MICROSTRUCTURE-BASED FATIGUE LIFE PREDICTION METHODS FOR NAVAL STEEL STRUCTURES

Prepared by

R. C. McClung
K. S. Chan
D. L. Davidson
T. Y. Tong

FINAL REPORT
July 1991–July 1994
SwRI Project No. 06-4414
ONR Contract No. N00014-91-C-0214

Submitted to

Office of Naval Research
800 N. Quincy Street
Arlington, VA 22217-5000

September 1994

SOUTHWEST RESEARCH INSTITUTE
SAN ANTONIO
DETROIT
HOUSTON
WASHINGTON, DC

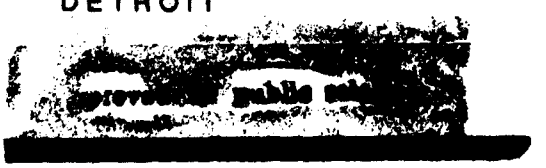

MICROSTRUCTURE-BASED FATIGUE LIFE PREDICTION METHODS FOR NAVAL STEEL STRUCTURES

Prepared by

R. C. McClung
K. S. Chan
D. L. Davidson
T. Y. Torng

FINAL REPORT
July 1991–July 1994
SwRI Project No. 06-4414
ONR Contract No. N00014-91-C-0214

Submitted to

Office of Naval Research
800 N. Quincy Street
Arlington, VA 22217-5000

September 1994

Approved:

S. J. Hudak, Jr.

Stephen J. Hudak, Jr., Director
Mechanics of Materials Department

SOUTHWEST RESEARCH INSTITUTE

6220 CULEBRA ROAD • POST OFFICE DRAWER 28510 • SAN ANTONIO, TEXAS, USA 78228-0510 • (210) 684-5111 • TELEX 244846

CERTIFICATION OF TECHNICAL DATA CONFORMITY

"Microstructure-Based Fatigue Life Prediction Methods for Naval Steel Structures"
ONR Contract No. N00014-91-C-0214
SwRI Project No. 06-4414

Final Report (July 15, 1991 - July 15, 1994)

The Contractor, Southwest Research Institute, hereby certifies that, to the best of its knowledge and belief, the technical data delivered herewith under Contract No. N00014-91-C-0214 is complete, accurate, and complies with all requirements of the contract.

9/12/94
Date

Ulric S. Lindholm, Vice President
Materials Engineering and Technology Division

Unclassified

ECURITY CLASSIFICATION OF THIS PAGE

REPORT DOCUMENTATION PAGE

Form Approved
OMB No. 0704-0188
Exp.Date: Jun 30, 1986

1a. REPORT SECURITY CLASSIFICATION Unclassified	1b. RESTRICTIVE MARKINGS
2a. SECURITY CLASSIFICATION AUTHORITY	3. DISTRIBUTION/AVAILABILITY OF REPORT Unlimited
2b. DECLASSIFICATION/DOW' ...G SCHEDULE	
4. PERFORMING ORGANIZATION REPORT NUMBER(S) 06-4414/3	5. MONITORING ORGANIZATION REPORT NUMBER(S)
6a. NAME OF PERFORMING ORGANIZATION Southwest Research Institute 6b. OFFICE SYMBOL *(If applicable)*	7a. NAME OF MONITORING ORGANIZATION Office of Naval Research
6c. ADDRESS *(City, State, and ZIP)* 6220 Culebra Road San Antonio, TX 78238-5166	7b. ADDRESS *(City, State, and ZIP Code)* 800 N. Quincy Street Arlington, VA 22217-5000
8a. NAME OF FUNDING/SPONSORING ORGANIZATION Office of Naval Research 8b. OFFICE SYMBOL *(If applicable)*	9. PROCUREMENT INSTRUMENT IDENTIFICATION NUMBER N00014-91-C-0214
8c. ADDRESS *(City, State, and ZIP)* 800 North Quincy Street Arlington, VA 22217-5000	10. SOURCE OF FUNDING NUMBERS PROGRAM ELEMENT NO. / PROJECT NO. / TASK NO. / WORK UNIT ACCESSION NO.

11. TITLE *(Include Security Classification)*
Microstructure-Based Fatigue Life Prediction Methods for Naval Steel Structures (Final Report)

12. PERSONAL AUTHOR(S)
R. C. McClung, K. S. Chan, D. L. Davidson, and T. Y. Tong

13a. TYPE OF REPORT	13.b TIME COVERED	14. DATE OF REPORT *(Year, Month, Day)*	15. PAGE COUNT
Technical	FROM 07/15/91 TO 07/15/94	94/09/12	153

16. SUPPLEMENTARY NOTATION

17. COSATI CODES			18. SUBJECT TERMS *(Continue on reverse if necessary and identify by block number)*
FIELD	GROUP	SUB-GROUP	Key Words: HSLA steels, fatigue life prediction, fatigue crack growth, small cracks, modeling, microstructure, copper precipitates, probabilistic fracture mechanics, welded structures

19. ABSTRACT *(Continue on reverse if necessary and identify by block number)*

The goal of the subject program has been to develop fundamental understandings of the relationships between microstructure and fatigue damage in structural steels of interest to naval applications. Quantitative descriptions of these relationships have been incorporated within practical engineering models for the prediction of fatigue life. Fatigue damage associated with microcrack nucleation and growth has been studied experimentally with *S-N* fatigue specimens of HSLA-80 steel. Some microstructures were modified with appropriate heat treatments, and the effects of microstructure on microcrack nucleation and growth have been characterized. Microstructural scaling laws have been developed and verified for both fatigue crack growth (FCG) and smooth specimen total life in a wide range of steels. The effects of microstructure on FCG have been described by a dimensionless microstructural parameter which is defined in terms of yield stress, fatigue ductility, dislocation cell size, and dislocation barrier spacing. FCG data from large and small flaws have been critically compared on the basis of engineering models for FCG rates, and the implications of this comparison for engineering fatigue life prediction are explored. A probabilistic treatment of the micromechanical scaling laws for FCG has been derived, permitting a direct evaluation of the relationship between microstructural variation and variability in FCG rates. Simulation modeling has been used to investigate different sources of apparent increased scatter in small crack data, and an enhanced lognormal random variable model has been derived to address the effects of this increased scatter on engineering fatigue life prediction.

...ED 3

20. DISTRIBUTION/AVAILABILITY OF ABSTRACT	21. ABSTRACT SECURITY CLASSIFICATION
☐ UNCLASSIFIED/UNLIMITED ☒ SAME AS RPT. ☐ DTIC USERS	Unclassified

22a. NAME OF RESONSIBLE INDIVIDUAL	22b. TELEPHONE *(Include Area Code)*	22c. OFFICE SYMBOL
R. C. McClung	(210) 522-2422	

DD FORM 1473 84 MAR

83 APR edition may be used until exhausted.
All other editions are obsolete.

SECURITY CLASSIFICATION OF THIS PAGE

Unclassified

Table of Contents

ABSTRACT

The goal of the subject program has been to develop fundamental understandings of the relationships between microstructure and fatigue damage in structural steels of interest to naval applications. Quantitative descriptions of these relationships have been incorporated within practical engineering models for the prediction of fatigue life. Fatigue damage associated with microcrack nucleation and growth has been studied experimentally with *S-N* fatigue specimens of HSLA-80 steel. Some microstructures were modified with appropriate heat treatments, and the effects of microstructure on microcrack nucleation and growth have been characterized. Microstructural scaling laws have been developed and verified for both fatigue crack growth (FCG) and smooth specimen total life in a wide range of steels. The effects of microstructure on FCG have been described by a dimensionless microstructural parameter which is defined in terms of yield stress, fatigue ductility, dislocation cell size, and dislocation barrier spacing. FCG data from large and small flaws have been critically compared on the basis of engineering models for FCG rates, and the implications of this comparison for engineering fatigue life prediction are explored. A probabilistic treatment of the micromechanical scaling laws for FCG has been derived, permitting a direct evaluation of the relationship between microstructural variation and variability in FCG rates. Simulation modeling has been used to investigate different sources of apparent increased scatter in small crack data, and an enhanced lognormal random variable model has been derived to address the effects of this increased scatter on engineering fatigue life prediction.

INTRODUCTION

The U.S. Navy currently employs HY-series steels in structural components such as submarine hulls. Since 1980, the Navy has also been evaluating the potential of HSLA (high-strength, low-alloy) steels for use in both ship and submarine construction. The introduction of these new steels has a complex impact on the design of naval structures. In some cases, design stress levels may increase to take advantage of improved properties, and this could cause significant decreases in fatigue crack initiation and propagation lives. As a result, fatigue cracking could become one of the greatest threats to structural integrity in future pressure hulls operating at higher stress levels. On the other hand, the development of new alloys with new microstructures and new welding process specifications provides the opportunity to improve the fatigue resistance of the material and, ultimately, of the structure itself.

The subject program has been motivated by the desire for improved understandings of the relationships between microstructure and fatigue damage in naval steel structures, with particular application to the prediction of fatigue life. Among the intended products of the study are improved methods for fatigue life prediction which give appropriate attention to different potential microstructures and associated microstructural influences on initiation and/or growth rates. The methods could be used to provide guidance in optimizing alloy chemistry, processing, and welding protocols for improved fatigue resistance, while also facilitating improved fitness-for-service assessments of actual or postulated cracking.

Fatigue design for naval structures is currently most often based on the stress-life (S-N) approach which relates applied stresses directly to the total life to "failure". This approach enables the analyst to take a "black box" approach to fatigue design in which relatively little must be known about the actual fatigue damage processes. But fatigue "science", such as the study of microstructural influences on fatigue damage, must look "inside" the black box to identify and characterize the physical damage processes as much as possible.

The total S-N life to "failure" is composed, in general, of three different life phases with specific physical damage processes: the nucleation of a microcrack, the growth of this microcrack until it reaches some engineering size (often on the order of millimeters), and the subsequent growth of the engineering crack to some definition of final failure. The total fatigue "life" is the sum of the lives associated with each phase. Under different conditions, one or more of the three phases may be dominant or negligibly small.

The basic technical approach of this program was first to identify the rate-controlling fatigue mechanisms and characterize the relevant microstructures for microcrack nucleation and growth. Quantitative relationships were established between microstructural and loading parameters and fatigue damage. Microcrack growth was identified as a potentially dominant phase of smooth specimen fatigue life. The second step was to develop practical engineering expressions to characterize the growth of both microcracks and large cracks and to predict total fatigue life. The third step of the program was to develop probabilistic models which incorporate both the microstructure-load-damage relationships developed in step one and the practical engineering approaches of step two. These stochastic models enabled a quantitative assessment of the probability of failure at a performance level of interest as a function of uncertainties in material/load/geometry input parameters.

The main body of this final report is a concise summary of the entire research program, highlighting key results and their implications. More complete presentations of the detailed procedures and results, along with more extensive discussions, are given in the six appendices. Each appendix is a reproduction of a full-length manuscript which has either been published, accepted for publication, submitted for publication, or which will be adapted for submission, all in refereed journals.

EXPERIMENTS

Complete details of the experiments, including material characterization, test matrices, and tabulated results, are given in Appendix A. For convenience, key details are summarized here.

Procedures

Most fatigue specimens were machined from the 10 mm thick flange region of welded I-beams manufactured by Bethlehem Steel Co. and sent to Lehigh University via Ingalls Shipbuilding Inc. Several specimens were cut from similar plate material obtained from the David Taylor Naval Ship Research and Development Center. Both plates satisfied the chemical composition specifications of MIL-S-24645 (9/24/90). The as-received microstructure consisted mostly of fine polygonal and accicular ferrite grains with sulfide inclusions. Ferrite grain sizes varied from 0.3 to 9 μm, with an average diameter around 2 to 4 μm, while inclusion sizes ranged from 2 to 12 μm. Copper precipitates ranged in size from 5 to 25 nm, with a peak at 8 to 12 nm. The 0.2% offset yield strength and ultimate strength of the as-received Lehigh plate were approximately 88 ksi (607 MPa) and 99 ksi (683 MPa), respectively. Several different heat treatment procedures were applied to the as-received material in order to study microstructural effects on the initiation and growth of fatigue cracks. Of particular interest was the lath-like microstructure commonly observed in the modified A710 and HSLA-100 steels.

Small fatigue cracks were studied with two different specimen designs. Beams of square cross-section 4 mm on a side by 52 mm long were loaded in 3-point bending (3PB) under nominal zero-max load cycling. Outer fiber stresses were required to exceed yield in these specimens order to initiate cracks, so the local (outer fiber) stress ratio (R) was not zero. In order to initiate cracks more easily, hourglass specimens with a minimum diameter of 0.1875 in. (4.76 mm) were loaded in rotating bending (RB), so that $R = -1$. Low stress machining and hand polishing techniques were used to minimize surface residual stresses in all specimens.

Crack growth was recorded by periodically taking acetate replicas of the specimen surface in the most highly-stressed regions. This technique made it possible to obtain FCG data from several different cracks on the same specimen. Tests were stopped when the largest cracks exceeded around 2 mm in surface length. Selected specimens were sectioned at the end of the test in order to determine typical aspect ratios for the surface cracks. Nearly all surface cracks were approximately semi-circular in shape. Secant and second-order incremental polynomial methods were used to compute da/dN from the raw a vs. N data. The nominal stress intensity factor, ΔK, was calculated from the surface half-crack length, a, and the nominal applied stress range, $\Delta\sigma$, according to the relationship $\Delta K = 1.3\ \Delta\sigma\ (a)^{1/2}$.

FCG data for large cracks in compact tension specimens were obtained from Lehigh University for the same heat of HSLA-80 material in the as-received condition [1] and from the Illinois Institute of Technology (IIT) for a comparable HSLA steel [2]. These tests were conducted at stress ratios of $R = 0.1$. These data exhibited a large crack threshold to exist at around $\Delta K_{th} = 7.5$ MPa•m$^{1/2}$.

A small number of additional low cycle fatigue (LCF) tests were conducted to characterize the strain-life relationship. These tests were conducted with smooth cylindrical specimens subjected to fully-reversed axial cycling under strain control.

Results

General observations about the effects of microstructure on fatigue crack initiation, growth, and total life follow in the next few paragraphs. Further details are available in Appendix A. The development of detailed micromechanical, engineering, and probabilistic models for these behaviors is treated in later sections.

Fatigue Crack Initiation

Microstructural changes greatly affected the sites at which fatigue cracks initiated. For example, cracks almost always initiated from inclusions in the as-received microstructure. In contrast, heat-treated microstructures containing lath-like features almost always exhibited initiation at these lath-like features.

However, these microstructural changes did not appear to have a significant impact on the total number of cycles required to initiate a crack. Initiation lives at comparable applied stresses were similar for as-received and heat-treated material.

The number of cracks that initiated was a function of stress level, increasing significantly with stress amplitude. Microstructure also appeared to have some effect on initiation frequency, more cracks initiating in as-received microstructures (inclusions) than in heat-treated microstructures (lath-like features).

Fatigue Crack Growth

Microstructural features appeared to have relatively little impact on the path and growth rates of the smallest microcracks in as-received material, as inclusions and other features were encountered during growth. However, the crack path was directly affected by microstructural features in heat-treated material. Cracks tended to initiate in the center portion of a grain and to grow in the lath direction until the crack reached a grain boundary. Crack direction was also easily correlated with lath orientation as the crack grew through subsequent grains. The relationship between microstructural features and crack growth in the weld material was not entirely clear. Crack growth rate data showed distinct periods of slower and more rapid crack advance. However, these observed rate changes were not linked to any specific microstructural features, such as grain boundaries.

The growth rates of small cracks (surface lengths ranging from 10 μm to 2 mm) were not, in general, significantly affected by microstructural changes. Figure 1 shows the scatterbands associated with all rotating beam small crack data. The only material conditions in which microstructure may have impacted microcrack growth rates was the weld and, to a smaller extent, one of the heat treated microstructures, but the differences were small in comparison to overall scatter. Growth rates for the smallest microcracks (< 200 μm) appeared to be slightly accelerated from the central tendencies of the other data.

Small cracks in all microstructures grew at ΔK values below the large crack threshold, thereby exhibiting one of the "small crack effects." However, these small cracks generally grew at rates which were consistent with the large crack Paris equation. Above about 10 MPa•m$^{1/2}$ (approximately 200 μm), large crack and small crack growth rate data were essentially identical. Below 10 MPa•m$^{1/2}$, small crack data were consistent with a downward extrapolation of the Paris line. However, the apparent scatter associated with these microcrack data was significantly larger than for the large crack data. These comparisons of large crack and small crack data are treated in more detail in subsequent discussions of modeling.

Collected large crack data for HSLA-80 and related steels exhibited a growth rate scatterband width of approximately 5x in the linear power-law regime. This variation is significantly smaller than typical small-crack scatter, but nevertheless large enough to have a significant impact on fatigue life. Transmission electron microscopy revealed that the higher growth rate corresponded to a steel containing Cu precipitates with an average diameter of 6.6 nm, while the lower crack growth rate corresponded to a steel with 17.5 nm Cu precipitates. This observation suggested that the size or mean free path of Cu precipitates might be a factor in determining the FCG response of this class of HSLA steels.

Total Smooth Specimen Life

Since the microstructural changes studied in this program had relatively little impact on fatigue crack initiation and small crack growth, it follows that microstructure had no significant impact on total smooth specimen life. Data for total life to "failure" (defined in these tests as the development of a 2 mm crack) were consistent with published data for similar materials.

The percentage of total smooth specimen life consumed in the nucleation of an identifiable microcrack ranged from 2% to 33%, with an average value around 12%. The nucleation life fraction tended to be larger at lower applied stresses (longer lives).

MICROMECHANICAL MODELS

A key objective of the research program was the development of microstructural scaling laws to describe the quantitative effects of microstructure (or lack thereof) on FCG rates and total fatigue lives. These scaling laws have been validated by comparisons to both the HSLA-80 data described above and other fatigue data available in the literature for other materials.

Microstructural Influences on Fatigue Crack Growth Rate

Fatigue crack growth (FCG) of large cracks in metals and alloys can generally be divided into three characteristic regimes: (1) a near-threshold regime where the growth response is sensitive to microstructure; (2) a power-law regime where microstructure typically has relatively little effect on the propagation rate, and (3) a rapid growth regime that is dominated by quasi-static crack extension and fracture toughness and is sensitive to microstructure. The power-law regime may sometimes be further subdivided into intermittent and continuous growth regimes. In the intermittent regime, cracks proceed discontinuously with periodic arrests and waiting periods between individual growth increments. Crack growth occurs on each cycle in the continuous growth regime.

A set of scaling laws was developed for describing both intermittent and continuous FCG in steels in the power law regime. The scaling laws were developed from the premise that FCG occurs as the result of low-cycle fatigue failure of a crack-tip element whose width and height correspond to the dislocation cell size and barrier spacing, respectively. The resulting crack growth equation is

$$\frac{da}{dN} = \xi^{1/b}(2s)^{1-1/b}\left[\frac{\Delta K^2}{E}\right]^{2/b} \tag{1}$$

where ξ is a dimensionless microstructural parameter defined as

$$\xi = \frac{Es}{4\sigma_y \varepsilon_f' d} \tag{2}$$

Here d is the dislocation barrier spacing, s the striation spacing, b the fatigue ductility exponent and ε_f' the fatigue ductility coefficient in a Coffin-Manson equation, E Young's modulus, and σ_y the yield strength. For continuous crack growth, $b = 1$, and Eqn. 1 reduces to

$$\frac{da}{dN} = \xi\left[\frac{\Delta K}{E}\right]^2 \tag{3}$$

This scaling law was validated through comparison to large crack FCG data for HSLA-80 and numerous other steels. Material inputs to the model (d, s, b, ε_f', etc.) were determined from independent microstructural and material property information wherever possible. The characteristic microstructural feature associated with the dislocation barrier spacing, d, changed appropriately from steel to steel, depending on the microstructure type. In the HSLA-80 steel, for example, d was taken as the mean free path of Cu precipitates. In ferritic/pearlitic steels, d was interpreted as the grain size, while d was the carbide spacing in tempered martensitic microstructures.

The calculated FCG curve for HSLA-80 is compared with experimental data in Figure 2. Agreement is excellent in both the intermittent and continuous crack growth regimes. Comparisons of model and experimental data for HY-80 and a comparable Q&T steel in the intermittent growth regime are shown in Figure 3. Other graphical comparisons are available in Appendix B.

The model was also used to investigate the postulated effect of Cu precipitate spacing on FCG rates, as noted in earlier experiments. The large variation in Cu precipitate mean free path (d = 0.46 to 0.79 μm) and related smaller variations in σ_y and ε_f' implied a significant change in ξ. The resulting effect on predicted growth rates was generally consistent with the observed experimental data, confirming that the Cu precipitates are the most significant microstructural feature for FCG rates.

This scaling law provides a rational basis for explaining the relatively weak influence of microstructure on FCG for steels in the power-law regime. Recall that da/dN scales with ξ, where $\xi = Es/(4\sigma_y\varepsilon_f'd)$. For steels with a fine microstructure, the value of d is small, but the values of ε_f' and σ_y are larger (following the Hall-Petch relation), as shown in Figure 4. Conversely, d is large

for steels with coarse microstructures, but the corresponding values for ε_f' and σ_y are lower. The consequence is that the product $\sigma_y\varepsilon_f'd$, and hence ξ and da/dN, are relatively insensitive to microstructure.

Complete details of model derivation, validation, and discussion are given in Appendix B. This manuscript, which was published in *Metallurgical Transactions A* [3], and its author, Dr. K. S. Chan, has been selected to receive the 1994 Marcus Grossman Young Author award from ASM International. The award honors the author(s) under 40 years of age whose paper was judged the best in a specific volume of *Metallurgical Transactions*.

In related research outside the scope of the subject contract, these microstructural scaling laws have also been applied to describe microstructural effects on FCG rates in titanium alloys and aluminides [4]. In contrast to steels, microstructure can have a pronounced effect on FCG rates in $\alpha+\beta$ titanium alloys, and the scaling laws described above were successful in characterizing this phenomenon.

Microstructural Influences on Total Smooth Specimen Life

A scaling law was also developed for total smooth specimen life, which is defined as "initiation" in some engineering applications. Like the crack growth scaling law, the starting point was the Coffin-Manson fatigue life relationship:

$$\frac{\Delta\varepsilon_p}{2} = \varepsilon_f'(2N_i)^{-b} \tag{4}$$

In the previous development of FCG scaling laws, the fatigue ductility coefficient ε_f' was found to depend on the dislocation barrier spacing according to a modified Hall-Petch relation, $\varepsilon_f' = \varepsilon_0'(d_0/d)^{1/2}$, where d_0 is a reference dislocation barrier spacing. These starting points lead to the final scaling law

$$N_i = C_i\left(\frac{d_0}{d}\right)^{\frac{1}{2b}} \tag{5}$$

with

$$C_i = \frac{1}{2}\left(\frac{2\varepsilon_0'}{\Delta\varepsilon_p}\right)^{\frac{1}{b}} \tag{6}$$

Comparisons of the experimental and calculated curves for four different steels are shown in Figure 5. Agreement appears to be strong. A similar comparison for the HSLA-80 steel is shown in Figure 6. In this case, the model calculation was based on $b = 0.5$ determined from the crack growth studies, while the actual life data suggest $b = 0.65$. This disagreement may be related to the earlier observation that microcrack nucleation in the as-received material condition nearly always occurred at sulfide inclusions. This may have reduced the N_i values and led to an apparent increase in the b value.

Further details and discussion of this scaling law are given in Appendix C, a manuscript which has been accepted for publication in *Scripta Met. et Mat.*

ENGINEERING MODELS

The scaling laws discussed above are of great significance in the quest to understand the fundamental nature of the relationship between microstructure and fatigue resistance. This understanding may be of particular benefit in efforts to develop materials with greater fatigue resistance or in efforts (discussed later) to understand and characterize scatter in observed fatigue resistance. However, there is also a need to develop improved engineering descriptions of fatigue resistance which may ultimately be employed to perform practical life predictions of engineering components and structures.

The smooth specimen experiments conducted at the outset of this research program demonstrated that a large portion of total smooth specimen life was consumed by the microcrack growth. This suggests that it should be possible to perform life calculations for smooth specimens from a fracture mechanics basis. However, the proper engineering relationship between this microcrack growth and the more commonly characterized growth of large fatigue cracks remains to be established.

Correlation of Small Crack and Large Crack Data

All crack growth data for both large and small cracks in the as-received HSLA-80 are compared on the basis of the nominal full-range ΔK (calculated from the full stress range σ_{max}-σ_{min}) in Figure 7. Note, first of all, that the small cracks grew at nominal ΔK values significantly lower than the large crack threshold value, ΔK_{th}, around 7.5 MPa•m$^{1/2}$. This is a commonly observed "small crack" effect. Second, note that the large and small crack data were not well-correlated by the nominal full-range ΔK. These data included widely differing stress ratios: large cracks at R = 0.1, small cracks at R = -1 (rotating beam) and -0.35 (square beam); and widely differing maximum stresses: near yield for the small cracks, far below yield for the large cracks.

Two different approaches were explored to "correct" the nominal ΔK to account for the effects of applied stress and stress ratio. One approach was based on the recommendations of ASTM Test Method E 647, "Standard Test Method for Measurement of Fatigue Crack Growth Rates." This test method instructs that $\Delta K = K_{max} - K_{min}$ when $R \geq 0$, but that ΔK should be calculated according to $\Delta K = K_{max}$ when $R < 0$ (i.e., take only the tensile portion of the stress intensity factor range). A second approach was based on considerations of plasticity-induced crack closure, employing the modified-Dugdale model of Newman [5] to estimate crack opening stresses at different maximum stresses and stress ratios.

The two approaches gave nearly identical results for these data, since calculated crack opening stresses were relatively close to zero stress for all three configurations. The correlation based on the "ASTM" approach is illustrated in Figure 8. This figure shows clearly that small crack data and large crack data are essentially identical above the near-threshold regime. At ΔK values below the large crack threshold, the microcrack data are satisfactorily represented by a downward extrapolation of the large crack Paris equation. The apparent scatter in the microcrack data is much larger, however, and this phenomenon is addressed further in the later discussion of probabilistic models. Further details of this engineering analysis are contained in Appendix D.

Implications for Engineering Life Prediction

Fatigue life prediction which is based on an explicit treatment of the crack growth phenomenon requires integration of the FCG equation. For the simple Paris equation or its equivalent, this integration results in the form

$$N_f = A(C, m, F)(\Delta\sigma)^{-m} \tag{7}$$

where C and m are the coefficient and exponent of the Paris equation and F is the geometry correction factor (here assumed to be constant) in the stress intensity factor expression. Equation (7) also assumes constant initial and final flaw sizes. This result implies that a traditional S-N equation can be constructed directly from a FCG relationship. For the HSLA-80 steel, the implied value of m based on FCG data is between 3 and 4. Furthermore, it has been demonstrated that this FCG relationship can be used to characterize the growth of fatigue microcracks as small as 10 to 30 μm. The remaining question is how accurately this FCG-derived relationship reflects actual S-N fatigue life data.

The answer to this accuracy question is dependent on the definition of "S-N" data. At least two definitions are meaningful for naval structural applications. The first definition is the life of a polished smooth specimen, and the second definition is the life of a large-scale welded component.

Available data for smooth specimen axial fatigue tests of HSLA-80 over a wide range of maximum stresses [6] indicate that the S-N "slope" m is about 10-12 for tests in which the stress amplitude was less than about 100 ksi (690 MPa). This observed value of m is significantly different from our implied value based on FCG data. The difference is due to the influence of the crack nucleation life phase. The nucleation phase tends to be negligibly small at relatively short lives but can be dominantly large (approaching 100% of total life) at very long lives. This general trend is evident in the fatigue tests conducted under the current contract, as noted earlier.

At higher applied stresses, when the nucleation life fraction is negligible, this FCG approach to smooth specimen life prediction will be entirely adequate. However, to address the complete range of smooth specimen behavior out to much longer lives, some further treatment of the nucleation phase will also be required. Traditional "initiation" models based on the Coffin-Manson type of equation, such as the microstructural scaling law presented earlier, may be useful here. However, it must be noted that these traditional models address the total life to specimen failure (which may include appreciable portions of crack growth, as demonstrated in this research program), not the true life to nucleation of a microcrack. Further work is required to partition the true nucleation life fraction and then to combine this with a true fracture mechanics model for microcrack growth.

However, as noted in the last paragraph, a treatment based entirely on integration of the FCG relationship for microcracks and large cracks will be satisfactory when nucleation occurs very early in life. This condition is satisfied for fatigue of many practical welded structures, which provide weldment defects and discontinuities as crack initiators. Recent data from fatigue tests of both large-scale and small-scale welded HSLA-80 structures [7, 8] suggest an S-N slope between 3 and 4, which agrees closely with the Paris exponent from the available FCG data. Simple estimates of total fatigue life based on fracture mechanics arguments (and using the same large crack baseline FCG data presented earlier in this report) were successful in predicting the observed trends in experimental lives.

Many large-scale welded structures such as bridges and steel buildings are engineered on the basis of fatigue design curves first developed by the American Association of State Highway and Transportation Officials (AASHTO) [9]. The slopes of these AASHTO design curves and similar curves published by other regulatory bodies have been fixed at $m = 3.0$, which is again consistent with known relationships for the FCG behavior. It is particularly interesting that the AASHTO curves appear to provide a reasonably accurate description of the Lehigh HSLA-80 welded structure *S-N* data [7], even though the AASHTO curves were developed from tests mostly on carbon-manganese steels. This coincidence occurs because, as demonstrated by the microstructural scaling laws, large crack FCG rates differ relatively little among different steel microstructures.

In general, the correct *S-N* slope for welded structures will vary as a function of initial weld quality. When initial weld quality is relatively low, cracks can initiate quickly and the *S-N* slope will approach the limiting value of 3 to 4 based on fracture mechanics arguments. When initial weld quality is higher, then the nucleation phase can again become important. Under these conditions, the *S-N* slope will be a larger number and may eventually approach that for smooth specimens in base metal, although in practice it will rarely reach this limit. Initial weld quality can also influence the initial size of the fatigue cracks, which has a further impact on *S-N* slope.

Further discussion of these engineering implications is available in Appendix D.

PROBABILISTIC MODELS

Fatigue crack growth data generally exhibit substantial scatter. This scatter arises from several factors, including microstructural variations, uncertainties in crack length measurements, and the intermittent nature of the FCG process itself. From a fundamental viewpoint, it is useful to understand these different sources of uncertainty, particularly as the scatter may be related to intrinsic microstructural factors. From an engineering viewpoint, it is often necessary to characterize this uncertainty in conjunction with life prediction and life management exercises. Each of these viewpoints was addressed with an appropriate probabilistic treatment in the subject program.

Probabilistic Treatment of Micromechanical Models

Many probabilistic treatments of FCG in the literature are based on simplistic engineering characterizations of the FCG process, such as the Paris equation. In these models, randomness in the FCG response is treated by taking one or both of the empirical constants (coefficient and exponent) of the Paris equation as random variables, without thought for the physical meaning of these variations or, in particular, the role of microstructure in the FCG process.

A micromechanical FCG model that incorporates microstructural size parameters was presented earlier in this report. This model, which provides an explicit relationship between *da/dN* and key microstructural size scales, was used as the starting point for the development of a new probabilistic FCG model. Specifically, each of the microstructure-dependent parameters in Eqn. 1 can be described as

$$M = \overline{M} X_M \tag{8}$$

where $M = E$, s, σ_y, ε_f', or d. $\overline{M}$ and X_M are the mean value and the randomness of the parameter M, respectively. For simplicity, however, randomness in E and s is ignored. The resulting probabilistic crack growth rate expression is given by

$$\frac{da}{dN} = (X_\xi)^{1/b} \bar{\xi}^{1/b} (2\bar{s})^{1-1/b} \left[\frac{\Delta K^2}{\bar{E}} \right]^{2/b} \tag{9}$$

Here

$$X_\xi = \frac{1}{X_{\sigma_y} X_{\varepsilon_f'} X_d} \tag{10}$$

is a function that incorporates the overall variation of the crack growth rate resulting from randomness in the microstructural variables. Correlations among the yield stress, the fatigue ductility coefficient, and the dislocation barrier spacing according to modified Hall-Petch relations permit further simplification of this expression. Further details are provided in Appendix E.

Compilations of yield stress and fatigue ductility coefficient data for steel as a function of dislocation barrier spacing, d, were presented previously in Figure 4. If the Hall-Petch exponents α (for σ_y) and β (for ε_f') are both assumed to be exactly 0.5, as is common for steels, then we obtain the slightly surprising result that the FCG rate is independent of the dislocation barrier spacing. Variations in the FCG rate then arise directly from variations in the Hall-Petch relationships (scatter in Figure 4). For other materials (e.g., titanium), α and β can be significantly different, so that variations in d also figure directly in the probabilistic FCG model.

Validation and demonstration of this model was carried out by performing statistical analysis of the available microstructural data to determine the appropriate X_i values. Available large crack FCG data for HSLA-80 was shown to be consistent with the predictions of the probabilistic model. In order to perform a total life calculation by integrating the crack growth law, additional information about the initial crack size was required. These data were obtained by assuming the initial flaw size in as-received HSLA-80 to be equivalent to the inclusion size, and fitting the available inclusion size data to a Weibull distribution. A performance function was defined by comparing the calculated crack growth life with an assumed service life. The resulting limit state problem was solved using FPI™, an advanced probabilistic code, based on fast probability integration (FPI) techniques. Outputs included the cumulative distribution function (CDF) of the crack growth life and the probability of failure, P_f. In addition, the probabilistic sensitivity factors (PSFs), which are the directional cosines of a unit vector from the origin to the most probable point on the limit-state surface in the standard normal space, were calculated to compare the relative importance between random variables. With further derivations, these PSFs become useful design information. The CDF and PSFs for a sample calculation for HSLA-80 steel are given in Figure 9. Further details are provided in Appendix E, along with contrasting calculations for a titanium alloy which were performed independent of the subject contract.

An advantage of this methodology over the traditional probabilistic approach is that the stochastic sensitivity of the various microstructure-dependent random variables can be predicted. This knowledge provides insight into how to modify the microstructure, the microstructure-

dependent parameters, and their corresponding randomness to improve the FCG rate resistance of structural alloys. Additionally, this information can be used as a basis for developing graded microstructures with favorable FCG characteristics.

Probabilistic Treatment of Engineering Models

The randomness associated with FCG may be most apparent and most significant for small cracks, when crack-microstructure interactions are also most significant. Small crack growth rate data are often characterized by great variability, especially in comparison to growth rate data for large cracks outside of the near-threshold region. Because of this large variability, simple deterministic schemes to compute microcrack-dominated life are often not satisfactory. Therefore, small crack growth is a particularly good candidate for probabilistic methodologies. Unfortunately, small crack growth also presents special obstacles to developing probabilistic models. In particular, it is often difficult to collect raw FCG data of sufficient quality and quantity to compute necessary probabilistic parameters.

The development of probabilistic fatigue life prediction methods based on the growth of both small and large cracks has been guided by two central criteria. The first criterion was that these methods reflect some genuine understanding of the physical sources of uncertainty in small crack and large crack growth, and that the mathematical methodologies, in some way, reflect this understanding. This criterion excluded some existing probabilistic FCG methodologies which cannot be linked to the physical process of small crack growth. The second criterion was that these methods retain sufficient mathematical simplicity to permit their practical use in engineering contexts. This criterion excluded other methodologies which may be theoretically attractive but are scientifically or mathematically complex.

Several different factors which influence uncertainty in crack growth behavior have been identified. These include variations in the crack growth increment rate, which is the microscopic variation along the crack path of a single specimen; errors in the measurement of crack length; and the crack superposition effect, which can be interpreted physically as an averaging effect. The available HSLA-80 crack growth data were analyzed to estimate these various factors, and a simple Monte Carlo simulation program was developed to illustrate the total effect on apparent FCG rates. The results for a sample simulation are shown in Figure 10. These results are qualitatively similar to the actual experimental data: large variability in the microcrack regime, and relatively smaller variability in the large crack regime. Further details and discussion of these simulations is provided in Appendix F. Simple conceptual models of this type provide a basis for comparing various sources of uncertainty more rigorously and thereby gaining fundamental insights into the behavior of microcracks.

An appropriate stochastic fatigue crack growth (SFCG) model for use in engineering applications should be as simple as possible while maintaining reasonable accuracy. This SFCG model should be able to address the large variability observed in the small crack regime, as well as the smaller variability observed in the large crack regime. Numerous SFCG models have been proposed in the literature. Unfortunately, very few of these models explicitly address small crack effects, and nearly all of the models require raw data of much greater quantity and quality than is feasible to obtain for small crack configurations.

When only limited data are available, a lognormal random variable (LRV) model proposed by Yang et al. [10] is useful. This model employs the simplest mathematical model for which the analytical solution may be derivable, and it can be easily understood by engineers. The lognormal random variable model takes the general form

$$\log\left(\frac{da}{dN}\right) = \log(f(\xi, K, a, R, etc.)) + \log(X(t)) \tag{11}$$

Here f is some user-defined FCG model, which may be a simple Paris equation or a more complex micromechanical relationship such as the scaling laws discussed earlier. The function $X(t)$ is a non-negative stationary lognormal random process which is used to account for the combined effect of unknown contributions towards changing the crack growth rate with time (cycles).

However, the standard LRV model does not admit an increase in the randomness for smaller crack sizes. In order to address this limitation, an enhanced LRV model was developed which accounted for the nonlinear variability exhibited by the actual FCG data. In order to accommodate the increased scatter in the small crack regime, the standard deviation σ_Z of the stochastic random variable $Z(t) = \log(X(t))$ was itself modeled as a time-dependent function. A conventional LRV model and an enhanced LRV model are compared with the original experimental data (combined large and small crack data) from which they were derived in Figure 11. Complete details of these LRV models is provided in Appendix F.

Complete solution of the probabilistic fatigue life problem requires not only the development of an appropriate SFCG model, but also the development of an appropriately robust, efficient, and accurate probabilistic method to solve the limit state problem. For the enhanced LRV model, some numerical integration or simulation approach is required. In the current program, an advanced mean value method [11] was used. Illustrative predictions of total propagation life for the HSLA-80 small crack data are shown in Figure 12 for both conventional and enhanced LRV models. Note that the enhanced LRV model predicts greater variability in the small crack regime than does the conventional LRV model, but as crack growth continues in the large crack regime, the enhanced LRV model will give realistically tighter bounds on total life.

DISCUSSION

The fundamental goals of this research program, as highlighted in the Introduction, were to supplement or replace traditional "black box" approaches to fatigue design/analysis with more scientific approaches which accurately describe true physical phenomena while retaining sufficient engineering simplicity. Significant progress towards these goals has been achieved in nearly every task.

For example, we have shown that traditional *S-N* life prediction methods for many welded structures can be replaced with prediction schemes based on integration of crack growth equations from extremely small initial crack sizes. This permits the direct evaluation of many different effects on total *S-N* life by studying the true mechanisms of damage growth rather than by fitting different empirical forms to data.

Furthermore, we have shown how it is possible to replace purely empirical FCG relationships with crack growth laws which more accurately characterize the crack advance mechanism in the specific material of interest. In particular, we have shown how it is possible to relate FCG rates directly to critical microstructural parameters through a series of micromechanical scaling laws. The implications of microstructure for total fatigue life can therefore be directly assessed.

We have also replaced traditional approaches to stochastic fatigue crack growth modeling, which are typically based on probabilistic treatments of empirical constants, with approaches which reflect the actual sources of uncertainty. For example, the probabilistic treatment of the microstructural scaling laws makes it possible to link variability in fundamental microstructural parameters and relationships to observed (or predicted) variability in FCG rates. Simulation modeling of small crack effects has made it possible to characterize and evaluate different sources of apparent variability in small crack data, providing guidance for the development of more realistic engineering models for stochastic FCG.

Development of these sound, fundamental understandings of the fatigue damage process now makes it possible to study a much broader range of fatigue life issues from a scientific perspective. Some of these potential future directions are described following the conclusions.

CONCLUSIONS

1. Microstructural changes in HSLA-80 following various heat treatments greatly affected the sites and frequency of fatigue crack nucleation, but had little effect on the number of cycles required to nucleate a fatigue microcrack. Microcracks nucleated at sulfide inclusions in as-received microstructures but at lath-like features in heat-treated microstructures.

2. The growth rates of small cracks did not appear to be significantly affected by the microstructural changes imposed. A slight acceleration of growth rates for the smallest microcracks may occur in the weld and one of the heat treated microstructures, but the differences were relatively small compared to overall scatter. Variations in FCG rates for large cracks appear to be related to the size or mean free path of Cu precipitates.

3. Microstructural changes had relatively little impact on total smooth specimen life. The percentage of total smooth specimen life consumed in the nucleation of an identifiable microcrack ranged from 2% to 33%, with an average value around 12%.

4. A set of scaling laws has been developed for describing both intermittent and continuous FCG in steels in the power-law regime. The scaling laws assume that FCG occurs as the result of low-cycle fatigue failure of a crack-tip element whose width and height correspond to the dislocation cell size and barrier spacing, respectively. The results show that the effects of microstructure can be described entirely in terms of a dimensionless microstructural parameter, ξ, which is defined in terms of yield stress, fatigue ductility, dislocation cell size, and dislocation barrier spacing.

5. Verification of the scaling laws for HSLA and conventional ferritic, ferritic/pearlitic, and martensitic steels reveals that the lack of a strong microstructural influence on FCG in the power-law regime is due to increasing yield stress and fatigue ductility with decreasing

dislocation barrier spacing, which leads to a narrow range of ξ values and crack growth rates. Variations of *da/dN* data with microstructure in HSLA-80 steels, including the effects of copper precipitates, have been explained in terms of the scaling laws.

6. A microstructural scaling law has also been developed for total smooth specimen life, sometimes described as "initiation life." This life is predicted to scale inversely with the dislocation barrier spacing. The scaling law has been verified by comparison with experimental data for several steels, including HSLA-80.

7. Large cracks and small cracks in HSLA-80 steel grow at similar rates in the traditional large crack power-law regime, when compared on the basis of a properly defined effective stress intensity factor range. This effective ΔK, which addresses differences in stress ratio and maximum stress, can be defined in terms of crack closure concepts or simply in terms of the tensile portion of the local stress range. For the data considered in this study, these two approaches gave similar results.

8. Small cracks in HSLA-80 steels can grow at applied stress intensity factors which are smaller than the traditional large crack threshold, ΔK_{th}. These cracks grow at rates which are consistent with a downward extrapolation of the large crack power-law trends.

9. Acceptably accurate characterization of total life *S-N* behavior for many welded structures based on an integration of FCG relationships for both small and large fatigue cracks is feasible. This approach is also feasible for smooth specimen behavior in the low cycle fatigue regime. Some additional attention to the nucleation phase may be necessary to characterize smooth specimen life in the high cycle regime or to treat welded structures with much higher initial weld quality.

10. A new stochastic fatigue crack growth model has been developed via a probabilistic treatment of the microstructural scaling law for FCG. The model demonstrates how variability in FCG rates and total fatigue lives is linked to variability in fundamental microstructural parameters and relationships. This model makes it possible to identify the most significant sources of variability and, hence, to identify the most promising opportunities for improved fatigue resistance through microstructural optimization.

11. Different sources of apparent variability in small crack FCG rate data include the crack growth increment rate, which is linked to microstructural factors; measurement errors; and the crack superposition effect, which can be interpreted physically as an averaging effect. A simple simulation model of small crack growth has been developed to demonstrate and evaluate the relative significance of these different sources of variability.

12. An enhanced lognormal random variable stochastic FCG model has been developed which addresses the increased scatter observed for small fatigue cracks, while maintaining much of the engineering simplicity of the traditional lognormal random variable model. The limit state problem based on this model can be solved with an appropriate fast probability integration method in order to obtain cumulative distribution information about total fatigue life.

FUTURE WORK

While the research investigations described above answered many key questions and provided insight on a variety of issues, they also serve to provoke a number of additional questions. Some potential extensions of these investigations to elucidate remaining uncertainties and to explore new issues are briefly described below. Other remaining questions and potential applications of these technologies were mentioned in the preceding discussions.

- The microstructural scaling laws were validated for a wide variety of steel microstructures and, in other work outside the current contract, for selected titanium microstructures. Further work is required to determine if these scaling laws can be applied to a broader range of materials, such as aluminum alloys and perhaps some advanced composites. The mutual applicability of the FCG scaling laws to both large and small cracks should also be explored further.

- Although these microstructural scaling laws were originally developed for dry ambient conditions, many naval applications involve aggressive environments such as sea water. Under these conditions, when mechanisms for crack advance are more complex, alternative scaling laws which address other microstructural phenomena may be required. Exploratory experimental and analytical studies are needed to assess these issues.

- Another necessary simplification in these initial investigations was simple constant amplitude loading at a limited number of stress ratios. Actual service loading is typical variable amplitude in nature and includes load excursions at many different stress ratios. Relatively little is known about microstructural influences or small crack effects under variable amplitude loading, although some available studies suggest significant differences in smooth specimen and small crack behavior for certain types of complex load histories. Fundamental work is required to address variable load histories from a sound theoretical basis, while retaining engineering simplicity.

- The application of greatest interest for many naval structures is crack growth in weldments. Limited investigations of small crack growth in welds under the current program found potential differences in crack growth rates which could not be fully explored. Other issues such as weld quality (initial defectiveness) and residual stresses are also important, and some of these issues may best be treated by a probabilistic microstructural approach.

- Studies of small crack growth under the current contract found that the large crack threshold was not preserved. It is not clearly understood, however, at what crack lengths or under what conditions the threshold may or may not become effective. This ambiguity is becoming increasingly important in many aeronautical applications, including both fixed wing and rotorcraft configurations, where durability and damage tolerance analyses (DADTA) must now be applied to smaller and smaller flaws. Lifetime predictions for these applications can be extremely sensitive to assumptions made about the nature of the "near-threshold" crack growth curve. The proper form of this curve, which is typically derived from large crack testing, is not known reliably from either an engineering or a microstructural perspective for cracks which are smaller and stresses which are larger.

- The probabilistic treatment of the micromechanical scaling laws permits the stochastic sensitivity of the various microstructure-dependent random variables to be predicted. This capability should be exploited further to investigate means of modifying the microstructure to improve the FCG rate resistance of structural alloys. Additionally, this information may provide guidance for the development of graded microstructures with favorable FCG characteristics.

- The simple simulation model developed to describe apparent scatter in small crack growth rates provides a powerful tool for additional investigations. Additional small crack data from original experiments and from the literature should be analyzed to better characterize different sources of uncertainty, and the simulation model itself should be exercised more extensively to compare and contrast these different contributions. It should prove particularly useful to distinguish real scatter from apparent scatter, since these should have different implications for lifetime prediction. The simulation model should also be more closely linked to the enhanced lognormal random variable model, so that the engineering model for stochastic FCG can be derived more directly from primitive physical variables.

- The general probabilistic model developed for FCG, which can accommodate both microstructural scaling and small crack scatter, also permits inclusion of other sources of variability such as stochastic load histories, dimensional variabilities (e.g., in weldment fit-up), probability of detection (POD) of defects during periodic inspection, etc. The usefulness of this formulation to solve the more comprehensive structural reliability problem should be explored further. Such a formulation could facilitate improved design optimization, in addition to improved life extension and management strategies which also address the effects of inspection and repair operations on structural reliability. This expansion would also permit a more meaningful assessment of microstructural variabilities in the context of total system variability.

PUBLICATIONS AND PRESENTATIONS

The following publications/presentations were directly generated by this research program:

"Scaling Laws for Fatigue Crack Growth of Large Cracks in Steels," by K. S. Chan, *Metallurgical Transactions A*, Vol. 24A, 1993, pp. 2473-2486.

"Scaling Laws for Fatigue Crack Growth of Large Cracks in Steels," by K. S. Chan, presented at the 1994 TMS Annual Meeting, San Francisco, CA, February 27 - March 3, 1994.

"Probabilistic Fatigue Life Prediction Methods for Small and Large Fatigue Cracks," by T. Y. Torng and R. C. McClung, Proc. 35th AIAA/ASME/ASCE/AHS/ASC Structures, Structural Dynamics, and Materials Conference, Hilton Head, South Carolina, April 1994, pp. 1514-1524.

"A Scaling Law for Fatigue Crack Initiation in Steels," by K. S. Chan, *Scripta Metallurgica et Materialia*, in press.

"Cu Bearing HSLA Steels: The Influence of Microstructure on Fatigue Crack Initiation and the Growth of Small Fatigue Cracks," by D. L. Davidson, K. S. Chan, and R. C. McClung, to be submitted.

"A Probabilistic Treatment of Microstructural Effects on Fatigue Crack Growth of Large Cracks," by K. S. Chan and T. Y. Torng, submitted to *ASME Journal of Engineering Materials and Technology*.

"Analysis of Small Fatigue Cracks in HSLA-80 Steel," by R. C. McClung and T. Y. Torng, to be submitted to *Engineering Fracture Mechanics*.

The following papers and presentations were not directly supported by the ONR contract, but represent immediate extensions of the technology developed under the ONR contract to other engineering applications.

"Microstructure/Fatigue Crack Growth Relationships in Titanium Alloys and Aluminides," by K. S. Chan, Proc. Harold Margolin Symposium, TMS, Warrendale, PA, 1994 (in press).

"Analysis of Small Crack Behavior for Airframe Applications," by R. C. McClung, K. S. Chan, S. J. Hudak, Jr., and D. L. Davidson, FAA/NASA International Symposium on Advanced Structural Integrity Methods for Airframe Durability and Damage Tolerance, Hampton, Virginia, May 4-6, 1994 (to be published as a NASA CP).

REFERENCES

1. A. C. Nussbaumer, R. J. Dexter, J. W. Fisher, and E. J. Kaufmann, "Propagation of Very Long Fatigue Cracks in a Cellular Box Beam," *Fracture Mechanics: 25th Volume, ASTM STP 1220*, 1994, in press.

2. J. A. Todd, L. Chen, E. Y. Yankov, and H. Tao, A comparison of the near-threshold corrosion fatigue crack propagation rates in Mil S-24645 HSLA steel and its weld metal, *ASME J. Offshore Mechanics and Arctic Engineering*, Vol. 115, 1993, pp. 131-136.

3. K. S. Chan, "Scaling Laws for Fatigue Crack Growth of Large Cracks in Steels," *Metallurgical Transactions A*, Vol. 24A, 1993, pp. 2473-2486.

4. K. S. Chan, "Microstructure/Fatigue Crack Growth Relationships in Titanium Alloys and Aluminides," Proc. Harold Margolin Symposium, TMS, Warrendale, PA, 1994 (in press).

5. J. C. Newman, Jr., "A Crack Opening Stress Equation for Fatigue Crack Growth," *International Journal of Fracture*, Vol. 24, 1984, pp. R131-R135.

6. T. W. Montemarano, B. P. Sack, J. P. Gudas, M. G. Vassilaros, and H. H. Vanderveldt, "High Strength Low Alloy Steels in Naval Construction," *Journal of Ship Production*, Vol. 2, 1986, pp. 145-162.

7. R. J. Dexter, J. W. Fisher, and J. E. Beach, "Fatigue Behavior of Welded HSLA-80 Members," ASME Offshore Mechanics and Arctic Engineering Conference, Glasgow, UK, June 1993.

8. S. Sarkani, D. P. Kihl, and J. E. Beach, "Fatigue of Welded Joints Under Narrowband Non-Gaussian Loadings," *Probabilistic Engineering Mechanics*, Vol. 9, 1994, 179-190.

9. *Standard Specification for Highway Bridges*, 14th ed., The American Association of State Highway Transportation Officials, Washington, DC, 1989.

10. J. N. Yang, W. H. Hsi, and S. D. Manning, *Stochastic Crack Propagation With Applications to Durability and Damage Tolerance Analyses*, AFWAL-TR-85-3062, 1985.

11. Y.-T. Wu, O. H. Burnside, and T. A. Cruse, "Probabilistic Methods for Structural Response Analysis," *Computational Probabilistic Methods*, AMD-Vol. 93, ASME, 1988, pp. 1-14.

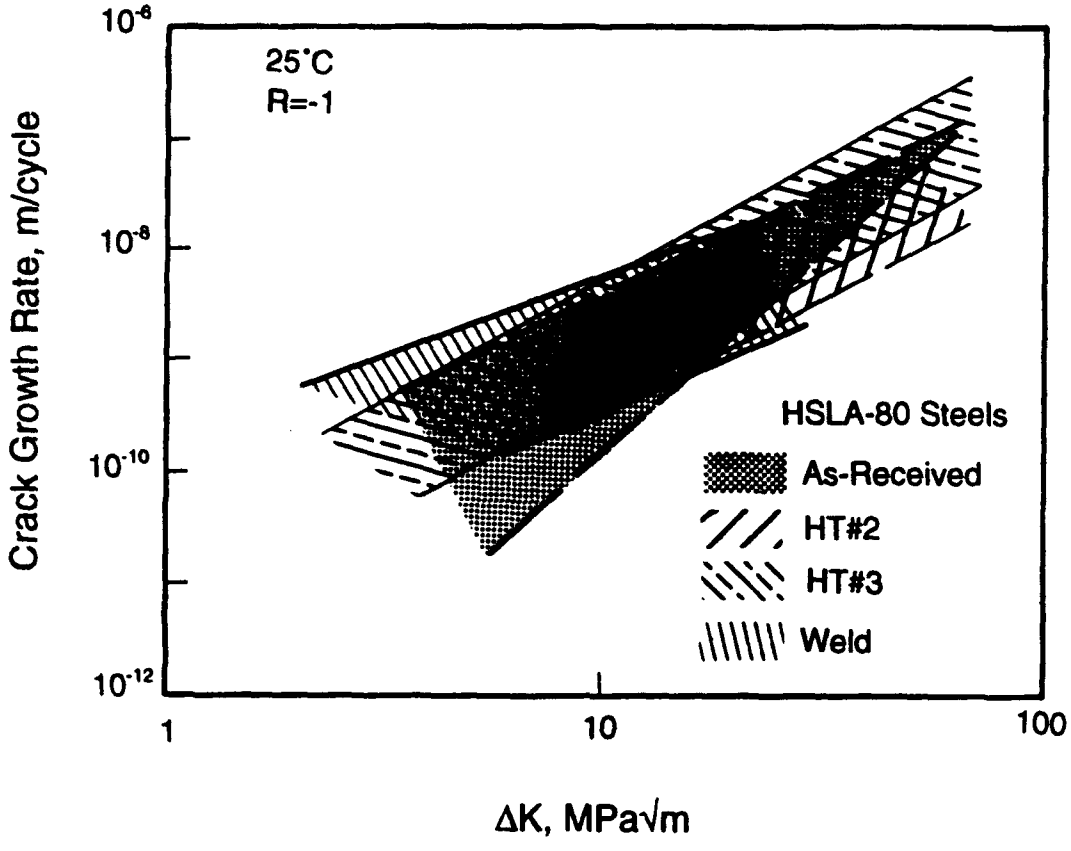

Figure 1. Comparison of small crack growth rates for various HSLA-80 microstructures

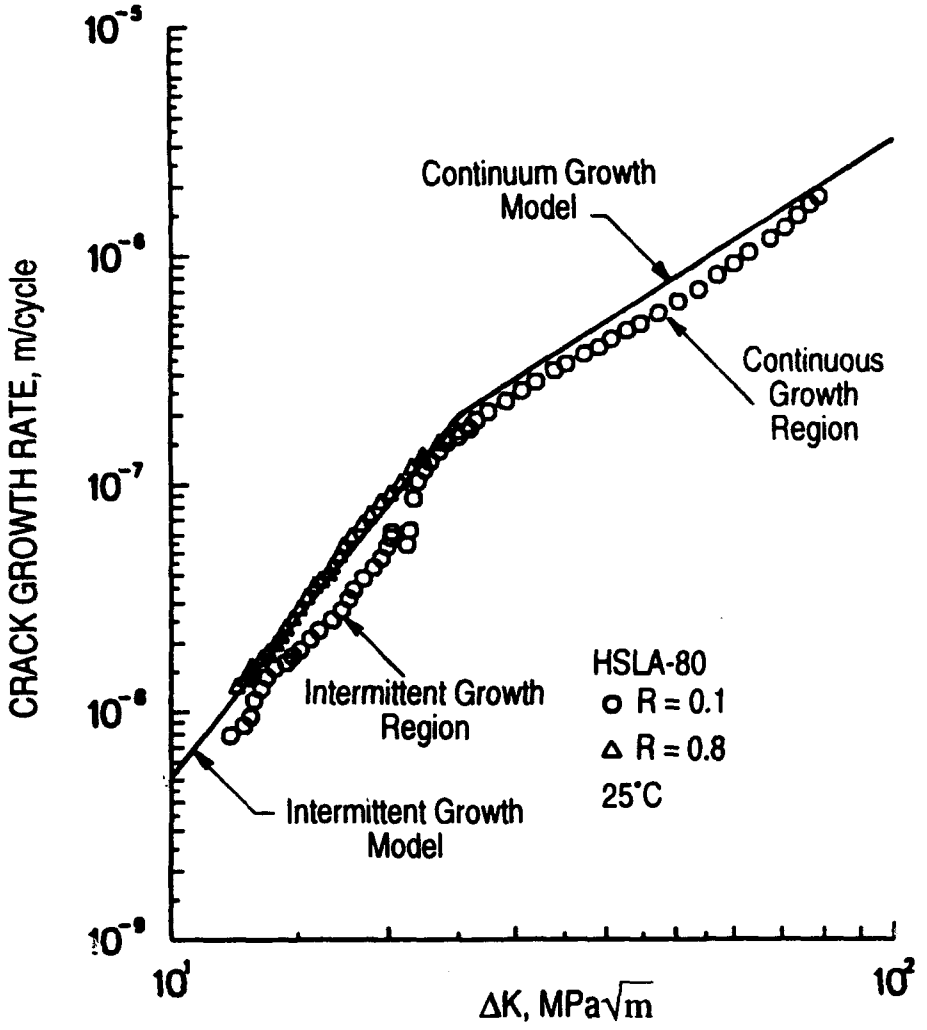

Figure 2. Comparison of experimental and calculated *da/dN* curves for HSLA-80 steels at $R = 0.1$ and 0.8

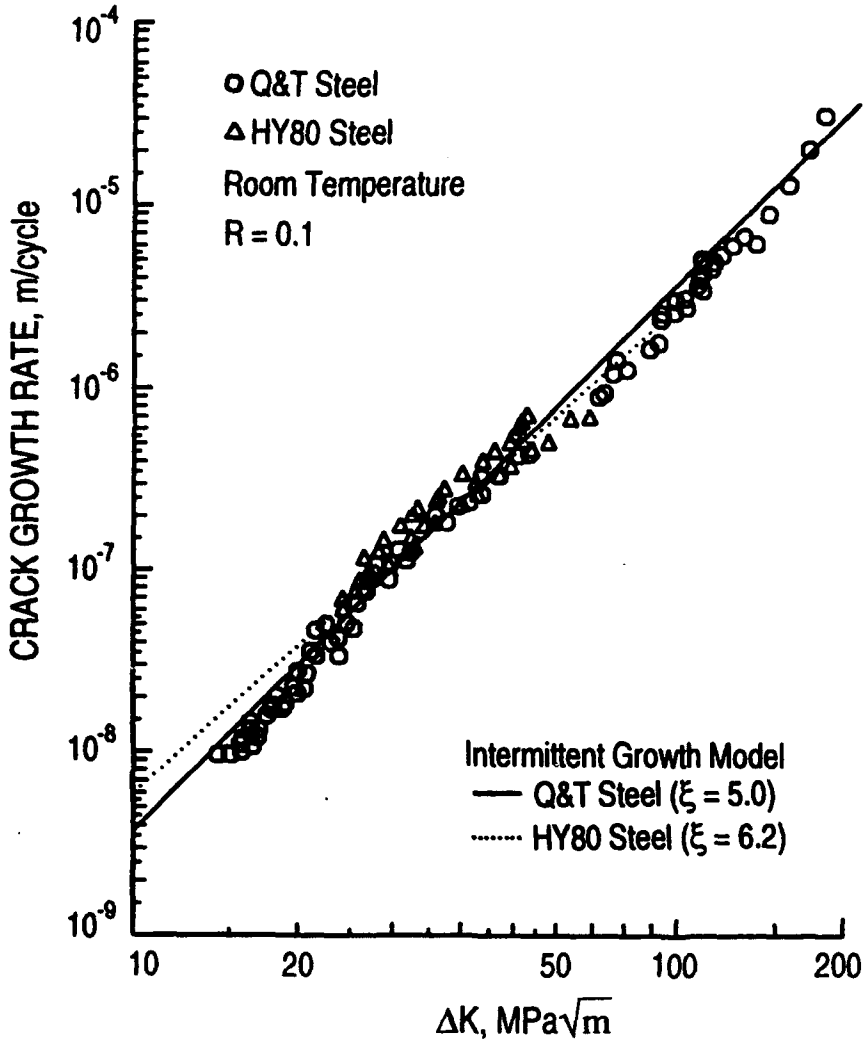

Figure 3. Comparison of model calculations with experimental data for HY80 and Q&T steels in the intermittent growth regime

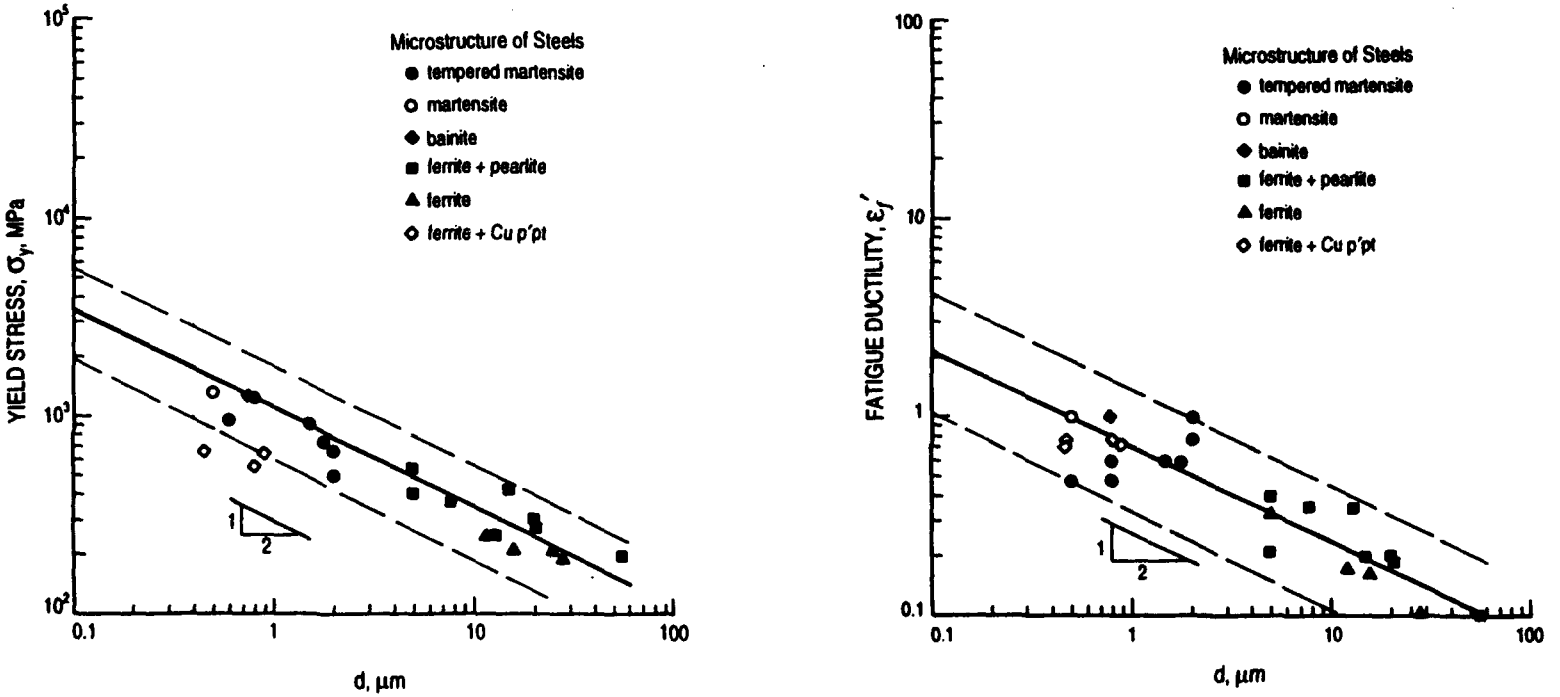

Figure 4. Correlations of yield stress and fatigue ductility coefficient with dislocation barrier spacing for steels: (a) yield stress, and (b) fatigue ductility coefficient

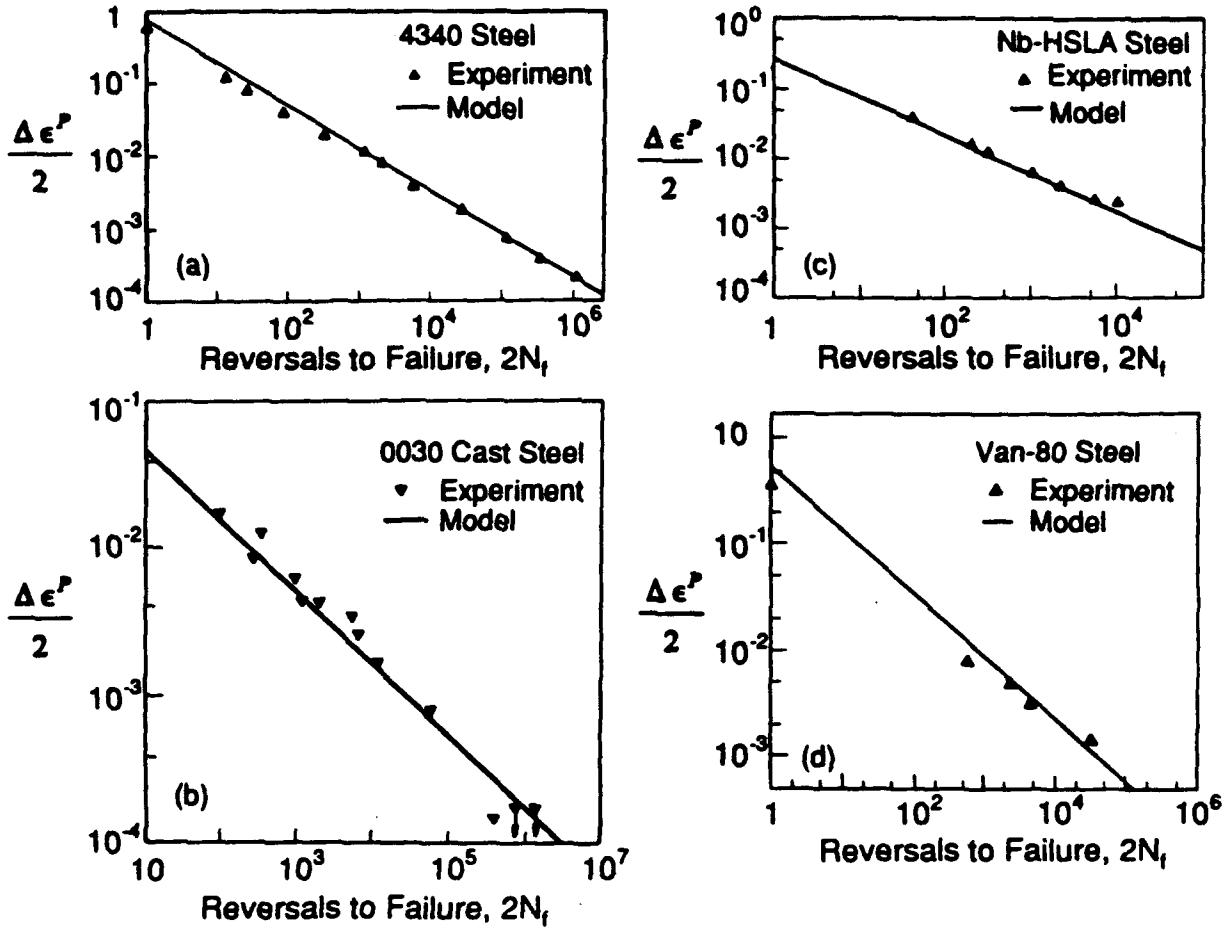

Figure 5. Comparison of calculated and experimental LCF curves for steels: (a) 4340 steel, (b) 0030 cast steel, (c) Nb-bearing steel, (d) Van 80 steel

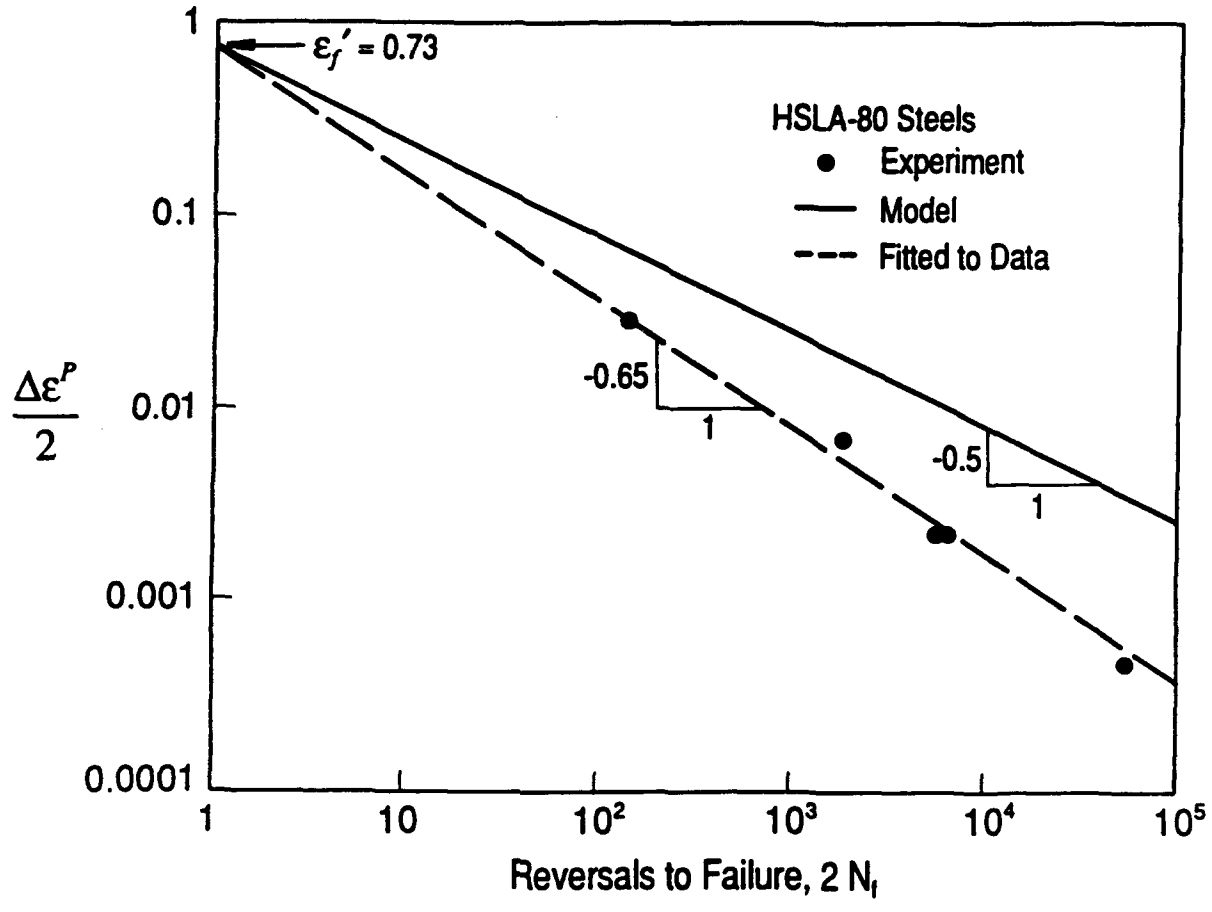

Figure 6. Comparison of calculated and experimental LCF curves for HSLA-80 steel

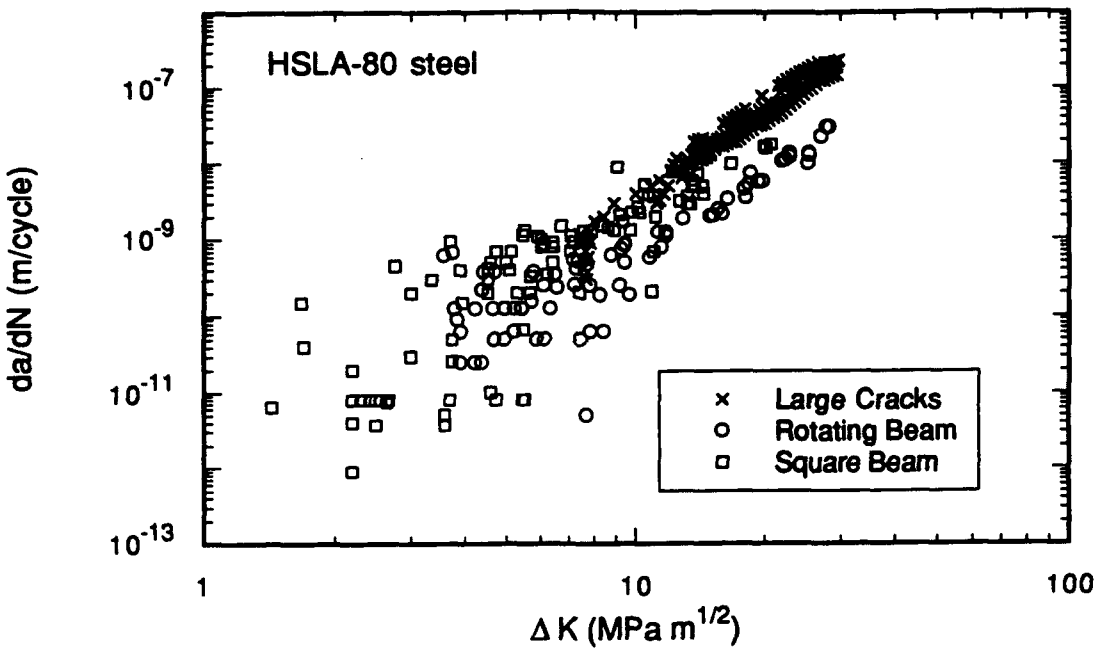

Figure 7. Small crack and large crack FCG data for HSLA-80 steel correlated by ΔK calculated from full stress range

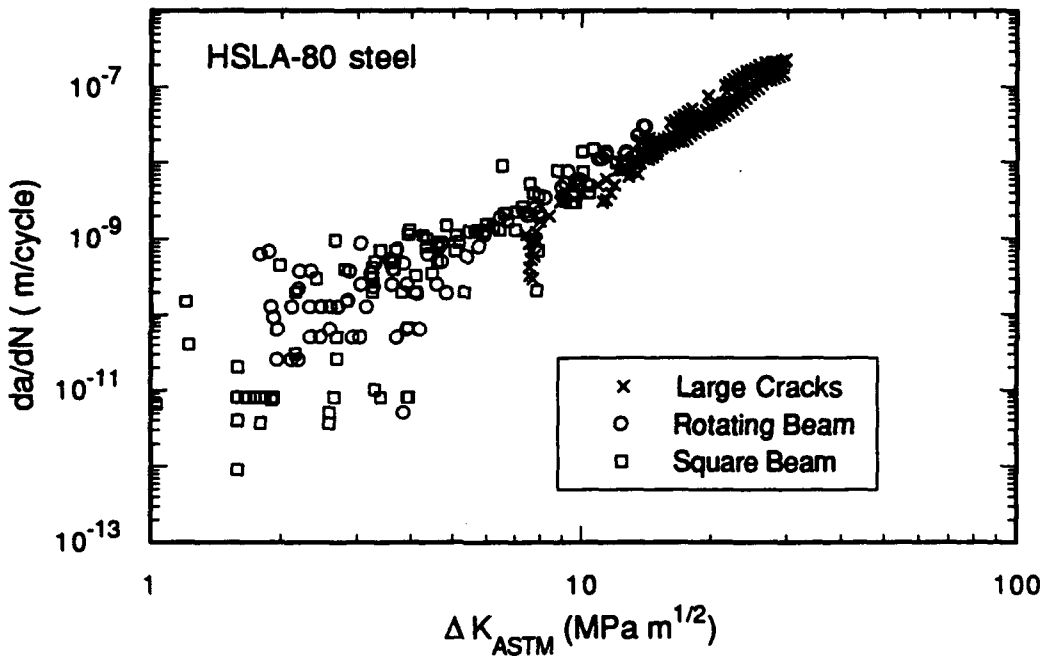

Figure 8. Small crack and large crack FCG data for HSLA-80 steel correlated by ΔK calculated as specified in ASTM Test Method E 647

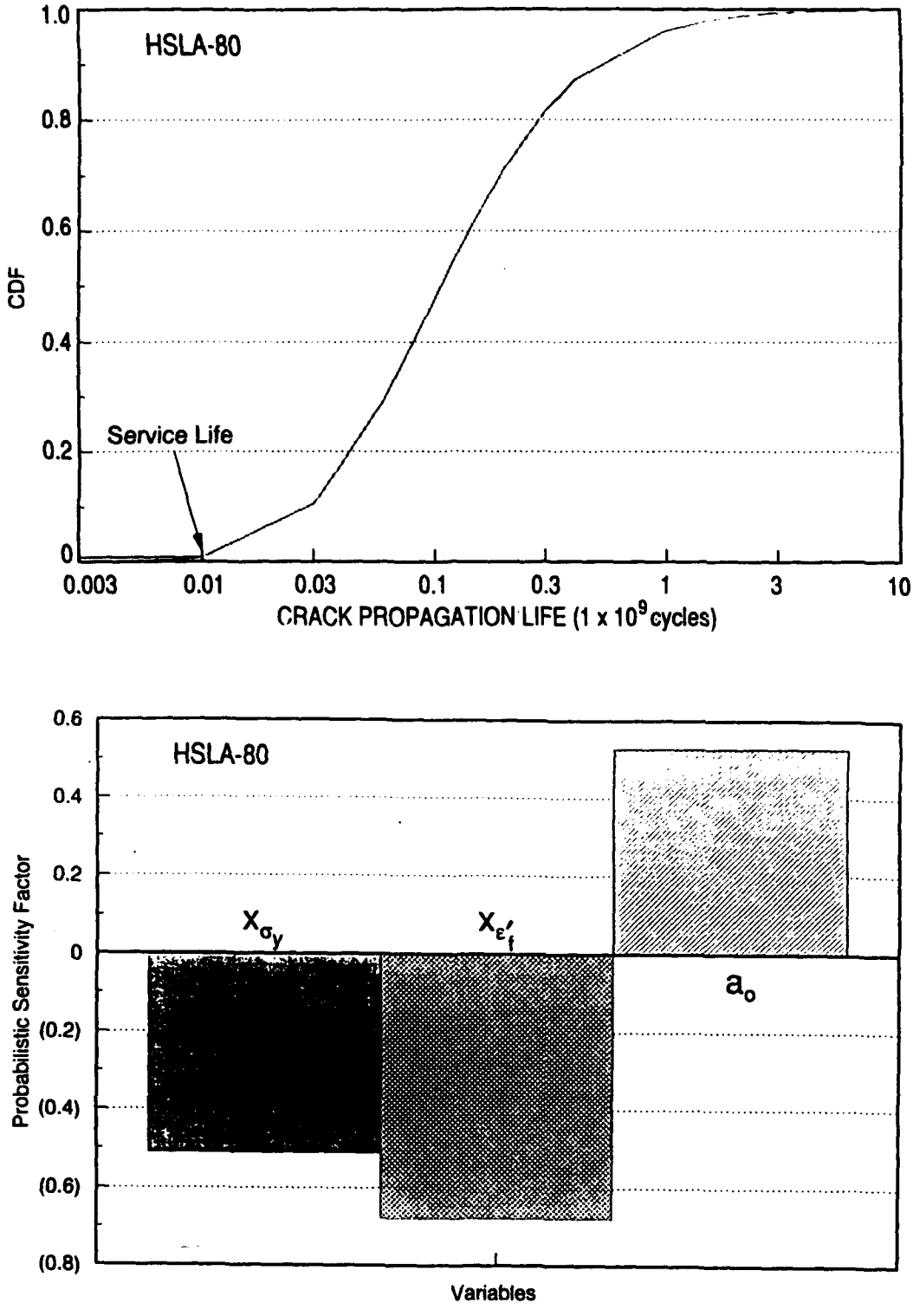

Figure 9. (top) Calculated cumulative distribution function for crack propagation life of HSLA-80 steel. The service life is assumed to be 10 $(10)^6$ cycles. (bottom) Calculated values of the probabilistic sensitivity factors corresponding to the CDF calculation in the top figure

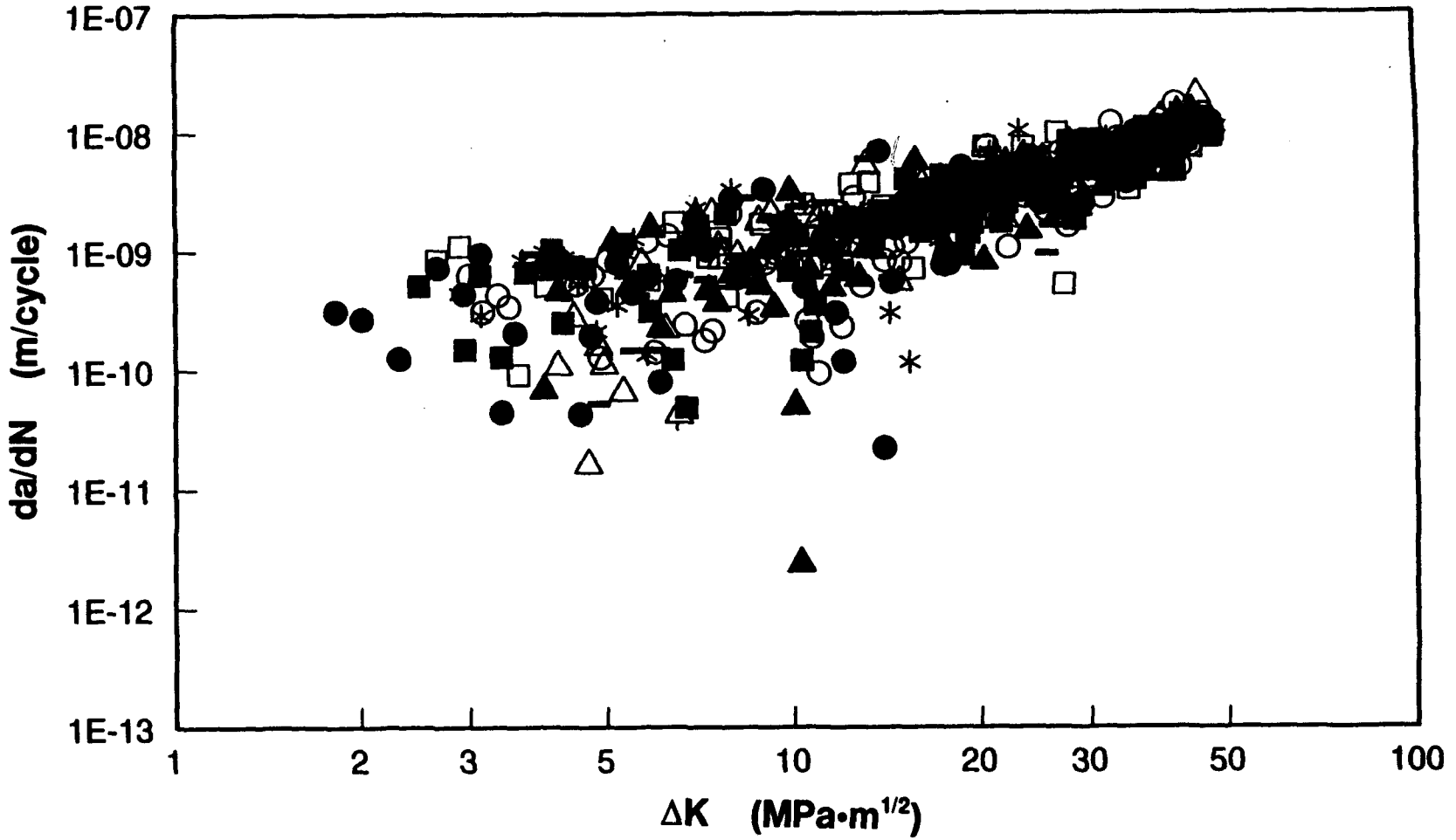

Figure 10. Simulated small crack data for HSLA-80 steel

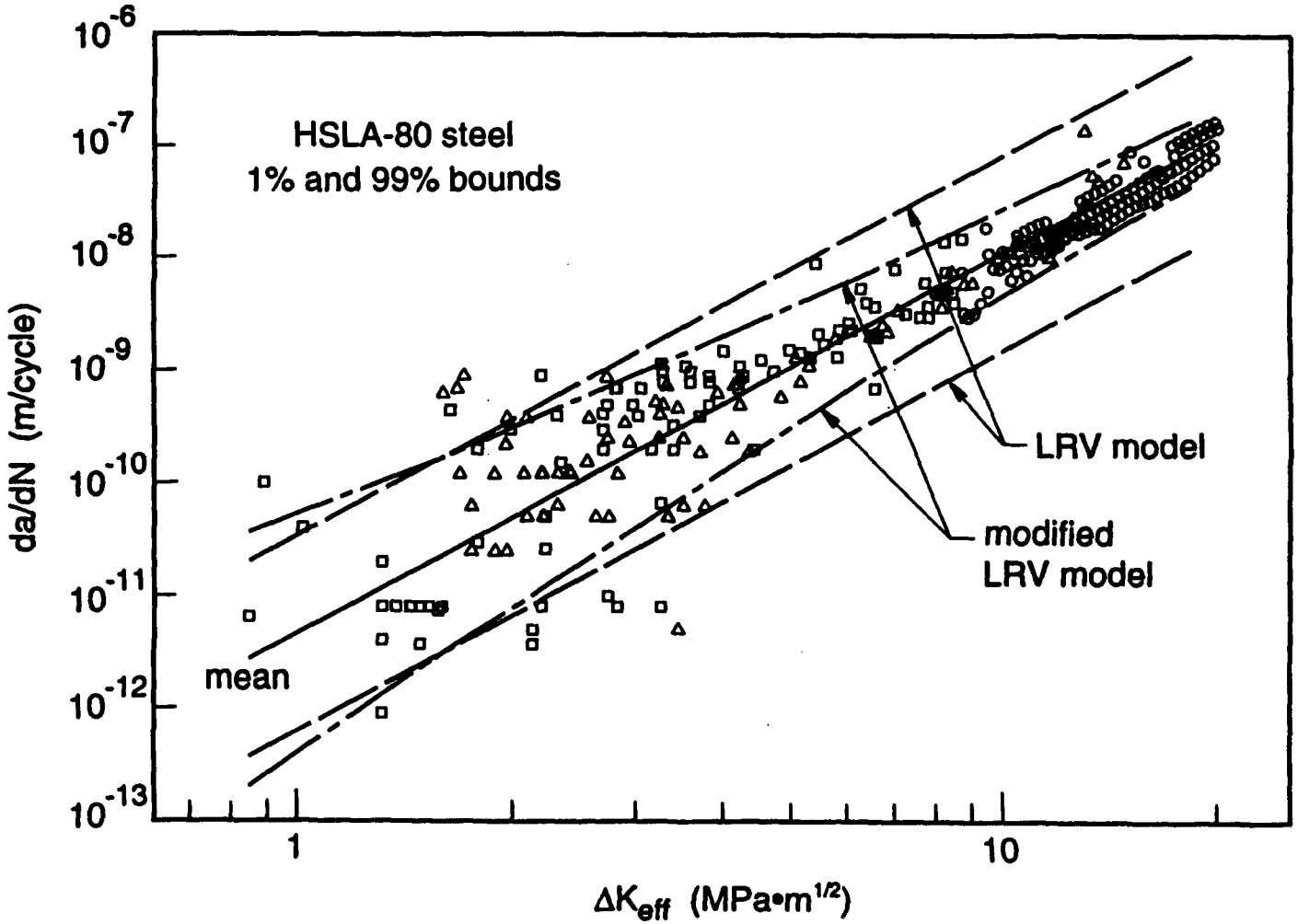

Figure 11. Stochastic treatments of large and small crack data for HSLA-80 steel, based on conventional and enhanced lognormal random variable models

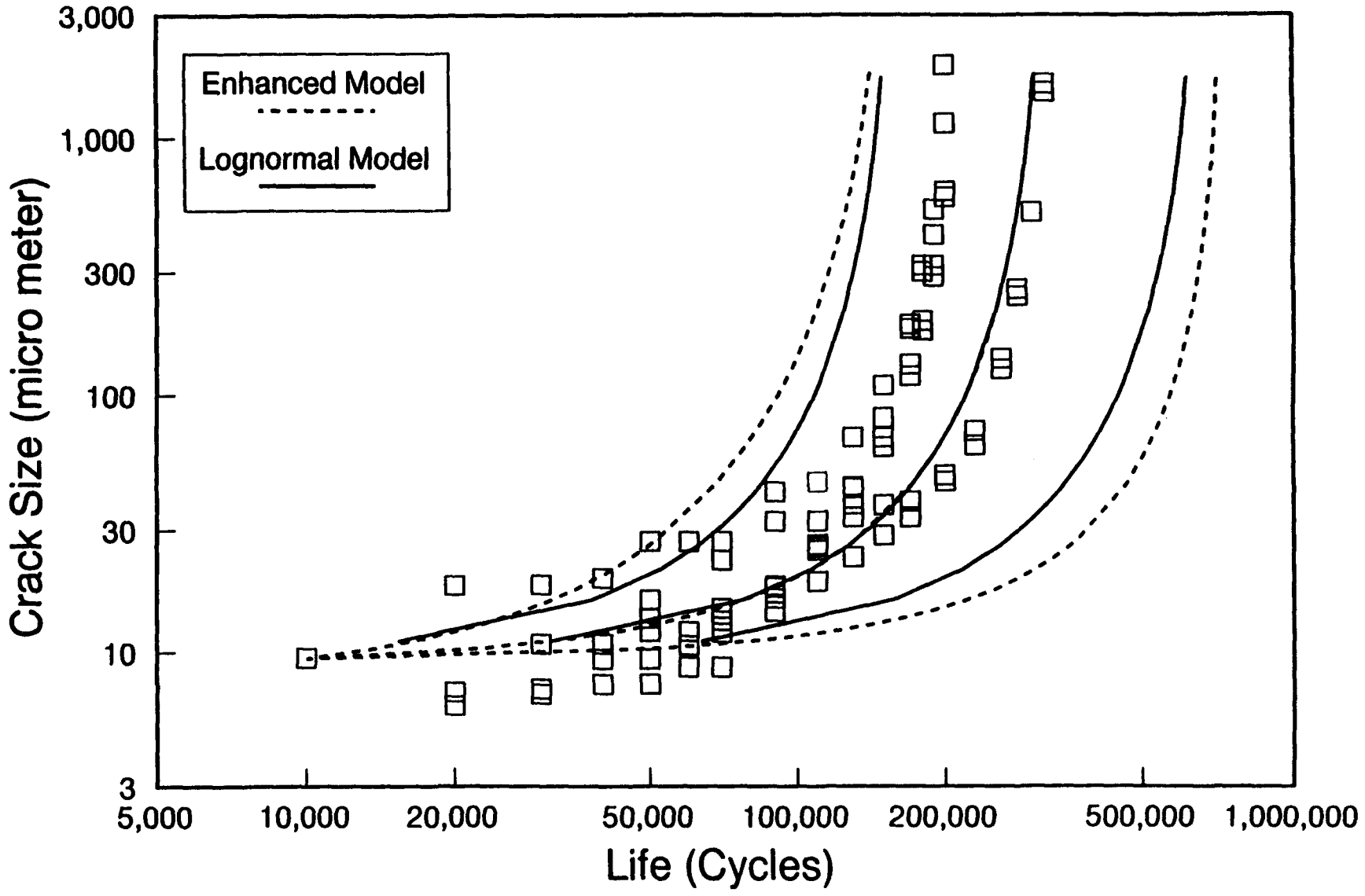

Figure 12. Sample life prediction results using lognormal and enhanced lognormal random variable models

APPENDIX A

"Cu Bearing HSLA Steels: The Influence of Microstructure on Fatigue Crack Initiation and the Growth of Small Fatigue Cracks"

D. L. Davidson, K. S. Chan, and R. C. McClung

[manuscript to be submitted for publication]

Cu Bearing HSLA Steels: The Influence of Microstructure on Fatigue Crack Initiation and the Growth of Small Fatigue Cracks

D.L. Davidson, K.S. Chan, and R.C. McClung
Southwest Research Institute
San Antonio, TX 78228

ABSTRACT

The fatigue characteristics of a Cu-bearing HSLA steel were investigated as a function of microstructure. Heat treatments and welding were used to alter microstructure. Small fatigue cracks were naturally initiated (≈ 30 μm long) in smooth specimens and grown past the transition to large fatigue crack growth behavior (≈ 200 μm), where they showed the characteristics of large fatigue cracks. The number of cycles to crack initiation depended on stress but not on microstructure, although the site of initiation was microstructurally dependent. Small cracks in all microstructures grew at ΔK values below the large crack threshold. The as-received (polygonal or equiaxed ferritic) microstructure and one of the lath microstructures that resulted from heat treatment exhibited the same growth rate correlation as large cracks in the linear (Paris) region, and could be considered as an extension of the large crack growth region down to the point of initiation. Small cracks in one of the heat treated and the weld microstructures grew at rates slightly faster than expected from extrapolation of the large crack correlation with ΔK.

INTRODUCTION

Small fatigue cracks growing in steels have been extensively studied since it was recognized that small cracks may have different growth kinetics than large cracks. There have been so many studies and they are published in such a diversity of journals and conference proceedings that no one has established a catalog of the results. A partial reading of the literature indicates that microstructure greatly influences the growth of small fatigue cracks in steels, as might be expected from the effects of microstructure on other properties.

In contrast to the growth kinetics of small cracks, fatigue crack initiation has not been extensively studied in steels, probably because it was shown in the 1970 - 80s that inclusions (ceramics, foreign matter, dirt, intermetallics) initiated most fatigue cracks in steels [1,2]. However,

in recent years, steels have become cleaner, and fatigue crack initiation may occur at sites other than inclusions [3].

The number of cycles to fatigue crack initiation and the growth of small fatigue cracks are important in assessments of the lifetimes of structures that are limited by fatigue. For large structures, such as oil production offshore platforms, cracks may be assumed to exist in the structures because of the fabrication methods used. But for smaller and more critical structures, such as aircraft landing gear, made of clean materials, there are probably no cracks in the as-fabricated structure. It was found that ≈ 70% of lifetime was occupied by the combined initiation and growth of fatigue cracks to a surface length of 1 mm [4]. Another study found that crack initiation, which was not at inclusions, was 10 to 20% of lifetime [5]. For the Cu bearing steel BIS 812 EMA, fatigue crack initiation was found to 50% of lifetime during tests in sea water [6].

As examples of the effects of microstructure on fatigue initiation sites, consider the work of Kunio, et al. [7], who found that cracks initiated in prior austenite grain boundaries for the low carbon martensitic steels investigated. De los Rios, et al. [8], reported about the same result for a 0.4 wt.% C steel of mixed pearlite and ferrite microstructure with the ferrite located in the prior austenite grain boundaries. Shang, et al. [9] observed that cracks initiated within ferrite grains in steels having 26 to 67% martensite. Tokaji, et al. [5] found that grain boundaries were implicated in a high strength ferritic steel with 10 μm diameter grains. Daeubler, et al. [3] found crack initiation parallel to the lamellae direction in a pearlitic steel. The nucleation sites of fatigue cracks in pure polycrystalline iron may be within grains or grain boundaries, depending on loading frequency [Guiu, et al. [10]. This effect is probably due to these tests being conducted in humid air, because water vapor has such a large effect on pure iron.

Once initiated, the growth of small cracks may also depend strongly on microstructure. Examples of this behavior may be found in the summary of Tokaji and Ogawa [11] who have illustrated through graphs of growth rate vs. crack length that crack arrest can occur (1) at grain boundaries in fine and coarse grained ferritic steels, (2) at prior austenitic grain boundaries in ferritic/martensitic steels, and (3) at the ferrite/pearlite boundaries in in pearlitic steels. However, cracks were also found to arrest at locations not associated with microstructure. This behavior is similar to that found for large fatigue cracks at low ΔK values in steels by Vaidya [12,13] who

made detailed surface observations similar to those often made on small cracks. He showed similar periods of temporary crack arrest often not associated in any apparent way with microstructural features. Similar observations of large crack behavior have also been made in a number of other materials [14]. Thus, the influence of microstructure on the growth of fatigue cracks is not necessarily related to crack size.

Alloying elements have been shown to have a large effect on the growth of large fatigue cracks in iron, and copper had the most effect per wt.% addition of the 12 elements studied [15]. The slope of the linear (Paris) portion of the da/dN vs. ΔK correlation increased from 3.6 to 5.2 with 1 wt.% Cu addition, and ΔK_{th} increased from 4.9 to 7.5 MPa$\sqrt{m}$. When Cu is added to steel, the amount of C and the tempering temperature were found to affect the rate of growth of large fatigue cracks [16]. A 0.28 C, 1.45 Cu (wt.%) steel showed the lowest rate of fatigue crack growth and the best resistance against fatigue crack initiation.

Data from Lukens Steel internal reports for A710, modified A710 and HSLA 100 steels show that the growth behavior of large fatigue cracks in these steels is similar, despite relatively large differences in microstructure. A710 steel consists of mostly fine polygonized (equiaxed) and accicular ferrites with less than 5% of pearlite, bainite and/or martensite [19]. In contrast, modified A710 and HY 100 steels have mainly lath-like ferrites with retained autenite and martensite particles located in the lath boundaries [19].

As deduced from the above summary, the prediction of fatigue crack initiation and growth for a steel not yet studied from the results of research on other steels, is not yet possible. This paper reports on the initiation and growth of small fatigue cracks in a copper-bearing steel that has not been investigated previously for these characteristics. Small crack growth rates are compared to those for large cracks in the same steel.

DESCRIPTION OF MATERIAL

Fatigue cracks were initiated and grown in several plates of high-strength, low-alloy (HSLA) steels, designated HSLA-80. Most of the specimens were cut from the flange region of 10 mm thick welded-construction I-beams manufactured by Bethlehem Steel Co. and sent to Lehigh University via Ingalls Shipbuilding Inc., designated "Plate #1." The

specimens removed from the welded part of the I-beam are designated "Weld." Several specimens were cut from similar material obtained from the David Taylor Naval Ship Research and Development Center, designated "Plate #2." Composition of the materials investigated, as determined by standard wet chemistry methods, are listed in Table 1.

Table 1
HSLA-80 Compositions
Weight %

Element	Plate #1 (Lehigh)	Weld (Lehigh)	Plate #2 (Navy)
C	0.05	0.06	0.06
Mn	0.54	0.95	*
Cu	1.03	0.68	0.98
Ni	0.72	1.48	0.76
Mo	0.20	0.33	*
Cr	0.72	0.55	0.70
Al	0.05	*	*
Si	0.27	0.34	0.21
P	0.009	0.013	*
S	0.001	*	*

* not measured

Compared to Military Standard 24645 of Sept. 24, 1990, Plate #1 was within standard ($1.0<Cu<1.3$ and $0.7<Ni<1.0$); the weld was low in Cu and high in Ni and Mn, but was otherwise with the standard; Plate #2 was low in Cu but was otherwise within the standard. These steels have low carbon to ensure good weldability and high copper for precipitation strengthening[17].

This entire investigation was made on Cu-containing steels, often designated as HSLA steels. These materials should not be confused with many of the non-Cu containing steels also designated HSLA steels. The standard heat treatment for these steels is: austenitize at 870 to 930°C followed by water quenching and ageing at 540 to 665°C for 0.5 hrs. The microstructure resulting from this heat-treatment contains polygonal and accicular ferrite, martensite, and retained austenite [18, 19], with the last

two constituents less than 5 vol.%. When cooling is relatively fast (<2°C/sec.), about 2% lower-bainite may form.

The most important aspect of heat treatment is the ageing step, which precipitates ε-copper spheres having sizes that range from 5 to 50 nm. When the precipitates are larger than about 5 nm they lose coherency [20].

The stress-strain curve was measured for Plate #1 in tension, giving an average yield stress of 607 MPa and an ultimate stress of 690 MPa [22].

HEAT TREATMENT

One of the goals of this research was to determine how the fatigue characteristics of this steel were affected by variations in the microstructure. Thus, the as-received microstructure was altered by heat treatment, and specimens were also cut from the weld portion of the I-beams. Hardness measurements and optical and transmission electron microscopy were used to characterize the resulting microstructures. Heat treatments used for microstructural alteration are listed in **Table 2**. Heat treatments that did not result in Cu precipitates were attempted but without success.

Table 2
Heat treatments for HSLA-80

Designation	Material	Heat Treatment	Hardness
HT#1	Plate #2	900°C for 48 hrs., water quench then 640°C for 0.5 hrs.	R_B 92
HT#2	Plate #1	1200°C for 1 hr., water quench	R_C 26
HT#3	Plate #1	1200°C for 1 hr., water quench then 593°C for 0.5 hrs.	R_C 31

MICROSTRUCTURAL CHARACTERIZATION

Ferrite grain sizes of the as-received microstructure were measured by optical microscopy to vary from about 0.3 to 9 μm, with the most common size around 2 μm. Inclusion size and occurrence were determined from analysis of 86 inclusions in Plate 2 using optical microscopy. Sizes ranged from ≈ 2μm to 12 μm, with the most frequent size around 5 μm. Inclusion size provided a lower limit to the smallest crack that was studied in this steel. The number of inclusions intercepting the specimen surface was calculated to be 800 per square mm, or 1.5% of the surface.

Heat-treatments #2 and #3 resulted in lath-like microstructures similar to those observed in A710 steel under high cooling rates and in modified A710 steels. Based on previous work [19, 19A], these HT structures are interpreted as being composed of accicular ferrite laths with a mixture of retained austenite and martensite particles within the lath boundaries. The weld microstructure has also been studied [19B] and found to consist of coarse ferrite grains containing small particles of either martensite or bainite.

Analysis of the copper precipitate size using transmission electron microscopy indicated that heat treatment did not alter either size or size distribution very much. The size range was 5 to 25 nm with a peak at 8 to 12 nm for as-received and heat treated specimens. Precipitate size distribution in the weld was not as broad, with a range of 7 to 17 nm and a peak at 8-12 nm.

EXPERIMENTAL PROCEDURES

Small fatigue cracks were studied using two specimen designs. Initially, beams of square cross section 4 mm on a side by 52 mm long were loaded in 3-point bending. Stresses of increasing magnitude were applied until cracks were initiated within a few hundred thousand cycles. But the stresses required to initiate cracks were so high that the outer fiber stress exceeded yield, so that the unloaded beam was no longer straight. The R-ratio (min. stress/max. stress) was maintained at nearly zero for the beam as a whole, but for the outer surface of the beam, the region in which the cracks started, R was closer to - 0.35 because of local plasticity. To overcome the problems caused by surface plasticity, subsequent experiments were conducted using a rotating beam specimen, having the

design shown in **Fig. 1**, where the applied R = -1. Even with this specimen, the as-received material showed remarkable resistance to crack initiation and the number of cycles required to initiate a crack was very sensitive to stress magnitude.

The surface preparation of specimens tested by these means is an important factor in the number of cycles to crack initiation. For this work, specimens were excised from the plates of material received using electric discharge machining (EDM). This machining method minimized residual stress and provided a good surface finish. The highly stressed regions of the specimens were hand polished using silicon carbide papers and finished with 0.1 μm diamond paste.

Plastic replicas were used to provide a history of the surface changes due to cyclic loading. The maximum stress regions of the specimens were periodically replicated at half maximum load, and examined by optical microscopy after the plastic was rendered opaque by vacuum depositing silver on the replica surface. Replicas were made at the beginning of each test, with the specimen both unloaded and loaded, and then periodically until cracks were grown to approximately 2 mm in length. The number of cycles between replication was determined by the stress level of the test and microstructure of the specimen. The number of cycles to crack initiation, the change in crack length with loading cycles, and the density of fatigue cracks initiated, were all determined from these replicas.

After the growth of the longest crack to about 2 mm, specimens were etched with 2% Nital and replicated. This was done in order to investigate the relationship between crack path and microstructure. Some of the specimens were broken to assess the shape of the microcracks and for measurement of striation spacing. The shape of the microcracks was approximately semicircular.

RESULTS

An overview of the experimental results can be gained from examining how the number of cycles to initiation, N_i, and number of cycles to grow the cracks to a length of 2 mm, N_f, varied as a function of stress, as shown in **Fig. 2**. The relation between stress amplitude and N from the present tests, which encompass several microstructures, are compared to previous results for a steel of similar composition, ASTM A 710 Grade A, [17] for the

microstructure derived by standard heat treatment only. As seen in Fig. 2, data from the current work are comparable to previous results, and data from the rectangular beam specimens are comparable to those from the rotating beam specimens. Testing conditions and results are listed in **Table 3** for all the experiments conducted. See Table 2 for a description of heat treatment. Stress amplitude for the sp. 1-3, tested at an applied R = 0.1 appears high compared to that used for sp. 4-9, but only because the stress amplitude for the latter is half the total stress applied, or 0 to maximum stress.

Table 3
HSLA-80 Fatigue Specimen Test Conditions

Spec. No.	Material & Condition	Spec. Type	Nominal R ratio	Stress Amplitude (MPa)	N_i	N_f	N_i/N_f	Initiation Site
					-- cycles --			
1	Plate#2, As-Rec.	3-P	0.1	690	4.3×10^6	no cracks		-
2	Plate#2, As-Rec.	3-P	0.1	840	1.6×10^5	1.2×10^6	0.13	inclusions
3	Plate #2, HT #1	3-P	0.1	840	3.2×10^5	9.6×10^5	0.30	inclusions
4	Plate#1, As-Rec.	Ro-Bm	-1.0	560	5.0×10^3	2.0×10^5	0.03	inclusions
5	Plate#1, As-Rec.	Ro-Bm	-1.0	520	4.0×10^4	3.2×10^5	0.12	inclusions
6	Plate#1, HT #2	Ro-Bm	-1.0	550	2.5×10^3	1.1×10^5	0.02	laths
7	Plate#1, HT #3	Ro-Bm	-1.0	520	3.5×10^4	1.9×10^5	0.18	laths
8	Plate#1, Weld	Ro-Bm	-1.0	520	5.0×10^3	1.6×10^5	0.03	slip?*
9	Plate#1, As-Rec.	Ro-Bm	-1.0	414	5.0×10^3	no cracks --		
				448	1.5×10^6	no cracks --		
				476	8.0×10^5	no cracks --		

3-P = 3-point bending specimen; Ro-Bm = Rotating beam specimen.
* In this complex microstructure, the reason for initiation was difficult to determine.

Initiation and Crack Path

Microstructure greatly affected the features and the number of sites at which fatigue cracks initiated. In the as-received microstructure (Lehigh material, Plate 2), cracks initiated from inclusions in almost every incidence. The heat treated microstructures contained lath-like features from which fatigue cracks initiated rather than at inclusions. This shift in initiation site is illustrated in **Fig. 3**. All the parts of Fig. 3 are at the same magnification, thus facilitating a direct comparison between microstructure and initiation site.

For the ferritic microstructures, Figs. 3(b) and (d), fatigue cracks initiated at inclusions, Figs. 3(a) and (c), almost always, but for heat treatments that resulted in lath structures, Figs. 3(f) and (h), fatigue cracks initiated in either within laths, or lath boundaries, Figs. 3(e) and (g).

A sequence of photographs showing crack growth from an inclusion initiated crack in as-received material is shown in **Fig. 4**. The crack initiated from one side of the inclusion but it grew approximately symmetrically - the initiating inclusion is marked by an arrow in Fig. 4(d); note the scale change. Secondary electron SEM images of several cracks grown in this microstructure are shown in **Fig. 5** (a) through (d). These figures suggest that microstructure had a small effect, if any, on crack growth because the trajectory of the crack was not altered as microstructural features were encountered during growth. For crack growth in the weld microstructure, Fig. 5(e) and (f), crack path did appear to be affected more than in the as-received structure by microstructural features.

For cracks initiated in lath microstructures, the crack path was directly affected by microstructural features, as shown in **Fig. 6**. The crack shown in the figure initiated in the lath structure, not at an inclusion. Figure 6(d) was made after etching, and shows that the crack initiated in the center portion of one grain, and subsequently grew in the lath direction until the crack reached a grain boundary; thence, crack growth to the left was across the lath direction of several small grains, while on the right, the crack grew more parallel to the laths. Similar behavior was exhibited by crack growth in another lath-like structure created by heat treatment, as shown in **Fig. 7**. Lath direction is easily correlated with crack direction for this microstructure.

The number of cracks that initiated was a function of stress level, microstructure, and R ratio. **Table 4** summarizes data on the numbers of microcracks that initiated. A comparison of Specimens 4 and 5 indicates that the number of cracks formed is a very strong function of stress level; this conclusion persists when comparing the remainder of the specimens tested at R = -1. By graphing the number of cracks (N) against the stress amplitude (σ), the following approximate functional relationship may be derived

$$\ln(N) = \ln(N_0) + \alpha\sigma \qquad (1)$$

where $N_0 = -15.6$ and $\alpha = 0.0415$. This relationship estimates the number of cracks found reasonably well for all specimens tested except for HT#3 (sp. 7).

Table 4
The Number of Cracks Initiated

Spec. No.	Material Cond.	Nominal R Ratio	Stress Ampl. MPa	Initiation Site	Number of Cracks	Note
2	Plate#2, As-Rec.	0.1	840	inclusions	7	
3	Plate#2, HT#1	0.1	840	inclusions	9	1
4	Plate#1, As-Rec.	-1.0	560	inclusions	5000	2
5	Plate#1, As-Rec.	-1.0	520	inclusions	160	
6	Plate#1, HT#2	-1.0	550	laths	1800	3
7	Plate#1, HT#3	-1.0	520	laths	18	
8	Plate#1, Weld	-1.0	520	slip?	371	4

Notes:
1. About half of the cracks were not inclusion initiated.
2. Average crack size = 12 μm, max. crack size = 35 μm.
3. Average crack size = 26 μm, max. crack size = 175 μm.
4. Cracks formed in a small band and readily coalesced.

The hypothesis that the "damage" to the specimen can be considered as a function of the number of cracks in the specimen has been examined by measuring the rate of crack formation in specimens 4 and 6 (Plate#1). The number of cracks normalized by the maximum number is compared as a function of the number of cycles normalized by the maximum number of cycles, in **Fig. 8**. These data on the number of cracks are compared to the

length of one of the fast growing cracks normalized by the maximum crack length.

The results in Fig. 8 indicate that the number of cracks is increasing in approximately the same way as the length of a fast growing small crack. Thus, the number of cracks can be considered as an indirect measure of the damage state. However, the length of a fast growing crack is a better measure because many of the cracks that formed did not grow, while it takes only one growing crack to break the specimen. The number of cracks is a good indication of stress level, regardless of the microstructure, as has been noted by other investigators.

Crack Growth Rates

The growth rates of small fatigue cracks have been compared to the growth rates of large fatigue cracks. A comparison of some of the large crack data available is shown in **Fig. 9**, where only the Todd, et al. [21] data were measured at sufficiently low rates to establish a threshold for fatigue crack growth, ΔK_{th}. The Dexter [22] data were obtained for the same Plate#1 material used for our tests. The data of Ikeda, et al. [10] were taken from a 0.28 C and 1.45 Cu steel tempered for 200 min. This steel had a higher C content than the other steels, but the similarity of the growth parameters indicates that C content ($0.08 < C < 0.28\%$) had little effect on the growth rates of large cracks.

The growth rates of small cracks through the microstructures illustrated in Figs. 3 through 7 are shown in **Figs. 10 -16**. Crack length change, Δa, was measured at each end of the crack from replicas, and crack growth rate was calculated by dividing Δa by the number of cycles between replicas, ΔN; periods when the crack was not growing are generally not shown. The minimum detectable crack growth rate, based on the resolution of the technique used, was about 8×10^{-12} m/cycle. The cyclic stress intensity factor, ΔK, correlated with crack growth rate at cycle N was determined from half the total surface crack length, a, and the applied stress range, $\Delta\sigma$, using the relationship

$$\Delta K = 1.3(\Delta\sigma/2)\sqrt{a} \qquad (2)$$

for specimens tested at both R = -1. For data obtained from the 3-point bend specimens, the yield stress, 607 MPa, was used for $\Delta\sigma/2$ in calculation

of ΔK. This procedure was based on the recommendation of ASTM Test Method E647 [24] which uses $\Delta K = K_{max} - K_{min}$ for $R \geq 0$ but $\Delta K = K_{max}$ for $R < 0$ (i.e., only the tensile portion of the stress amplitude was used.)

These crack growth data were used to examine several questions that are usually asked about the growth of small fatigue cracks : (1) Did the small cracks grow at ΔK levels below the fatigue threshold for large cracks, ΔK_{th}; (2) Did small cracks grow faster than large cracks at the same ΔK levels; (3) Did microstructure affect the growth of small cracks?

The first question is easily answered as "yes;" small cracks grew below the threshold for large cracks in all microstructures. For small and large crack growing in at about the same ΔK, crack growth rates were approximately the same; thus the answer to question 2 is also yes. The generally good agreement between the growth of small and large cracks at equal values of ΔK is indicative that the assumption used in eq.(2) was reasonable. The effect of microstructure on the growth rates of small cracks, question 3, is less clear because of the large variation in crack growth rates.

Crack growth data for the as-received microstructure and HT#1 all appear to lie within the same band of variation which is approximately along an extension of the linear region of the large crack growth rate curve. Thus, all data (both large and small cracks) for the as-received microstructure were taken together and a regression analysis was used to determine the B and s in the correlation

$$da/dN = B\Delta K^s \qquad (3)$$

The analysis gave $s = 3.23$ and $B = 3\times10^{-12}$ m/cycle with a correlation coefficient of 0.93. For comparison these values for the large crack data alone are $s = 3.65$ and $B = 1\times10^{-12}$ m/cycle.

In **Fig. 17** are shown a dashed line which is an extension of the Todd large crack data, and a solid line that is the regression line for all as-received large and small crack data. It is concluded that the small crack growth rate data may be considered an extension of the large crack growth data. Also shown in Fig. 17 are the scatterbands for the as-received small crack data, along with the envelopes of crack growth rate data for sp. 7, HT#3, and sp. 8, weld. Both of these envelopes lie above the mean value

correlation lines established for the as-received microstructure, although there is some overlap with the as-received scatterbands. The slope of both HT#3 and weld data appears to be about 1.5. It is not possible to draw definite conclusions from the limited available data, but small crack growth rates in the weld and HT#3 conditions may be slightly accelerated relative to the as-received condition.

Another illustration of differences between crack growth rates in the weld microstructure and the base material is shown in **Fig. 18**. The number of loading cycles N has been adjusted in this figure by subtracting the number of cycles required for initiation, Table 3; i.e, both cracks start growing at 1 kilocycle in this comparison. Only crack growth up to 100 μm is shown because of crack coalesance above about 200 μm in the weld. About twice as many cracks initiated in the weld as in the base material at the same stress level, Table 4.

DISCUSSION

The most significant effect of microstructural changes made by heat treating this Cu-bearing steel was the change in fatigue crack initiation sites. The as-received plates initiated fatigue cracks from inclusions in almost every incidence, but the microstructures resulting from heat-treatment contained lath-like features from which fatigue cracks initiated, rather than at inclusions. The number of loading cycles applied prior to the initiation of the first crack did not appear to be microstructurally dependent, and the number of cracks that eventually initiated in all microstructures showed a large dependence on stress, but not microstructure.

The lack of a microstructural dependence on the number of cycles to initiation may not be surprising since heat treatment did not alter the size or volume fraction of the strengthening Cu precipitates. In this sense, microstructure was not modified by heat treatment. Conversely, the presence of retained austenite and martensite particles at the lath boundaries in HT#3, the lath microstructure, might explain why fatigue cracks initiatiated in that location. Previous work on modified A710 steel showed that these particles may be of equiaxed shape and 0.2 to 1.5 μm in diameter or of elongated shape and 3 to 10 μm long by 0.25 μm wide [19A]. In addition, a high density of dislocations has been found at lath interfaces [19]. These second phase particles may provide fatigue crack initiation

sites similar to the sulfide inclusions in carbon steels. If cracks did initiate at these lath boundary inclusions, then it would explain why the number of cycles to initiation in the lath microstructure was about the same as for the as-received microstructure, in which cracks also initiated mainly at inclusions.

The growth of small fatigue cracks in the as-received steels of both Plates #1 & #2 (Figs. 2 and 4) and HT#1 and HT#2 appear to be approximately independent of microstructure, independent of stress over the stress range investigated, and independent of R ratio for the ΔK definitions used. As shown in Fig. 17, the slope of the large crack Paris region may be extrapolated through the small crack data. Thus, the growth of small and large fatigue cracks may be treated with the same linear relation over the whole range of sizes from initiation (about 30 μm) to failure ($\approx$ 10 mm), although the equation used for surface crack ΔK should be changed above about 2 mm to account for geometric changes. Because a linear relationship is valid over such a wide range of crack size, or ΔK range, it appears as though the large crack threshold, ΔK_{th} is an artifact of the testing technique used for measuring the growth rate of large fatigue cracks.

The microstructure of the HT#3 (sp. 7) and the weld (sp. 8) does appear to slightly affect the growth of small fatigue cracks, although the limited available data make it difficult to draw definitive conclusions. Potential reasons for this behavior are not known. The ferritic microstructure was transformed to a lath structure by HT#3, and the weld microstructure was clearly different from the others; however, the size of the Cu-precipitates was not found to be altered very much. These microstructural changes did not appear to alter fatigue crack initiation, so why the growth of small fatigue cracks may have been faster is not clear. The effect of the higher growth rates of HT#3 and the weld could potentially result in significant changes in the lifetime prediction for a structure. Based on the mean value growth rates of the available data, the number of cycles required for growth of a small crack from initiation ($\approx$ 30 μm) to the transition to large

crack behavior (≈ 200 μm) was about 100,000 cycles for a slope of ≈ 1.5 (HT#3 and the weld), but was about 260,000 cycles for the as received microstructures (slope ≈ 3.6), a factor of 2.5 difference. Thus, the increased crack growth rates caused by this microstructural alteration could be important in lifetime estimates for structures of HSLA-80 steels when the growth of small cracks is a large proportion of structural lifetime.

SUMMARY AND CONCLUSIONS

1. For Cu-bearing HSLA-80 steel, fatigue initiation site was altered by heat treatment, although the number of cycles to first crack initiation was, surprisingly, unaffected. The initiation sites were changed from inclusions for as-received material to laths for HT#2 and HT#3. The number of fatigue cracks that initiated increased with cycling, but the ultimate number of cracks initiated depended more on stress than on microstructure.

2. Small fatigue cracks in all the microstructures tested grew at ΔK values below the large crack threshold, estimated from published work to be about 7.5 MPa$\sqrt{m}$, thereby exhibiting one of the "small crack effects." It is deduced that the large crack threshold is an artifact of the test methods used for large fatigue cracks.

3. The correlation da/dN vs. ΔK for small cracks in the as-received microstructures and in HT#1 and HT#2 had a slope of 3.23, and can be considered an extension of the large crack growth rates down to $\Delta K \approx 1$ MPa$\sqrt{m}$. However, the available small crack data for HT#3 and the weld were slightly faster for cracks smaller than ≈ 200 μm ($\Delta K \approx 10$ MPa$\sqrt{m}$).

ACKNOWLEDGMENTS

The patient and skillful laboratory fatigue work was performed by Byron Chapa. Harold Saldana prepared samples for transmission electron microscopy, Dr. Yi-Ming Pan obtained the micrographs, and Jim Spencer measured precipitate size and volume fraction from these micrographs. This work was funded by the Office of Naval Research, N00014-91-C-0214, Dr. A.K. Vasudevan, Program Officer. The authors gratefully acknowledge the technical assistance of these colleagues and the sponsorship of ONR.

REFERENCES

1. J. Lankford, Int. J. Fract., v. 12, 1976, pp. 155-156.

2. J. Lankford and F.N. Kusenberger, Met. Trans., v. 4, 1973, pp. 553-559.

3. M.A. Daeubler, A.W. Thompson, and I.M. Bernstein "Influence of microstructure on fatigue behavior and surface fatigue crack growth of fully pearlitic steels" Met. Trans. A, v. 21A, 1990, pp. 925-933.

4. M. Goto and H. Nisitani "Fatigue life prediction of heat treated carbon steels and low alloy steels based on small crack growth law" Fat. Fract. Engng. Mater. Struct., v. 17, 1994, pp. 171-184.

5. K. Tokaji, T. Ogawa, and Y. Harada "Evaluation of limitation of linear elastic fracture mechanics for small fatigue crack growth" Fat. Fract. Engng. Mater. Struct., v. 10, 1987, pp. 281-289.

6. M.Z.S. Khan and I.A. Burch "Effect of seawater on the fatigue life and crack growth behavior of a new microalloyed steel for submarine hull application" Int. J. Fatigue, v. 14, 1992, pp. 313-318.

7. T. Kunio, M. Shimizu, K. Yamada, M. Enomoto, and A. Yoshitake "The role of prior austenite grains in fatigue crack initiation and propagation in low carbon martensite" Fat. Eng. Mat. Struct., v. 2, 1979, pp. 237-249.

8. E.R. de los Rios, Z. Tang, and K.J. Miller "Small crack fatigue behavior in a medium carbon steel" Fatigue Engng. Mater. Struct., v. 7, 1984, pp. 97-108.

9. J.K. Shang, J.-L. Tzou and R.O. Ritchie "Role of crack tip shielding in the initiation and growth of long and small fatigue cracks in composite microstructures" Met. Trans. A, v. 18A, 1987, pp. 1613-1627.

10. F. Guiu, R. Dulniak, and B.C. Edwards "On the nucleation of fatigue cracks in pure polycrystalline alpha iron" Fat. Eng. Mat. Struct., v. 5, 1982, pp. 311-321.

11. K. Tokaji and T. Ogawa "The growth behavior of microstructurally small fatigue cracks in metals" in Short Fatigue Cracks, K.J. Miller and E.R. de los Rios, eds., Mech. Eng. Publ. Ltd., London, 1992, pp. 85-99.

12. W.V. Vaidya "Near threshold fatigue crack propagation behavior of a heterogeneous microstructure" Fat. Eng. Mat. Struct., v. 9, 1986, pp. 305-317.

13. W.V. Vaidya "An evaluation of crack front effect on threshold and crack propagation" Scripta Met., v. 23, 1989, pp. 27-32.

14. D.L. Davidson and J. Lankford "Fatigue crack growth in metals and alloys: mechanisms and micromechanics" Int. Mat. Revs., v. 37, 1992, pp. 45-76.

15. H. Ishii, T, Kawarazaki, and Y. Fujimura "Fatigue in binary alloys of bcc iron" Mat. Trans. A, 15A, 1984, pp. 679-691.

16. S. Ikeda, T. Sakai, and M.E. Fine "Fatigue behavior of precipitation-hardening medium C steels containing Cu" J. Mater. Sci., 12, 1977, pp. 675-683.

17. T.W. Montemarano, B.P. Sack, J.P. Gudas, M.G. Vassilaros, and H.H. Vandervelt, J. Ship Production, v. 2, 1986, pp. 145-162.

18. R.J. Jessman and G.J. Murphy, J. Heat Treat., v. 3, 1984, pp. 228-236.

19. G.R. Speich and T.M. Scoonover, Processing Microstructure and Properties of HSLA Steels, A.J. Deardo, ed., TMA-AIME, Warrendale, PA, 1988, pp. 265-287.

19A. S.W. Williams, D.J. Colvin, and G. Krauss, Scripta Met., v. 22, 1988, pp. 1069-1074.

19B. T.M. Scoonover, W.E. Lukens, and C.S. Pande

20. M.T. Miglin, J.P. Hirth, A.R. Rosenfield and W.A.T. Clark, Met. Trans. A, v. 17A, 1986, pp. 791-798.

21. J.A. Todd, L. Chen, and E.Y. Yankov, ASME J. Offshore Mech. & Arctic Eng., v. 115, No. 3, 1993, pp. 154-161.

22. A.C. Nussbaumer, R.J. Dexter, J.W. Fisher, and E.J. Kaufmann in Fracture Mechanics: 25th volume, ASTM STP 1220, F. Erdogen and R.J. Hartranft, eds., Am. Soc. Test. Mat., Philadelphia, PA, 1994 (in press).

23. K.S. Chan, Met. Trans. A., v. 24A, 1993, pp. 2473-2486.

24. ASTM Test Method E 647 "Standard Test Method for Measurement of Fatigue Cracks Growth Rates" 1994 Annual Book of ASTM Standards, Vol. 03.01, Am. Soc. Test. Mat., Philadelphia, PA, 1994, pp. 569-596.

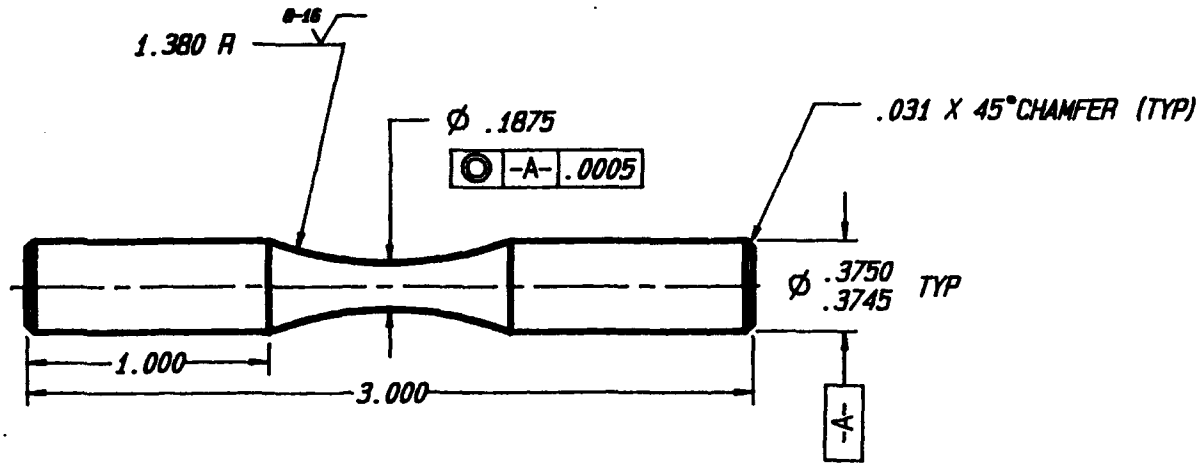

NOTE:
1. USE LOW STRESS MACHINING IN GAGE SECTION.
2. SMALL CENTERS ARE PERMISSIBLE.

Fig. 1 Rotating beam specimen used for small crack growth study.

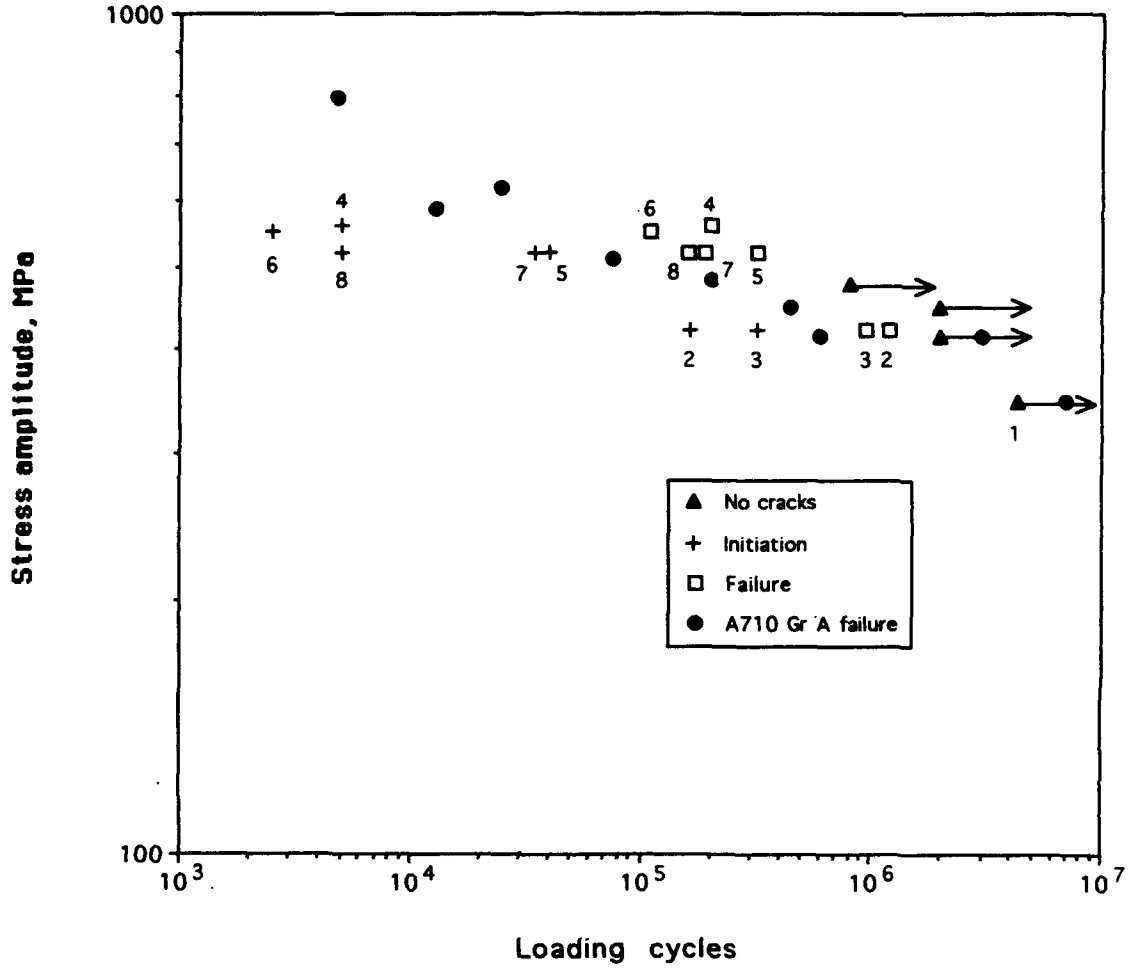

Fig. 2 Stress-cycles to crack initiation and growth to 2 mm length. Data points with arrows are for specimens that did not initiate cracks.

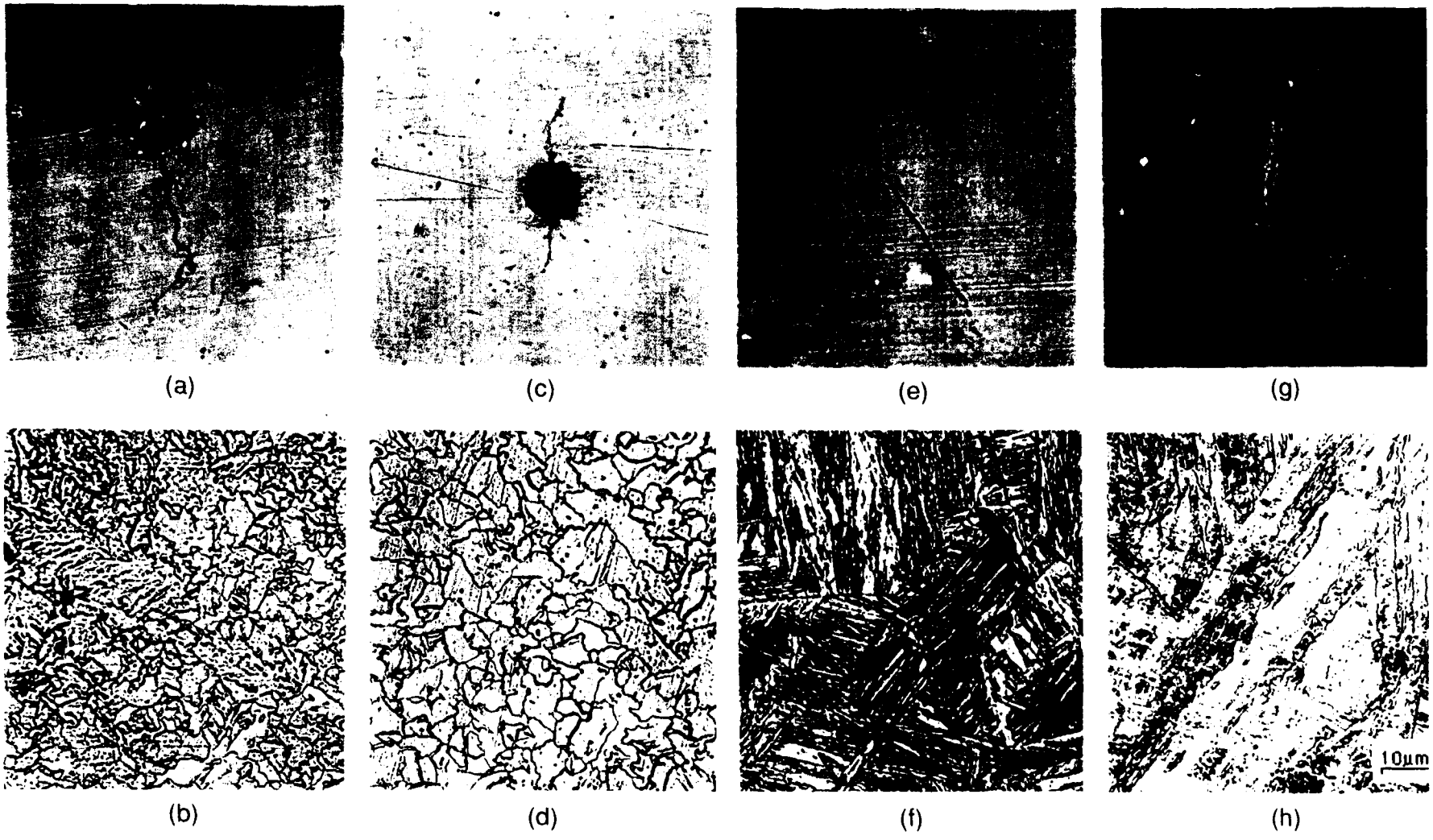

Fig. 3 The relationship between microstructure and crack initiation sites. All photographs have the same scale. (a) and (b) Plate#2, As-received (ferritic) microstructure; (c) and (d) HT#1, sp. 3 (large grained ferritic); (e) and (f)Plate#1, HT#2, sp. 6 (lath), and (g) and (h) Plate#1 HT#3, sp. 7 (lath). Stress axis horizontal.

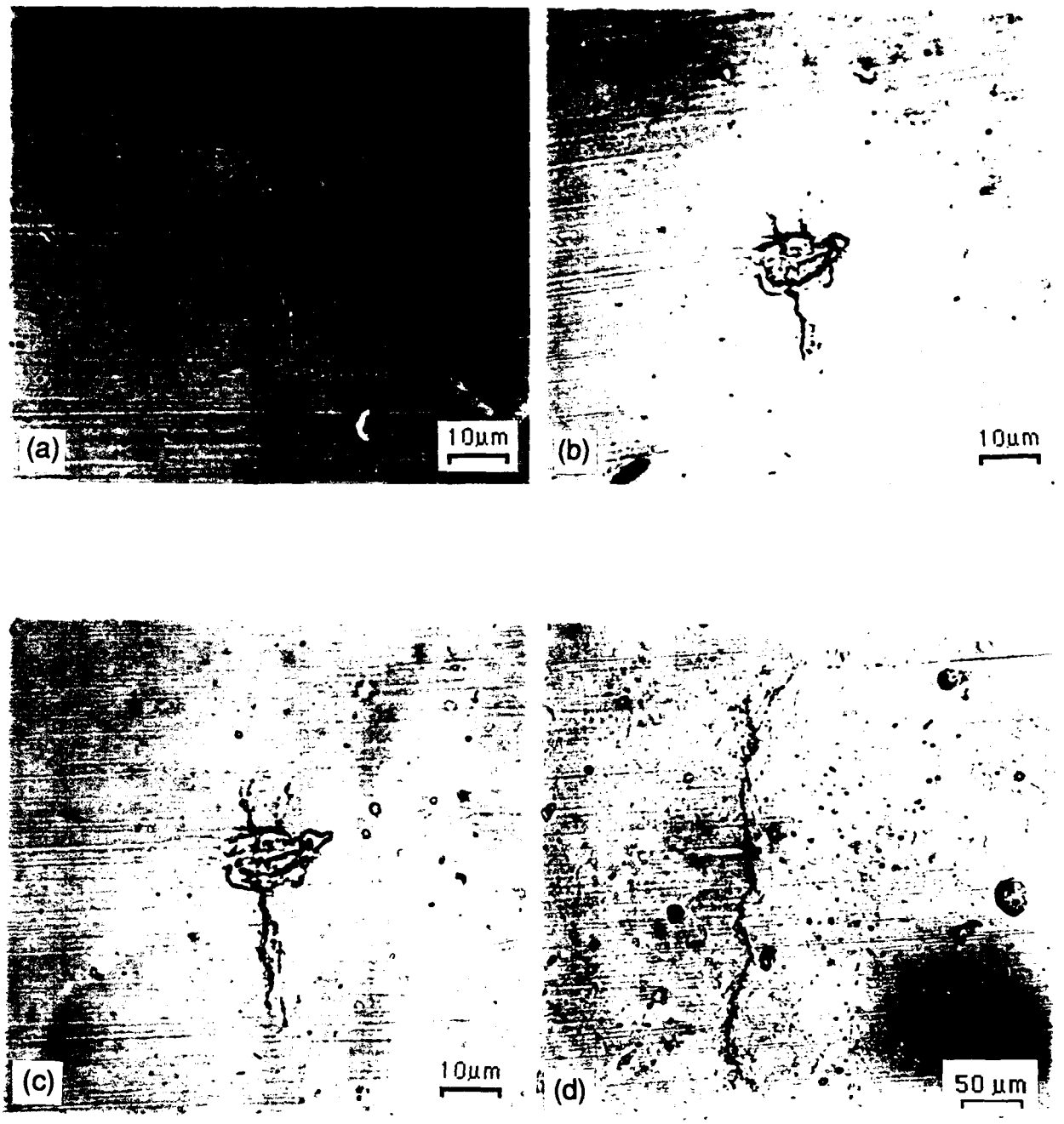

Fig. 4 Crack initiation and growth sequence, Plate#1, as-received, sp. 4. (a) 20 kcy, (b) 30 kcy, (c) 70 kcy and (d) 170 kcy. Stress axis horizontal.

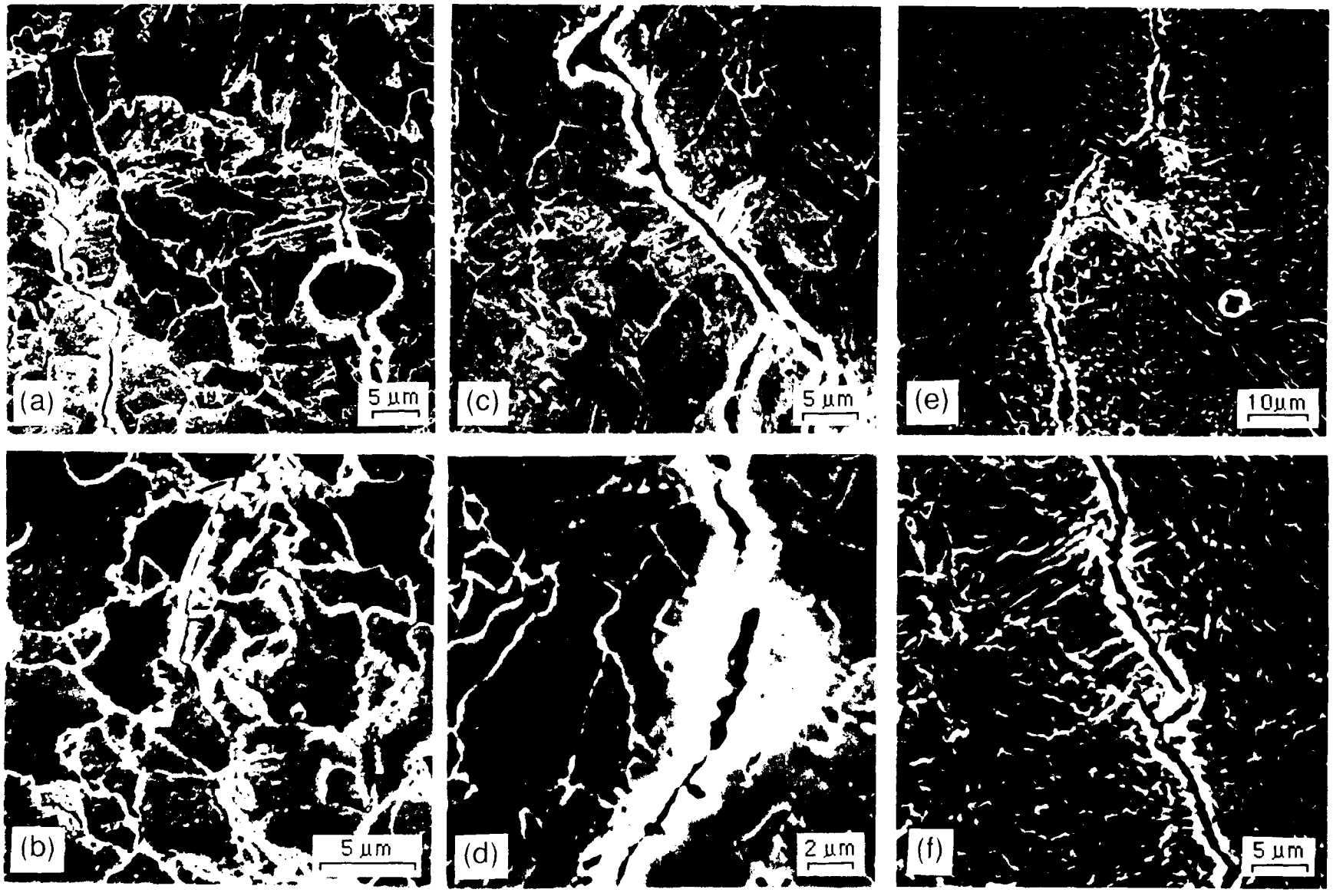

Fig. 5 Crack path in relation to microstructural features. (a,b) Plate#2, sp. 2, as-received, (c,d) Plate#1, as-received, sp. 4, and (e,f) weld, sp. 8. Stress axis horizontal.

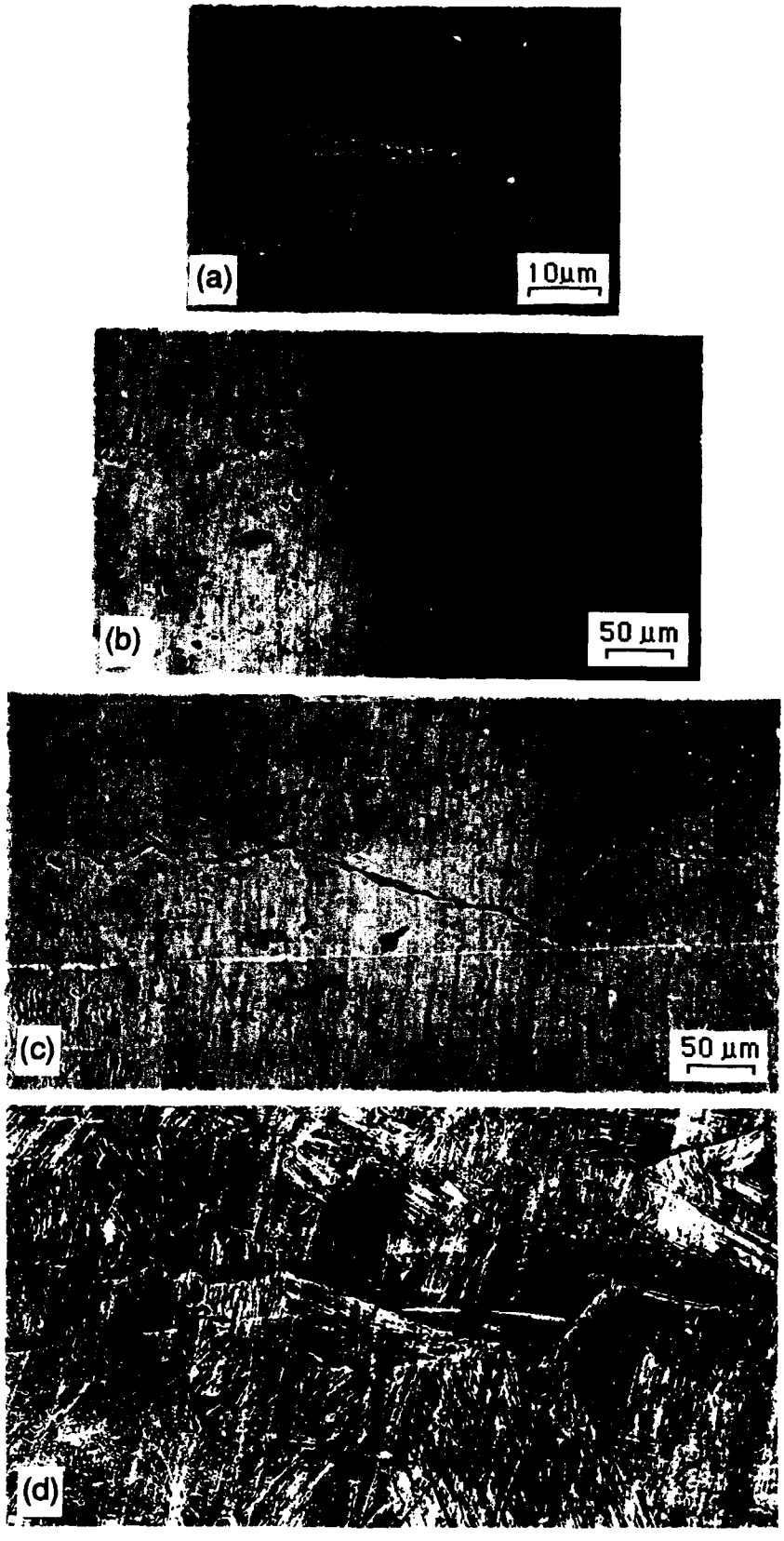

Fig. 6 Crack initiation and growth sequence, HT#3, sp.8. (a) 70 kcy, (b) 140 kcy, (c) 180 kcy, and (d) 180 kcy after etching. Stress axis vertical.

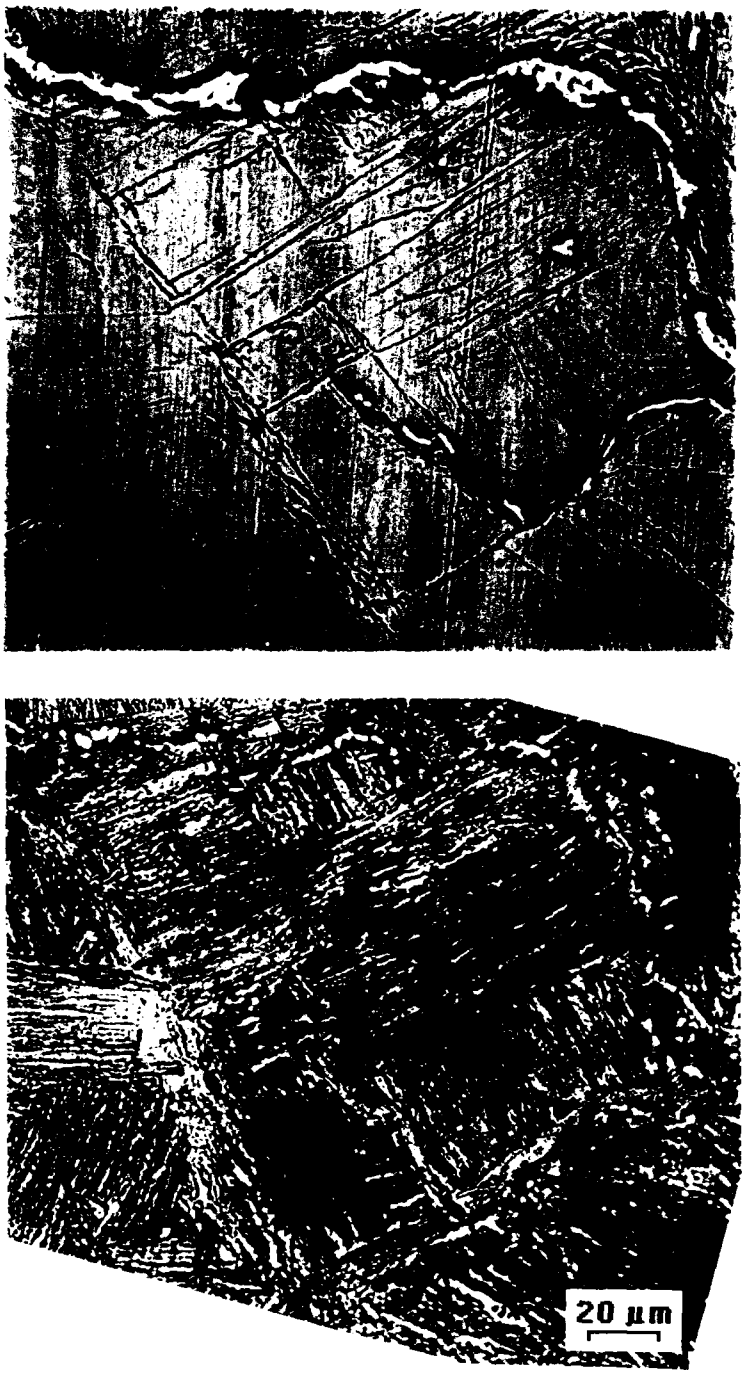

Fig. 7 Crack path in relationship to microstructure, HT#2, sp. 6 after 110 kcy. Before and after etching. Stress axis vertical.

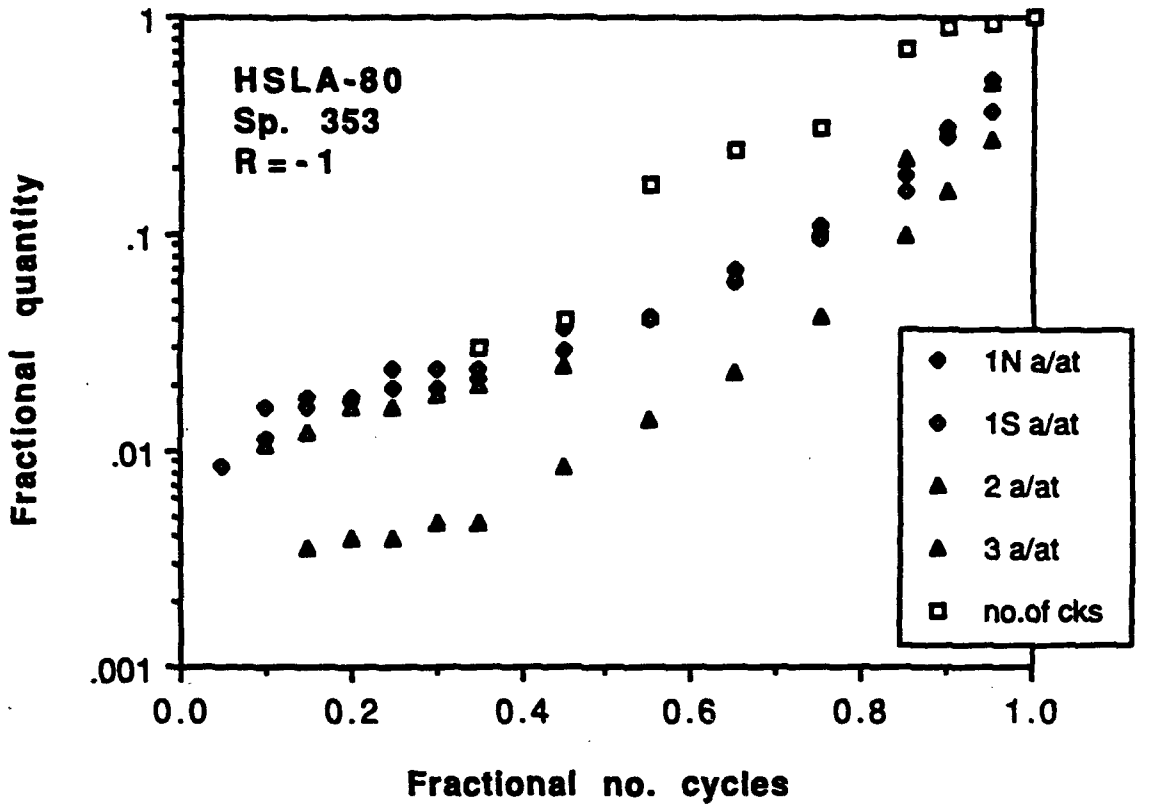

Fig. 8 - A comparison showing the similarity between the rates of crack initiation and the growth of a small crack.

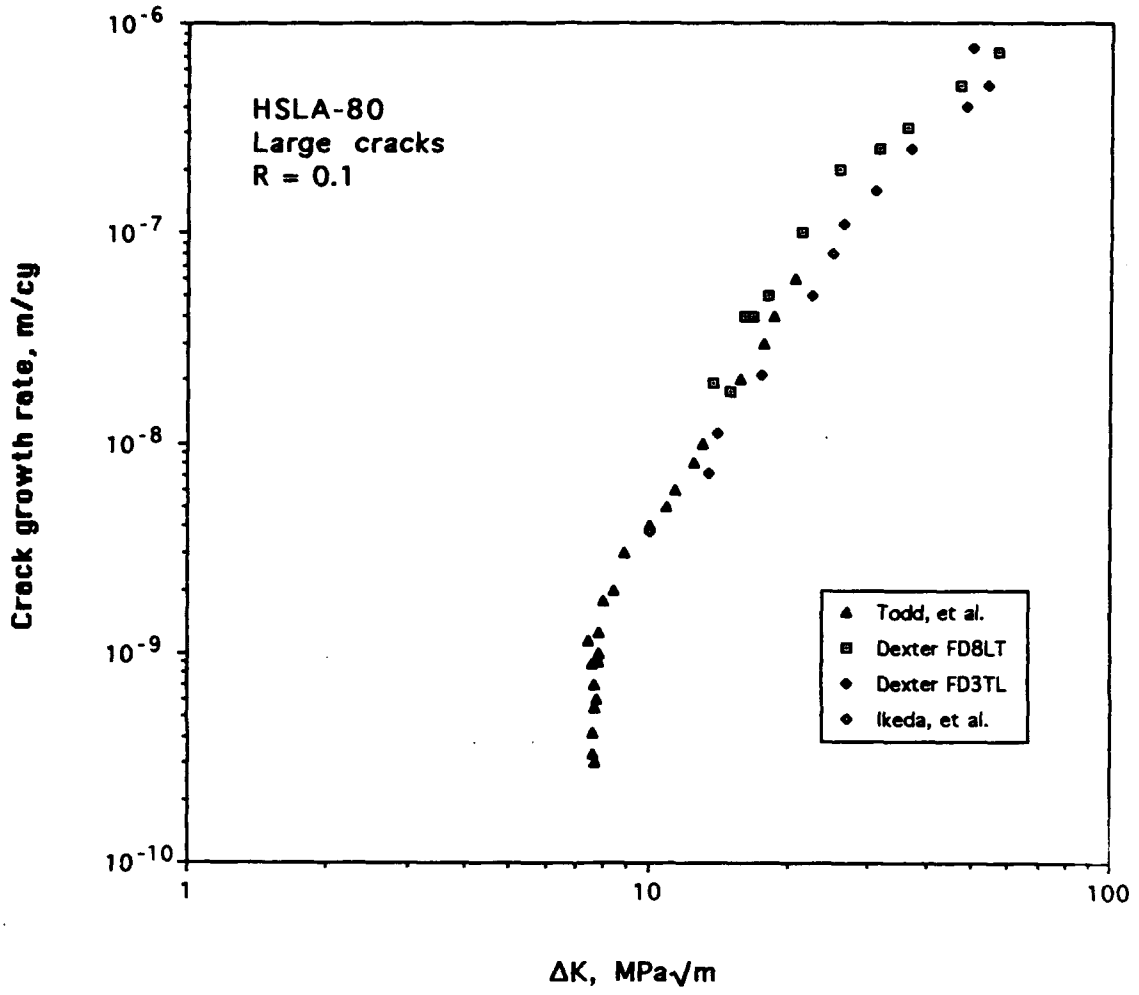

Fig. 9 Comparison of growth rates for large fatigue cracks in Cu-bearing HSLA steels.

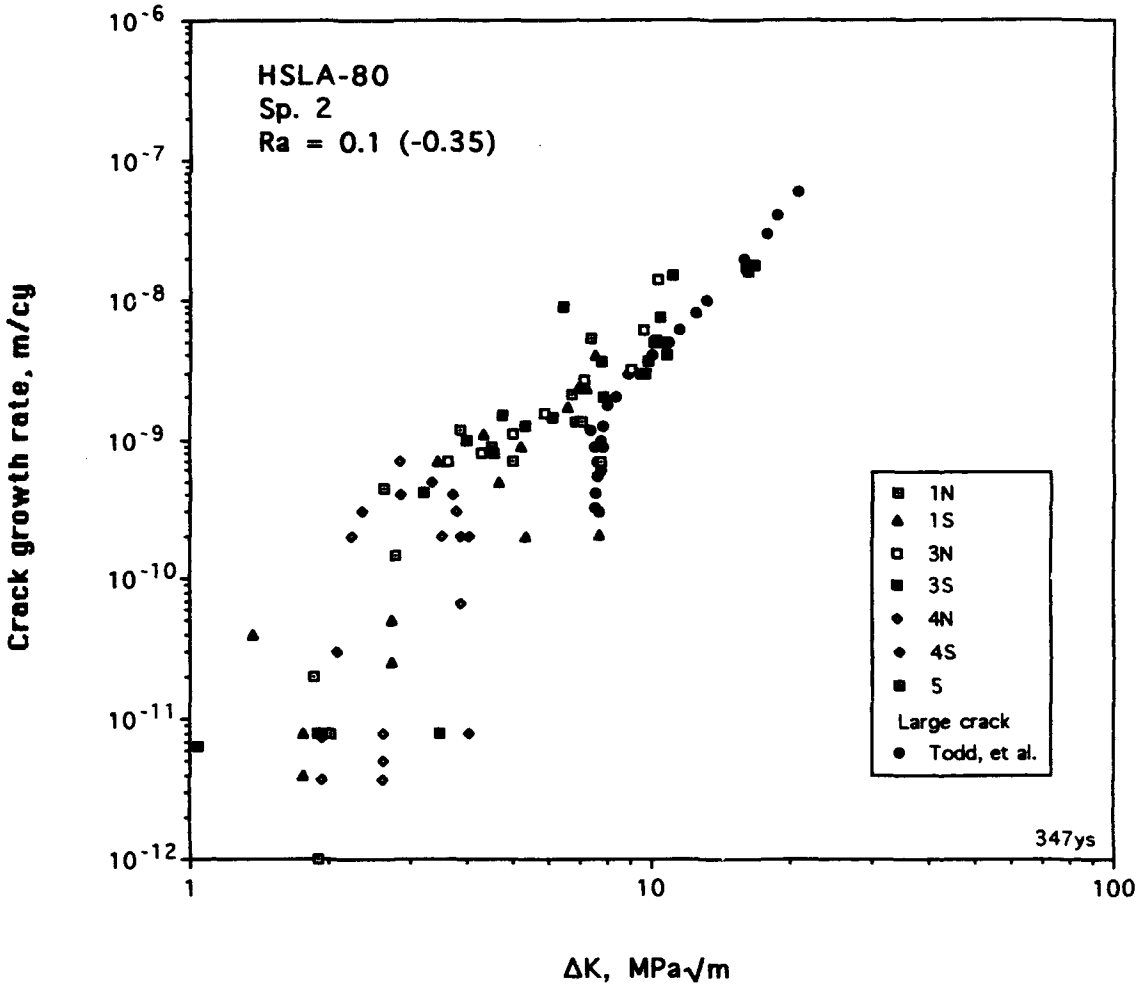

Fig. 10 Fatigue crack growth rate from Plate#1, as-received (ferritic) material, 3-point bend bar, sp. 2,

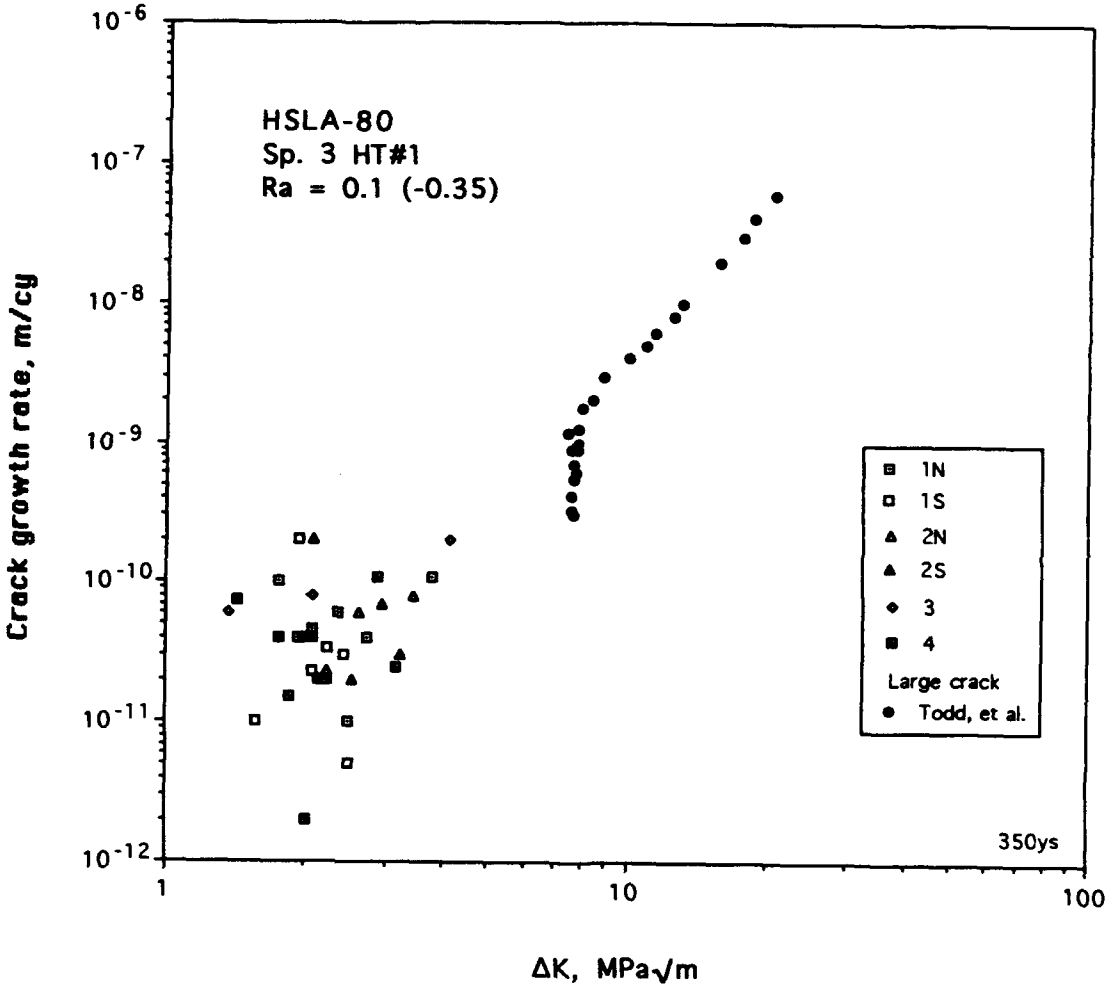

Fig. 11 Fatigue crack growth rate from Plate#2, HT#1 (ferritic material), 3-point bend bar, sp. 3.

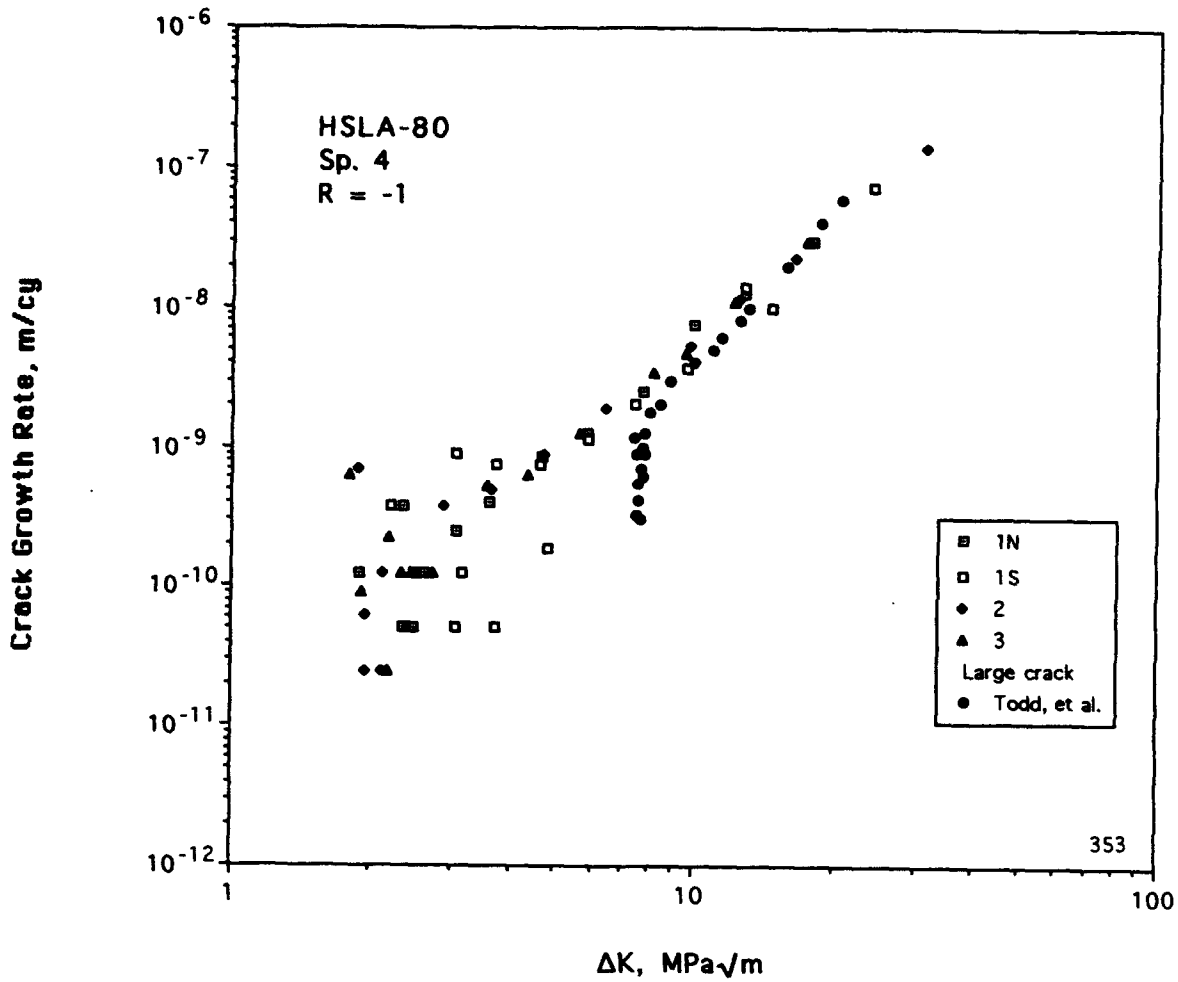

Fig. 12 Fatigue crack growth rate from Plate#1, as-received (ferritic) material, rotating beam, sp. 4.

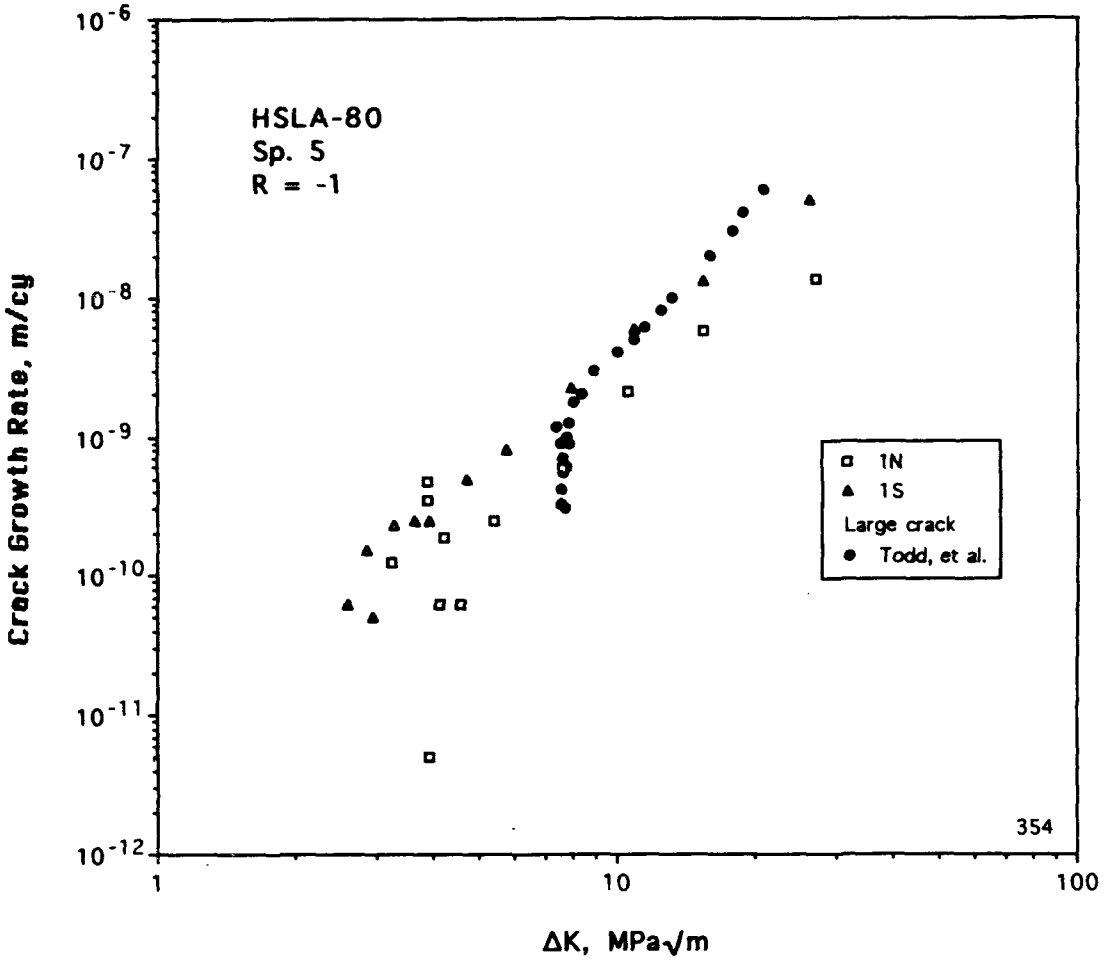

Fig. 13 Fatigue crack growth rate from Plate#1, as-received (ferritic) material, rotating beam, sp. 5.

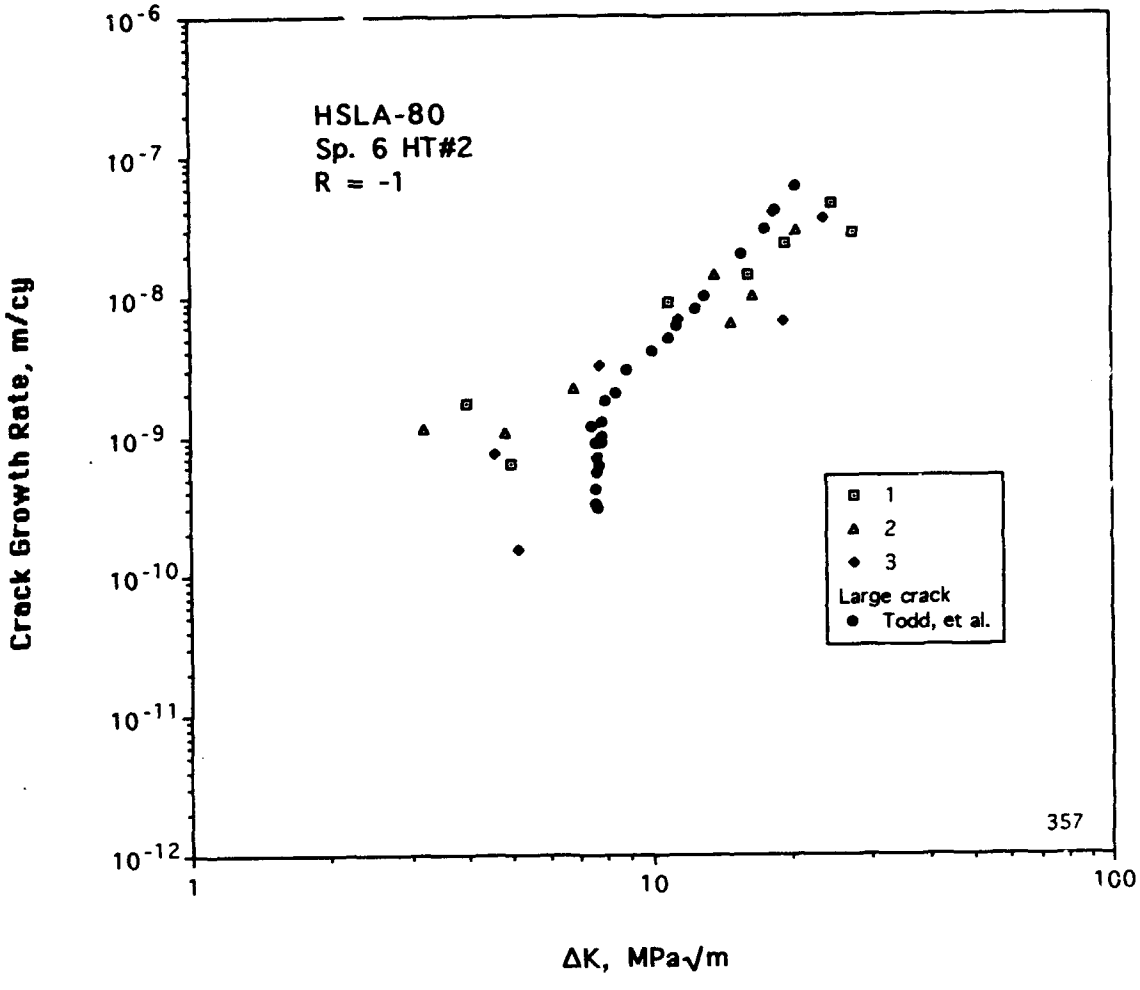

Fig. 14 Fatigue crack growth rate from Plate#1, HT#2 (lath structure), rotating beam, sp. 6.

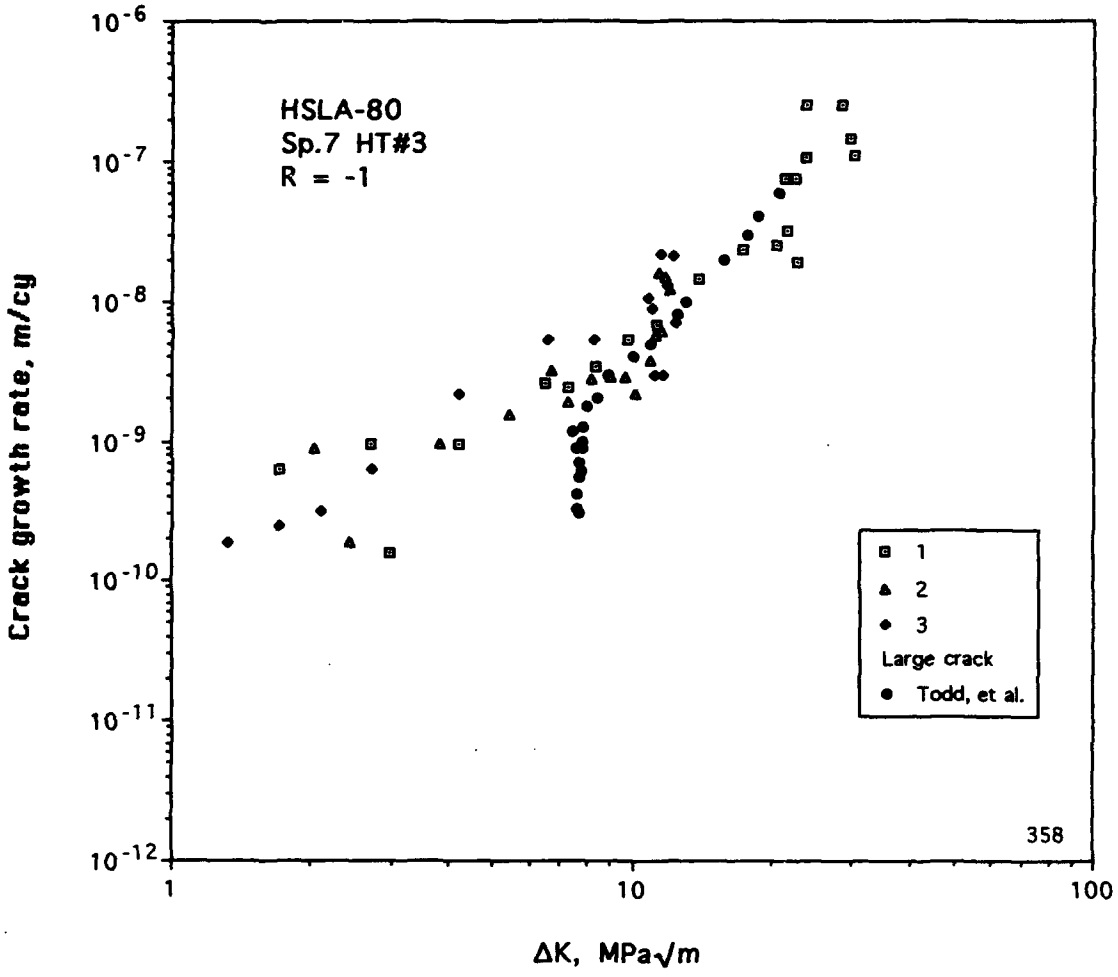

Fig. 15 Fatigue crack growth rates: Plate#1, HT#3 (lath structure), rotating beam, sp. 7.

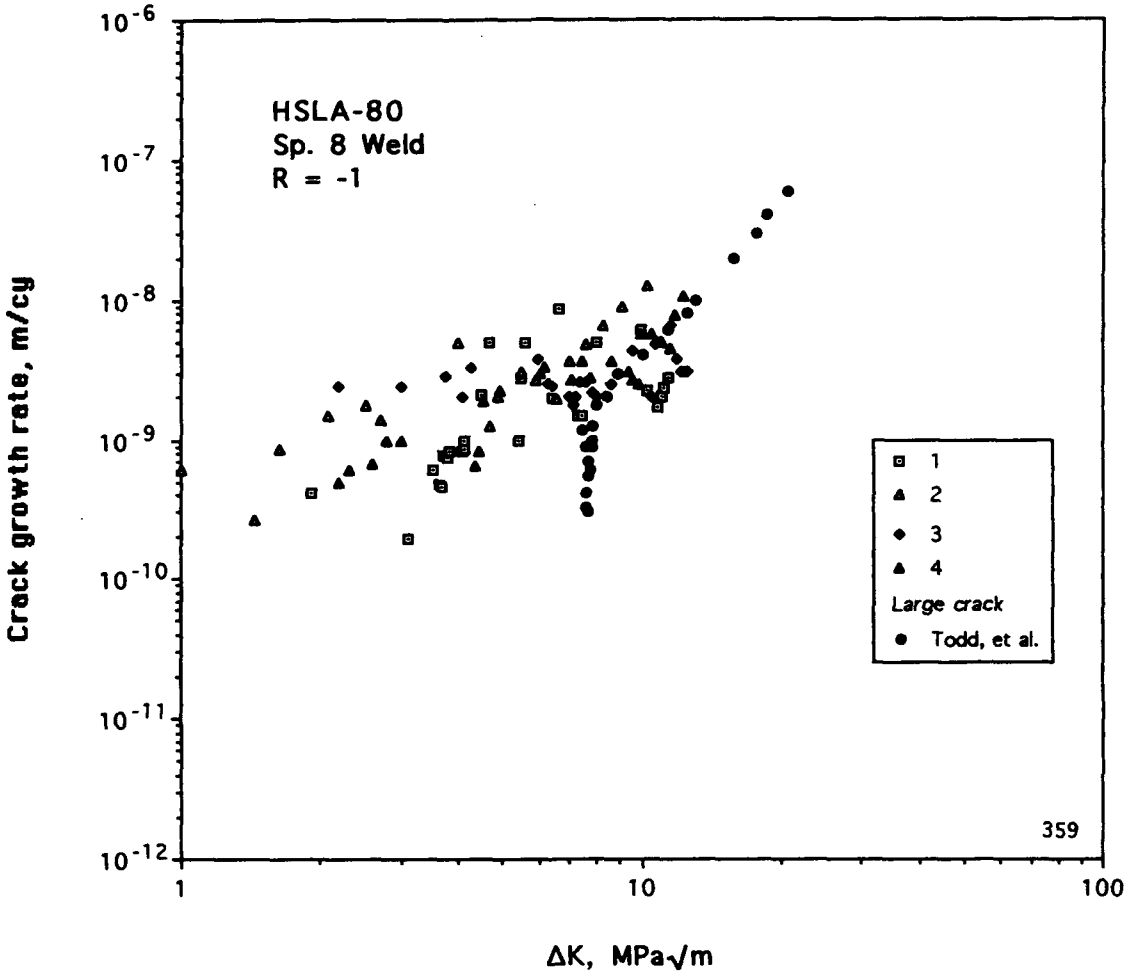

Fig. 16 Fatigue crack growth rates: Plate#1, weld metal, rotating beam, sp. 8.

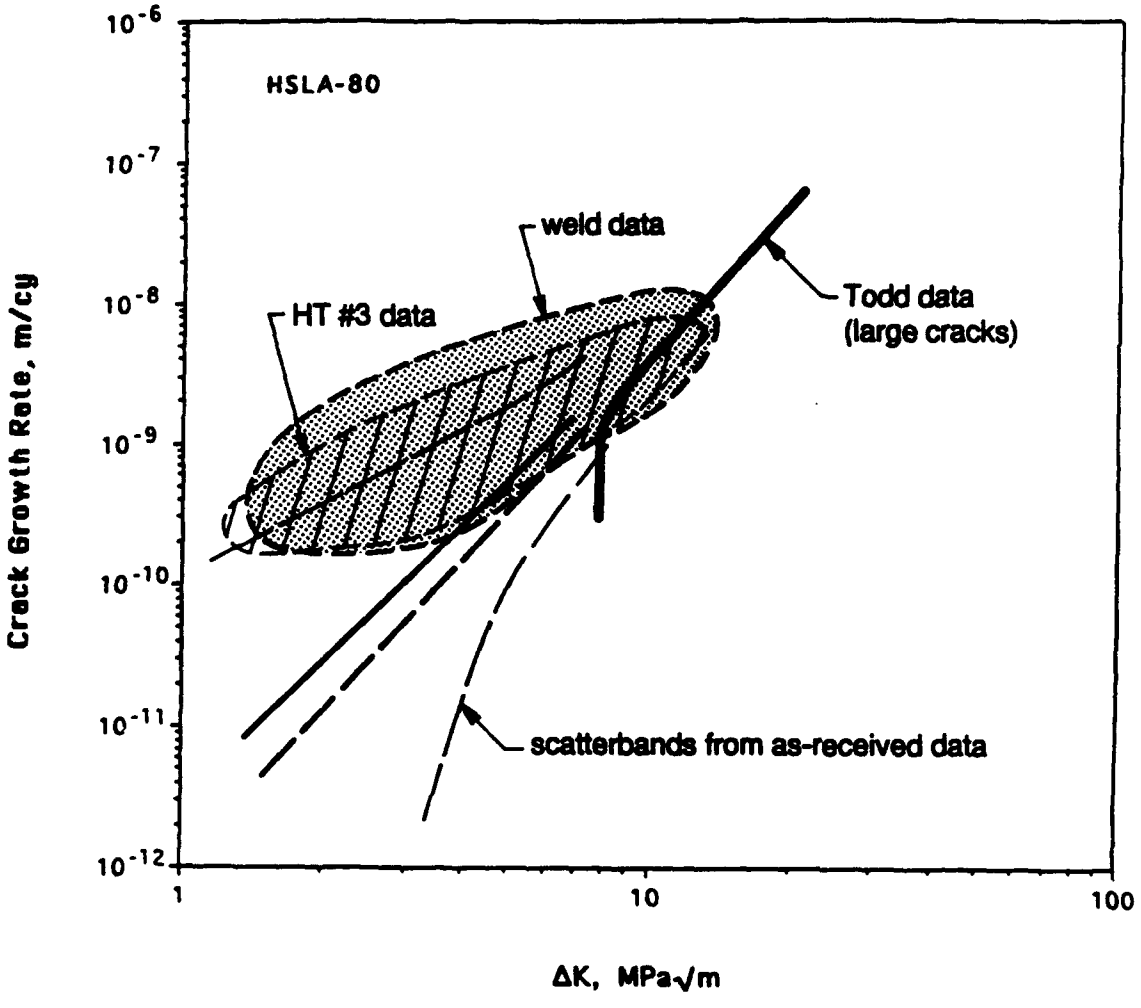

Fig. 17 Comparison of crack growth rates. The straight dashed line represents an extension of the growth rate data for large cracks, and the straight solid line is a regression through all of the large and small crack data from the as-received microstructure (note also the scatterbands from this data). Crack growth rates for HT#3 and the weld are shown as envelopes encompassing the available small crack data for each microstructure.

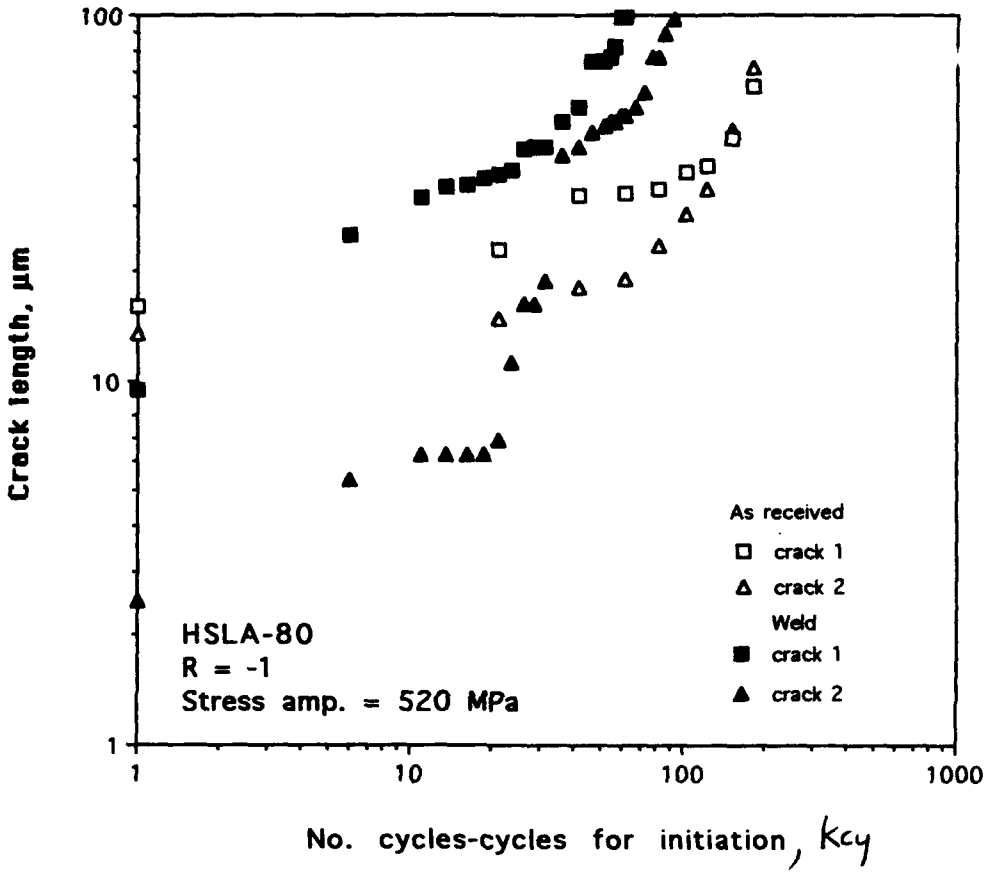

Fig. 18 Comparison of crack lengths for cracks grown in as-received material, sp. 5, Plate#1, and weld metal, sp. 8, showing the faster growth of cracks in the weld at the same stress amplitude. The effect of differences in initiation have been removed by subtracting the number of cycles for crack initiation.

APPENDIX B

"Scaling Laws for Fatigue Crack Growth of Large Cracks in Steels"

K. S. Chan

Published in *Metallurgical Transactions A*
Vol. 24A, November 1993, pp. 2473-2486.

Scaling Laws for Fatigue Crack Growth of Large Cracks in Steels

K.S. CHAN

A set of scaling laws has been developed for describing intermittent as well as continuous fatigue crack growth of large cracks in steels in the power-law regime. The proposed scaling laws are developed on the basis that fatigue crack growth occurs as the result of low-cycle fatigue (LCF) failure of a crack-tip element whose width and height correspond to the dislocation cell size and barrier spacing, respectively. The results show that the effects of microstructure on fatigue crack growth can be described entirely in terms of a dimensionless microstructural parameter, ξ, which is defined in terms of yield stress, fatigue ductility, dislocation cell size, and dislocation barrier spacing. For both discontinuous and continuum crack growth, the crack extension rate, da/dN, scales with ξ and $(\Delta K/E)^m$, where ΔK is the stress intensity range, m is the crack growth exponent, and E is Young's modulus. Application of the model to high-strength low-alloy (HSLA) and conventional ferritic, ferritic/pearlitic, and martensitic steels reveals that the lack of a strong microstructural influence on fatigue crack growth in the power-law regime is due to increasing yield stress and fatigue ductility with decreasing dislocation barrier spacing, which leads to a narrow range of ξ values and crack growth rates. Variation of da/dN data with microstructure in HSLA-80 steels is explained in terms of the proposed model. Other implications of the scaling laws are also presented and discussed in conjunction with several fatigue models in the literature.

I. INTRODUCTION

FATIGUE crack growth of large cracks in metals and alloys can generally be divided into three characteristic regimes:[1] (1) a near-threshold regime where the growth response is sensitive to microstructure, (2) a power-law regime where microstructure has little effect on the propagation rate, and (3) a rapid growth regime that is dominated by quasi-static crack extension and fracture toughness (*e.g.*, the K_{IC} value) and is sensitive to microstructure. As shown in Figure 1, the power-law regime may be subdivided into intermittent and continuous growth regimes. For many alloys, there is considerable overlap between the intermittent and continuous growth regimes such that they become indistinguishable and appear as a single power-law regime. Excellent reviews of the effects of microstructure on fatigue crack growth have been presented by Ritchie,[1] Suresh,[2] and Davidson and Lankford,[3] as well as by others.[4]

While the lack of microstructural influence in the Paris (power-law growth) regime[5] is well recognized, its existence is poorly understood. The conventional explanation for microstructure-insensitive fatigue crack growth is that the cyclic plastic zone size is larger than a characteristic microstructural unit size and behaves in a continuum manner. As a result, crack growth is dominated by the cyclic crack-tip opening displacement and occurs on every cycle (continuous or continuum growth). One possible criticism of this explanation is that continuum growth theories[6-9] predict an inverse relationship between fatigue crack growth rate and yield stress. Since the yield stress depends on microstructure, one would think the fatigue crack growth rate should depend at least mildly on microstructure. Yet, numerous studies[10-13] have shown that the fatigue crack growth rates of a large number of metals,[13] including steels,[10,11,12] aluminum,[11] and titanium alloys,[10,11] correlate with the elastic modulus only in the continuum growth regime. On the other hand, compilation of fatigue crack growth data for steels of various yield strengths shows a wide scatter band and not a single curve,[14] suggesting that the yield strength, if not the microstructure, might be of some importance.

Recent work has revealed that fatigue crack growth does not occur on a cycle-by-cycle basis in the lower-ΔK end of the power-law regime.[3,15-17] Instead, crack growth proceeds intermittently with periodic arrests and waiting periods between individual growth increments (intermittent growth). The incremental growth distance, as determined by the striation spacing, is relatively constant and ranges from 0.1 to 0.3 μm, which is on the order of the dislocation cell size.[3,17] The intermittent growth process is generally modeled by considering that the crack-tip process zone behaves like a low-cycle fatigue (LCF) specimen.[17-26] During strain cycling, the crack-tip LCF element accumulates fatigue damage and fails in accordance with the Coffin-Manson equation.[27,28] The intermittent growth models predict that fatigue crack growth is discontinuous, and the corresponding rate is sensitive to the size of the crack-tip LCF element, which is generally related to a characteristic microstructural length.

The conflicting views about the role of microstructure in fatigue crack growth in the power-law regime are of interest when considering fatigue crack growth in Cu-containing, high-strength low-alloy (HSLA) steels such as HSLA-80[29] (or A710, Grade A, Class 3 in ASTM designation[30]). This class of steels derives its high strength from a combination of fine grain size (1 to 2 μm) and precipitation hardening by small ε-Cu precipitates on the order of 5 to 20 nm in diameter.[31-35] Fatigue crack growth

K.S. CHAN, Staff Scientist, is with the Materials and Mechanics Department, Southwest Research Institute, San Antonio, TX 78228-0510.

Manuscript submitted February 9, 1993.

characterization of HSLA-80 and A710 steels showed a large scatter band with a magnification of five times variation in crack growth rates at a given K level.[29] Transmission electron microscopy (TEM) has revealed that the higher crack growth rate corresponds to a steel (designated as the FZZ plate) containing Cu precipitates with an average diameter of 6.6 nm, while the lower crack growth rate corresponds to a steel (designated as the GAH plate) with 17.5 nm Cu precipitates, as shown in Figure 2.[35] The observation suggests that the size or mean free path of Cu precipitates might be a factor in determining the fatigue crack growth response of this class of HSLA steels.

The objective of this article is to present the results of an investigation whose goal was to develop scaling laws for describing the fatigue crack growth behavior of Cu-bearing HSLA steels. The impetus of the modeling effort was the lack of understanding on the effects of microstructural size scale on fatigue crack growth of large cracks in the power-law regime. In this article, fatigue crack growth laws will be reviewed to highlight the current understanding of the role of microstructure in the power-law growth regime. A generalized model that relates the crack growth kinetics of large cracks directly to relevant microstructural size parameters will be presented. Application of the model to HSLA-80 steels will then be illustrated. Finally, the validity of the model will be tested against experimental results in the literature for ferritic, ferritic/pearlitic, bainitic, and martensitic steels. The purpose of the comparison is twofold: (1) to test the range of applicability of the model and (2) to provide possible explanations for the apparent lack of microstructural influence on fatigue crack growth of large cracks in steels. The use of two normalized parameters for scaling the fatigue crack growth rate of large cracks in steels will be demonstrated in the power-law regime.

II. REVIEW OF FATIGUE CRACK GROWTH LAWS

Numerous fatigue crack growth laws have been proposed over the last 30 years. Formulated in terms of linear-elastic fracture mechanics, these crack growth laws relate the incremental crack extension per fatigue cycle, da/dN, to the stress intensity range, ΔK. The most well-known fatigue crack growth law is the Paris power-law relation given by:[15]

$$\frac{da}{dN} = C\Delta K^m \qquad [1]$$

where C and m are empirical constants. Modifications of the Paris equation to treat stress ratio effects or the presence of a growth threshold are also available in the literature. Most of these models are empirical and provide little information about the effects of microstructural size scale on the crack growth kinetics.

Fatigue crack growth occurs during every cycle at high ΔK. In this continuum growth regime, the crack growth rate, which is in the range of 10^{-6} to 10^{-3} m/cycle, is dominated by the cyclic crack-tip opening displacement, ΔCTOD. For this reason, continuum growth models are generally based on the assumption that the incremental growth distance per cycle is one unit,[7] or a fraction, of the ΔCTOD;[36] thus,

$$\frac{da}{dN} = C_1\Delta\text{CTOD} \qquad [2]$$

where C_1 is usually taken to be 0.5.[34] For small-scale yielding,[7]

$$\Delta\text{CTOD} = \frac{\Delta K^2}{4\sigma_y E} \qquad [3]$$

leading to[7]

$$\frac{da}{dN} = \frac{C_1\Delta K^2}{4\sigma_y E} \qquad [4]$$

when Eqs. [2] and [3] are combined. Equation [4] indicates that the crack growth rate scales with $\Delta K^2/(\sigma_y E)$, where E is Young's modulus and σ_y is yield stress. Comparison of this model with experimental results indicates that Eq. [4] generally overpredicts the fatigue crack growth rate, meaning that the value for C_1 should be less than 0.5. Furthermore, experimental crack growth rates have been found to correlate with $(\Delta K/E)^2$, specifically, empirical relations of the form[10,11,12]

$$\frac{da}{dN} = C_2\left[\frac{\Delta K}{E}\right]^2 \qquad [5]$$

where C_2 is a fitting parameter. Reported values of C_2 are $\approx$3,[10] 5.4,[11] and 8.[12] Like Eq. [1], Eqs. [4] and [5] provide no insight on the role of microstructural scale in continuum fatigue crack growth. In fact, Eq. [5] implies that microstructure plays no role in the continuum growth regime. Theoretical models of Frost *et al.*,[37] and Weertman,[38] which relate the fatigue crack growth rate to the blunting of the crack tip whose radius is dictated by the surface energy, are in the form as given by Eq. [5]. The values of C_2 were predicted to be $\approx$3.[37,38]

It is well recognized that fatigue crack growth in the intermediate ΔK range occurs intermittently.[3] Early models of the discontinuous fatigue growth behavior were developed based on the assumption that fatigue damage accumulated at every cycle. Crack extension occurred when the accumulated fatigue damage reached a critical value.[7,8,36,39] Proposed measures of fatigue damage included the absorbed hysteresis energy,[7] ΔCTOD,[8,39] and plastic strain range.[36] Both the absorbed hysteresis energy and ΔCTOD criteria led to[7,8,39]

$$\frac{da}{dN} = \frac{C_3\Delta K^4}{\sigma_y^2 EU} \qquad [6]$$

where C_3 is a numerical constant and U is the total absorbed hysteresis energy per newly created surface area as the result of fatigue crack propagation. Note that most of the hysteretic work is spent in deforming the material located within the cyclic plastic zone and is dissipated as heat. A significant difference between continuum and discontinuous crack growth is in the increase of the crack growth exponent, m, from 2 to 4.

McClintock[36] was the first person to introduce the concept of a "structural size" over which accumulation

of cyclic plastic strain occurred. By applying the Coffin-Manson strain-life relation[27,28] to a microstructural element located at a characteristic distance, l, ahead of the crack tip, McClintock showed that accumulation of cyclic plastic strain within the structural element during fatigue would lead to a fatigue crack growth that is proportional to $(1/l)(\omega^*/\gamma_f)^2$, where ω and γ_f are the reverse plastic zone size and fracture strain in shear, respectively. For small-scale yielding, McClintock's crack growth equation can be expressed as[7]

$$\frac{da}{dN} = \frac{C_4}{l}\left[\frac{\varepsilon_y}{\varepsilon_f'}\right]^2\left[\frac{\Delta K}{\sigma_y}\right]^4 \qquad [7]$$

where ε_y and ε_f' are the static yield strain and fatigue ductility coefficient,[40,41] respectively. Subsequent crack growth models based on the concept of a microstructural unit size where the damage criterion is applied include those by Antolovich and co-workers,[21,22] Kujawski and Ellyin,[24] Mazumdar,[25] and Lanteigne and Baïlon.[20] In the models of Majumdar and Morrow,[18] Chakrabortty,[19] and Starke *et al.*,[26] a series of LCF specimens was considered to lie at various distances within the cyclic plastic zone ahead of the crack tip. The crack growth laws were then developed by treating failure of individual LCF specimens in terms of the linear fatigue damage rule.

In Davidson's fatigue crack growth model,[23] fatigue damage was envisioned to commence when slip, initiated from the crack tip, was blocked by obstacles located ahead of the crack tip. The obstacle spacing, or slip blockage distance, was then considered the unit size of the microstructural element whose failure would lead to an incremental crack growth. As in other models,[21–26] failure of the crack-tip microstructural element was treated *via* the Coffin-Manson LCF relation.[27,28] Unlike other models, the crack extension distance was considered to be different from the slip distance. This view of the fatigue crack growth process is similar to that subsequently employed by Roven and Nes[17] to develop their fatigue model. While conceptually similar, the Roven and Nes model[17] is considerably simpler and contains fewer empirical constants than Davidson's model.[23] The former crack growth model is used heavily in this investigation and will be described in detail in Section III.

III. A MICROSTRUCTURE-BASED FATIGUE CRACK GROWTH MODEL

The model of Roven and Nes[17] considers the LCF failure of a crack-tip element of width s and height d, where s and d are striation and dislocation barrier spacing, respectively, as shown schematically in Figure 3. In most metals, the incremental crack growth distance corresponds to the striation spacing but differs from the dislocation barrier spacing; thus, s and d are generally different. Figure 3(a) shows that the crack-tip element is embedded in the cyclic plastic zone, while Figure 3(b) illustrates the LCF failure process of the crack-tip element by irreversible motion of dislocations between the dislocation barriers. The dislocation structure shown in Figure 3(b) is formed by rearrangement of dislocations into a wall-like or ladder structure during strain cycling.

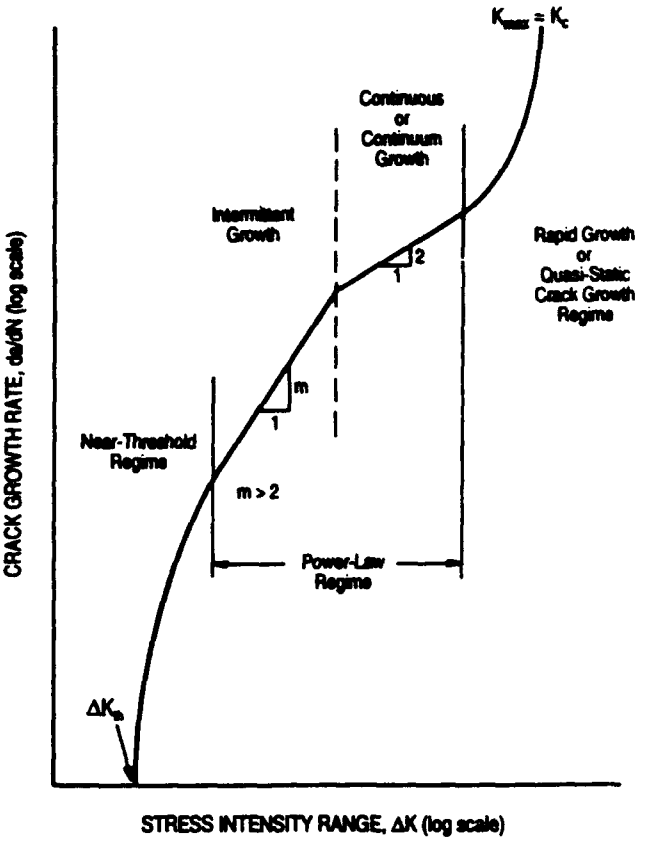

Fig. 1 — A schematic showing the various growth regimes in a fatigue crack growth curve.

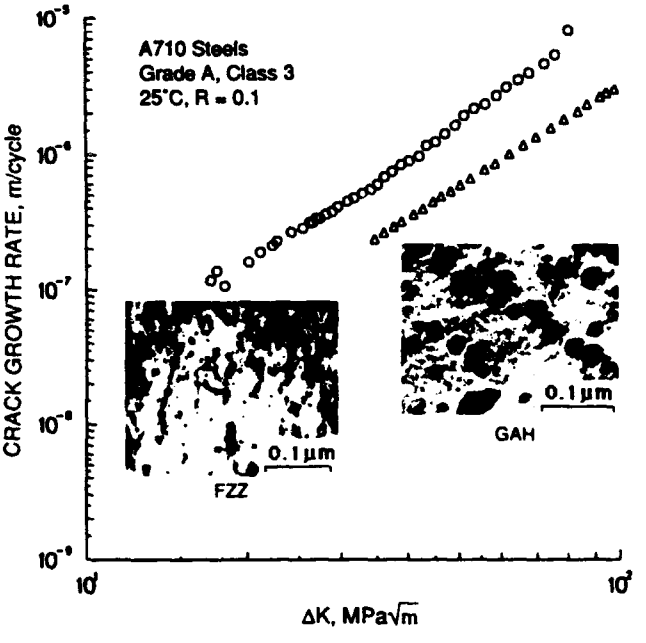

Fig. 2 — Dependence of fatigue crack growth rate on the size of ε-copper precipitates in FZZ and GAH plates.[35]

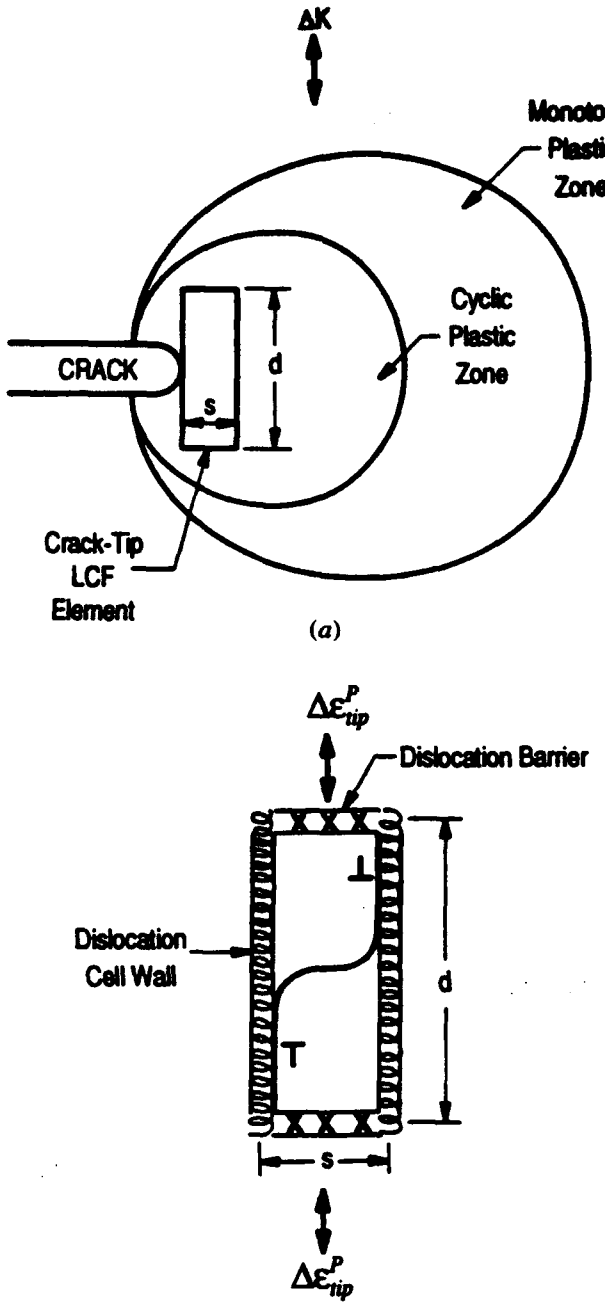

Fig. 3—Schematics of the proposed LCF crack-tip element for modeling fatigue crack growth: (*a*) location of the crack-tip element relative to the cyclic and monotonic plastic zones and (*b*) characteristic microstructural lengths of the crack-tip element.

The selection of striation spacing as the width of the crack-tip element was motivated by the observation that discontinuous fatigue crack growth in iron and low-carbon steels is characterized by a constant striation spacing in the range of 0.1 to 0.3 μm.[17] Additionally, the striation spacing appears to correlate with either dislocation cell size or wall spacing, which are also on the order of 0.1 to 0.3 μm.[17] This implies that the incremental crack growth distance (striation spacing) corresponds to failure of a dislocation cell element in the width direction. On this basis, the fatigue crack growth rate associated with LCF failure of a crack-tip element is given by[17,23]

$$\frac{da}{dN} = \frac{s}{N_s} \qquad [8]$$

where N_s is the number of fatigue cycles required to cause the observed crack extension (striation spacing), s.

Fatigue failure of the crack-tip element is considered to be governed by the Coffin-Manson relation described by[27,28]

$$\frac{\Delta\varepsilon^P}{2} = \varepsilon_f' (2N_s)^{-b} \qquad [9]$$

where $\Delta\varepsilon^P$ is the plastic strain range and b is the fatigue ductility exponent.[40] Note that Eq. [9] is written such that b is positive, while the fatigue ductility exponent is generally given as a negative quantity in the literature.[40,41] The cyclic crack-tip opening displacement and plastic strain range can be related to the dislocation barrier spacing, d, according to

$$\Delta\varepsilon^P_{tip} = \frac{\Delta\text{CTOD}}{d} \qquad [10]$$

with ΔCTOD given by Eq. [3]. Substituting Eqs. [3] and [10] into Eq. [9] leads to

$$\frac{1}{N_s} = \left[\frac{1}{4}\left(\frac{1}{2^{1-b}\sigma_{ys}\varepsilon_f' d}\right)\left(\frac{\Delta K^2}{E}\right)\right]^{1/b} \qquad [11]$$

which gives

$$\frac{da}{dN} = \xi^{1/b}(2s)^{1-1/b}\left[\frac{\Delta K}{E}\right]^{2/b} \qquad [12]$$

with

$$\xi = \frac{Es}{4\sigma_{ys}\varepsilon_f' d} \qquad [13]$$

when Eq. [11] is substituted into Eq. [8].

Equation [12] is a general expression for discontinuous fatigue crack growth and has the same form as the Paris power law with $m = 2/b$ and C a function of E, s, and the dimensionless parameter, ξ, which contains all of the microstructure-dependent parameters (σ_{ys}, ε_f', d, and s). For the special case of $b = 0.5$ in the Coffin-Manson law, Eq. [12] becomes

$$\frac{da}{dN} = \frac{\xi^2}{2s}\left[\frac{\Delta K}{E}\right]^4 \qquad [14]$$

which is somewhat similar to Eq. [6] due to Rice,[7] Weertman,[8] and Mura.[39]

For continuum crack growth, $b = 1$, and crack extension occurs at every cycle. Eq. [12] is reduced to

$$\frac{da}{dN} = \xi\left[\frac{\Delta K}{E}\right]^2 \qquad [15]$$

which can be re-expressed as

$$\frac{da}{dN} = \phi\Delta\text{CTOD} \qquad [16]$$

with

$$\phi = \frac{s}{\varepsilon_f' d} \qquad [17]$$

and ΔCTOD given by Eq. [3]. Note that Eq. [15] is identical to Eq. [5], which is based on experimental observations, while Eq. [16] is identical to Eq. [2], which is based on a continuum formulation. The potential advantage of Eqs. [12], [15], and [16] over Eqs. [2] and [5] is that they provide additional information about the role of microstructure-related parameters including yield stress (σ_y), fatigue ductility coefficient (ε_f'), dislocation cell size (s), and dislocation barrier spacing (d) in determining the crack growth rate.

Crack closure or a growth threshold, ΔK_{th}, can be incorporated into the proposed model by recognizing the fact that these two related phenomena only affect the driving force for crack growth, and they have no effect on intrinsic fatigue properties of a particular microstructure, which the microstructural parameter, ξ, signifies. Altering the proposed model to include crack closure or a growth threshold can be accomplished by replacing the stress intensity range, ΔK, in Eqs. [3], [11], [12], [14], and [15] with an effective stress intensity range, ΔK_{eff}, given by[3]

$$\Delta K_{eff} = \Delta K - \Delta K_{cl} \qquad [18]$$

or

$$\Delta K_{eff} = \Delta K - \Delta K_{th} \qquad [19]$$

where ΔK_{cl} is the stress intensity range due to crack closure and ΔK_{th} is the growth threshold. The remainder of this article will evaluate various implications of the proposed model against experimental data of steels with a variety of microstructures.

IV. APPLICATION OF THE FATIGUE MODEL TO STEELS

The microstructure-based fatigue model has been applied to elucidate the possible influence of microstructure on the fatigue crack growth behavior of HSLA steels[29,31,42–45] and conventional ferritic,[46] ferritic/pearlitic,[47–52] bainitic,[11] and martensitic steels.[53–56] Specifically, the fatigue model has been exercised to obtain the crack growth curves for steels with various microstructures, and the calculated curves are compared against experimental results in the literature. The evaluation is limited to the power-law growth regime only, as the effects of microstructure on the near-threshold or threshold of steels are well established.[1,3,57]

Material inputs to the fatigue model include the yield stress (σ_y), fatigue ductility coefficient (ε_f'), fatigue ductility exponent (b), striation spacing (s), and the dislocation barrier spacing (d). When available, reported results of these parameters were used. Otherwise, estimates or measurements of these parameters were made. In most cases, the value of b was obtained from the slope of the da/dN *vs* ΔK curve in a log-log plot. Recall that $m = 2/b$. Reported values of static yield stress were used in all cases. Static yield stress was used rather than the cyclic yield stress, because the former is reported more frequently. Microstructural information was not always reported. Under this circumstance, the barrier spacing was measured from published micrographs when available or estimated based on steels with similar strength and microstructure. If none was available, the barrier spacing was estimated based on the yield strength using the relations of yield strength and mean free path established by Gurland.[58] Reported values of ε_f' were generally used. In some cases, a value of ε_f' for similar steels with equivalent strength and microstructure was used. Values of ε_f' compiled by Hertzberg[40] and Boardman[41] were utilized. For HSLA-80 steels, ε_f' was taken to be the reduction-in-area, because it was numerically similar to the ε_f' value reported for a high-Nb HSLA steel.[59] Additionally, attempts to equate ε_f' to the true fracture strain, ε_f, calculated according to $\varepsilon_f = \ln [1 - RA]^{-1}$ had led to overprediction by the model, meaning ε_f' is less than ε_f, as observed in many steels.[60] When no information was available or poor agreement was obtained between model and experiment, the value of ε_f' was adjusted to fit the model to the experimental curve. The rationale here was that the value of ε_f' for the crack-tip element of the size $s \times d$ could be different from that of a conventional LCF or tensile specimen of a larger size. The dislocation cell size, s, was taken to be 0.1 μm in most cases, but $s = 0.2$ μm[17] was also used for ferritic/pearlitic steels. The value of Young's modulus, E, was taken to be 2×10^5 MPa for all steels. A summary of the microstructural parameters is presented in Table I.

Critical experiments were also performed on HSLA-80 steels to verify the model calculations. The critical experiments included characterization of striation spacing as a function of stress intensity range and characterization of the mean free path of ε-Cu precipitates in HSLA-80 steels. The HSLA-80 crack growth data utilized in the study were originally obtained at the Naval Air War Center (NAWC) and Lehigh University. Some of the test specimens were obtained from these two sources for the characterization tests. Using scanning electron microscopy (SEM), fatigue striation spacings were characterized on compact-tension fatigue crack growth specimens from Lehigh University. Transmission electron microscopy was performed on the FZZ and GAH specimens of HSLA-80 supplied by NAWC to determine the size, volume fraction, and mean free path of ε-Cu precipitates. Details of the experimental procedures are described elsewhere.[35]

A. *HSLA Steels*

The calculated fatigue crack growth curve for HSLA-80 steel is compared with experimental data[45] in Figure 4.

Table I. Summary of Yield Stress (σ_y), Fatigue Ductility Coefficient (ϵ_f'), Dislocation Barrier Spacing (d), Cell Size (s), Fatigue Ductility Exponent (b), Crack-Growth Exponent (m), and the Dimensionless Microstructural Parameters ϕ and ξ for Various Steels

Steel	σ_y, MPa	ϵ_f'	d, μm	s, μm	b	$m = 2/b$	ϕ	ξ	Microstructure*	Characteristic Length
HSLA-80[45]	620.0	0.71[42]	0.89[35]	0.1	0.5 (1)	4 (2)	0.16	12.8	F + Cu precipitates	mean free path of Cu precipitates
(GAH)[29,42]	559.2[42]	0.75[42]	0.79[35]	0.1	0.5 (1)	4 (2)	0.17	15.1	F + Cu precipitates	mean free path of Cu precipitates
(FZZ)[29,42]	633.0	0.71[42]	0.46[35]	0.1	0.5 (1)	4 (2)	0.31	24.2	F + Cu precipitates	mean free path of Cu precipitates
VAN-80[51,52]	560.0	0.21[52]	5[52]	0.2	0.571 (1)	3.5 (2)	0.19	17.0	F + P	grain/colony size
HY80[53]	655.0	0.77**	2†	0.1	0.65	3.1	0.06	5.0	tempered M	carbide spacing
HY130[53]	965.3	0.48[40]	0.8[75]	0.1	(1)	(2)	0.26	13.5	tempered M	carbide spacing
A533B[111]	503.0	1.0‡	2[77]	0.1	(1)	(2)	0.05	5.0	tempered M	carbide spacing
A514J[54]	744.7	0.60[40]	1.8†	0.1	(1)	(2)	0.09	6.2	tempered M	carbide spacing
10Ni steel[111]	1255.0	0.60[40]	0.8§	0.1	(1)	(2)	0.20	8.3	tempered M	carbide spacing
QT steel[52]	910.0	0.6[40]	1.5[52]	0.1	0.67	2.98	0.11	6.1	tempered M	carbide spacing
4340[56]	1241.0	0.48[40]	0.8§	0.1	0.6 (1)	3.33 (2)	0.26	10.5	tempered M	carbide spacing
4Cr-0-35C[55]	1324.0	1.0‡	0.5[76,61]	0.1	0.75	2.67	0.21	7.6	M	lath width
Ni-Mo-V steel[111]	1240.0	1.0‡	0.75#	0.1	(1)	(2)	0.13	5.4	B	carbide spacing
A36[48]	248.2	0.35‡	13[58]	0.1	0.65	3	0.02	4.4	F + P	grain size
A537[48]	406.8	0.40†	5[58]	0.1	0.65	3	0.05	6.1	F + P	grain size
1020[47]	366.0	0.35[40]	7.8[47]	0.2	0.571	3.5	0.07	10.0	F + P	grain size
	275.0	0.18‡	20.5[47]	0.2	0.571	3.5	0.05	9.9	F + P	grain size
	194.0	0.10‡	55[47]	0.2	0.571	3.5	0.04	9.4	F + P	grain size
0030 cast steel[49,50]	303.0	0.20‡	20[49]	0.2	0.5	4	0.05	8.3	F + P	grain size
0050A cast steel[49,50]	434.0	0.20‡	15[49]	0.2	0.5	4	0.07	7.7	F + P	grain size
Plain C steel[46]	253.8	0.19[41]	12[46]	0.2	0.571	3.5	0.09	17.3	F	grain size
	211.7	0.19[41]	16[46]	0.2	0.571	3.5	0.07	15.5	F	grain size
	201.9	0.12‡	25[46]	0.2	0.571	3.5	0.07	16.5	F	grain size
	192.1	0.12‡	28[46]	0.2	0.571	3.5	0.06	15.5	F	grain size

Note: The parenthesized values for b and m correspond to values used in the continuum growth regime, while the unparenthesized values are for the intermittent growth regime. The relevant microstructures and the characteristic length corresponding to the dislocation barrier spacing, d, for individual steels are indicated in the last two columns.

*F = ferrite; P = pearlite; M = martensite; and B = bainite.

**Estimated based on HSLA-80 data.

†Estimated based on Q&T steel data.

‡Fitted to crack growth rate.

§Estimated based on HY130 data.

#Measured from SEM micrographs.

In the model calculation, both the intermittent growth model (Eq. [14]) and the continuum growth model (Eq. [15]) were used to compute the respective crack growth rates at a given ΔK level. The minimum of these two crack growth rates was taken to be the appropriate da/dN for that ΔK level. In all cases, intermittent growth dominated in the lower ΔK regime, while continuum growth dominated at high ΔK levels, resulting in a change in slopes in the calculated curve shown in Figure 4. The experimental data included crack growth at stress ratios of $R = 0.1$ and 0.8, where R is the ratio of minimum stress to maximum stress during a fatigue cycle. Note the absence of a marked R-ratio effect in the experimental data, which suggests crack closure is minimal in this data set. The calculated curve is in good agreement with the experimental data for both $R = 0.1$ and $R = 0.8$. Both the calculated and observed crack growth curves are bilinear. The slope of the lower ΔK curve is 4, while it is 2 in the high ΔK regime. This result suggests that intermittent growth occurs at low ΔK, while continuum growth dominates at high ΔK.

Fatigue striation measurements indicated that the striation spacing was relatively constant with an average value of $\approx$ 0.1 to 0.2 μm for ΔK levels less than 33 MPa$\sqrt{m}$, as shown in Figure 5. More importantly, the striation spacing was larger than the calculated and the observed crack growth rates, confirming the contention that intermittent growth dominated in this regime. At ΔK levels above 33 MPa$\sqrt{m}$, the striation spacing was larger and increased with ΔK. Additionally, the striation spacing was approximately equal to the calculated and observed crack growth rates, meaning that crack growth indeed occurred on a cycle-by-cycle basis, extending at increments of one or more cell sizes at each fatigue cycle. Thus, the observed change in slope in the da/dN curve in HSLA-80 steels is indeed the consequence of a transition from an intermittent growth to a continuum growth process. Furthermore, both the intermittent and continuum growth processes scale with the same microstructural parameter, ξ, even though the exponent depends on the nature of the crack growth process.

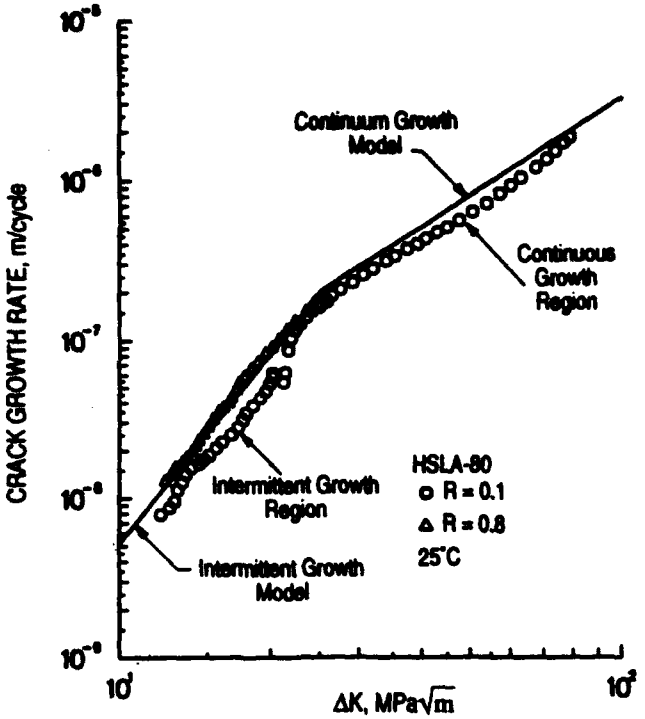

Fig. 4—Comparison of experimental and calculated da/dN curves for HSLA-80 steels at $R = 0.1$ and 0.8. Experimental crack growth data are from Dexter.[45]

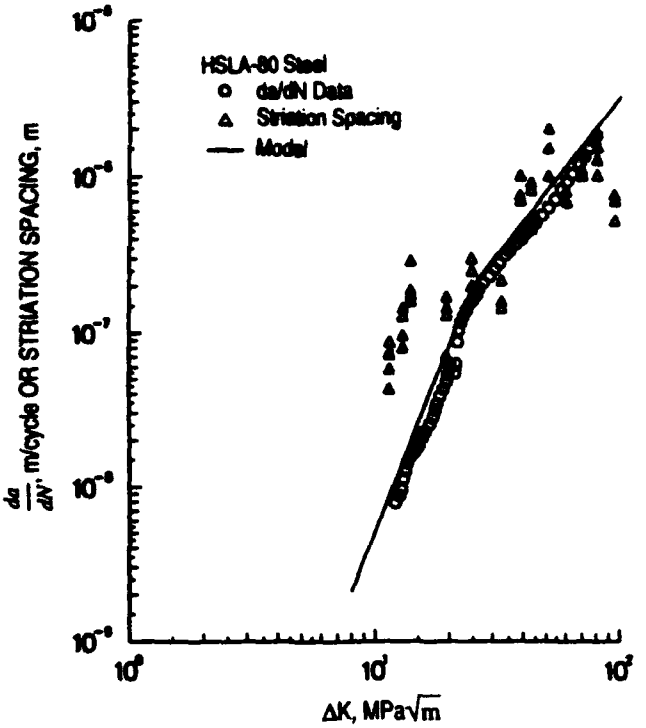

Fig. 5—Comparison of experimental and calculated da/dN curves with striation spacings for HSLA-80 steel at $R = 0.1$. Experimental crack growth data are from Dexter.[45]

As indicated earlier, the crack growth data of HSLA-80 steels varied by a factor of 5 among nominally identical, though not necessarily microstructurally identical, specimens.[35] To resolve this difference, crack growth calculations were performed for individual HSLA-80 specimens using their measured properties as input to the fatigue model. The designations of the specimens were FZZ, GAH, and FD1LT. The FZZ specimen corresponded to the top of the scatter band of the HSLA-80 crack growth data base, while the GAH and FD1LT were near the bottom of that band. The calculated curves are compared with experimental results in Figure 6, together with their corresponding ξ values. The data of Todd *et al.*[43] is also included in Figure 6, because the data set contains da/dN results for ΔK less than 10 MPa$\sqrt{m}$. Though not perfect, the good agreement between calculation and experiment nonetheless suggests that the variation in fatigue crack growth rate in HSLA-80 steels originates from variations in yield stress, fatigue ductility coefficient, and Cu-precipitate spacing, which form the dimensionless microstructural parameter, ξ, defined according to Eq. [13]. In particular, FZZ exhibited a higher crack growth rate and ξ value, while FD1LT and GAH manifested lower crack growth rates and ξ values. The result suggests that the relevant microstructural feature in HSLA-80 steels is the mean free path of the ε-Cu precipitates.

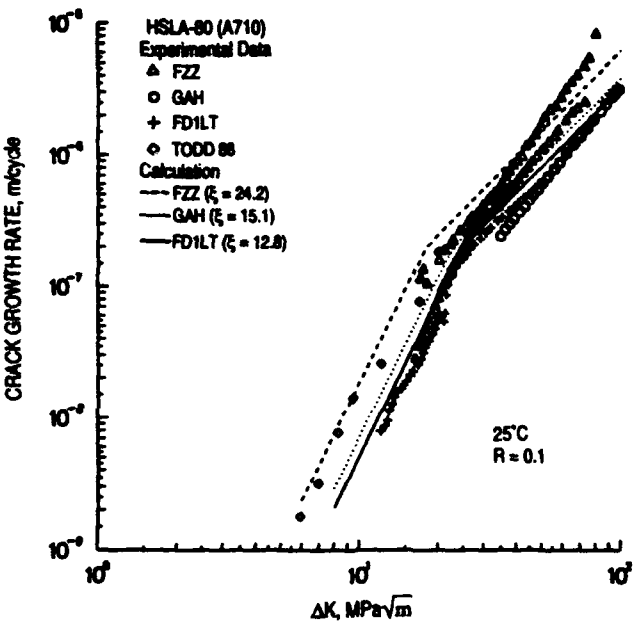

Fig. 6—Comparison of experimental and calculated da/dN curves for individual HSLA-80 steel specimens. Experimental data are from Dexter,[45] Montemarano *et al.*,[42] and Todd *et al.*[43]

A comparison of the model calculations and experimental results for VAN-80 steel,[51,52] which is a vanadium-containing HSLA steel containing a fine ferritic/pearlitic microstructure, is shown in Figure 7. It is also an independent comparison, because all relevant material properties[52] were measured and reported together with the crack growth data in the original studies.[51,52] The excellent agreement gives credence to the proposed model. Notice that the VAN-80 steel also showed evidence of a transition from intermittent growth to continuum growth

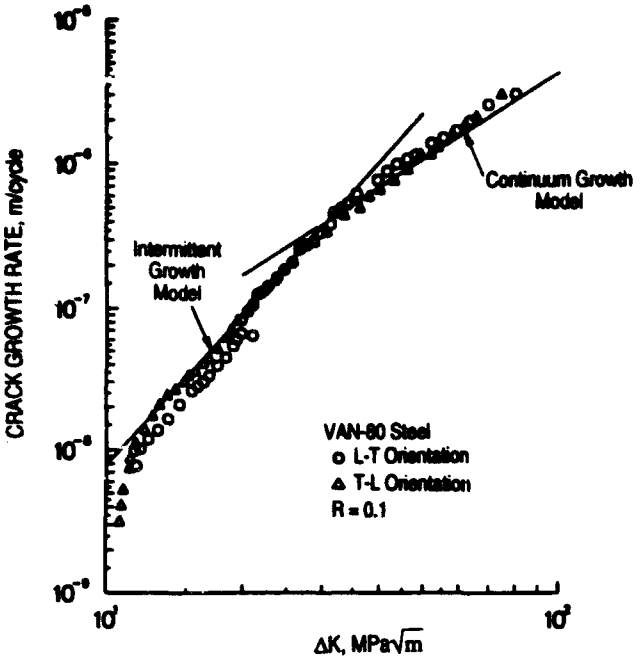

Fig. 7—Comparison of model calculation with experimental data of VAN-80 steel from Hertzberg and co-workers.[51,52]

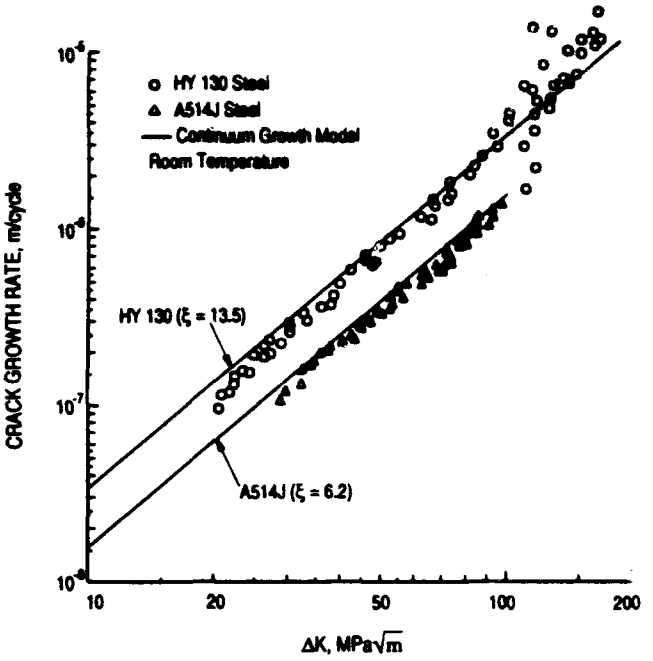

Fig. 8—Comparison of model calculation with experimental data of HY130[53] and A514J[54] steels in the continuum growth regime.

at high ΔK levels, supporting the observation made in HSLA-80 steels.

B. *Martensitic Steels*

Most of the martensitic steels examined contained tempered martensite. The variation in the relevant microstructural feature was the carbide spacing. One steel with untempered martensite[55] was examined, and the relevant feature was the width of the martensitic laths, as pointed out previously by Yoder *et al.*[61] One bainitic steel[11] was examined. Like steels with tempered martensite, the relevant microstructure for the bainitic steel was carbide spacing. Because of the large number of steels examined, only selected examples will be presented here.

Figure 8 shows a comparison of the calculated and measured crack growth curves for HY130[53] and A514J[54] steels in the continuum growth regime. The ξ value for HY130 is 13.5 compared to 6.2 for A514J. The higher ξ value for the former is due to a higher yield strength and lower values for carbide spacing and fatigue ductility. A comparison of the model calculations and experiment in the intermittent growth regime is presented for HY80[53] and a quenched and tempered (QT) steel[52] in Figure 9. In this case, the microstructural parameters of these two steels are relatively similar, leading to similar ξ values and crack growth curves.

C. *Ferritic/Pearlitic Steels*

The relevant microstructural feature for the ferritic or ferritic/pearlitic steels examined appeared to be grain or colony size. A comparison of the calculated and experimental crack growth curves for A36 and A537A, which contain a ferritic microstructure with pearlite, is shown in Figure 10. Both steels show subtle differences

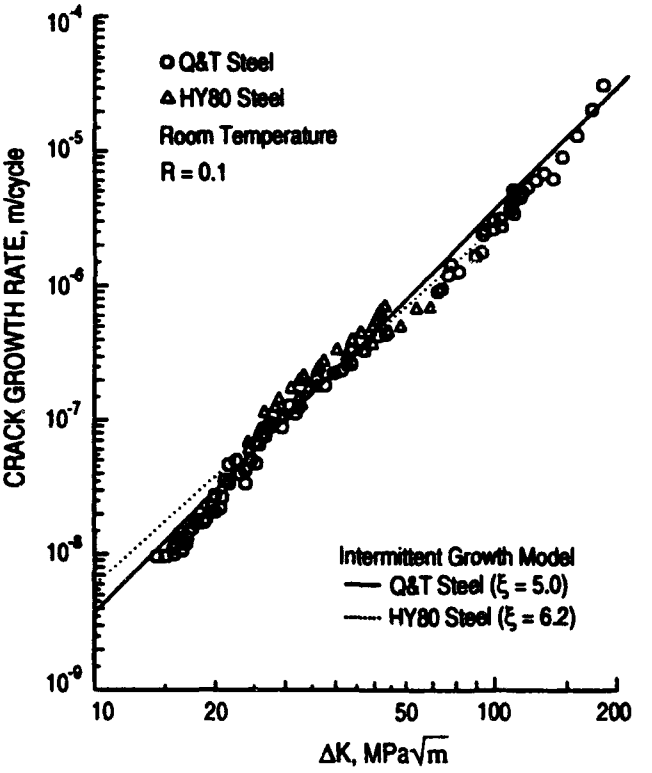

Fig. 9—Comparison of model calculation with experimental data of HY80[48,53] and QT steels[52] in the intermittent growth regime.

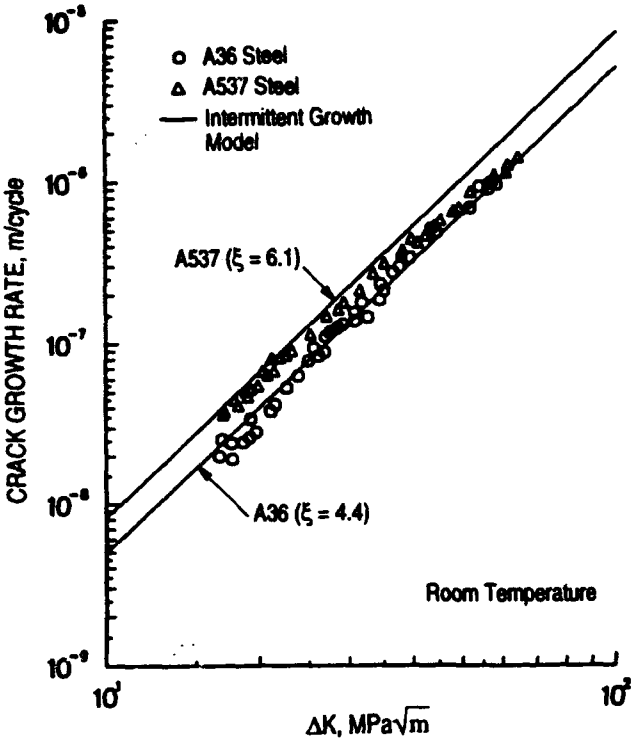

Fig. 10—Comparison of calculated and experimental *da/dN* curves for A36 and A537A steels.[48]

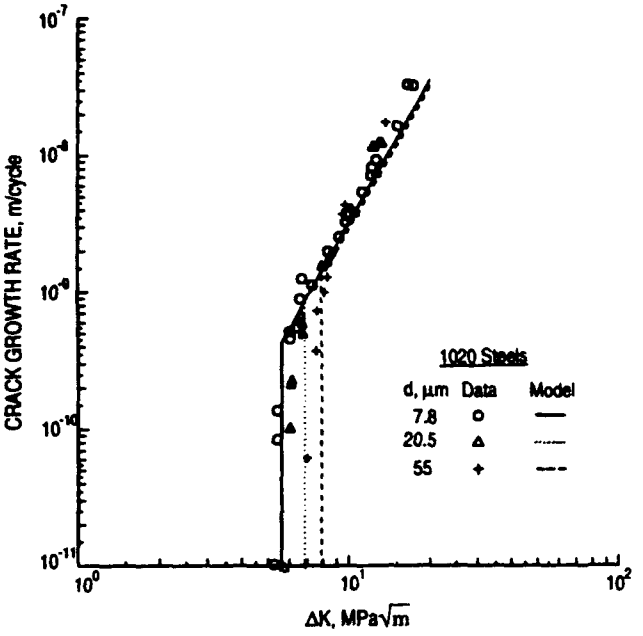

Fig. 11—Calculated *da/dN vs* ΔK curves compared to experimental data of 1020 steels. Experimental data are from Taira *et al.*[47]

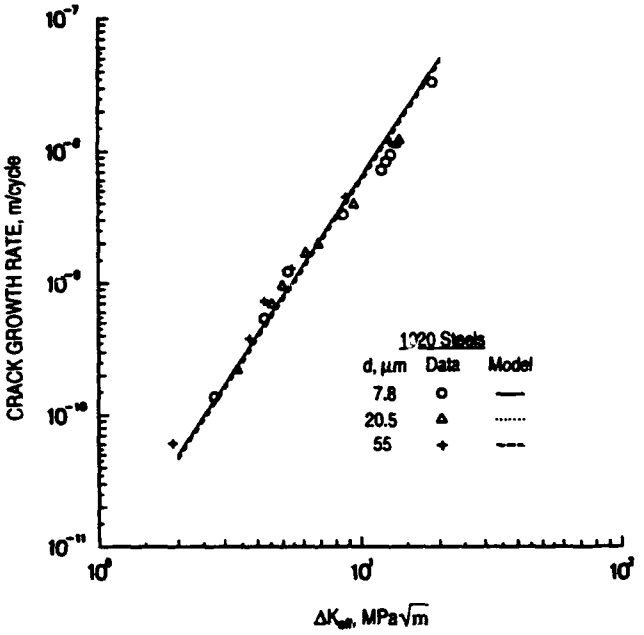

Fig. 12—Calculated *da/dN vs* effective ΔK curves compared to experimental data of 1020 steels. Experimental data are from Taira *et al.*[47]

in yield strength, grain size, fatigue ductility, and fatigue-ductility exponent. The consequence is minor differences in the ξ value and fatigue crack growth rate, as shown in Figure 10.

A comparison of the model calculations and experimental data for 1020 steels heat-treated to three different grain sizes is shown in Figure 11. For these steels, the combination of yield stress, fatigue ductility, and grain size led to similar ξ values and fatigue crack growth rates for all three steels at ΔK levels above the growth threshold, ΔK_{th}. In an earlier study, Yoder *et al.*[61] have shown that the growth threshold of a number of steels is given by the expression

$$\Delta K_{th} = 5.5\sigma_y\sqrt{d} \qquad [20]$$

where d is the ferrite grain size in this case. Equation [20] was used in conjunction with the intermittent growth model to obtain the calculated curves shown in Figure 11.

The 1020 steel data shown in Figure 11 were taken from Taira *et al.*[47] Crack closure was measured for these steels, and *da/dN* data were also correlated with the effective ΔK, ΔK_{eff}, by Taira *et al.*,[47] as shown in Figure 12. Application of the intermittent growth model to the closure-corrected crack growth data of 1020 steels required replacing ΔK with ΔK_{eff} and a new value for b, Figure 12. Specifically, b was reduced from 0.571 to 0.543, while the dimensionless microstructure parameter, ξ, remained unchanged. This closure independence provides another support for the contention that ξ is the relevant microstructural parameter for scaling *da/dN* and $(\Delta K/E)^m$.

V. DISCUSSION

A. *Role of Microstructure in Crack Growth*

One of the significant findings of this investigation is that fatigue crack growth rate scales with the dimensionless microstructural parameter, ξ, and $(\Delta K/E)^m$ in both the intermittent growth and continuum growth regimes. Since ξ encompasses all relevant microstructural

parameters, one only needs to examine variables contained within ξ that are microstructure dependent, *i.e.*, yield stress, fatigue ductility, and dislocation barrier spacing, to elucidate the role of microstructure in fatigue crack growth in the power-law regime. Figure 13 shows a log-log plot of yield stress *vs* barrier spacing for all the steels examined. Despite the scatter, the yield stress is seen to increase with decreasing dislocation barrier spacing according to the Hall-Petch relation;[62,63] *i.e.*,

$$\sigma_y \propto (d)^{-1/2} \quad [21]$$

Similarly, a plot of log (ε_f') *vs* log (d) in Figure 14 shows increasing fatigue ductility with decreasing barrier spacing according to

$$\varepsilon_f' \propto (d)^{-1/2} \quad [22]$$

Motivated by these findings, $\sigma_y\varepsilon_f'$ is plotted against d in a log-log plot in Figure 15. The result is a scatter band whose average value is represented by a linear curve with a slope of -1, as shown in Figure 15. Thus, the relationship between $\sigma_y\varepsilon_f'$ and d is given by

$$\sigma_y\varepsilon_f' d = U_d \quad [23]$$

where U_d, the cumulative plastic work-per-unit area of crack growth, appears to vary among the various steels.

The apparent lack of microstructural influence on fatigue crack growth in the power-law regime can be explained in terms of the results shown in Figures 13 through 15. Recall that da/dN scales with ξ and $\xi = Es/(4\sigma_y\varepsilon_f' d)$. For steels with a fine microstructure, the value of d is small but the values of σ_y and ε_f' are larger. Conversely, d is large for steels with coarse microstructures, but the corresponding values for σ_y and ε_f' are lower. The consequence is that the product of $\sigma_y\varepsilon_f' d$, or U_d, is relatively insensitive to microstructure, leading to small variations in the ξ value and, thus, the crack growth rate. Since σ_y and ε_f' show considerable scatter when correlated with d (Figures 12 and 13), variations in these parameters lead to a range of ξ values and crack growth rates. Thus, part of the experimentally observed crack growth variation actually originates from the microstructure, as observed in HSLA-80 steels in Figure 6.

The ε_f' value for HSLA-80 steels, which ranges from 0.71 to 0.75, was assumed to have the same value as the reduction-in-area. These assumed values are consistent with $\varepsilon_f' = 0.80$, measured for a Nb-bearing HSLA

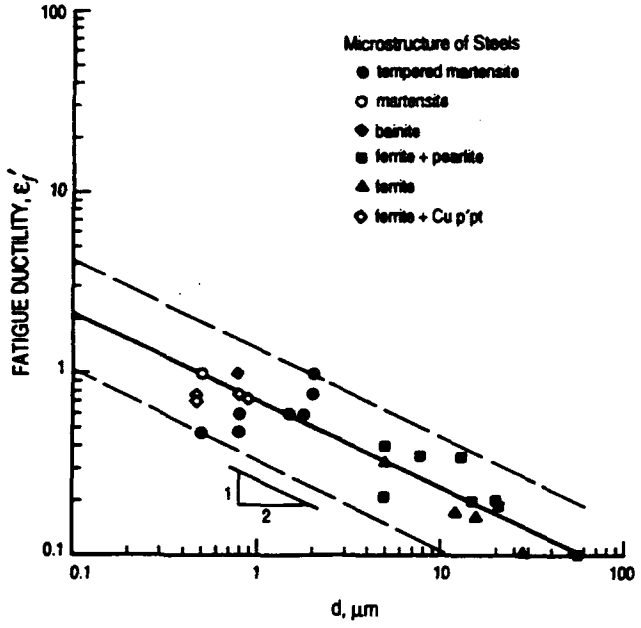

Fig. 14 — Dependence of fatigue ductility on dislocation barrier spacing, d.

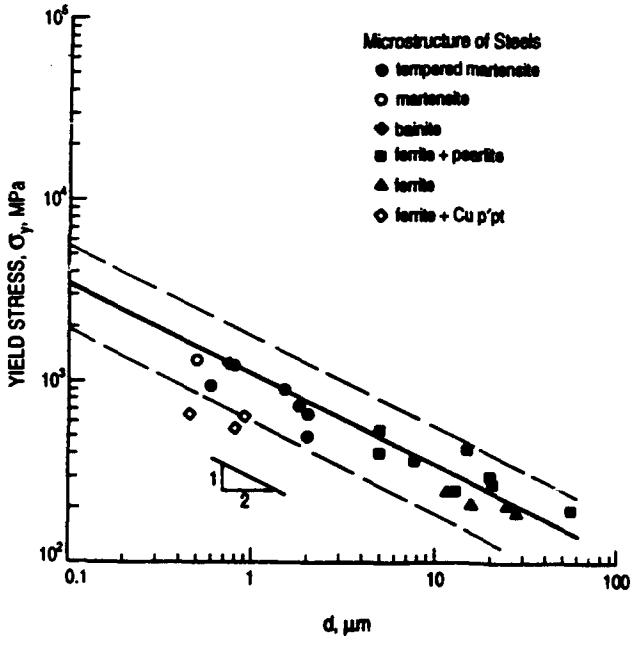

Fig. 13 — Dependence of yield stress on dislocation barrier spacing, d.

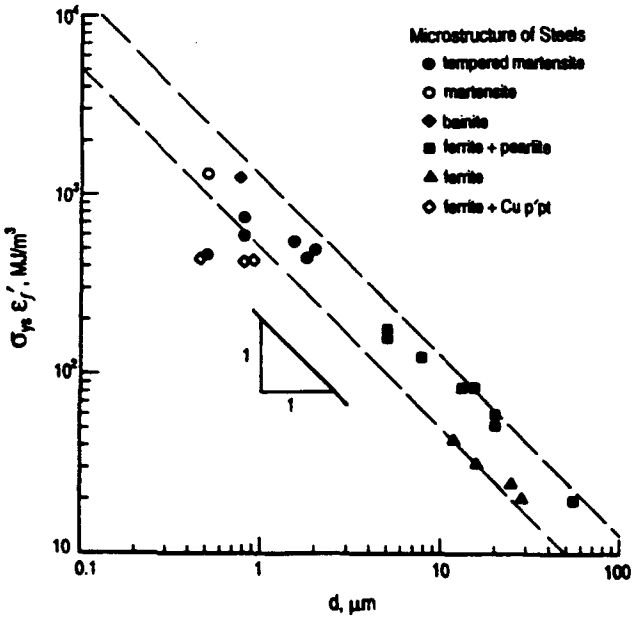

Fig. 15 — Dependence of $\sigma_y\varepsilon_f'$ on dislocation barrier spacing, d.

steel containing a high Nb content,[59] but are larger than $\varepsilon_f' = 0.20$ to 0.24 for low-Nb HSLA steels.[59] These values of ε_f' (0.71 to 0.75) for HSLA-80 steels are ≈54 pct of the true fracture strain values calculated on the basis of $\varepsilon_f = \ln (1 - RA)^{-1}$. This ratio of ε_f' to ε_f is consistent with the experimental data compiled by Ong.[60] Some of the ε_f' values (A36, A537, A533B, 1020, and low-carbon steels) were obtained by fitting the model to the crack growth data. Those results are therefore not an independent verification of the model. For the two cast steels, a value of $\varepsilon_f' = 0.20$ was required to obtain good agreement between model and experiment. The reported values for these two cast steels were ≈0.35 to 0.40.[49,50] As indicated earlier, the discrepancies might be attributed to differences in the size of the crack-tip element and the conventional LCF specimen or to inadequacies of the model. Overall, the ε_f' value for the steels examined ranges from 0.1 to 1, which is within the experimental range.[40,41]

The use of static yield strength, σ_y, instead of its cyclic counterpart, σ_y', may introduce errors in the calculated crack growth rate. A review of published values for σ_y and σ_y'[40] indicates that σ_y' can be as low as $0.6\sigma_y$ for cyclically softened steels and can be as high as $2.8\sigma_y$ for cyclically hardened steels. Using an average value of $b = 0.6$, this range of σ_y' values ($\sigma_y' = 0.6\sigma_y$ to $2.8\sigma_y$) leads to variations in fatigue crack growth rate of about −36 and +46 pct, respectively. These errors for the worst-case situations are considered reasonable, since experimental fatigue crack growth rate data can vary by a factor of 2. In most cases, σ_y differs from σ_y' by about 20 pct. This leads to a potential error of about ±14 pct in the fatigue crack growth rate, which is considered negligible.

B. *Comparison with Previous Crack-Growth Models*

As indicated earlier, the microstructure-based model yields a crack growth equation that is identical to the continuum growth model of Rice.[7] The main difference between the two models is that in the microstructure-based model, the dimensionless parameter, ϕ, depends on microstructure-sensitive parameters as defined by Eq. [17], while ϕ is assumed to be 1/2 in the continuum model. Figure 16 shows that the values of ϕ observed in the steels examined range from 0.02 to 0.3, with ϕ increasing with decreasing values of d/s. Interestingly, the value of ϕ extrapolates to 1/2 at the limit of $d/s = 1$. Since d relates ΔCTOD to $\Delta\varepsilon_{tip}^{p}$ (Eq. [10]), the fatigue crack growth rate is directly related to how the ΔCTOD is accommodated by the cyclic plastic flow within the crack-tip element, whose dimensions correspond to characteristic features of the fatigue microstructure.

One form of the present model (Eq. [15]) firmly establishes that the experimental correlation between da/dN and $\Delta K/E$ (Eq. [5]) is indeed relevant. In fact, such a correlation applies to both the continuum and intermittent growth regime, as observed experimentally.[10–13,64] Different values of C_2 observed by various investigators[10–13] in the continuum growth regime[10,11,12] can now be explained in terms of variations in yield stress, fatigue ductility coefficient, dislocation barrier spacing, and dislocation cell size, *i.e.*, the fatigue microstructure.

Figure 17 shows the values of ξ as a function of the ratio of dislocation barrier spacing to cell size, d/s, with no obvious correlation between the two parameters. Thus, Eq. [23] is essentially valid to the first order. The variation in ξ, which ranges from 4 to 25, arises mainly from different values of U_d and partly from variations in the cell size, s. The models of Frost *et al.*,[37] and Weertman[38] are of the same form described by Eq. [5] as alluded to in Section II. The scaling parameters in these models, however, are a constant approximately equal to 3, which is lower than that observed in most steels.

The parameter U_d is reminiscent of the U term in Eq. [6]. However, it should be noted that they are parameters with somewhat different physical meanings. The U_d term represents the cumulative plastic work-per-unit crack area associated with LCF fracture of a crack-tip element of height, d, and width, s (Figure 3), while U is generally measured over the length of the plastic zone.[65–68] As a result, the value of U is considerably larger than U_d. The implication is that most of the energy supplied by the external load does not go to producing an incremental crack growth. Instead, most of this expended energy goes to deform material within the crack-tip plastic zone and dissipates as heat.

Recent TEM observations have revealed that fatigue cycling of iron and steels[17,69,70] leads to the formation of dislocation subcells at low accumulated plastic strains. The dislocation subcells subsequently rearrange to form dislocation wall-like structures.[69] In both cases, the size of the dislocation subcells and the spacing between dislocation walls are generally between 0.1 to 0.2 μm.[17,69,70] The effect of continued strain cycling was to refine the dislocation cell structure by increasing the population of dislocation cells and wall spacing that is in the 0.1 to 0.2 μm range. This point is best illustrated in Figure 18, which is prepared based on TEM micrographs of Keller

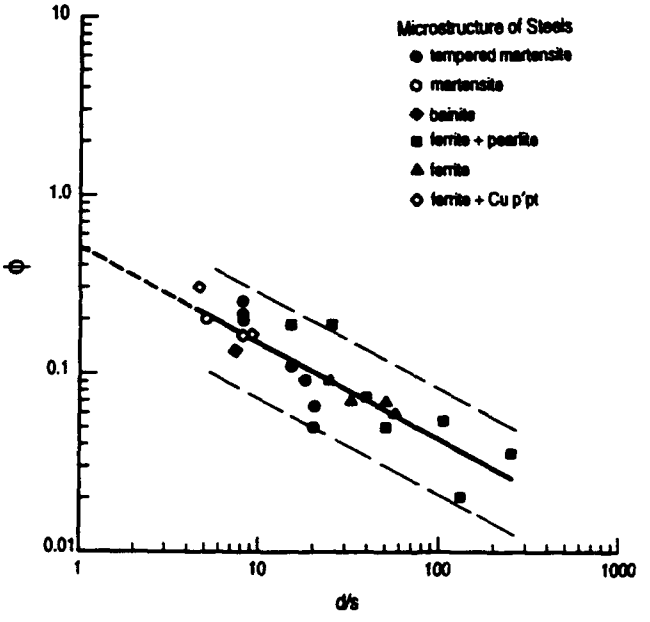

Fig. 16—The dependence of the dimensionless microstructural parameter, $\phi = s/(\varepsilon_f' d)$, on the ratio of dislocation barrier spacing to dislocation cell size, d/s.

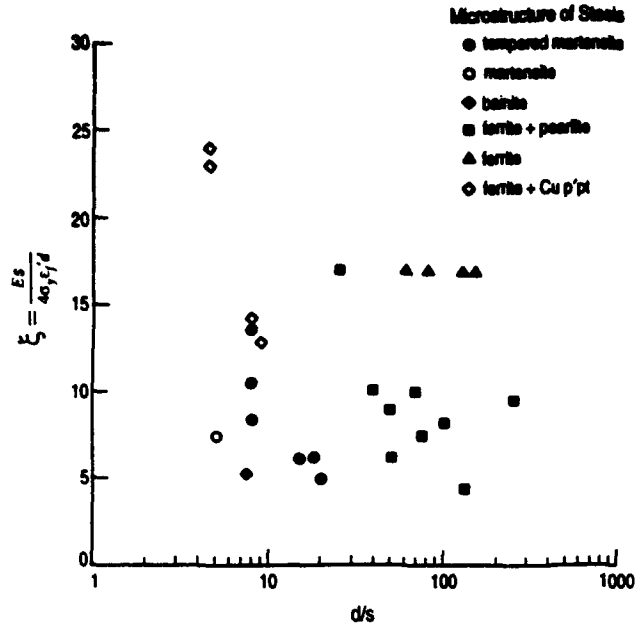

Fig. 17—The lack of dependence of the dimensionless microstructural parameter, $\xi = Es/\sigma_y\varepsilon_f'd$, on the ratio of dislocation barrier spacing to dislocation cell size, d/s.

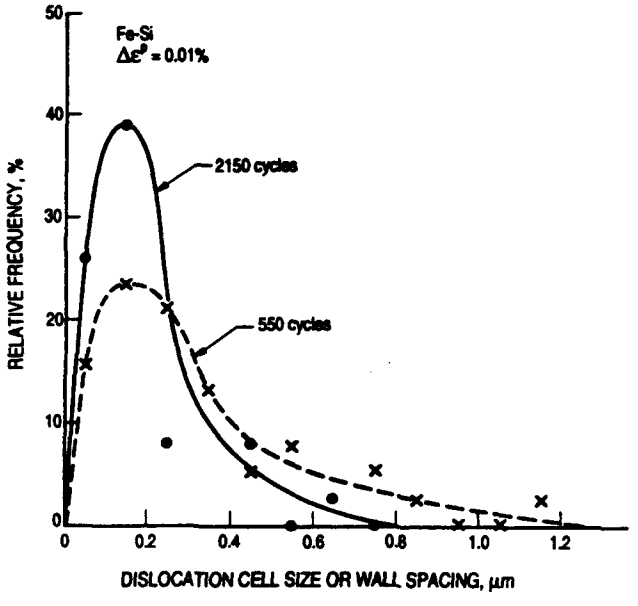

Fig. 18—Distribution of dislocation cell size showing refinement of cell size with increasing fatigue cycles. Based on results of Keller *et al.*[69]

et al.[69] showing dislocation structures in the interior of fatigue specimens of a Fe-Si alloy. The dislocation cell size near a crack tip in iron has also been shown by Katagiri *et al.* to be about 0.1 to 0.2 μm.[71] Additionally, the dislocation cell size increases with increasing distance from the crack tip.[71] Taken together, these TEM observations suggest most of the cyclic plastic work, U, is expended into refining the dislocation structure within the crack-tip plastic zone, probably *via* dislocation mechanisms as suggested by Kuhlmann-Wilsdorf and Laird[72] and Laird *et al.*[73] The smallest size that a dislocation cellular element can attain is about $s \times d$, with $s \approx 0.1$ to 0.2 μm. Further refining of this element size might be impossible, and attempts to do so would lead to LCF failure of the cellular element, producing an incremental growth of length, s, at an energy expenditure of U_d.

The present model is quite similar to that of Antolovich *et al.*[122] The essential difference between the two models is that the role of the dislocation cell size, s, and dislocation barrier spacing, d, is considered in the former model, while only the dislocation cell size is considered in the latter model. The model of Antolovich *et al.*[122] can be expressed in a form similar to Eq. [12], resulting in a scaling parameter that is a function of $E/(\sigma_y\varepsilon_f')$ but is otherwise independent of an explicit microstructural length parameter.

The proposed model is conceptually similar to that of Davidson[123] and is essentially identical to that of Roven and Nes,[17] with the exception of a factor of 1/4 in the ΔCTOD and ΔK relation (Eq. [17]). The model of Roven and Nes is expressed in terms of ΔK_{eff}, while ΔK is used in the present model. As shown in Figures 10 and 11, the different use of the crack driving force parameter results in a small change in the fatigue ductility exponent, b, and has no effect on the dimensionless ξ parameter that scales da/dN with either ΔK or ΔK_{eff}. The value of b ranges from 0.5 to 0.75 in the intermittent growth regime, compared to the range of 0.39 to 0.77 observed for a wide range of steels.[40,41] Thus, the b values derived from the crack growth data are reasonable. However, for materials such as stainless steels[74] whose crack growth exponent is about 6 to 8, the proposed model would have some difficulties unless b values as low as 0.25 to 0.3 are allowed. It should also be noted that the proposed model is difficult to apply to microstructures whose dislocation barriers are not obvious, for example, ferritic[46] or austenitic steels[74] with very large grain size (>100 μm) or single-crystal alloys. Under these circumstances, the dislocation barrier spacing, d, is obviously not the grain size, as the cyclic plastic zone is embedded well within a single grain. As a result, another characteristic length, which might well be related to the underlying dislocation structure, should be used for d. It is envisioned that the proposed scaling laws can be readily extended to materials that do not form cellular dislocation structures (*e.g.*, planar slip materials) by relating the dimensions (s and d) of the crack-tip LCF element to appropriate microstructural length dimensions. Identification of the proper dislocation barrier spacing and crack extension distance for these materials, however, might not be an easy task.

VI. CONCLUSIONS

1. The effects of microstructure on fatigue crack growth in the power-law regime can be described entirely in terms of a dimensionless microstructure parameter, ξ, defined in terms of yield stress, fatigue ductility, dislocation cell size, and dislocation barrier spacing. For both intermittent and continuum crack growth, the crack extension rate, da/dN, scales with ξ and

$(\Delta K/E)^m$, where ΔK is the stress intensity range, m is the crack growth exponent, and E is Young's modulus.

2. The lack of a strong microstructural influence on fatigue crack growth in the power-law regime of steels is due to increasing yield stress and fatigue ductility coefficient with decreasing dislocation barrier spacing, which results in a narrow range of ξ values and crack growth rates. The value of ξ ranges from 4 to 24 for the steels examined.
3. In the continuum growth regime, the crack growth rate is a small fraction of the cyclic crack-tip opening displacement. The scaling constant between da/dN and ΔCTOD is a dimensionless microstructural parameter, ϕ, which is the ratio of dislocation cell size to the product of dislocation barrier spacing and fatigue ductility. The value of ϕ ranges from 0.02 to 0.3 for the steels examined.
4. Variation of da/dN data among HSLA-80 steel specimens is partly due to variations in the mean free path of ε-Cu precipitates, yield stress, and fatigue ductility among individual specimens.
5. The change in the crack growth exponent from 4 to 2 with increasing ΔK levels in HSLA-80 steels is due to the transition from an intermittent growth mechanism to a continuum growth process. The striation spacing is on the order of the dislocation cell size (0.1 to 0.2 μm) and is relatively constant during intermittent growth. The striation spacing is considerably larger and increases with increasing ΔK during continuum growth.

ACKNOWLEDGMENTS

This work was supported by the Office of Naval Research through ONR Contract No. N00014-91-C-0214. The encouragement by Program Monitor, Dr. A.K. Vasudevan, is acknowledged. The author is also thankful to Dr. R.J. Dexter, ATLSS Center, Lehigh University, for supplying HSLA-80 data and tested specimens and to Dr. T.M. Scoonover at NAWC for supplying the GAH and FZZ specimens. Technical assistance by Dr. Y.-M. Pan (SwRI) with the TEM and Mr. J. Campbell (SwRI) with the SEM is acknowledged. The author is thankful to Drs. D.L. Davidson and R.C. McClung, both at SwRI, for their constructive comments and to Ms. J.A. McCombs for typing the manuscript.

REFERENCES

1. R.O. Ritchie: *Int. Met. Rev.*, 1979, vol. 24, pp. 205-30.
2. S. Suresh: *Fatigue of Materials*, Cambridge University Press, London, 1991.
3. D.L. Davidson and J. Lankford: *Int. Met. Rev.*, 1992, vol. 37, pp. 45-76.
4. *Fatigue and Microstructure*, M. Meshii, ed., ASM, Metals Park, OH, 1979.
5. P.C. Paris and F. Erdogan: *J. Basic Eng. Trans. ASME, Ser. D*, 1963, vol. 85, pp. 528-34.
6. R.W. Lardner: *Phil. Mag.*, 1968, vol. 17, pp. 71-82.
7. J.R. Rice: in *Fatigue Crack Propagation*, ASTM STP 415, ASTM, Philadelphia, PA, 1967, pp. 247-311.
8. J. Weertman: in *Fatigue and Microstructure*, M. Meshii, ed., ASM, Metals Park, OH, 1979, pp. 279-306.
9. P.E. Irving and L.N. McCartney: *Met. Sci.*, 1977, vol. 11, pp. 351-61.
10. R.J. Donahue, H.M. Clark, P. Atanmo, R. Kumble, and A.J. McEvily: *Int. J. Fracture Mech.*, 1972, vol. 8, pp. 209-19.
11. R.C. Bates and W.G. Clark, Jr.: *Trans. ASM*, 1969, vol. 62, pp. 380-89.
12. G.T. Hahn, R.G. Hoagland, and A.R. Rosenfield: AF33615-70-C-1630, Battelle Memorial Institute, Columbus, OH, 1971, Aug.
13. M.O. Speidel: in *High-Temperature Materials in Gas Turbines*, P.R. Sahm and M.O. Speidel, eds., Elsevier Scientific Publishers, Amsterdam, Holland, 1974, pp. 207-51.
14. D.P. Wilhem: in *Fatigue Crack Propagation*, ASTM STP 415, ASTM, Philadelphia, PA, 1967, pp. 363-83.
15. N.M. Grinberg: *Int. J. Fatigue*, 1984, vol. 6, pp. 229-42.
16. H.J. Roven, M.A. Langøy, and E. Nes: in *Fatigue '87*, R.O. Ritchie and E.A. Starke, eds., Engineering Materials Advisory Services, Warley, United Kingdom, 1987, vol. 1, pp. 175-84.
17. H.J. Roven and E. Nes: *Acta Metall. Mater.*, 1991, vol. 39, pp. 1735-54.
18. S. Majumdar and J. Morrow: in *Fracture Toughness and Slow-Stable Cracking*, ASTM STP 559, ASTM, Philadelphia, PA, 1974, pp. 159-82.
19. S.B. Chakrabortty: *Fatigue Eng. Mat. Struct.*, 1979, vol. 2, pp. 331-44.
20. J. Lanteigne and J.-P. Baïlon: *Metall. Trans.*, 1981, vol. 12A, pp. 459-66.
21. G.R. Chanani, S.D. Antolovich, and W.W. Gerberich: *Metall. Trans.*, 1972, vol. 3, pp. 2661-72.
22. S.D. Antolovich, A. Saxena, and G.R. Chanani: *Eng. Fract. Mech.*, 1975, vol. 7, pp. 649-52.
23. D.L. Davidson: *Acta Metall.*, 1984, vol. 32, pp. 707-14.
24. D. Kujawski and F. Ellyin: *Eng. Fract. Mech.*, 1984, vol. 20, pp. 695-704.
25. P.K. Mazumdar: *Acta Metall.*, 1986, vol. 34, pp. 2487-92.
26. E.A. Starke, Jr., F.S. Lin, R.T. Chen, and H.C. Heikkenen: in *Fatigue Crack Growth Threshold Concepts*, D.L. Davidson and S. Suresh, eds., TMS-AIME, Warrendale, PA, 1984, pp. 43-61.
27. L.F. Coffin, Jr.: *Trans. ASME*, 1954, vol. 76, pp. 931-50.
28. S.S. Manson and M.H. Hirschberg: in *Fatigue: An Interdisciplinary Approach*, Syracuse University Press, Syracuse, NY, 1964, pp. 133-78.
29. T.W. Montemarano, B.P. Sack, J.P. Gudas, M.G. Vassilaros, and H.H. Vanderveldt: *J. Ship Prod.*, 1986, vol. 2, pp. 145-62.
30. *1987 Annual Book of ASTM Standards*, ASTM A710/A710M-85a, 1987, vol. 01.04, ASTM, Philadelphia, PA, p. 664.
31. A.D. Wilson, C.R. Roper, Jr., and E.G. Hamburg: SAE Paper No. 870790, 1988, pp. 2.1127-2.1146.
32. R.J. Jesseman and G.J. Murphy: *J. Heat Treating*, 1984, vol. 3 (3), pp. 228-36.
33. G.R. Speich and T.M. Scoonover: in *Processing, Microstructure, and Properties of HSLA Steels*, A.J. DeArdo, ed., TMS-AIME, Warrendale, PA, 1988, pp. 265-87.
34. M.T. Miglin, J.P. Hirth, A.R. Rosenfield, and W.A.T. Clark: *Metall. Trans.*, 1986, vol. 17A, pp. 791-98.
35. K.S. Chan, D.L. Davidson, and R.C. McClung: "Microstructure-Based Fatigue Life Prediction Methods for Naval Steel Structures," First Annual Report, ONR Contract No. N00014-91-C-0214, Southwest Research Institute, San Antonio, TX, July 1992.
36. F.A. McClintock: *Fracture of Solids*, D.C. Drucker and J.J. Gilman, eds., John Wiley, New York, NY, 1963, pp. 65-102.
37. N.E. Frost, K.J. Marsh, and L.P. Pook: *Metal Fatigue*, Clarendon Press, Oxford, 1974, p. 235.
38. J. Weertman: in *Mechanics of Fatigue*, ASME, New York, NY, 1981, vol. 47, pp. 11-19.
39. T. Mura and C.T. Lin: *Int. J. Fract.*, 1974, vol. 10, pp. 284-87.
40. R.W. Hertzberg: *Deformation and Fracture Mechanics of Engineering Materials*, John Wiley & Sons, New York, NY, 1976, pp. 448-51.
41. B. Boardman: in *ASM Metals Handbook*, 10th ed., ASM, Metals Park, OH, 1990, vol. 1, pp. 673-88.
42. T.W. Montemarano, R.T. Brenna, T.E. Caton, D.A. Davis, R.L. McCaw, L.J. Roberson, T.M. Scoonover, and R.J. Wong: DTNSRDC TM-28-84-17, David W. Taylor Naval Ship Research and Development Center, 1984.
43. J.A. Todd, P. Li, G. Lin, and V. Ramon: *Scripta Metall.*, 1988, vol. 22, pp. 745-50.
44. L.R. Link: in *Fatigue and Fracture Testing of Weldments*, ASTM

STP 1058, H.I. McHenry and J.M. Potter, eds., ASTM, Philadelphia, PA, 1990, pp. 16-33.
45. R.J. Dexter: Lehigh University, Bethlehem, PA, unpublished research, 1993.
46. T. Yokobori, I. Kawada, and H. Hata: in *Reports of Research Institute for Strength and Fracture of Materials*, Tohoku University, Sendai, Japan, 1973, vol. 9(2), pp. 35-64.
47. S. Taira, K. Tanaka, and M. Hoshina: in *Fatigue Mechanisms*, ASTM STP 675, ASTM, Philadelphia, PA, 1979, pp. 135-162.
48. J.M. Barsom: *Trans. ASME, Ser. B, J. Eng. Ind.*, 1971, vol. 93, pp. 1190-96.
49. R.I. Stephens, J.H. Chung, S.G. Lee, H.W. Lee, A. Fatemi, and C. Vacas-Oleas: in *Fatigue at Low Temperatures*, ASTM 857, R.I. Stephens, ed., ASTM, Philadelphia, PA, 1985, pp. 140-60.
50. R.I. Stephens: in *Fatigue Life: Analysis and Prediction*, V.S. Goel, ed., ASM, Metals Park, OH, 1986, pp. 69-77.
51. P.E. Bretz, B.L. Braglia, and R.W. Hertzberg: in *Weldments: Physical Metallurgy and Failure Phenomena*, Proc. 5th Bolton Landing Conf., R.J. Christoffel, E.F. Nippes, and H.D. Solomon, eds., General Electric Company, Schenectady, NY, 1979, pp. 271-83.
52. R.W. Hertzberg and R.H. Goodenow: in *Microalloying '75*, Union Carbide Corp., Niagara Falls, NY, 1981, pp. 503-16.
53. J.M. Barsom, E.J. Imhof, and S.T. Rolfe: *Eng. Fract. Mech.*, 1971, vol. 2, pp. 301-17.
54. M. Parry, H. Nordberg, and R.W. Hertzberg: *Weld. J.* 1972, vol. 51 (2), pp. 485-90.
55. M.F. Carlson and R.O. Ritchie: *Scripta Metall.*, 1977, vol. 11 (12), pp. 1113-18.
56. E.J. Imhof and J.M. Barsom: in *Progress in Flaw Growth and Fracture Toughness Testing*, ASTM STP 536, ASTM, Philadelphia, PA, 1973, pp. 182-205.
57. M.E. Fine and R.O. Ritchie: in *Fatigue and Microstructure*, M. Meshii, ed., ASM, Metals Park, OH, 1979, pp. 245-78.
58. J. Gurland: in *Stereology and Quantitative Metallography*, ASTM STP 504, ASTM, Philadelphia, PA, 1972, pp. 108-18.
59. Y.H. Kim and M.E. Fine: *Metall. Trans.*, 1982, vol. 13A, pp. 59-72.
60. J.H. Ong: *Int. J. Fatigue*, 1993, vol. 15, pp. 13-19.
61. G.R. Yoder, L.A. Cooley, and T.W. Crooker: in *Fracture Mechanics: 14th Symp.—Vol. I: Theory and Analysis*, ASTM STP 791, J.C. Lewis and G. Sines, eds., ASTM, Philadelphia, PA, 1983, pp. I-348-I-365.
62. E.O. Hall: *Proc. Phys. Soc., London, Sect. B*, 1951, vol. 64, pp. 747-53.
63. M.J. Petch: *J. Iron Steel Inst.*, 1953, vol. 174, pp. 25-28.
64. S. Pearson: *Nature*, 1966, vol. 211, pp. 1077-78.
65. S. Ikeda, Y. Izumi, and M.E. Fine: *Eng. Fract. Mech.*, 1977, vol. 9, pp. 123-36.
66. P.K. Liaw, M.E. Fine, and D.L. Davidson: *Fatigue Eng. Mat. Struct.*, 1980, vol. 3, pp. 59-74.
67. P.K. Liaw, S.I. Kwun, and M.E. Fine: *Metall. Trans. A*, 1981, vol. 12A, pp. 49-55.
68. P.K. Liaw: *Eng. Fract. Mech.*, 1985, vol. 22, pp. 237-45.
69. R.R. Keller, W. Zielinski, and W.W. Gerberich: *Scripta Metall. Mater.*, 1992, vol. 26, pp. 1523-28.
70. W.J. Bartina, M. Aziza, A.C. Rinella, and S. Yue: in *HSLA Steels: Metallurgy and Applications*, ASM, Metals Park, OH, 1986, pp. 763-70.
71. K. Katagiri, J. Awatani, A. Omura, K. Koyanagi, and T. Shiraishi: in *Fatigue Mechanisms*, J.T. Fong, ed., ASTM STP 675, ASTM, Philadelphia, PA, 1979, pp. 106-28.
72. D. Kuhlmann-Wilsdorf and C. Laird: *Mater. Sci. Eng.*, 197[illegible], vol. 27, pp. 137-56.
73. C. Laird, P. Charsley, and H. Mughrabi: *Mater. Sci. Eng.*, 1986, vol. 81, pp. 433-50.
74. A.W. Thompson: *Eng. Fract. Mech.*, 1975, vol. 7, pp. 61-68.
75. K.D. Challenger, R.B. Brucker, W.M. Elger, and M.J. Sorek: *Weld. Res. Suppl.*, 1984, Aug. pp. 254-S-262-S.
76. M.F. Carlson, B.V. Narasimha Rao, and G. Thomas: *Metall. Trans. A*, 1979, vol. 10A, pp. 1273-84.
77. *Metals Handbook*, 8th ed., ASM, Metals Park, OH, 1972, vol. 7.

APPENDIX C

"A Scaling Law for Fatigue Crack Initiation in Steels"

K. S. Chan

To appear in *Scripta Metallurgica et Materialia*

A SCALING LAW FOR FATIGUE CRACK INITIATION IN STEELS

Kwai S. Chan
Southwest Research Institute
San Antonio, TX 78238

Introduction

The beneficial effect of a fine grain size on crack initiation and low-cycle fatigue (LCF) life is well known (Previous studies have shown that the cycle to failure in many alloys is increased with decreasing grain or microstructu unit size (1). Despite this qualitative understanding, a quantitative description of the dependence of LCF life microstructural unit size does not appear available in the literature. Because of this, how crack initiation or LCF life sca with microstructural unit size remains an open question.

The objective of this article is to propose a scaling law for treating fatigue crack initiation and LCF failure metals or alloys. In particular, the dependence of crack initiation or LCF life on microstructural unit size scale quantified. Evaluation of the scaling law against experimental LCF data for a number of steels is presented. While m of the experimental data were obtained from the literature, LCF data for a Cu-bearing HSLA steel, whose fatigue cra growth behavior is controlled by ε-Cu precipitates in the nanometer size range, was also generated for the purpose verifying the proposed model. Finally, the different roles of microstructural unit size on fatigue crack initiation a growth are elucidated and discussed.

The Proposed Model

In a recent paper by the author (2), a set of scaling laws was proposed for describing fatigue crack grow responses of large cracks in the continuum and intermittent growth regimes of steels. The scaling laws have be developed on the basis of a crack-tip element whose failure is described in terms of the Coffin-Manson relation (3, Like the crack growth model, the starting point of the scaling law for fatigue crack initiation is also based on t Coffin-Manson relation given by (3,4)

$$\frac{\Delta\varepsilon^p}{2} = \varepsilon_f'(2N_i)^{-b} \qquad (1)$$

where $\Delta\varepsilon^p$ is the plastic strain range, $2N_i$ is the reversal to failure by crack initiation, ε_f' is the fatigue ductility coefficie and b is the fatigue ductility exponent. Eq. (1) is written such that b is positive, while the fatigue ductility exponent generally given as a negative quantity in the literature.

In recent studies (2,5), the fatigue ductility coefficients for steels (2) and Ti alloys (5) were found to depend the dislocation barrier spacing according to a modified Hall-Petch relation (6,7)

$$\varepsilon_f' = \varepsilon_o'\left(\frac{d_o}{d}\right)^{\frac{1}{2}} \qquad (2)$$

where ε_o' is the fatigue ductility coefficient at the reference dislocation barrier spacing, d_o. Combining Eq. (2) wit Eq. (1) leads one to

$$\frac{\Delta\varepsilon^p}{2} = \varepsilon_o' \left(\frac{d_o}{d}\right)^{\frac{1}{2}} (2N_i)^{-b} \quad (3$$

which can be rearranged to give

$$N_i = C_i \left(\frac{d_o}{d}\right)^{\frac{1}{2b}} \quad (4$$

with

$$C_i = \frac{1}{2}\left(\frac{2\varepsilon'_o}{\Delta\varepsilon^p}\right)^{\frac{1}{b}} \quad (5$$

for relating the fatigue crack initiation (or LCF) life explicitly to the dislocation barrier spacing, d.

Comparison of Model and Experiment

The material parameters in the proposed model include ε_o', d_o, and b. Previous work (2) has determined tha $\varepsilon_o' = 0.75$ at $d_o = 1$ μm for steels, while the value of b ranges from 0.5 to 0.8. The dislocation barrier spacing for variou steels has been reported earlier (2), and the results are summarized in Table 1. These d and b values were used as inpu to the proposed model to compute the LCF curves.

Comparisons of the experimental and calculated LCF curves for 4340 (8) and 0030 (9) cast steels are presented in Figures 1(a) and (b), respectively. Similar comparisons of model calculations and experimental data for Nb-bearing (10) and V-bearing (11) HSLA steels are shown, respectively, in Figures 1(c) and (d). In all cases, agreement between model and experiment was excellent.

Steel	d, μm	b
4340	0.8	0.6
0030	20	0.5
005A	15	0.5
HSLA-80	0.89	0.50
Nb-HSLA (400-5H)	9.5	0.54
Nb-HSLA (hot-rolled)	1.0	0.58
Nb-HSLA (annealed)	9.5	0.58
VAN-80	2	0.58

TABLE 1. Values of dislocation barrier, d, and fatigue ductilit coefficients, b, for the various steels (2,3,9,10,13).

A comparison of model prediction and experimental data for HSLA-80 (12), a Cu-bearing HSLA steel, is presented in Figure 2. For the model calculation, the b value used was 0.5, which was previously determined based on the slope of the crack growth data. The LCF data was obtained using smooth, round bar specimens subjected to full reverse strain-controlled cycles. The value of ε_f obtained for the HSLA-80 steel was 0.73, which was identical to the on predicted from Eq. (2) using the appropriate value for the dislocation barrier spacing, d = 8.9 μm (2). At a given plast strain range, the experimental LCF life was slightly less than that calculated from the model, as shown in Figure 2. Th observed value of the fatigue ductility exponent, b, was 0.65, compared to b = 0.5 used in the model calculatio Metallographic examination revealed that fatigue crack initiation in the HSLA-80 steel generally occurred at sulfic inclusions (12). This observation suggests that crack initiation at inclusions might have reduced the N_i values and led an apparent increase in the observed b value.

At a given plastic strain range, the number of reversals to failure, $2N_f(=2N_i)$, is predicted to decrease wi increasing dislocation barrier spacing. A comparison of this model prediction with experimental data for several stee is shown in Figure 3 for $\Delta\varepsilon^p = 0.02$. Since the fatigue ductility exponent, b, ranges from 0.5 to 0.65 for these steel calculated curves for b values of 0.5, 0.55, and 0.65 are shown in the figure. All of the experimental data show go

agreement with the calculated curves and lie within the upper and lower bounds that correspond to the curves for b values of 0.5 and 0.65, respectively. Figure 3 also shows that the observed number of reversals to crack initiation, $2N_i$, decreases with increasing dislocation barrier spacing, in accordance with the proposed model.

Discussion

The result of this investigation demonstrated that within experimental scatter, the cycle-to-crack initiation, N_i, decreases with increasing dislocation barrier spacing, d, according to the power law of Eq. (4), whose exponent to the microstructural size parameter, d, is $-\frac{1}{2b}$. Additionally, the LCF result for HSLA-80 steel indicated that the presence of inclusions in the microstructure reduced the N_i values at various plastic strain ranges by different amounts, leading to an increase in the observed value for the fatigue ductility exponent, b. Thus, the fatigue ductility coefficient, b, appears to depend on the inclusion content.

In previous papers (2,5), the scaling law for fatigue crack growth in steels (2) and Ti-base alloys (5) was found to be (5)

$$\frac{da}{dN} = \left[\frac{d}{d_o}\right]^{\frac{\alpha+\beta-1}{b}} \left\{\xi_o^{1/b} (2s)^{1-1/b} \left[\frac{\Delta K}{E}\right]^{2/b}\right\} \tag{6}$$

with

$$\xi_o = \frac{Es}{4\sigma_o \varepsilon_o' d_o} \tag{7}$$

where E is Young's modulus; s is the striation spacing (crack jump distance); σ_o is the yield stress at the reference dislocation barrier spacing, d_o (d_o = 1 μm); and α and β are exponents in the modified Hall-Petch relations for yield stress and fatigue ductility coefficients (5), respectively. Eq. (6) indicates that da/dN scales with $[d]^{\frac{\alpha+\beta-1}{b}}$, since all of the parameters within the large parenthesis in the right-hand side of Eq. (6) are independent of the dislocation barrier spacing, d.

The crack growth life, N_g, obtained by integration of Eq. (6) is

$$N_g = C_g \left[\frac{d}{d_o}\right]^{\frac{1-\alpha-\beta}{b}} \tag{8}$$

where

$$C_g = \int_{a_i}^{a_f} \left\{\xi_o^{1/2} (2s)^{1-\frac{1}{b}} \left[\frac{\Delta K}{E}\right]^{\frac{2}{b}}\right\}^{-1} da \tag{9}$$

is a constant that is independent of microstructure for a given set of initial, a_i, and final, a_f, crack lengths. Crack closure effects can be incorporated into Eq. (9) by replacing ΔK with an effective ΔK.

Comparison of Eqs. (4) and (8) reveals that N_i and N_g depend on the dislocation barrier spacing in quite different ways. While $N_i \propto d^{-\frac{1}{2b}}$ and always decreases with increasing d value, $N_g \propto d^{\frac{1-\alpha+\beta}{b}}$ and may or may not increase with the dislocation barrier spacing, depending on the values α and β. For steels, α = β = 0.5 and N_g is independent of the microstructural size parameter, d. In contrast, α = 0.12 and β = 0.5 for Ti-base alloys, and N_g increases with increasing values of the microstructural size parameter, d. Thus, the microstructural unit size can lead to opposite effects on fatigue crack initiation and intrinsic crack growth resistance. This point is illustrated schematically in Figure 4, which shows log N_i decreases linearly with log(d) with a slope of $\frac{-1}{2b}$, while log N_g increases linearly with log(d) with a slope of $\frac{1-\alpha-\beta}{b}$. Since $N_f = N_i + N_g$ and both α and β have values between zero and 0.5, the log N_f - log(d) curve shows a minimum at d^*

as shown in Figure 4. The implication from the result in Figure 4 is that one can increase N_f by improving either th fatigue initiation life (N_i) or the fatigue crack growth life (N_g) through control of microstructural unit size, but one canno maximize N_f through optimizing N_i and N_g by manipulating the microstructural unit size alone.

Conclusions

1. The crack initiation life, N_i, scales inversely with the dislocation barrier spacing, d, according to $N_i \propto d^{-\frac{1}{2b}}$, where the fatigue ductility exponent, b, may depend on the inclusion content.

2. The intrinsic crack growth life, N_g, scales with the dislocation barrier spacing, d, according to $N_g \propto d^{\frac{1-\alpha-\beta}{b}}$, where α and β are exponents in the Hall-Petch relations for yield stress and fatigue ductility coefficient, respectively.

3. The microstructural unit size, d, can lead to opposite effects on fatigue crack initiation and intrinsic crack growth resistance. A minimum is present in a plot of log N_f versus log d, where N_f ($=N_i + N_g$) is the total fatigue life.

Acknowledgements

This work was supported by the Office of Naval Research through ONR Contract No. N00014-91-C-021 (Dr. A. K. Vasudevan, Program Monitor). The editorial and clerical assistance by Ms. D. J. Stowitts and Ms. J. A. McCombs, Southwest Research Institute, are appreciated.

References

1. E. A. Starke, Jr., and G. Lutjering, in **Fatigue and Microstructure**, edited by M. Meshii, p. 205, ASM, Metals Park, OH (1979).
2. K. S. Chan, **Met. Trans. A.**, 24A, 2473 (1993).
3. L. F. Coffin, Jr., **Trans. ASME**, 76, 931 (1954).
4. S. S. Manson and M. H. Hirschberg, **Fatigue: An Inter-Disciplinary Approach**, p. 133, Syracus University Press, Syracuse, NY (1964).
5. K. S. Chan, in **Proc. Harold Margolin Symposium**, TMS, Warrendale, PA, in press (1994).
6. E. O. Hall, **Proc. Phys. Soc. London**, Section B, 64, 747 (1951).
7. M. J. Petch, **J. Iron Steel Inst.**, 74, 25 (1953).
8. R. W. Landgraf, in **Achievement of High Fatigue Resistance in Metals and Alloys**, ASTM STP 467, p. 3 ASTM, Philadelphia, PA (1970).
9. R. I. Stephens, in **Fatigue Life: Analysis and Prediction**, edited by V. S. Goel, p. 69, ASM, Metals Park, OH (1986).
10. S. I. Kwun and R. A. Fournelle, **Met. Trans. A.**, 11A, 1429 (1980).
11. P. Watson and T. H. Topper, SAE Paper 710597, SAE, NY (1971).
12. D. L. Davidson and K. S. Chan, unpublished research, Southwest Research Institute, San Antonio, TX (1994).
13. David Ouesnel, Ph.D. Dissertation, Dept. of Mat. Sci. and Eng., Northwestern University (1977).

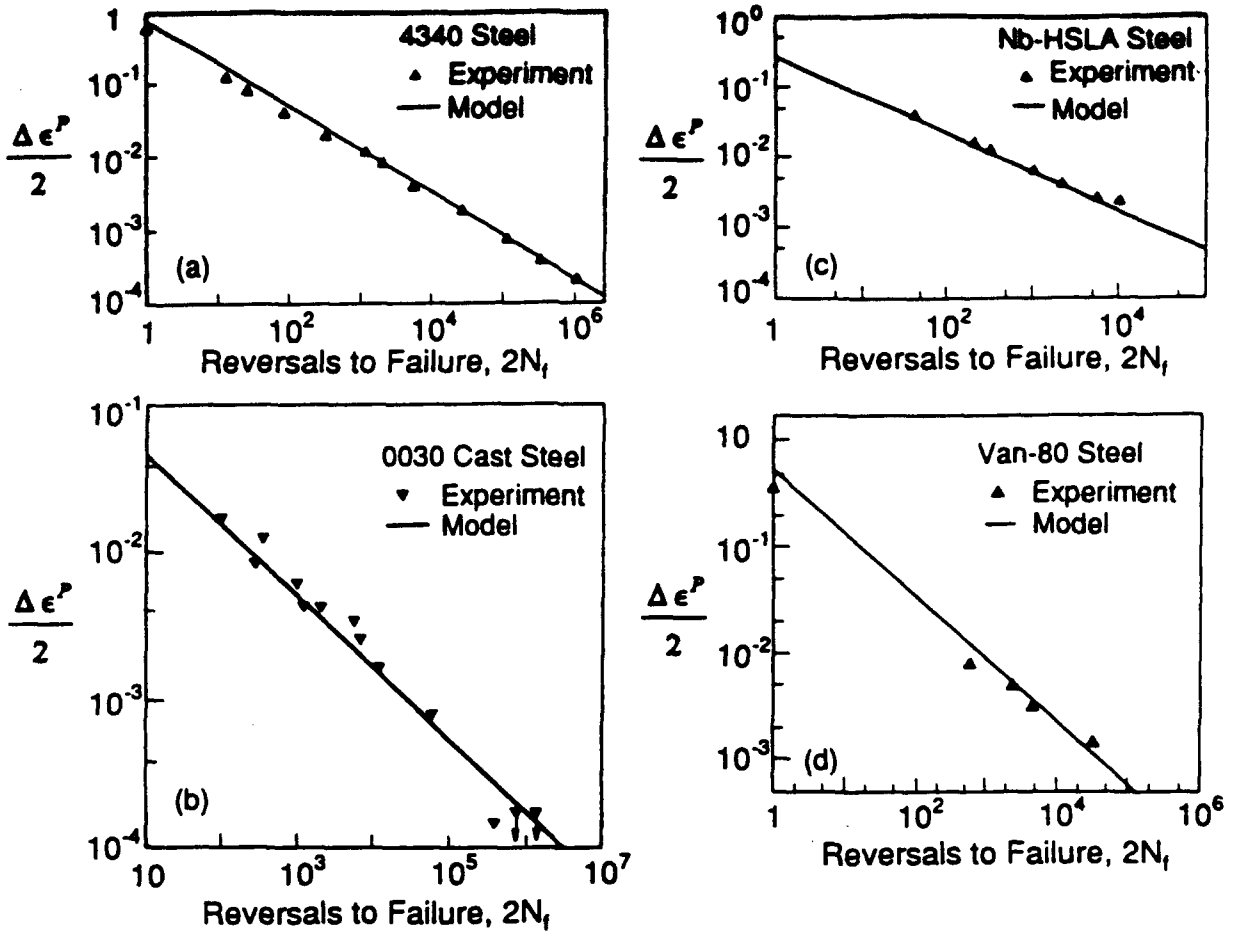

FIGURE 1. Comparison of calculated and experimental LCF curves for steels: (a) 4340 steel, (b) 0030 cast steel, (c) Nb-bearing HSLA steel, and (d) Van 80 steel.

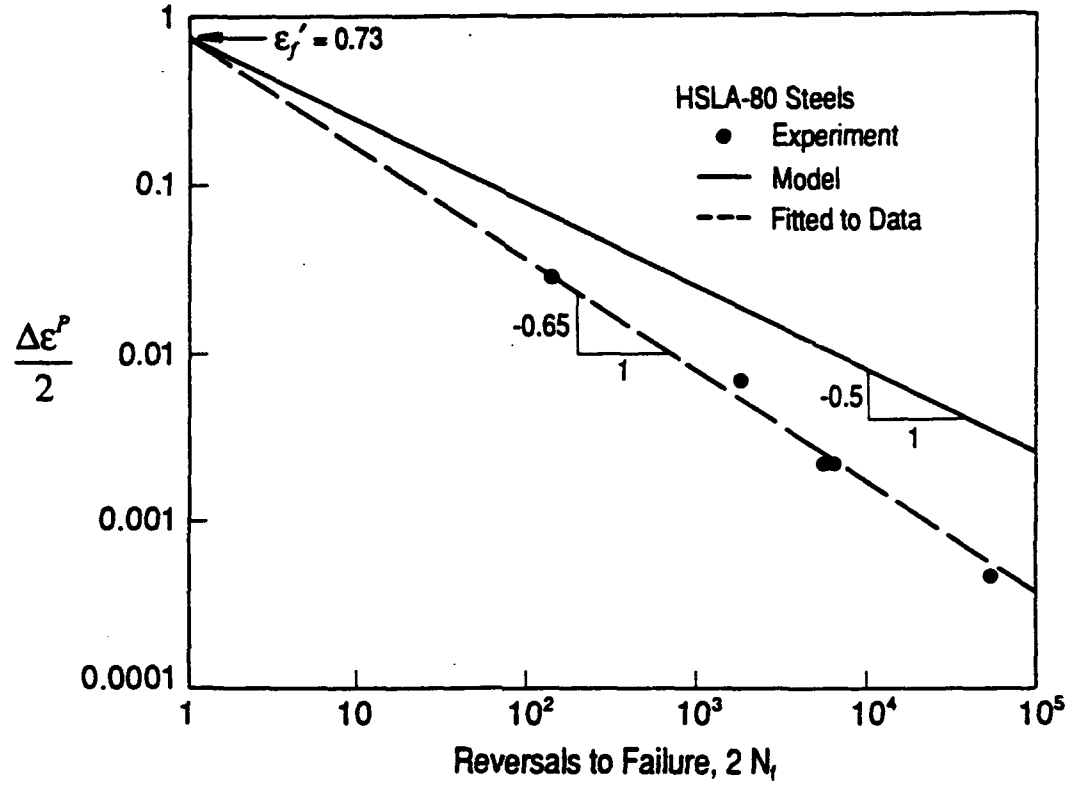

FIGURE 2. Comparison of calculated and experimental LCF curves for HSLA-80.

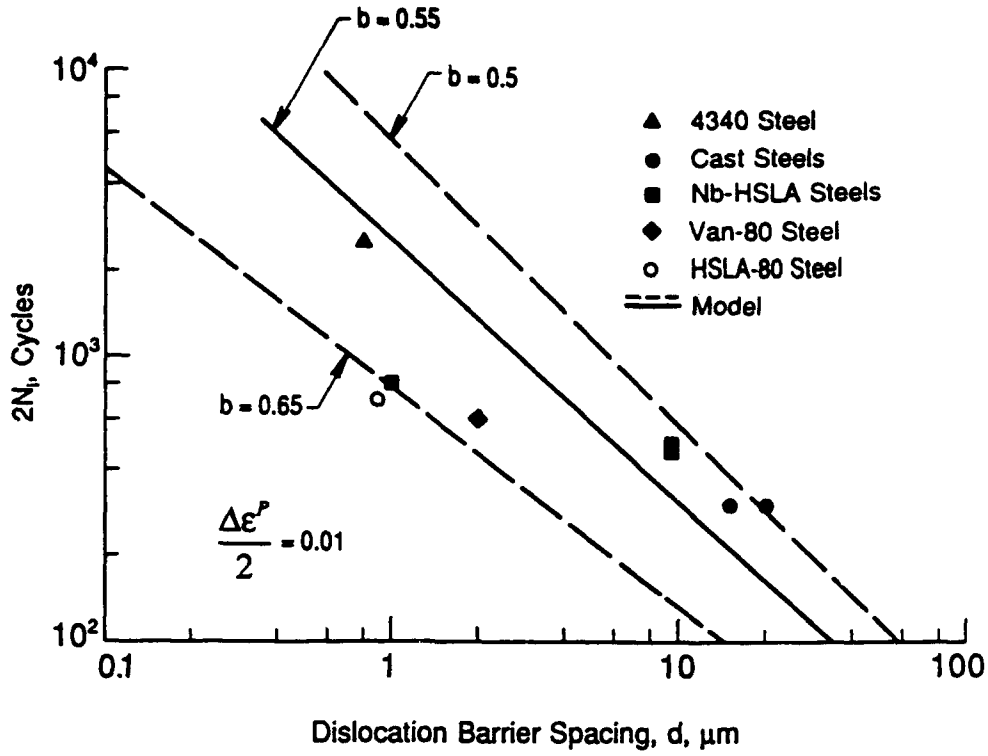

FIGURE 3. Inverse dependence of $2N_i$ on the dislocation barrier spacing, d, observed in steels and compared with model calculations.

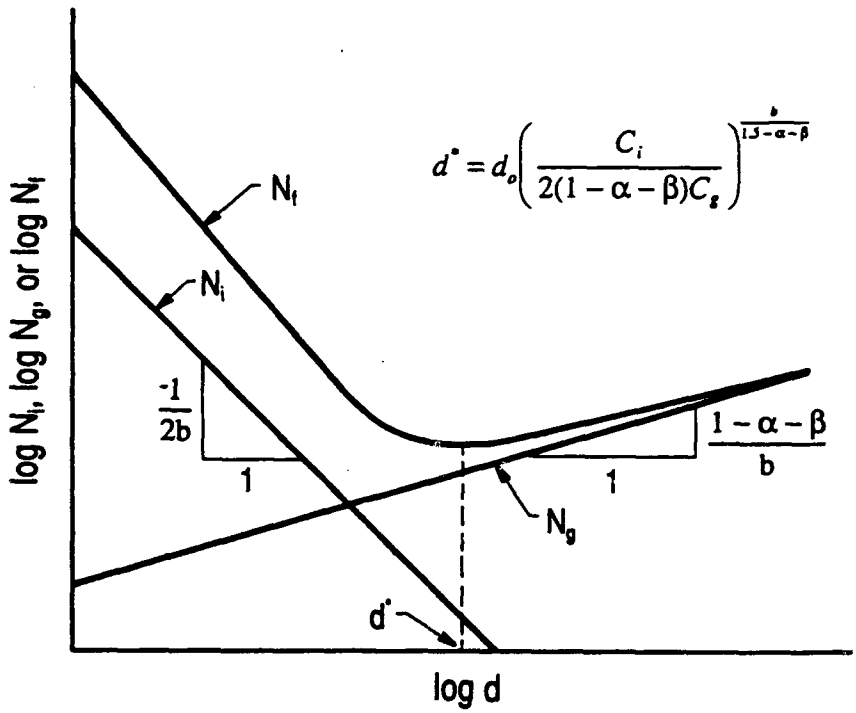

FIGURE 4. A schematic shows opposite effects of dislocation barrier spacing, d, on the crack initiation life, N_i, and crack growth life, N_g, resulting in a minimum in the total life, N_f.

APPENDIX D

"Engineering Analysis of Small Crack FCG Data and Implications for Fatigue Life Prediction"

R. C. McClung

[Selected portions of this appendix and Appendix F have been combined to develop a manuscript entitled, "Analysis of Fatigue Cracks in HSLA-80 Steel," by R. C. McClung and T. Y. Torng, to be submitted for publication]

ENGINEERING ANALYSIS OF SMALL CRACK FCG DATA AND IMPLICATIONS FOR FATIGUE LIFE PREDICTION

R. C. McClung
Southwest Research Institute

INTRODUCTION

The analysis of small fatigue cracks is becoming increasingly important for assuring the reliability of engineering structures.

Historically, fatigue design and analysis have often been based on empirical bulk damage approaches, such as stress-life (S-N) and strain-life (ε-N) methods. These methods relate applied stresses or strains directly to the total life to "failure." Although this "black box" approach is attractive for its simplicity, it is limited by its inability to characterize the progressive development of damage in terms of physically meaningful quantities (such as crack size). These limitations frequently become apparent during attempts to address more sophisticated issues such as load history or microstructural effects on fatigue life.

Another common approach to fatigue analysis is the damage tolerance methodology, which explicitly addresses fatigue crack growth (FCG) in the structure. This approach facilitates a more rigorous treatment of damage development. However, traditional damage tolerance applications have focused on the growth of relatively large cracks. Relatively large initial flaw sizes are typically assumed, usually based on the capabilities of common nondestructive evaluation (NDE) techniques.

Evolving requirements for structural performance and reliability are motivating changes to both approaches. "Safe-life" analyses based on S-N and ε-N approaches are being replaced by crack growth analyses in some applications. In the low cycle fatigue (LCF) regime, a majority of the life of a smooth fatigue specimen (which defines S-N and ε-N life) is commonly consumed by the growth of small cracks. On the other hand, small cracks are beginning to be considered more often in traditional damage tolerance applications. Motivations for these changes include improvements in NDE techniques and the increasing realization that in some situations, such as multiple-site damage in aging aircraft, small cracks can play a significant role in the reduction of damage tolerance capability.

There is no shortage of published research on small cracks available in the scientific literature. The technical community now has a reasonably comprehensive understanding of the fundamental mechanisms associated with various types of small crack growth. However, the current challenge is to develop and validate practical methodologies to analyze small crack growth for engineering structures. These methodologies will also require more rigorous fundamental treatments of applications issues such as geometry and load history effects on small cracks.

A proper understanding of the relationship between small crack and large crack growth behavior is particularly important. The small crack growth phase is often the dominant fatigue life fraction, and so accurate modeling of this regime is often of greatest significance for accurate life predictions. On the other hand, experimental FCG rate data are most often available for large cracks

(small crack tests are much more expensive to conduct) and most theoretical models for FCG behavior are derived and validated for large crack data. The scaling laws developed under the present contract, for example, were verified through extensive comparison to large crack data. In principle, these scaling laws should also be applicable to small cracks, but this requires a certain amount of similitude between small crack and large crack behavior. If small crack behavior is found to be significantly different from large crack behavior in some way, then the applicability of large crack models may be called into question.

In this appendix, small-crack FCG data for HSLA-80 steel are analyzed from a practical engineering perspective and critically compared with FCG data for large cracks. The potential use of FCG relationships to perform fatigue life predictions in the place of traditional *S-N* approaches is explored.

EXPERIMENTS

Small Cracks

Small-crack tests were performed with two different specimen designs. Beams of square cross-section 4 mm on a side by 52 mm long were loaded in 3-point bending (3PB) under nominal zero-max load cycling. Outer fiber stresses were required to exceed yield in these specimens order to initiate cracks, so the local (outer fiber) stress ratio (R) was not zero. In order to initiate cracks more easily, hourglass specimens with a minimum diameter of 0.1875 in. (4.76 mm) were loaded in rotating bending (RB), so that $R = -1$. Low stress machining and hand polishing techniques were used to minimize surface residual stresses in all specimens.

Small crack tests were conducted on the material in the as-received condition and in three alternative conditions created through additional heat treatments, plus one specimen fabricated from weld material. To eliminate possible sources of confusion, these comparisons with large crack data incorporate only the small crack tests in the as-received condition. This data base includes multiple cracks from one square beam specimen (347) and two rotating bending specimens (353 and 354). Specimen 347 experienced a total stress range of 840 MPa (122 ksi), Specimen 353 a total stress range of 1120 MPa (162 ksi), and Specimen 354 a total stress range of 1040 (151 ksi). From tensile tests conducted on the same heat of HSLA-80 at Lehigh University, the average yield strength is about 88 ksi (607 MPa) and the average ultimate strength about 99 ksi (683 MPa).

Crack growth was recorded by periodically taking acetate replicas of the specimen surface in the most highly-stressed regions. This technique made it possible to obtain FCG data from several different cracks on the same specimen. Tests were stopped when the largest cracks exceeded around 2 mm in surface length. Selected specimens were sectioned at the end of the test in order to determine typical aspect ratios for the surface cracks. Nearly all surface cracks were approximately semi-circular in shape.

Secant and second-order incremental polynomial methods were used to compute da/dN from the raw a vs. N data. The nominal stress intensity factor, ΔK, was calculated from the surface half-crack length, a, and the nominal applied stress range, $\Delta\sigma$, according to the relationship $\Delta K = 1.3\ \Delta\sigma\ (a)^{1/2}$.

Large Cracks

The available large crack data of greatest interest is presented in Figure 1. Shown here are data from four specimens tested at Lehigh University [1] on the same heat of HSLA-80 being studied at SwRI. All tests were conducted at a stress ratio of $R = 0.1$. The specimen identification codes denote tests on both TL and LT orientations from both the web and flange of a structural I-beam. The data indicate that these distinctions have relatively little influence on FCG rates; differences in growth rates between the two nominally identical F-LT tests are no smaller than the differences between different configurations. These data unfortunately do not provide direct information about near-threshold behavior. In order to evaluate this regime, independent data from Todd at IIT [2] for another heat of HSLA-80 are superimposed on the figure. The Todd data clearly agree closely with the Lehigh data in the regime where the two sets overlap, but the Todd data also establish a clearly defined large crack threshold around $\Delta K_{th} = 7.5$ MPa$\sqrt{m}$.

Least-squares regression of the combined data (all five large crack data sets) between $\Delta K =$ 9 MPa$\sqrt{m}$ and 23 MPa$\sqrt{m}$ gives a Paris law slope of 3.77. The scatterbands shown on Figure 1 represent ±2x in FCG rate.

COMPARISONS OF SMALL CRACK AND LARGE CRACK DATA

Analysis

All crack growth data for both large and small cracks are compared on the basis of the nominal full-range ΔK in Figure 2. Here the entire stress range $\Delta\sigma$ is used to calculate ΔK regardless of stress ratio. Note, first of all, that the small cracks grew at nominal ΔK values significantly lower than the large crack threshold value, ΔK_{th}, around 7.5 MPa•m$^{1/2}$ (as estimated from the Todd data). This is a commonly observed "small crack" effect. Second, note that the large and small crack data, which included widely differing stress ratios and maximum stresses, were not well-correlated by the nominal full-range ΔK. The slopes of the data appear to be generally similar, but differences in the intercepts leads to an apparent "layering" of the data, including disagreements between the two sets of small crack data.

There are several differences between the various data sets which could admit some rational basis for calculating an adjusted ΔK. The most obvious difference is that of stress ratio. The large cracks are growing at $R = 0.1$ and the rotating bending small cracks are growing at $R = -1$. The square beam small cracks are growing in a local stress field with an estimated stress ratio of about $R = -0.35$. This local stress ratio was estimated by assuming that the maximum local stress at the outer fiber was approximately equal to the yield stress due to plastic deformation at the outer fiber, but that the stress range was still equal to the full applied (elastic) outer fiber bending stress range. A more subtle difference between the different specimens which may also have some effect is that the small crack tests were conducted with maximum stresses near the yield stress, while the large crack tests were conducted at much lower stresses.

Two alternative approaches to addressing these differences have been investigated. The first approach, which is identified here as the "nominal ASTM approach," is based on the recommendations of ASTM Test Method E 647, "Standard Test Method for Measurement of Fatigue Crack Growth Rates." This test method instructs that $\Delta K = K_{max} - K_{min}$ when $R \geq 0$, but that ΔK

should be calculated according to $\Delta K = K_{max}$ when $R < 0$ (i.e., take only the tensile portion of the stress intensity factor range). For the particular tests under consideration here, we will write an appropriately "adjusted" $\Delta K_{eff} = U\Delta K$, where ΔK is always computed as $K_{max} - K_{min}$ and any stress ratio "adjustment" is expressed by the fraction U. The large crack tests have $U = 1$, the rotating bending tests have $U = 0.5$, and square beam tests have an estimated $U = 0.72$.

A second approach is based on the phenomenon of plasticity-induced crack closure. Of several different proposed mechanisms for crack closure, the development of a plastic wake and the corresponding influence on residual stress fields is thought to be the most significant outside of the near-threshold regime [3]. Several different mechanics approaches have been developed to characterize plasticity-induced closure, including simple analyses based on a modified Dugdale strip-yield model, finite element analyses, superdislocation models, and boundary element models. These different formulations are nearly unanimous in their conclusions that crack opening levels outside the near-threshold regime are, in general, a function of maximum stress, stress ratio, and stress state. Many experimental observations are available to support these theoretical projections.

The closure-corrected effective stress intensity factor range, ΔK_{eff}, is related to the nominal full-range ΔK according to $\Delta K_{eff} = U\,\Delta K$, where U is the effective stress intensity factor range ratio,

$$U = \frac{\sigma_{max} - \sigma_{open}}{\sigma_{max} - \sigma_{min}} \tag{1}$$

The specific task at hand is to estimate the magnitude of the adjustment factor U, which here functions as the effective stress intensity *factor range ratio*. An analytical approach based on published closure models was chosen in order to eliminate the opportunity of inserting an arbitrary fudge factor. The approach is identical to a robust closure strategy under development as part of a comprehensive methodology for elastic-plastic fatigue crack growth rate prediction to be applied to aerospace propulsion systems [4]. The approach is based on the modified-Dugdale model of Newman, which has been conveniently expressed as a simple closed-form equation giving $\sigma_{open}/\sigma_{max}$ as a function of $\sigma_{max}/\sigma_{flow}$, R, and the stress state (plane stress vs. plane strain) [5]. Here σ_{flow} is the average of the yield and ultimate strengths. The stress state is quantified by the constraint factor α, where $\alpha = 1$ for plane stress, $\alpha = 3$ for full plane strain, and intermediate values represent partial constraint. The Newman model is based on a center crack in an infinite plate. This model can be applied satisfactorily to other geometries by reinterpreting $\sigma_{max}/\sigma_{flow}$ as K_{max}/K_{flow}, where $K_{flow} = \sigma_{flow}\sqrt{\pi a}$ [6].

Based on the measured tensile properties, the flow stress was estimated as 93.5 ksi (645 MPa). The stress state was identified as plane strain ($\alpha = 3$) for the large crack tests on the basis of a comparison of the crack tip plastic zone sizes with characteristic specimen dimensions [7]. The estimated stress state varies for the small crack tests, but the differences between plane stress and plane strain closure stresses under these conditions (large maximum stresses) were negligible. The maximum stress for the rotating bending specimens was just the stress amplitude $\Delta\sigma/2$, which varied from 75 to 81 ksi (520 to 560 MPa). The local stress ratio for the square beam specimens was estimated as $R = -0.35$ by assuming that the maximum local stress at the outer fiber was approximately equal to the yield stress due to plastic deformation at the outer fiber, but that the stress range was still equal to the full applied (elastic) outer fiber bending stress range. The ratio of K_{max}/K_{flow} to

$\sigma_{max}/\sigma_{flow}$ for the semi-circular surface cracks which formed in the small crack tests was equal to the geometry correction factor on the stress intensity factor solution used here, 0.73. The maximum stresses (loads) for the large crack tests were small enough that no strong dependence of $\sigma_{open}/\sigma_{max}$ on K_{max}/K_{flow} was present. On the basis of these numbers and methods, the effective stress range ratio U was calculated as approximately $U = 0.8$ for the large crack tests, $U = 0.45$ for the rotating bending tests, and $U = 0.6$ for the square beam tests.

Crack closure levels are known to change significantly for large cracks in the immediate near-threshold regime, increasingly sharply with decreasing ΔK [8]. The resulting sharp decrease in ΔK_{eff} is consistent with the sharp decrease in FCG rate very near the threshold. However, since specific experimental information about this near-threshold closure effect was not available for HSLA-80, no attempts were made to correlate the large crack data very near the threshold on a consistent basis with the small crack data. For convenience, the very near-threshold large crack data were simply censored from the ΔK_{eff} calculations.

Comparisons of the large crack and small crack data based on these two approaches, the nominal ASTM approach and the closure approach, are presented graphically in Figures 3 and 4. Note that the two approaches give similar results, since the estimated U values are similar. The comparison based on an explicit treatment of crack closure appears to give slightly closer agreement between large crack and small crack data in the region where the two sets overlap, but at this point it is not our primary concern to evaluate which approach is "correct" or preferable. Instead, we only conclude from the mutual agreement that these are valid means of comparing the large crack and small crack data, which is our primary goal here.

The agreement between the so-called "ASTM" and "crack closure" approaches might be interpreted to mean that closure considerations are not important. However, it should be noted that the "ASTM" approach itself makes an implicit assumption about the effective stress range which may reflect assumptions about "crack closure". The condition that $\Delta K = K_{max}$ when $R < 0$ is consistent with the common assumption that the crack is closed when the nominal stresses are compressive. This assumption that $\sigma_{open} = 0$ appears to be an acceptably accurate estimate for small cracks under large, fully-reversed stresses, and for large cracks (outside of the near-threshold regime) under relatively small applied stresses, which are precisely the conditions in these tests. It is possible, however, that this "ASTM" approach may break down if the true closure behavior for either large or small cracks changes significantly.

Conclusions

What can be concluded from these comparisons of large crack and small crack data? First of all, it appears that small cracks and large cracks grow at similar rates in the traditional large-crack power-law regime (in this case, above about 10 MPa•m$^{1/2}$). This agreement suggests that large crack FCG relationships (including scaling laws) should also be applicable to small cracks.

Second, it is clear that small cracks can grow at applied stress intensity factors which are smaller than the traditional large crack threshold values, ΔK_{th}. The small cracks exhibit no clear threshold behavior, even at smaller ΔK values. The small crack data do exhibit occasional crack arrests at extremely low ΔK, but these are not consistently observed. The occasions of crack arrest which are observed may be due to unique microstructural interactions when the crack size is on the

same order as the microstructure. Of greater importance to the fatigue life prediction problem, however, is the conclusion that the FCG laws used to describe small crack growth should not, in general, include a large crack threshold. Further study of large crack FCG growth very near the (large crack) threshold has not been pursued, since the phenomenon is not significant for fatigue life prediction based on small crack growth relationships.

Along this line, it should be noted that no special attempt has been made to correlate the very-near-threshold large crack data with the other data presented. It may be the case that very near the threshold, the crack closure levels increase significantly. This increase would cause a sharp decrease in the calculated driving force, ΔK_{eff}, near threshold, which might bring the near-threshold da/dN data into line with the other data. These changes in crack closure behavior for near-threshold large cracks have been measured for other engineering materials [8]. Similar data are not currently available for HSLA-80 steels, so this possibility cannot be currently evaluated.

A third conclusion of note is that small cracks which grow at ΔK values below the large crack threshold appear to grow at rates which are generally consistent with a downward extrapolation of the power-law trends from the large crack regime. In other words, the large crack power-law FCG relationship may be equally applicable to the very smallest microcracks (in addition to longer microcracks, which were addressed above in the first conclusion). From an engineering standpoint, it is relatively easy to address the small crack and large crack data on an entirely consistent basis. Figure 5 shows that a single power-law fit to the combined large crack and small crack data is very satisfactory. The slope of this particular Paris line is $m = 3.23$, which is only slightly smaller than the regression of the large crack data alone.

Our engineering conclusion, then, is that the small crack data and large crack data can be treated in a similar manner for the purposes of fatigue life prediction. Scaling laws derived for large crack behavior should also be applicable to the small crack regime for HSLA-80 steels. The primary differences between the large crack and small crack regimes involve the statistical dispersion of the data.

ENGINEERING LIFE MODELS

Fatigue life prediction which is based on an explicit treatment of the crack growth phenomenon requires integration of the FCG equation. Consider the common choice of the simple Paris law for FCG,

$$\frac{da}{dN} = C(\Delta K)^m \tag{2}$$

where ΔK is given by the general expression

$$\Delta K = F \Delta\sigma \sqrt{\pi a} \tag{3}$$

Note that these same expressions can be written in terms of some ΔK_{eff} if an alternative formulation for the driving force is more appropriate. All expressions are written in terms of a simple ΔK for

convenience here. If the geometry correction factor F can be treated as approximately independent of crack length, which is roughly correct for small crack problems, then the total crack propagation life, N_p, can be calculated as

$$N_p = \frac{2}{(m-2)C(F\sqrt{\pi})^m(\Delta\sigma)^m}\left\{\frac{1}{a_i^{(m-2)/2}} - \frac{1}{a_f^{(m-2)/2}}\right\} \tag{4}$$

when m not equal to 2. Here a_i and a_f are the initial and final crack sizes. The final crack size is a function of applied stress, based on fracture mechanics arguments. This dependence, however, often has little impact on total predicted lives, since $1/a_f^{(m-2)/2} << 1/a_i^{(m-2)/2}$ in many applications. If both of these crack sizes are taken to be constants independent of applied stress, which is therefore an acceptable approximation from an engineering perspective, then Eqn. 6 can be simplified to the general *S-N* form

$$N_p = A(C,m,F)(\Delta\sigma)^{-m} \tag{5}$$

This result implies that a traditional *S-N* equation can be constructed directly from a FCG relationship. For our HSLA-80 steel, the implied value of m is between 3 and 4 for crack growth in the small crack or intermittent FCG regimes. The remaining question is how accurately this derived relationship reflects actual *S-N* fatigue life data.

The answer to this accuracy question is dependent on the definition of "*S-N*" data. At least two definitions are meaningful for naval structural applications. The first definition is the life of a polished smooth specimen, loaded either axially or in bending. The second definition is the life of a large-scale welded component. Each definition will be considered separately.

Smooth Specimen *S-N* Behavior

Available data for smooth specimen axial fatigue tests of HSLA-80 in air [9] indicate that the *S-N* "slope" m should be about 10-12 for tests in which the stress amplitude was less than about 100 ksi (690 MPa). See Figure 6. This slope corresponds to a fatigue strength exponent (the exponent in the conventional stress-life expression, $\Delta\sigma/2 = \sigma_f'(2N_f)^c$) $c = -1/m$ of about -0.08 to -0.10, which is a typical value for this class of steels. This observed value of m is significantly different from our implied value based on FCG rates. The difference is due to the influence of the crack nucleation life phase. The total *S-N* "life" can be thought of as consisting of three independent phases: nucleation, small crack growth, and large crack growth. Under different conditions, one or more of the life phases may dominate the total life.

In particular, the nucleation phase tends to be negligibly small at relatively short lives (high stresses) and dominantly large at very long lives (low stresses). This trend is clearly evident in the HSLA-80 small crack growth tests. The average nucleation life fraction, N_i/N_{total}, was 0.233 for tests at a stress amplitude of 420 MPa, 0.113 at a stress amplitude of 520 MPa, and 0.024 at a stress amplitude of 560 MPa. The generally accepted rule of thumb is that very close to the fatigue limit, the nucleation life fraction approaches 1. This trend implies that the dependence of nucleation life on stress is extremely strong. For situations in which the nucleation phase is a significant fraction of the total life, a simple integration of the small crack growth law will not give an entirely satisfactory

description of total life. For the particular small crack tests conducted in this program, the nucleation life fraction was typically small, and so this integration should give reasonably good life results. This method, however, will likely fail when applied to a much wider range of applied stresses.

In order to treat the total smooth specimen *S-N* problem more accurately, explicit attention must be given to the nucleation phase of life. The nucleation lives can be modeled by a general Coffin-Manson type of equation which relates the applied (plastic) strain range directly to N_i. It was previously observed (see Appendix A), based on experimental results, that microstructure could have a pronounced effect on crack nucleation, and the nucleation equation may be able to incorporate microstructural effects explicitly. For example, if nucleation occurs at inclusions (as was the case for all fatigue tests of as-received material), then the inclusion size and the volume fraction of inclusions may be significant quantitative variables in a nucleation equation. It follows naturally that any treatment of the probabilistic *S-N* problem under these conditions must also address variability in the nucleation event.

It should be emphasized, however, that this quantitative treatment of the complex nucleation problem is required only when the nucleation life phase is a non-negligible fraction of the total life. When nucleation occurs relatively early in life, then a treatment based entirely on integration of the small crack FCG equation may be satisfactory.

Welded Component *S-N* Behavior

Recent data from fatigue tests of both large-scale [10] and small-scale [11] welded structures fabricated from HSLA-80 suggests an *S-N* slope m between 3 and 4, as shown in Figure 7. In contrast to the smooth specimen results, this slope agrees closely with the Paris exponent from the available fatigue crack growth rate data. In these structural fatigue tests, cracks initiated at relatively large defects and discontinuities in the weldments, and crack nucleation lives were relatively insignificant in comparison to total propagation lives. Simple estimates of total fatigue life based on fracture mechanics arguments (and using the same large crack baseline FCG data presented earlier in this report) were relatively successful in predicting the observed trends in experimental lives [12].

Many large-scale welded structures such as bridges and steel buildings are engineered on the basis of fatigue design curves first developed by the American Association of State Highway and Transportation Officials (AASHTO) [13]. These design curves are a set of standard *S-N* relationships which correspond to categories of welded details grouped according to their relative fatigue strengths. The AASHTO curves are based on the lower 95% confidence limit (using log-normal statistics) of full-scale fatigue test data. The slopes of these AASHTO design curves and similar curves published by other regulatory bodies have been fixed at $m = 3.0$, which is again consistent with known relationships for the fatigue crack growth behavior. It is particularly interesting that the AASHTO curves appear to provide a reasonably accurate description of the Lehigh HSLA-80 welded structure *S-N* data (see again Figure 7), even though the AASHTO curves were developed from tests mostly on carbon-manganese steels. This coincidence occurs because, as noted earlier in Section 2, large crack FCG rates differ relatively little among different steel microstructures.

Total life scatter in the Lehigh HSLA-80 welded structure tests was relatively large, as much as a factor of 10 for nominally identical conditions. Preliminary investigations into the origins of this scatter concluded that variations in the size of the initiating weldment defect contributed relatively little to the overall variation in life for longitudinal fillet welds. Scatter in defect size appeared to be more significant for transverse groove weld specimens. Other factors, such as variations in local weldment and crack geometry, residual stresses, material microstructure, and small flaw growth rates, will also contribute to total scatter, but these effects were not characterized in the Lehigh research.

In general, the correct *S-N* slope for welded structures will vary as a function of initial weld quality. When initial weld quality is relatively low from a fatigue perspective, cracks can initiate quickly and the *S-N* slope will approach the limiting value of 3 to 4 based on fracture mechanics arguments. When initial weld quality is higher, perhaps due to more careful welding procedures, post-weld treatments (e.g., to remove local stress concentrators), or improved nondestructive inspection, then the nucleation phase can again become important. Under these conditions, the *S-N* slope will be a larger number and may eventually approach that for smooth specimens in base metal, although in practice it will rarely reach this limit [14]. Initial weld quality can also influence the initial size of the fatigue cracks, which has a further impact on *S-N* slope.

In conclusion, acceptably accurate characterization of total life *S-N* behavior for welded structures based on an integration of appropriate FCG relationships appears to be feasible. Detailed attention to the crack nucleation phase of life does not appear to be necessary, although variability in the size of the initial defect (crack) may need to be addressed explicitly.

CONCLUSIONS

1. Large cracks and small cracks in HSLA-80 steel grow at similar rates in the traditional large crack power-law regime, when compared on the basis of a properly defined effective stress intensity factor range.

2. The effective stress intensity factor range, which addresses differences in stress ratio and maximum stress, can be defined in terms of crack closure concepts or simply in terms of the tensile portion of the stress range. For the data sets considered in this study, these two approaches gave similar results.

3. Small cracks can grow at applied stress intensity factors which are smaller than the traditional large crack threshold, ΔK_{th}.

4. Small cracks which grow at ΔK values below the large crack threshold appear to grow at rates which are generally consistent with a downward extrapolation of the power-law trends from the large crack regime.

5. Acceptably accurate characterization of total life *S-N* behavior for welded structures based on an integration of FCG relationships for both large and small cracks appears to be feasible. This approach is also feasible for smooth specimen behavior in the low cycle fatigue regime. Some additional attention to the nucleation phase may be necessary to characterize smooth specimen life in the high cycle regime.

REFERENCES

1. A. C. Nussbaumer, R. J. Dexter, J. W. Fisher, and E. J. Kaufmann, "Propagation of Very Long Fatigue Cracks in a Cellular Box Beam," *Fracture Mechanics: 25th Volume, ASTM STP 1220*, 1994, in press.

2. J. A. Todd, L. Chen, E. Y. Yankov, and H. Tao, A comparison of the near-threshold corrosion fatigue crack propagation rates in Mil S-24645 HSLA steel and its weld metal, *ASME J. Offshore Mechanics and Arctic Engineering*, Vol. 115, 1993, pp. 131-136.

3. R. C. McClung, "The Influence of Applied Stress, Crack Length, and Stress Intensity Factor on Crack Closure," *Metallurgical Transactions A*, Vol. 22A, 1991, pp. 1559-1571.

4. "Elastic-Plastic and Fully Plastic Fatigue Crack Growth," NASA Contract NAS8-37828, Southwest Research Institute Project No. 06-5013, 1992-1994.

5. J. C. Newman, Jr., "A Crack Opening Stress Equation for Fatigue Crack Growth," *International Journal of Fracture*, Vol. 24, 1984, pp. R131-R135.

6. R. C. McClung, "Finite Element Analysis of Specimen Geometry Effects on Fatigue Crack Closure," Topical Report to NASA George C. Marshall Space Flight Center, NASA Contract NAS8-37828, April 1993.

7. R. C. McClung, "Closure and Growth of Mode I Cracks in Biaxial Fatigue," *Fatigue and Fracture of Engineering Materials and Structures*, Vol. 12, 1989, pp. 447-460.

8. R. C. McClung and D. L. Davidson, "High Resolution Numerical and Experimental Studies of Fatigue Cracks," *Engineering Fracture Mechanics*, Vol. 39, 1991, pp. 113-130.

9. T. W. Montemarano, B. P. Sack, J. P. Gudas, M. G. Vassilaros, and H. H. Vanderveldt, "High Strength Low Alloy Steels in Naval Construction," *Journal of Ship Production*, Vol. 2, 1986, pp. 145-162.

10. R. J. Dexter, J. W. Fisher, and J. E. Beach, "Fatigue Behavior of Welded HSLA-80 Members," ASME Offshore Mechanics and Arctic Engineering Conference, Glasgow, UK, June 1993.

11. S. Sarkani, D. P. Kihl, and J. E. Beach, "Fatigue of Welded Joints Under Narrowband Non-Gaussian Loadings," *Probabilistic Engineering Mechanics*, Vol. 9, 1994, 179-190.

12. G. R. Kober, R. J. Dexter, E. J. Kaufmann, B. T. Yen, and J. W. Fisher, "The Effect of Welding Discontinuities on the Variability of Fatigue Life," *Fracture Mechanics: 25th Volume, ASTM STP 1220*, in press.

13. *Standard Specification for Highway Bridges*, 14th ed., The American Association of State Highway Transportation Officials, Washington, DC, 1989.

14. S. J. Hudak, Jr., and J. D. Smith, "Fatigue Design Criteria for High Strength Steels Used Offshore," submitted to 1995 ASME Offshore Technology Conference.

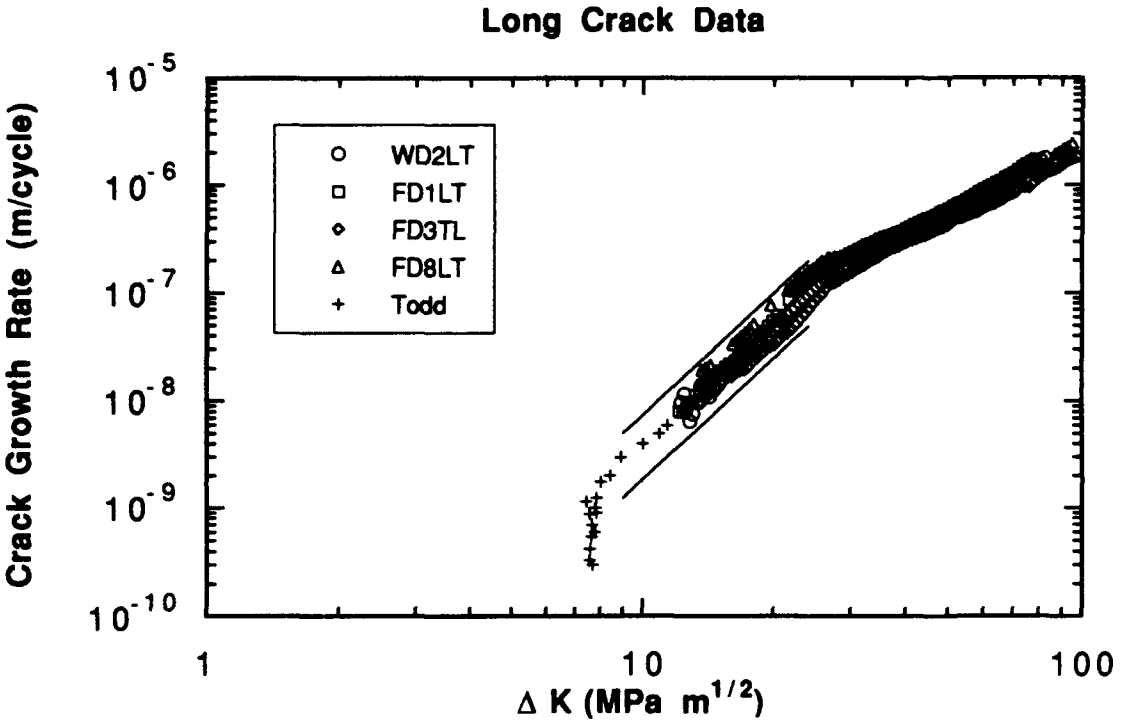

Figure 1. Large crack FCG data for HSLA-80 steel

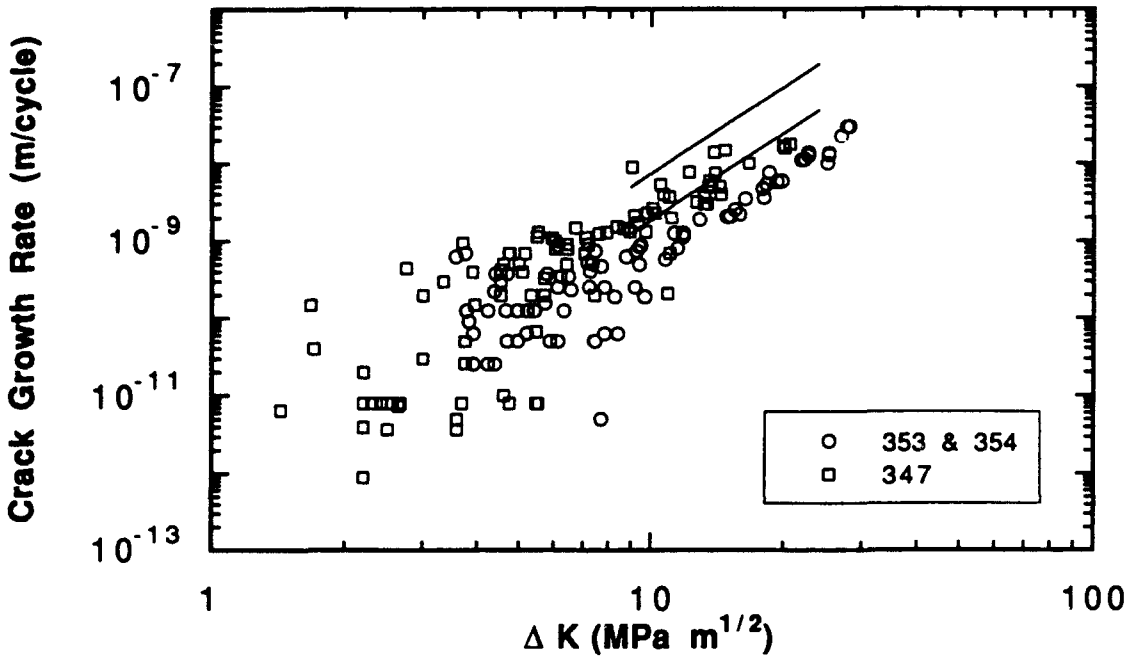

Figure 2. Comparison of large crack and small crack data based on full range ΔK

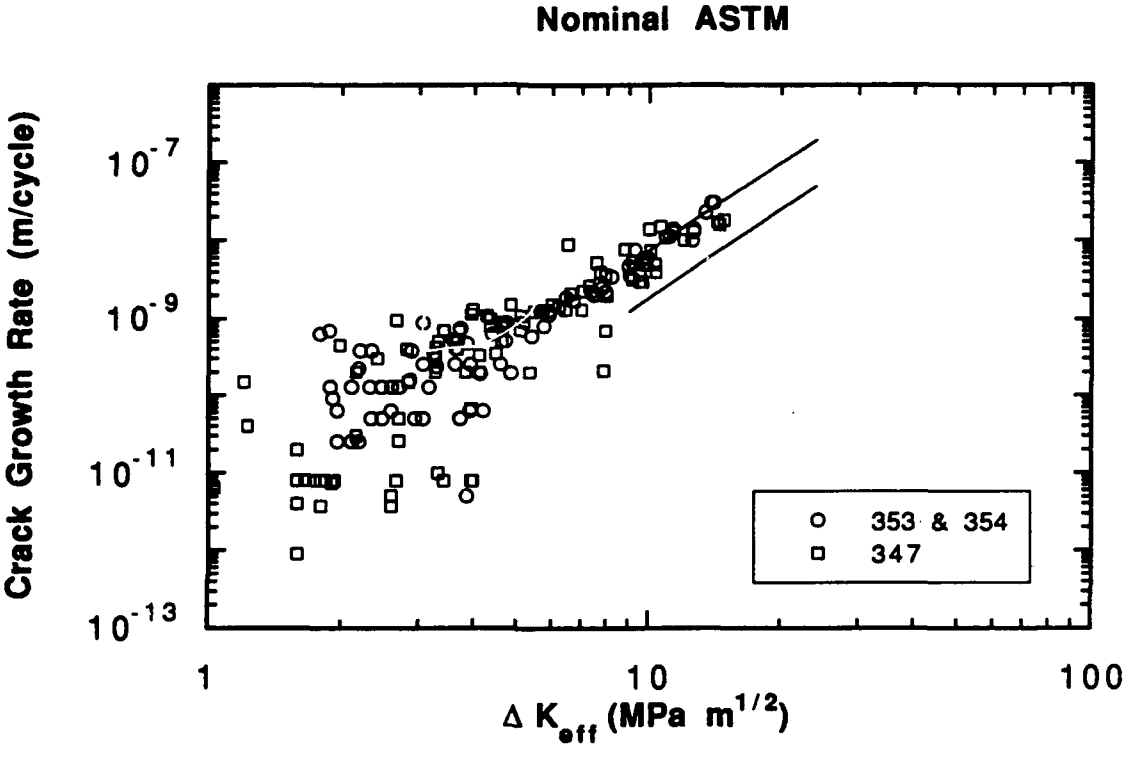

Figure 3. Comparison of large crack and small crack data based on effective ΔK defined by the nominal ASTM approach

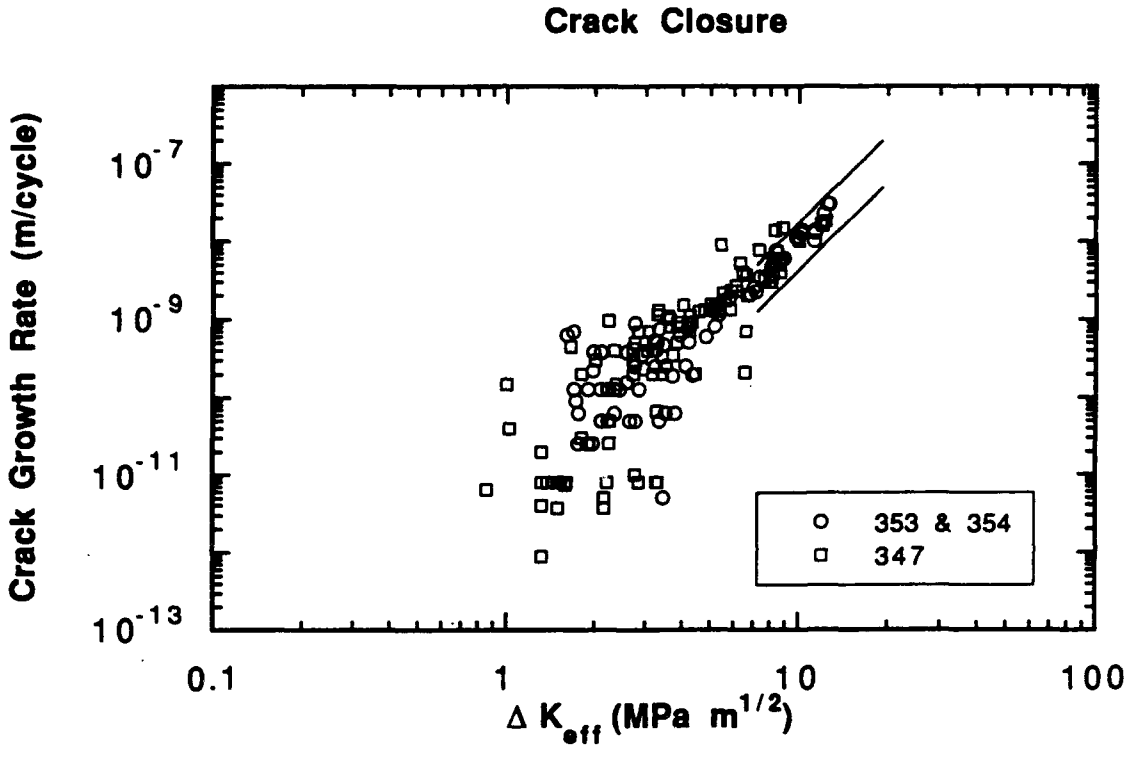

Figure 4. Comparison of large crack and small crack data based on effective ΔK defined by the Newman crack closure approach

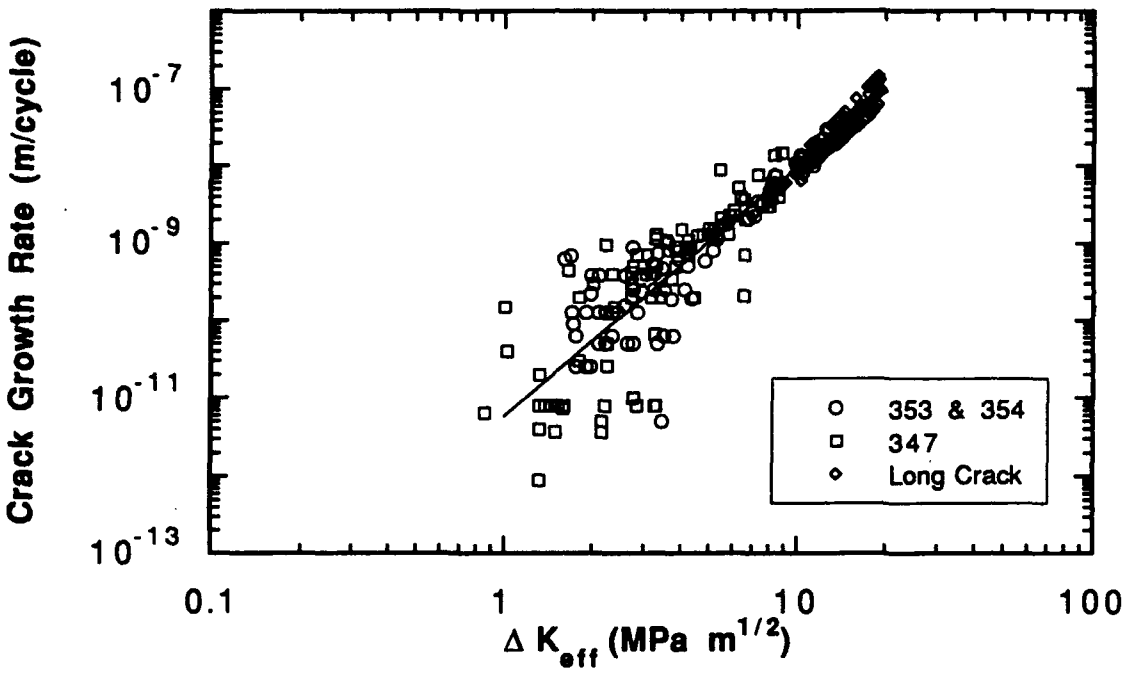

Figure 5. Comparison of large crack and small crack data, showing linear regression of all combined data

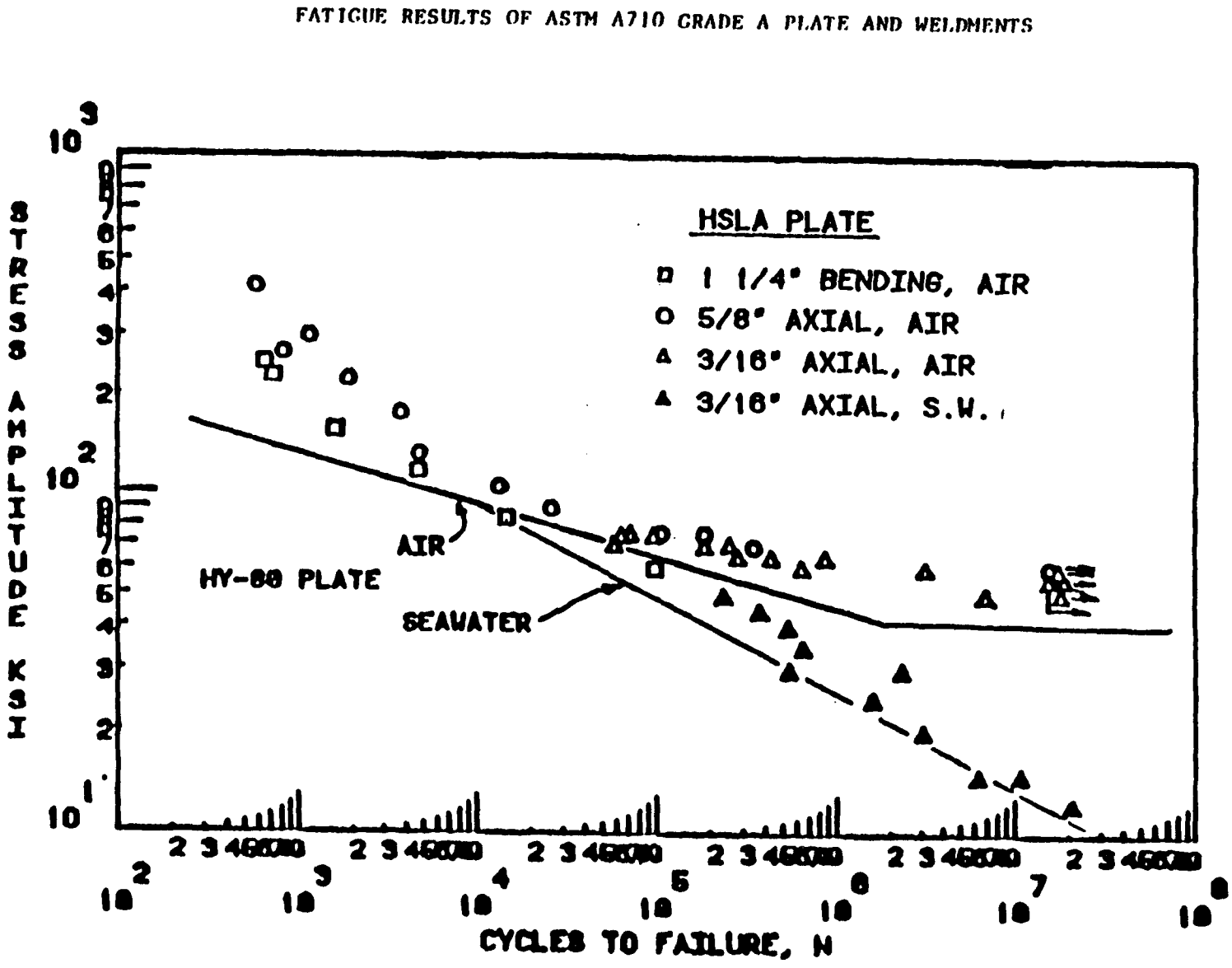

Figure 6. Smooth specimen *S-N* data for HSLA-80 [9]

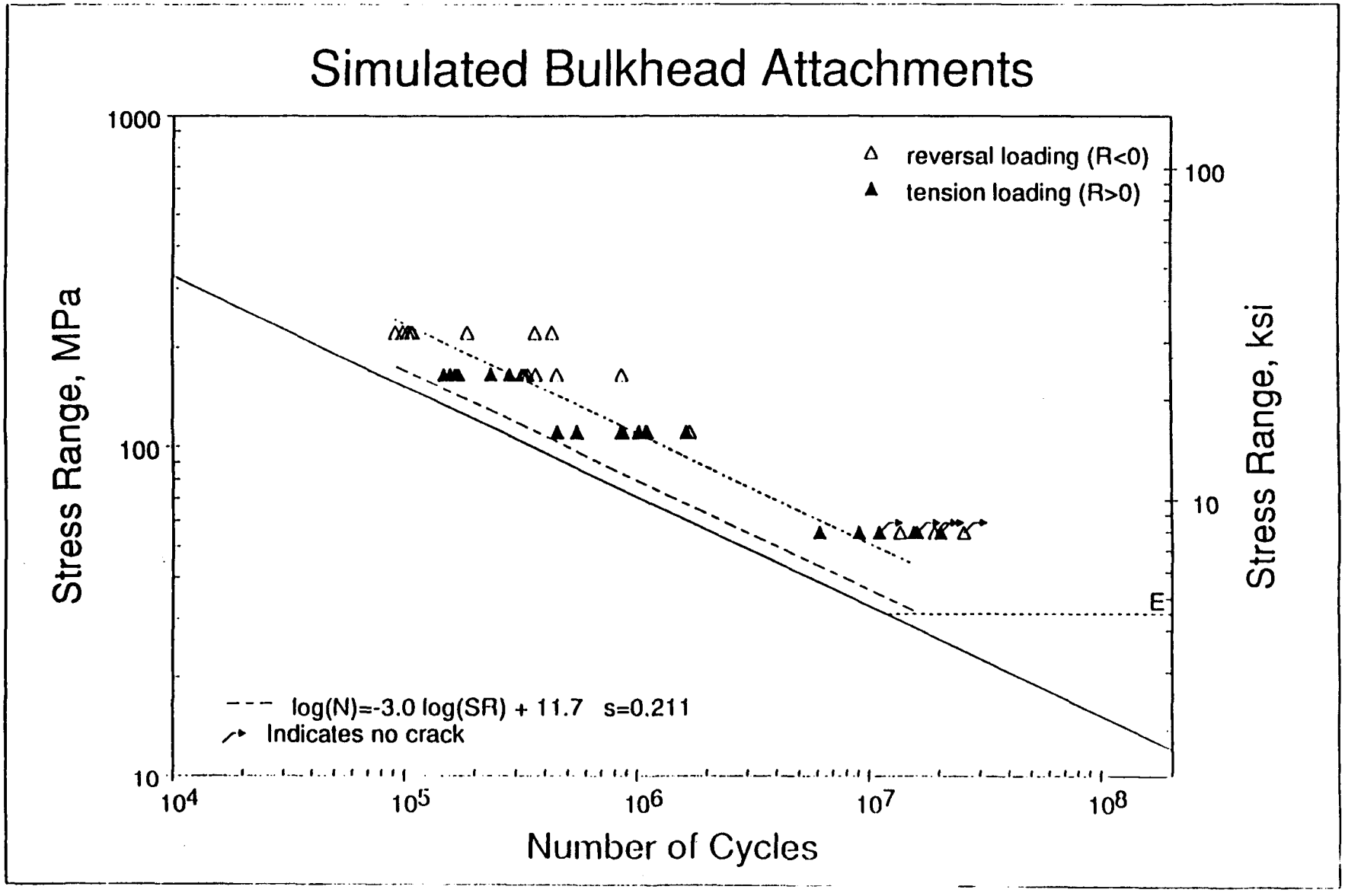

Figure 7. Welded structure *S-N* lata for HSLA-80 [10]

APPENDIX E

"A Probabilistic Treatment of Microstructural Effects on Fatigue Crack Growth of Large Cracks"

K. S. Chan and T. Y. Torng

Submitted to *ASME Journal of Engineering Materials and Technology*

A PROBABILISTIC TREATMENT OF MICROSTRUCTURAL EFFECTS ON FATIGUE CRACK GROWTH OF LARGE CRACKS

K.S. Chan and T.Y. Torng

Southwest Research Institute
San Antonio, TX 78238

ABSTRACT

A probabilistic model has been developed for treating the effects of microstructural variation on the fatigue crack growth response of large cracks in structural alloys. The proposed methodology is based on a microstructure-based fatigue crack growth law that relates the crack growth rate, da/dN, to the dislocation barrier spacing, yield stress, fatigue ductility coefficient, Young's modulus, and the dislocation cell size or crack jump distance. Probabilistic treatment of these microstructure-dependent variables has led to a fatigue crack growth law that includes explicitly the randomness of the yield stress, fatigue ductility coefficient, and the dislocation barrier spacing in the response equation. Applications of the probabilistic crack growth model to structural reliability analyses for steels and Ti-alloys are illustrated, and the probabilistic sensitivities of individual random variables are evaluated.

INTRODUCTION

Fatigue crack growth data generally exhibit substantial scatter. The origins of the scatter vary among several factors, ranging from microstructural variations, uncertainties in crack length measurements, residual stresses, and the intermittent nature of the fatigue crack growth process. Despite the use of averaging procedures, fatigue crack growth rate, da/dN, data generally shows a large scatter band when correlated with the stress intensity range, ΔK. Because of this, statistical treatment of the da/dN data is usually a necessity when the data is used in the life prediction of a structural component *(Johnston, 1983)*.

Several probabilistic procedures are available in the literature for treating various aspects of the statistical nature of fatigue crack growth and for applications in structural reliability analysis. Most, if not all, of the probabilistic models are based on the Paris power-law equation *(Paris and Erdogan, 1963)*,

$$\frac{da}{dN} = C\Delta K^m \tag{1}$$

for relating da/dN to the stress intensity range, ΔK. In these models, randomness in the fatigue crack growth response is treated by taking the empirical constants, C and m, in the Paris equation as random variables *(Johnston, 1983; Ostergaard and Hillberry, 1983; Ortiz and Kiremidjian, 1989)*, without considering the role of microstructure in the fatigue crack growth process.

The objective of this article is to present a new probabilistic treatment of fatigue crack growth that includes explicitly the effects of microstructural unit size on the fatigue crack growth behavior. A generalized framework of the approach is presented first. The model is then applied to treating da/dN variations observed in Ti-alloys and steels. Finally, the role of microstructure variations in the crack growth kinetics of these materials is elucidated.

PROBABILISTIC MODEL DEVELOPMENT

A fatigue crack growth model that incorporates microstructural size parameters was developed recently by Chan *(1993)*. The model has been developed on the basis that fatigue crack growth occurs as the result of accumulation of plastic strain range at a crack-tip element whose failure is governed by the Coffin-Manson relation *(Coffin, 1954; Manson, 1964)*. The height and width of the crack-tip element correspond to the dislocation barrier spacing, d, and the crack jump distance, s, respectively, as shown schematically in Figure 1. In cell-forming materials, the crack jump distance, s, also corresponds to the dislocation cell size.

The crack growth rate, da/dN, obtained for this fatigue process is *(Chan, 1993)*

$$\frac{da}{dN} = \xi^{1/b}(2s)^{1-1/b}\left[\frac{\Delta K}{E}\right]^{2/b} \tag{2}$$

where ΔK is the stress intensity range, E is Young's modulus, b is the fatigue ductility exponent, and ξ is a dimensionless parameter given by *(Chan, 1993)*

$$\xi = \frac{Es}{4\sigma_y \varepsilon_f' d} \tag{3}$$

that incorporates all of the microstructure-dependent parameters including the yield stress, σ_y, the fatigue ductility coefficient, ε_f', Young's modulus, dislocation barrier spacing, d, and the dislocation cell size or crack jump distance, s.

This microstructure-based crack growth model, which gives an explicit relationship between da/dN and the microstructural size scale, was used as the starting point for the development of the probabilistic fatigue crack growth model. Specifically, each of the microstructure-dependent parameters in Eq. (3) can be described as

$$M = \overline{M} X_M \tag{4}$$

where M = E, s, σ_y, ε_o', or d; $\overline{M}$ and X_M are the mean value and the randomness of the parameter M, respectively. For simplicity, however, randomness in E and s is ignored so that $X_E = X_s = 1$. Under this circumstance, combining Eqs. (2) and (3) leads one to the probabilistic crack growth rate expression given by

$$\frac{da}{dN} = (X_\xi)^{1/b} \overline{\xi}^{1/b} (2\overline{s})^{1-1/b} \left[\frac{\Delta K}{\overline{E}} \right]^{2/b} \tag{5}$$

where

$$X_\xi = \frac{1}{X_{\sigma_y} X_{\varepsilon_o'} X_d} \tag{6}$$

is a function that incorporates the overall variation of the crack growth rate resulting from randomness in the selected microstructural variables. Correlations between the yield stress, fatigue ductility coefficient, and the dislocation barrier spacing, d, allow one to further simplify Eq. (5).

This can be accomplished by recognizing that both the yield stress and the fatigue ductility coefficient are related to the dislocation barrier spacing according to modified Hall-Petch *(Hall, 1951; Petch, 1953)* relations given by *(Chan, 1993)*

$$\sigma_y = \sigma_o \left(\frac{d_o}{d} \right)^{\alpha} \tag{7}$$

and

$$\varepsilon_f' = \varepsilon_o' \left(\frac{d_o}{d} \right)^{\beta} \tag{8}$$

where σ_o and ε_o' are the yield stress and fatigue ductility coefficients at the reference dislocation barrier spacing, d_o, respectively, and α and β are nondimensional, empirical constants.

APPLICATION TO TI-ALLOYS

Previous studies have shown that fatigue crack growth in Ti-base alloys is very sensitive to the microstructure. In this section, application of the proposed probabilistic fatigue crack growth model to Ti-base alloys is illustrated. Compilation of yield stress and fatigue ductility coefficient as a function of the dislocation barrier spacing for various Ti-base alloys is shown in Figure 2(a) and (b), respectively *(Yoder et al., 1979; Chan, 1994)*. These correlations reveal that both yield strength and fatigue ductility coefficients can be considered to exhibit a uniform uncertainty that is independent of the size of dislocation barrier spacing, which is the grain or packet size for Ti-alloys *(Yoder et al., 1979)*. In other words, the same uncertainty occurs at different dislocation barrier spacings. Based on this observation, Eqs. (7) and (8) can be rewritten as

$$\sigma_Y = \sigma_0 \left(\frac{d_0}{d} \right)^{\alpha} X_{\sigma_Y} \tag{9}$$

and

$$\varepsilon_f' = \varepsilon_0' \left(\frac{d_0}{d} \right)^{\beta} X_{\varepsilon_f'} \tag{10}$$

for describing the randomness in σ_y and ε_f'. Eqs. (9) and (10) can then be combined with Eq. (5) to give

$$\frac{da}{dN} = \left(\frac{1}{X_{\sigma_y} X_{\varepsilon_f'}}\right)^{1/b} \left(\frac{\bar{d} X_d}{d_o}\right)^{\frac{\alpha+\beta-1}{b}} \left[\xi_{so}^{1/b} (2s)^{1-1/b} \left(\frac{\Delta K}{E}\right)^{2/b}\right] \tag{11}$$

with

$$\xi_{so} = \frac{Es}{4\sigma_0 \dot{\varepsilon}_0 d_0} \tag{12}$$

as the crack growth response equation. In Eq. (12), ξ_{so} is the value of ξ evaluated at the reference dislocation spacing, d_o. For the Ti-alloys examined, $\alpha = 0.12$, $\beta = 0.5$, $d_o = 1$ μm, $\sigma_0 = 1200$ MPa, and $\dot{\varepsilon}_0 = 0.2$. Additionally, $b = 0.57$, $s = 0.2$ μm, and $E = 1.2E5$ MPa; X_{σ_y} is modeled by a lognormal distribution with a mean of 1.03044 and a standard deviation of 0.25617. The distribution for $X_{\varepsilon_f'}$ is a normal one with a mean of 1 and a standard deviation of 0.078782. The dislocation barrier spacing, d, is a random variable described by

$$d = \bar{d} X_d \tag{13}$$

where $\bar{d}$, the mean value of d, is 128.64 μm, and X_d is an extreme value distributed random variable with the mean = 1 and standard deviation = 0.7. The randomness of d was evaluated from the grain (or packet) size measurements for Ti-alloys reported by Yoder *et al* (1979). Substituting the appropriate parameters into Eq. (12) leads to

$$\frac{da}{dN} = 2.8665 \times 10^{-15} \left[(d)^{-0.67} \left(X_{\sigma_y} X_{\varepsilon_f'}\right)^{-1.75} \Delta K^{3.51}\right] \quad \text{m/cycle} \tag{14}$$

where ΔK is the stress intensity range in $MPa\sqrt{m}$, and d is in μm. This stochastic fatigue crack growth rate is thus a function of the random variables, X_{σ_y}, $X_{\varepsilon_f'}$, X_d, and $\bar{d}$ by virtue of Eq. (13).

To examine the effect of these random variables, a plot of da/dN vs. d was obtained for $\Delta K = 40\ MPa\sqrt{m}$. When ΔK is a constant, da/dN is a function of X_{σ_y}, $X_{\varepsilon_f'}$, and the dislocation barrier, d, spacing. A family of da/dN vs d lines, which represents different confidence levels, is

shown in Figure 3. Because d has been taken as the independent variable, the uncertainty of d has no effect on the probability results, and only uncertainties of yield strength and fatigue ductility coefficient have an effect. When d equals to 1 μm, the 1%, 10%, 50%, 90%, and 99%, crack growth rate equal to 2.33E-6, 3.73E-6, 6.64E-6, 1.19E-5, and 1.93E-5 m/cycle, respectively. The ratio in crack growth rate between 99% and 1% confidence levels is very close to one order of magnitude. To check the accuracy of this model, the experimental data from Yoder *et al.* (1979), are also presented in Figure 3.

Figure 4(a) shows a comparison of the crack growth curves for d values of 15 μm, 150 μm and 400 μm. When $\Delta K = 10\ MPa\sqrt{m}$, the mean crack growth rate for d = 15 μm, 150 μm and 400 μm, are 8.43E-9, 1.82E-9, and 9.44E-10 m/cycle, respectively. The ratio in crack growth rate for d = 15 μm and 400 μm is about one order of magnitude. To offer a comparison with different probability levels, Figure 4(b) shows crack growth curves for the 1% and 99% confidence levels for the three average dislocation barrier spacings examined. The results in Figures 3 and 4 clearly show that variation in the microstructure unit size (i.e., dislocation barrier spacing) has a significant effect on the fatigue crack growth response of Ti-alloys.

APPLICATION TO STEELS

Compilations of yield stress and fatigue ductility coefficient data of steel are presented as a function of dislocation barrier spacing, d, in Figures 5(a) and (b), respectively. The values of α and β are both 0.5 for steels. Substituting these values of α and β into Eq. (12) leads one to

$$\frac{da}{dN} = \left(\frac{1}{X_{\sigma_y} X_{\varepsilon'_f}}\right)^{1/b} \left\{\xi_o^{1/b} (2s)^{1-1/b} \left[\frac{\Delta K}{E}\right]^{2/b}\right\} \tag{15}$$

which indicates the fatigue crack growth rate is independent of the dislocation barrier spacing, d, but depends on the randomness of σ_y and ε_f'. Thus, the Hall-Petch exponents (α and β) in the yield stress and ductility equation determine whether or not the fatigue crack growth rate depends explicitly on the dislocation barrier spacing, d.

For the steels considered, $d_0 = 1\mu m$, $\sigma_0 = 1149 MPa$, $b = 0.5$, $s = 0.1\mu m$, $E = 2.E5 MPa$, and $\dot{\varepsilon_0} = 0.75$. Furthermore, X_{σ_Y} = lognormal (mean = 1.028, standard deviation = 0.2452), and $X_{\dot{\varepsilon_f}}$ = lognormal (mean = 1.05, standard deviation = 0.3362). Using these data, the uncertainty of crack growth rate, da/dN, was examined as a function of ΔK using X_{σ_Y} and $X_{\dot{\varepsilon_f}}$ as the only random variables. When ΔK = 1, the da/dN rates at confidence levels of 99%, 90%, 50%, 10%, and 1%, are 6.716E-13, 2.86E-13, 1.05E-13, 3.87E-14, and 1.6488E-14 m/cycle, respectively. The ratio in crack growth rate for the 99% and 1% confidence levels is ≈ 40. In addition to the probabilistic results, five experimental data sets for HSLA-80 steels *(R.J. Dexter, 1993; Todd et al., 1993)* were also plotted to check the developed model. As shown in Figure 6, almost all data fall within 99% and 1% confidence levels. The HSLA-80 steels exhibited a change in the slope of the crack growth from ≈ 4 to ≈ 2 at high ΔK levels, which corresponds to a change from the intermittent growth mechanism to continuous growth mechanism. For simplicity, the changes in the crack growth mechanism and the slope of the crack growth curve are ignored here.

PROBABILISTIC LIFE PREDICTION

The application of the microstructure-based fatigue crack growth equation for life prediction and structural reliability analysis is straightforward. Specifically, the fatigue crack growth life was obtained by integrating the da/dN equation from the limits of an initial crack size, a_o, to a critical crack length, a_f. For illustration purposes, the stress intensity factor was assumed to be given by

$$\Delta K = 1.3\Delta\sigma\sqrt{a} \tag{16}$$

where $\Delta\sigma$ represents the stress range and a represents the crack size. The initial crack size, a_o, was taken to equal the inclusion size. Based on the available inclusion size data for HSLA-80 steel *(Chan et al., 1992)*, a Weibull distribution (mean = 3.83 μm, standard deviation = 2.495 μm) was used to fit the data as shown in Figure 7. As for the critical crack size, a_c, a deterministic value of 0.05 m was assumed. These assumptions led to

$$N_g = N\left(X_{\sigma_Y}, X_{\dot{\varepsilon_f}}, a_0\right) = \int_{a_o}^{a_c} \left[\frac{da}{dN}\left(X_{\sigma_Y}, X_{\dot{\varepsilon_f}}, a\right)\right]^{-1} da \tag{17}$$

for steels, and

$$N_g = N\left(X_{\sigma_Y}, X_{\varepsilon_f'}, X_d\, a_0\right) = \int_{a_o}^{a_c} \left[\frac{da}{dN}\left(X_{\sigma_Y}, X_{\varepsilon_f'}, a, d\right)\right]^{-1} da \tag{18}$$

for Ti-alloys. Because X_{σ_Y}, $X_{\varepsilon_f'}$, a_0, and in the case of Ti-base alloys, d, are random variables, the crack growth life, N_g, is also a random property. A desired service life, N_S, of 10 million cycles was required; the limit-state (or performance) function was defined as

$$g_N = N_g - N_S \tag{19}$$

which was then solved using FPI™, an advanced probabilistic code developed and licensed by Southwest Research Institute (SwRI) *(Wu et al., 1989)*, to obtain the cumulative distribution function (CDF) of the cycle life and the probability of failure, P_f. In addition, the probabilistic sensitivity factors, which are the directional cosines of a unit vector from the origin to the most probable point on the limit-state surface in the standard normal space *(Wu, 1993)*, are calculated to compare the relative importance between random variables. With further derivations *(Torng and Yang, 1993)*, these probabilistic sensitivity factors become useful design information.

Figure 8 shows the cumulative distribution function of the cycle life for the simulated life prediction calculation for HSLA-80 steel. The probability of failure, P_f, is 7.9E-3 at a service life of 10 million cycles. The probable sensitivity factors at the service life levels are presented in Figure 9. The result indicates that $X_{\varepsilon_f'}$ has the largest effect on the probability of failure for the problem considered. A similar life prediction calculation was also performed for the Ti-alloys. The cumulative distribution factor of the cycle life for the Ti-alloy problem is presented in Figure 10. For this case, the probability of failure at a service life of 10 million cycles is 0.48. The probability of failure depends on the randomness of σ_{ys}, ε'_f, a_o, and d. Among these random variables, a_o and X_d exerted the largest influence on the failure probability, as shown in Figure 11.

DISCUSSION

The result of this investigation reveals that fatigue crack growth rate of large cracks is generally dependent on the microstructure, either directly on the dislocation barrier spacing, which characterizes the relevant microstructural unit size, or indirectly on microstructure-dependent parameters such as yield stress and ductility coefficient. Microstructural variation results in randomness in the yield stress, fatigue ductility coefficient, and the dislocation barrier spacing, which, in turn, leads

to stochastic variations in the fatigue crack growth response. The proposed model explains the large variation in fatigue crack growth response observed in Ti-alloys and steels. Furthermore, the model also explains the strong dependence of the crack growth rate on the microstructural unit size in Ti-alloys *(Yoder et al., 1979)*, and the apparent lack of microstructural size effect in steels *(Chan, 1993)*.

The study also demonstrated that probabilistic procedures developed for the Paris power-law equation can be applied directly to the microstructure-based fatigue crack growth equation. A possible advantage of the proposed methodology over the traditional one is that stochastic sensitivity of the various microstructure-dependent random variables can be predicted. This knowledge provides a venue for controlling the microstructure, the microstructure-dependent parameters, and their corresponding randomness to improve the fatigue crack rate resistance of structural alloys. Additionally, this information can also be used as a basis for developing graded microstructures with favorable fatigue crack growth characteristics.

CONCLUSIONS

The conclusions reached in this investigation are as follows:

1. Microstructure variation can lead to randomness in the yield stress, fatigue ductility coefficient, and the dislocation barrier spacing, which in turn results in variation in the fatigue crack growth rate.

2. When fatigue crack growth response is independent of the microstructural unit size, microstructure variation effects fatigue crack growth rate through randomness in the yield stress and the fatigue ductility coefficient.

3. Stochastic sensitivity of the random variables of yield stress, fatigue ductility, and dislocation barrier spacing varies with structural alloys. Manipulation of microstructural variation according to the most sensitive random variable might be a possible means of tailoring fatigue crack growth response.

ACKNOWLEDGEMENTS

This work was supported by the Office of Naval Research through ONR Contract No. N00014-91-C-0214 (Dr. A. K. Vasudevan, Program Monitor). The editorial and clerical assistance by Ms. D. J. Stowitts and Ms. J. A. McCombs, Southwest Research Institute, are appreciated.

REFERENCES

Chan, K.S., Davidson, D.L., and McClung, R.C., 1992, "Microstructure-Based Fatigue Life Prediction Methods for Normal Steel Structures," SwRI Report for Project No. 06-4414, First Annual Report for ONR Contract No. N00014-91-C-0214, Southwest Research Institute, San Antonio, TX.

Chan, K.S., 1993, "Scaling Laws for Fatigue Crack Growth of Large Cracks in Steels," *Metall. Trans. A.*, vol. 24A, pp. 2473-2486.

Coffin, L.F., 1954, "A Study of the Effects of Cyclic Thermal Stresses on a Ductile Metal," *Trans. ASME*, vol. 76, pp. 931-950.

Dexter, R.J., 1993, Lehigh University, Bethlehem, PA, unpublished research.

Hall, E.O., 1951, "The Deformation and Ageing of Mill Steel: III, Discussion of Results," *Proceedings of Phys. Soc.*, London, sect. B, vol. 64, pp. 747-753.

Johnston, G.O., 1983, "Statistical Scatter in Fracture Toughness and Fatigue Crack Growth Rate Data," *Probabilistic Fracture Mechanics and Fatigue Methods: Application for Structural Design and Maintenance*, ASTM STP 798, J.M. Bloom and J.C. Ekvall, eds., ASTM, pp. 42-66.

Manson, S.S., and Hirschberg, M.H., 1964, in "Fatigue: An Inter-Disciplinary Approach," Syracuse University Press, Syracuse, NY, pp. 133-178.

Ortiz, K., and Kiremidjian, A.S., 1988, "Stochastic Modeling of Fatigue Crack Growth," *Eng. Fract. Mech.*, vol. 29, no. 3, pp. 317-334.

Paris, P.C., and Erdogan, F., 1963, "A Critical Analysis of Crack Propagation Laws," Trans. ASME, *J. of Basic Engineering*, vol. 85, series D(4), pp. 528-534.

Petch, M.J., 1953, "The Cleavage Strength of Polycrystals," *J. Iron Steel Inst.*, vol. 174, pp. 25-28.

Todd, J.A., Chen, L., Yankov, E.Y., and Tao, H., 1993, "A Comparison of the Near-Threshold Corrosion Fatigue Crack Propagation Rates in Mil S-24645 HSLA Steel and Its Weld Metal," Transaction ASME, *J. Offshore Mechanics and Artic Eng.*, vol. 115, pp. 131-136.

Torng, T.Y., and Yang, R.J., "Robust Structural System Design Strategy Based On Reliability-Based Optimization Method," presented at the International Union of Thoretical & Applied Mechanics (IUTAM), San Antonio, TX, June 7-10, 1993, and to be published in an IUTAM Bound Volume.

Wu, Y-T., Burnside, O.H., and Cruse, T.A., 1989, "Probabilistic Methods for Structural Response Analysis," *Computational Probabilistic Methods*, AMD-Vol. 93, ASME; *Computational Mechanics of Reliability Analysis*, W.K. Liu and T. Belytschko (eds.), Elmepress International, ch. 7, pp. 182-195.

Wu, Y-T., 1993, "Computational Methods for Efficient Structural Reliability and Reliability Sensitivity Analysis," *Proceedings of the 34th Structures, Structural Dynamics, and Materials Conference*, AIAA 93-1626-CP, pp. 2817-2826.

Yoder, G.R., Cooley, L.A., and Crooker, T.W., 1979, "50-Fold Difference in Region-II Fatigue Crack Propagation Resistance of Titanium Alloys: A Grain-Size Effect," *J. Eng. Mat. Tech.*, vol. 101, pp. 86-90.

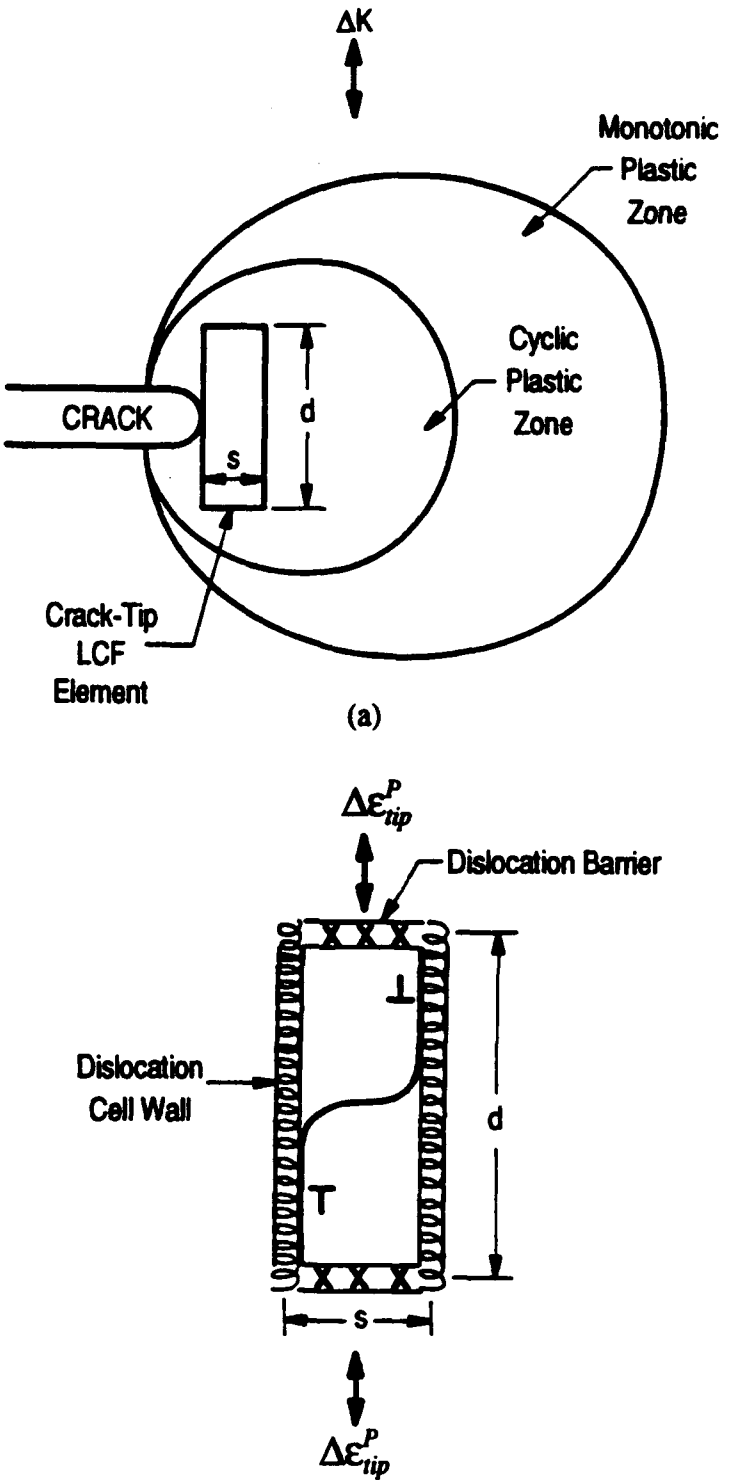

Figure 1. Schematics of the proposed low-cycle fatigue crack-tip element for modeling fatigue crack growth: (a) location of the crack-tip element relative to the cyclic and monotonic plastic zones, and (b) characteristic microstructural lengths of the crack-tip element *(Chan, 1993)*.

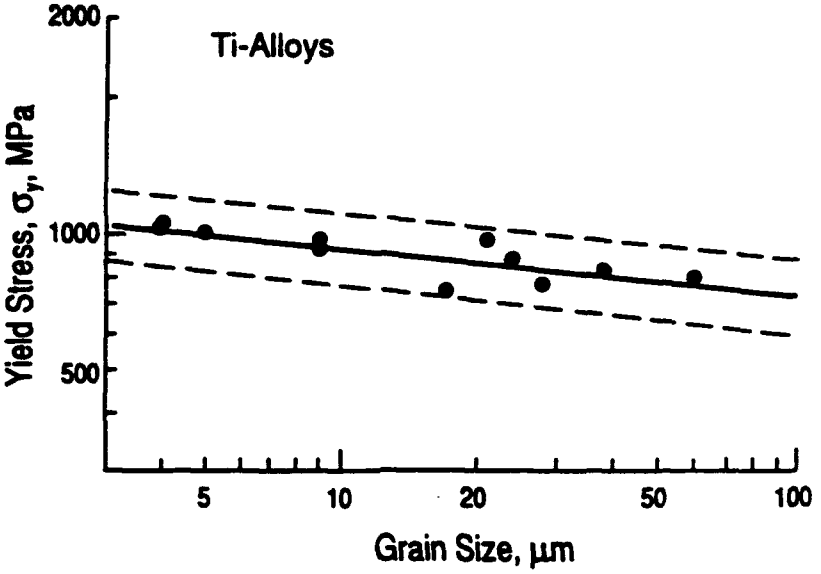

(a)

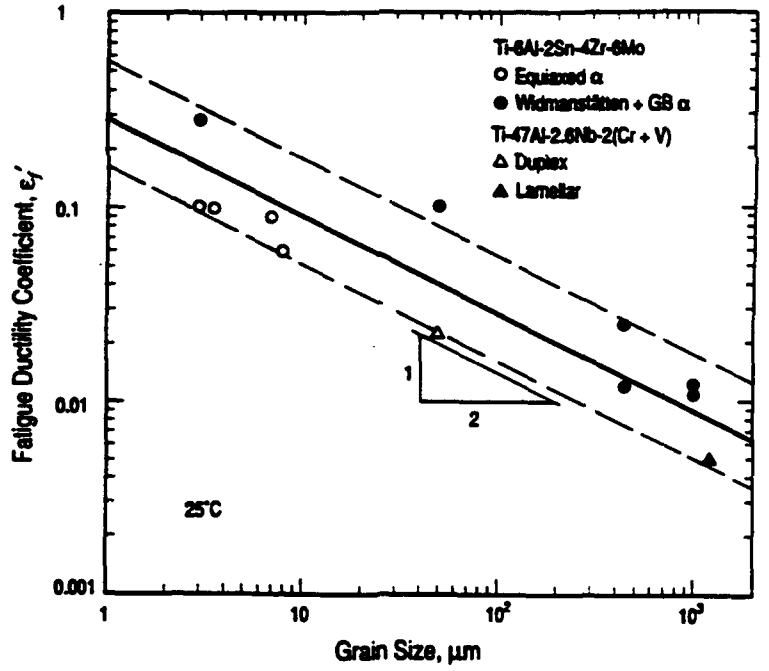

(b)

Figure 2. Correlations of yield stress and fatigue ductility coefficient with grain size for Ti-alloys: (a) yield stress *(Yoder et al., 1979)*, and (b) fatigue ductility coefficient *(Chan, 1993)*.

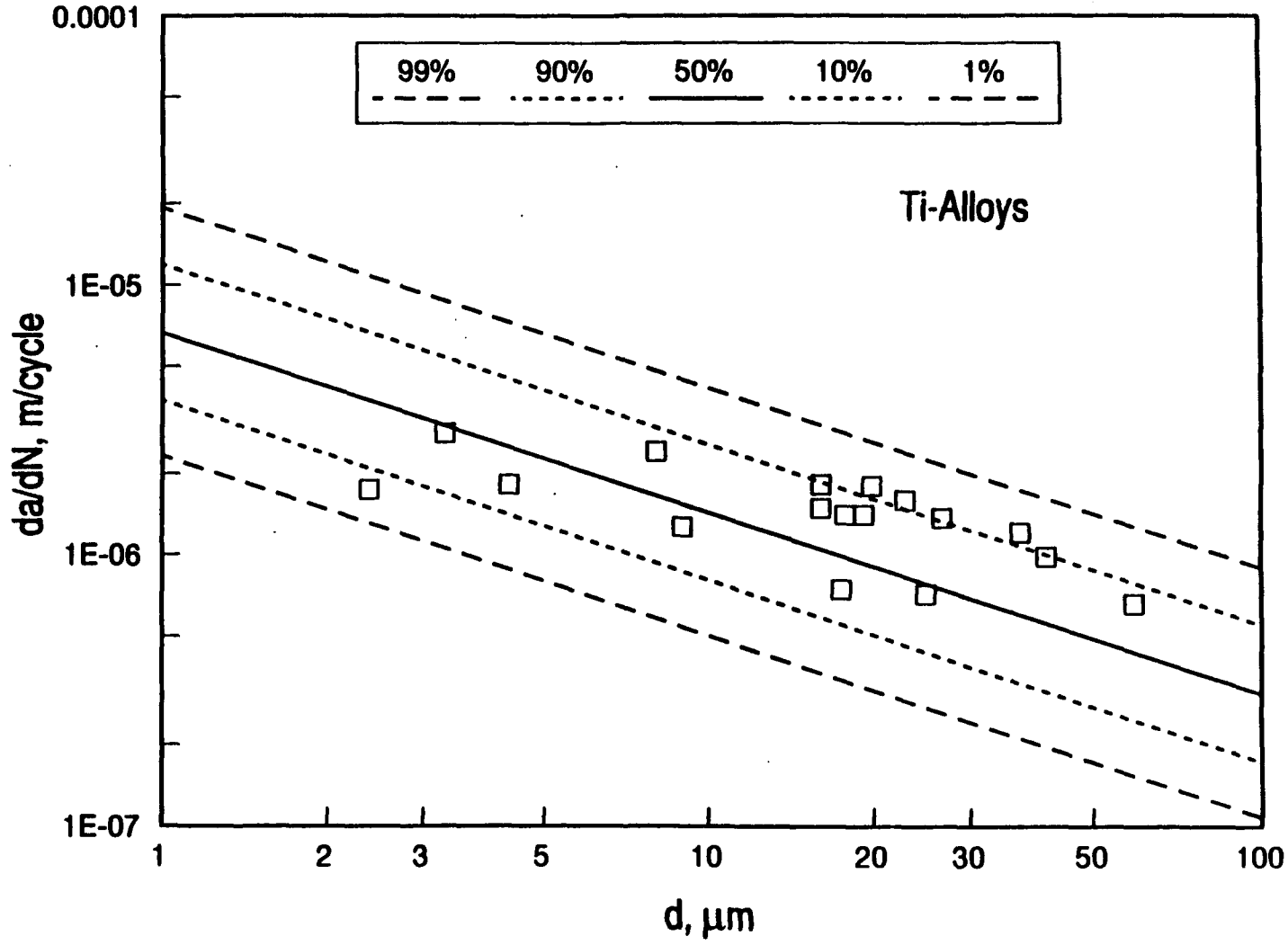

Figure 3. Stochastic model calculation compared against experimental crack growth data *(Yoder et al. 1979)* for Ti-alloys showing decreasing crack growth rate with increasing dislocation barrier spacing, which corresponds to grain or packet size for Ti-alloys.

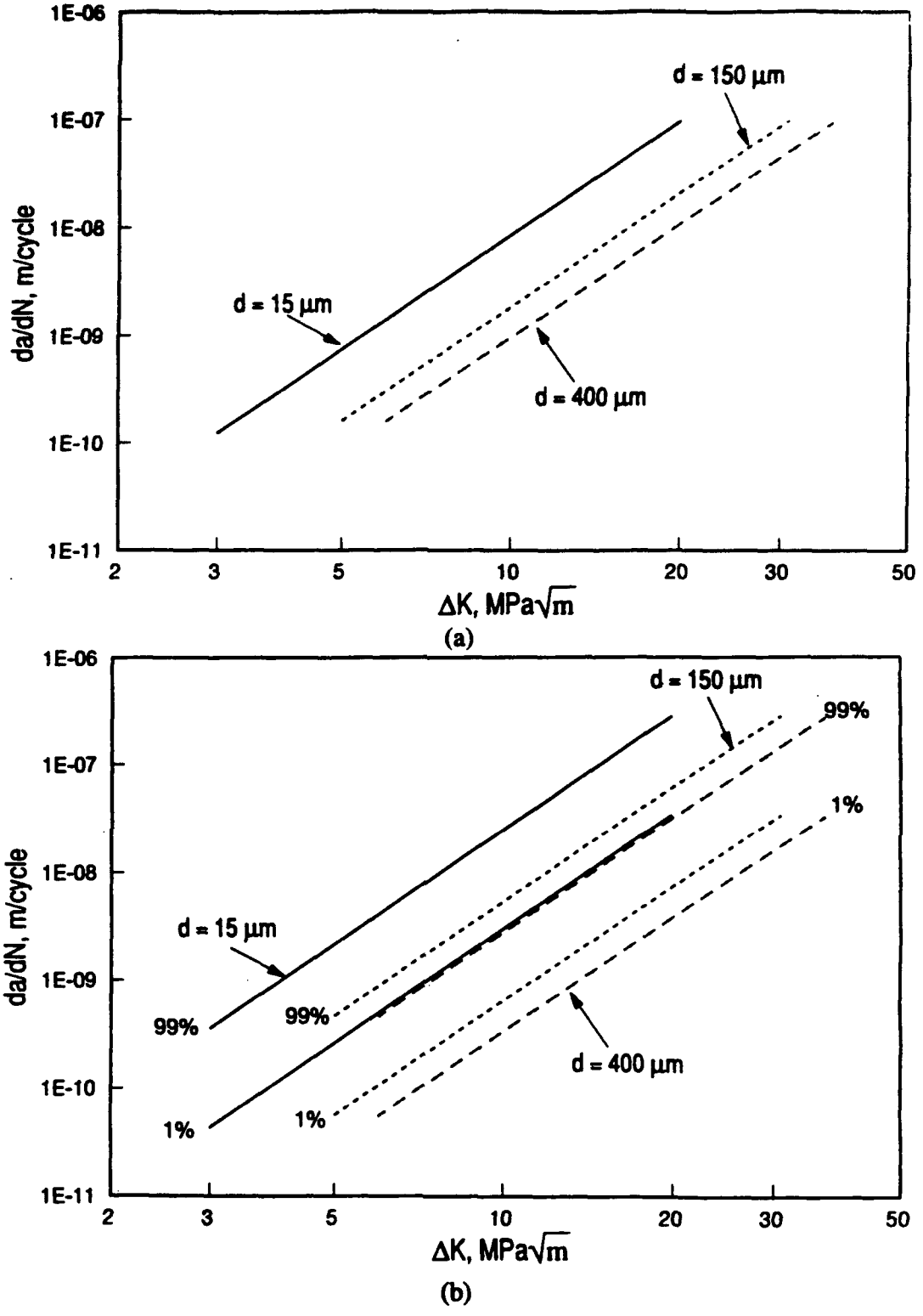

Figure 4. Dependence of fatigue crack growth rate on the grain or packet size predicted by the stochastic fatigue crack growth model: (a) mean curves, and (b) crack growth curves at 1% and 99% confidence levels.

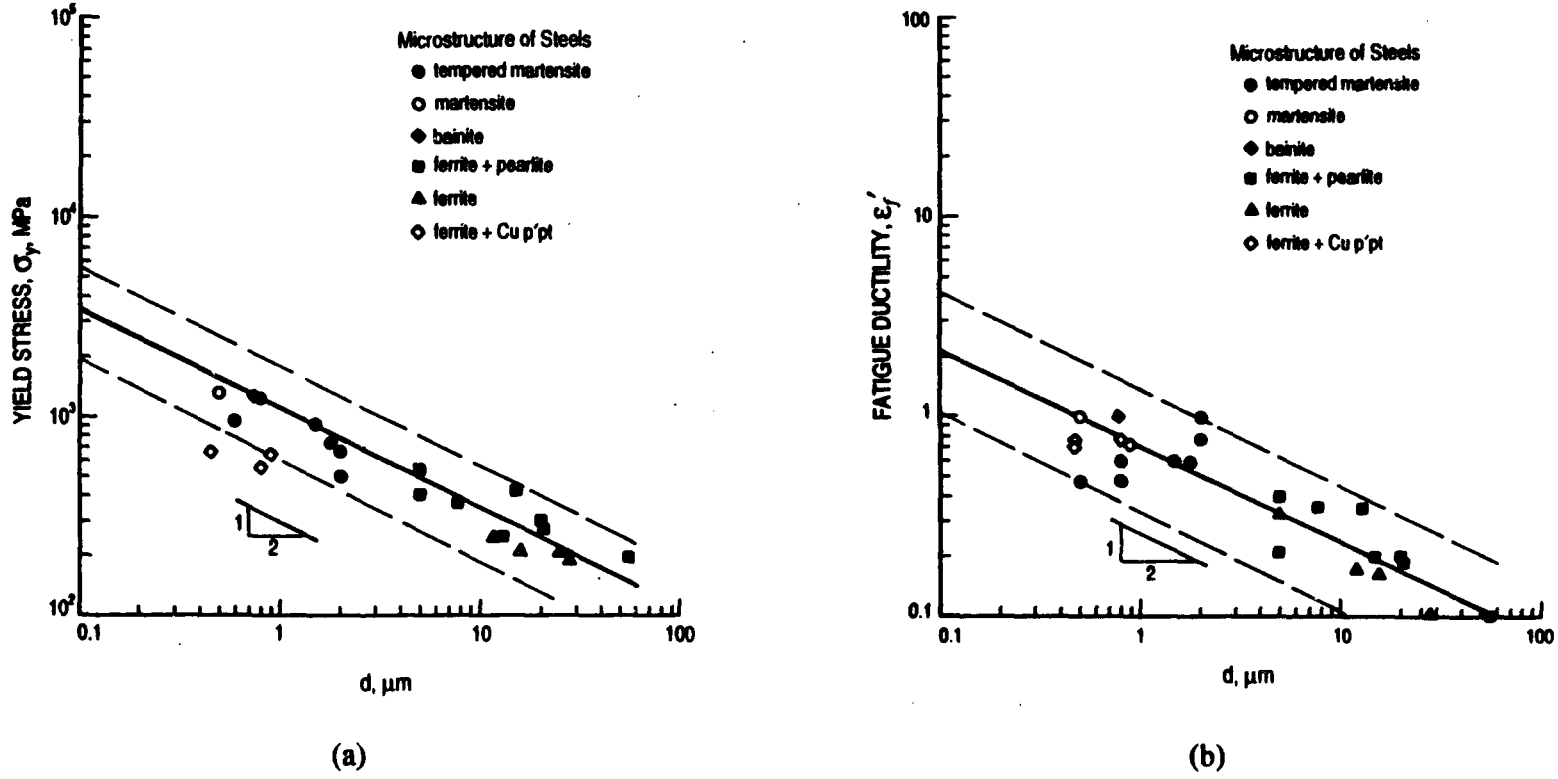

Figure 5. Correlations of yield stress and fatigue ductility coefficient with dislocation barrier spacing for steels: (a) yield stress, and (b) fatigue ductility coefficients *(Chan, 1993)*.

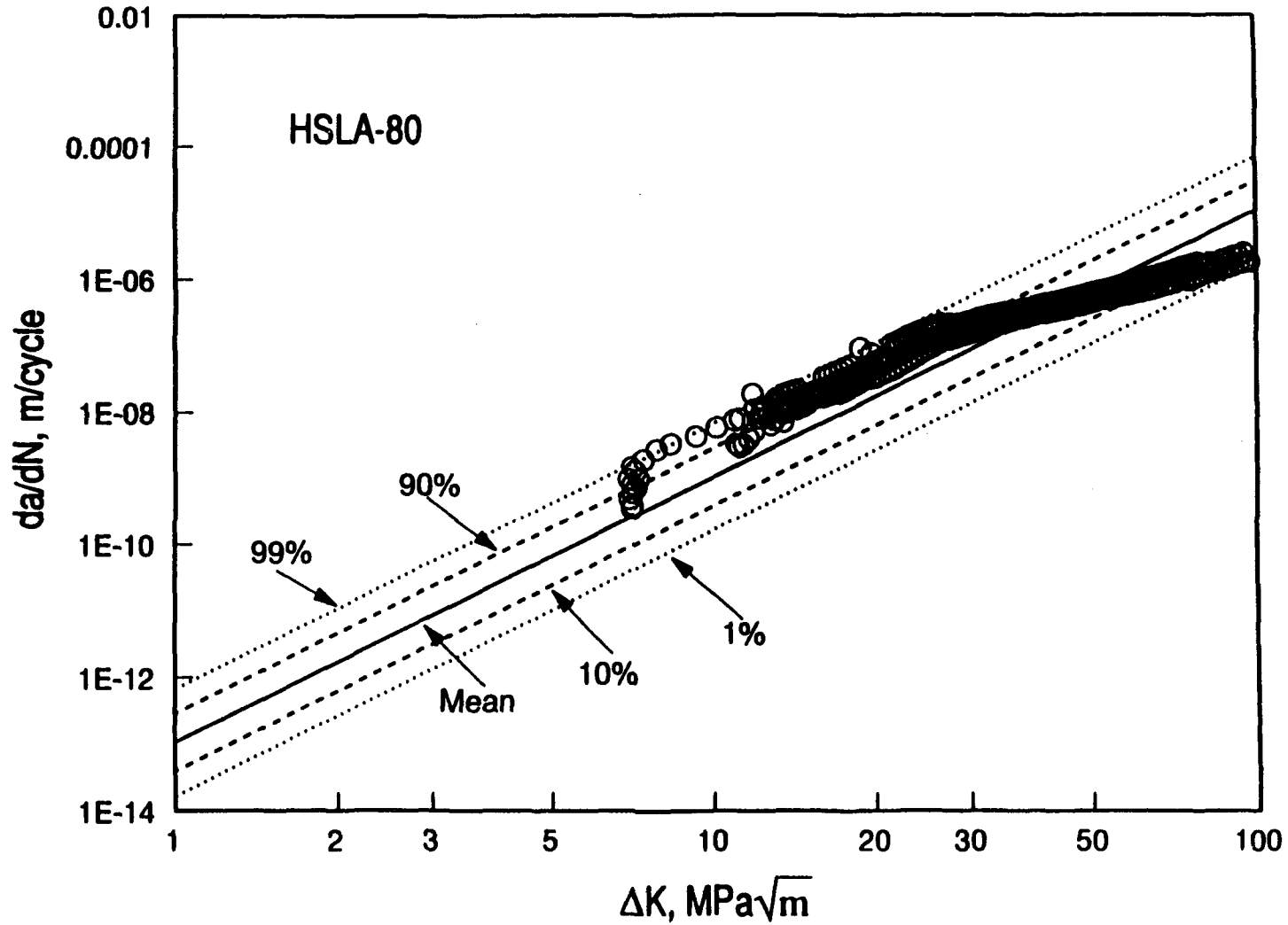

Figure 6. Stochastic model calculation compared against experimental crack growth data *(Dexter, 1993; Todd et al., 1993)* for HSLA-80 steels.

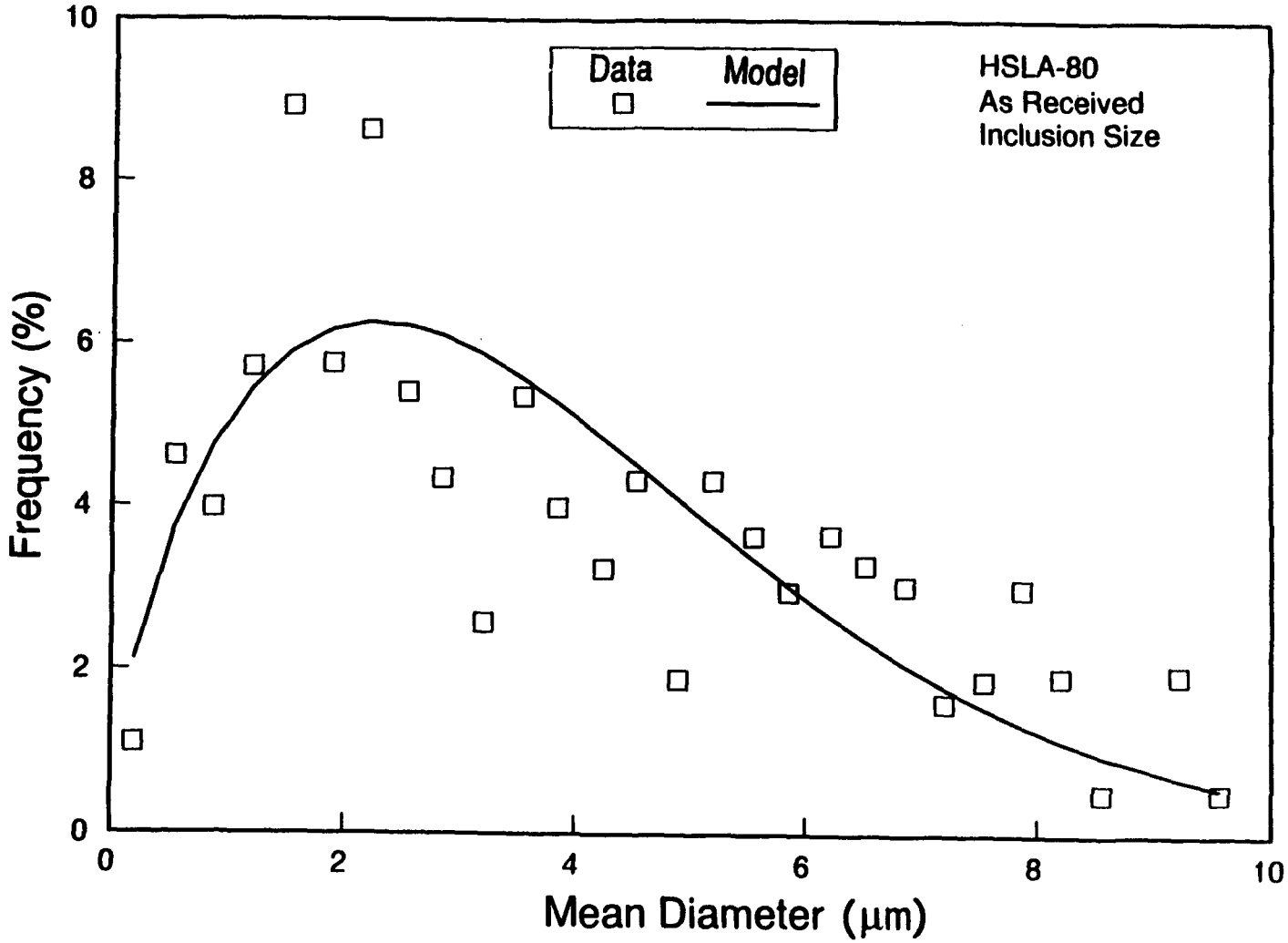

Figure 7. Calculated and measured inclusion size distribution for HSLA-80 steels in the as-received condition.

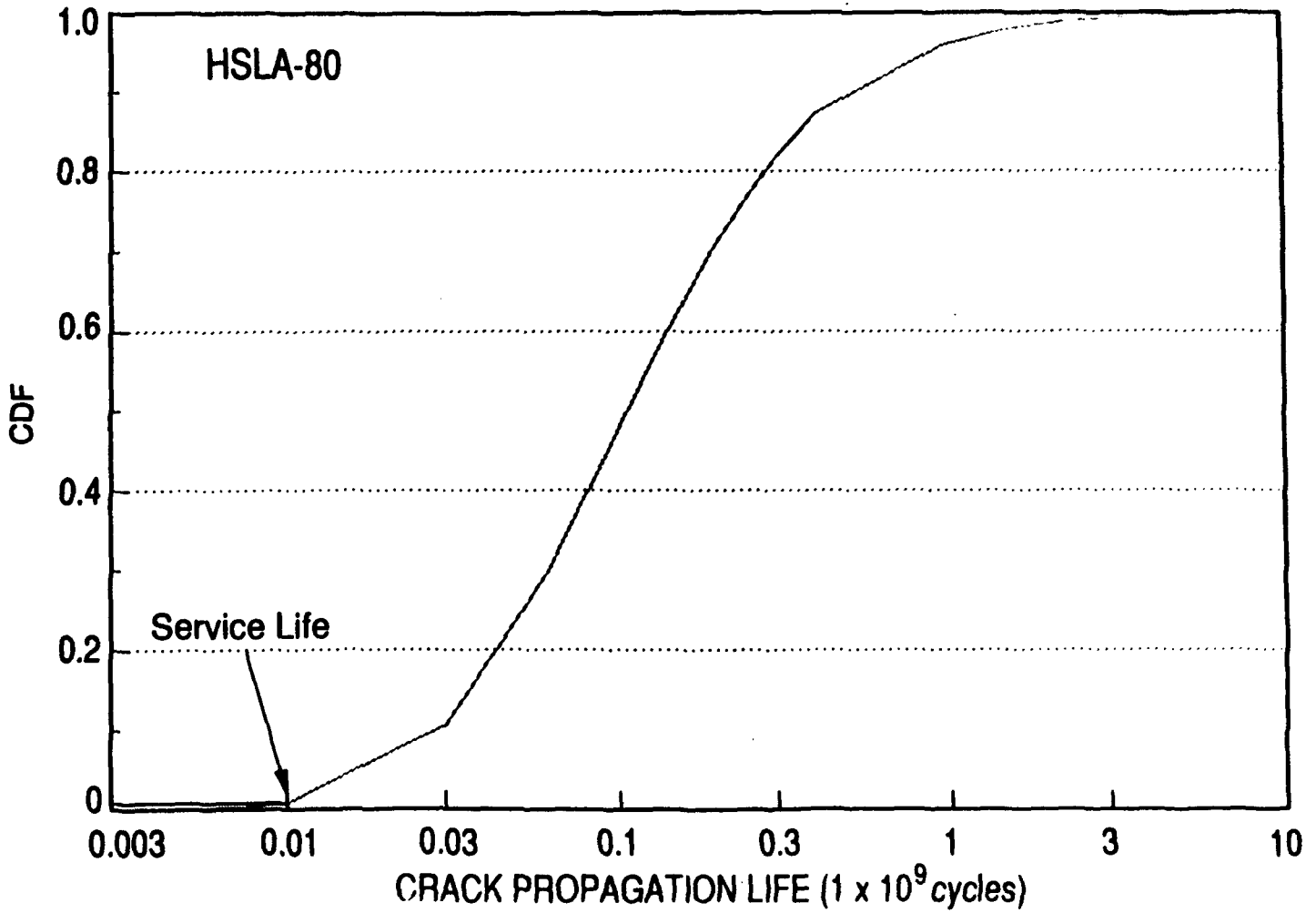

Figure 8. Calculated CDF plot for crack propagation life of the HSLA-80 steel. The probability of failure is 7.9×10^{-3} at a desired service life of 10 million cycles.

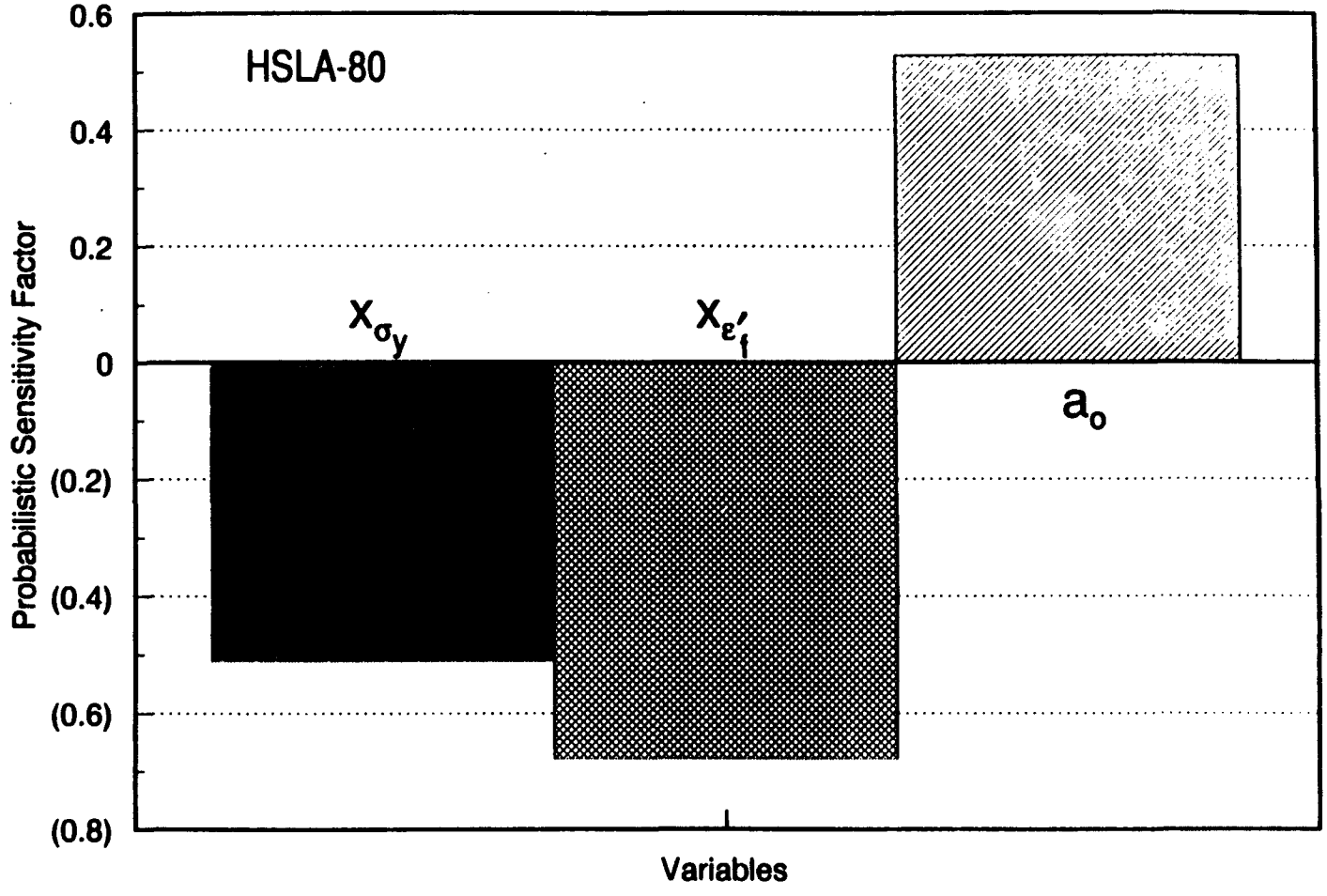

Figure 9. Calculated values of the probabilistic sensitivity factor for the yield stress, fatigue ductility, and initial crack size random variables for the CDF calculation for HSLA-80 steels.

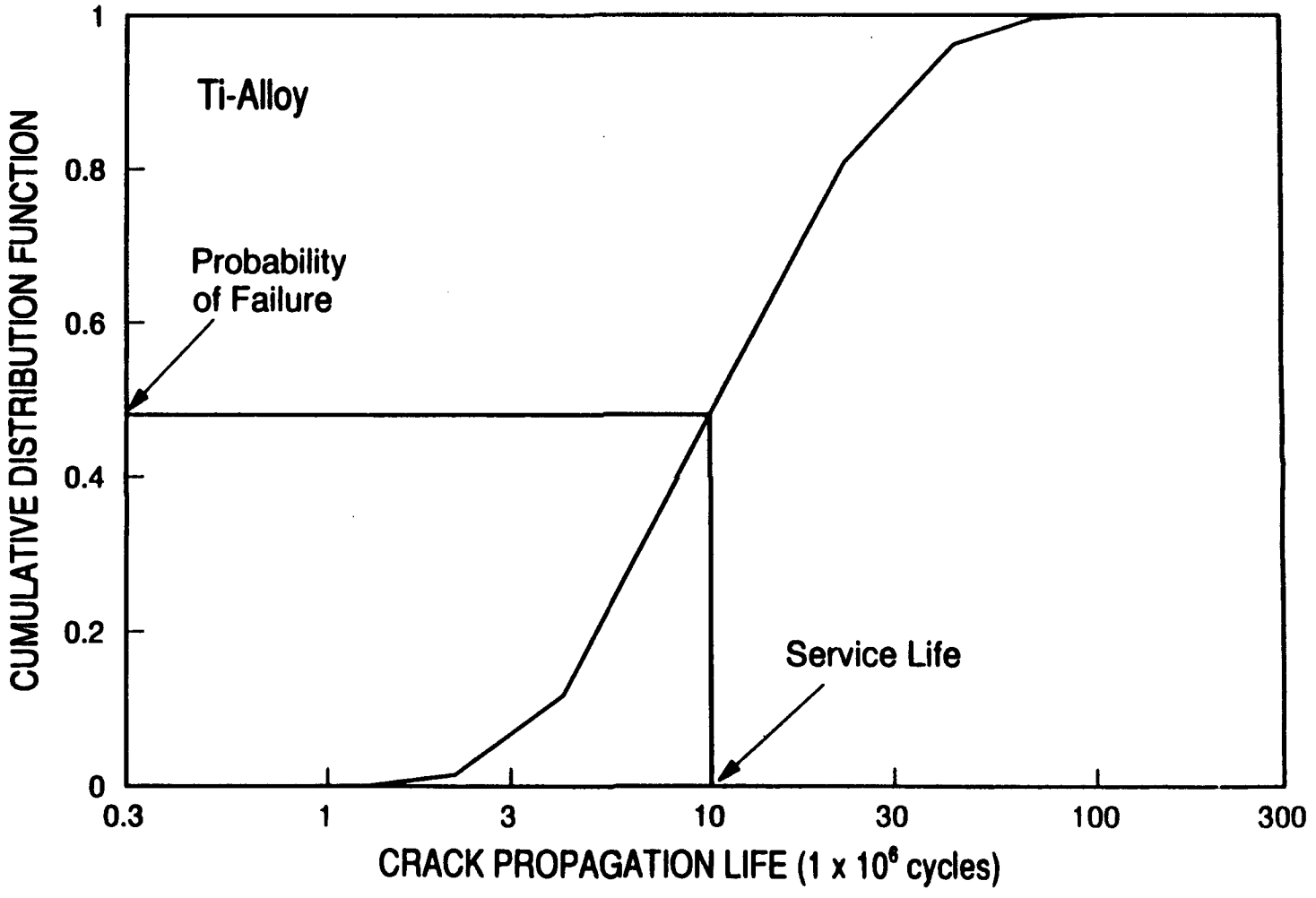

Figure 10. Calculated CDF plot for crack propagation life of a Ti-alloy. The probability of fatigue is 0.497 at a desired service life of 10 million cycles.

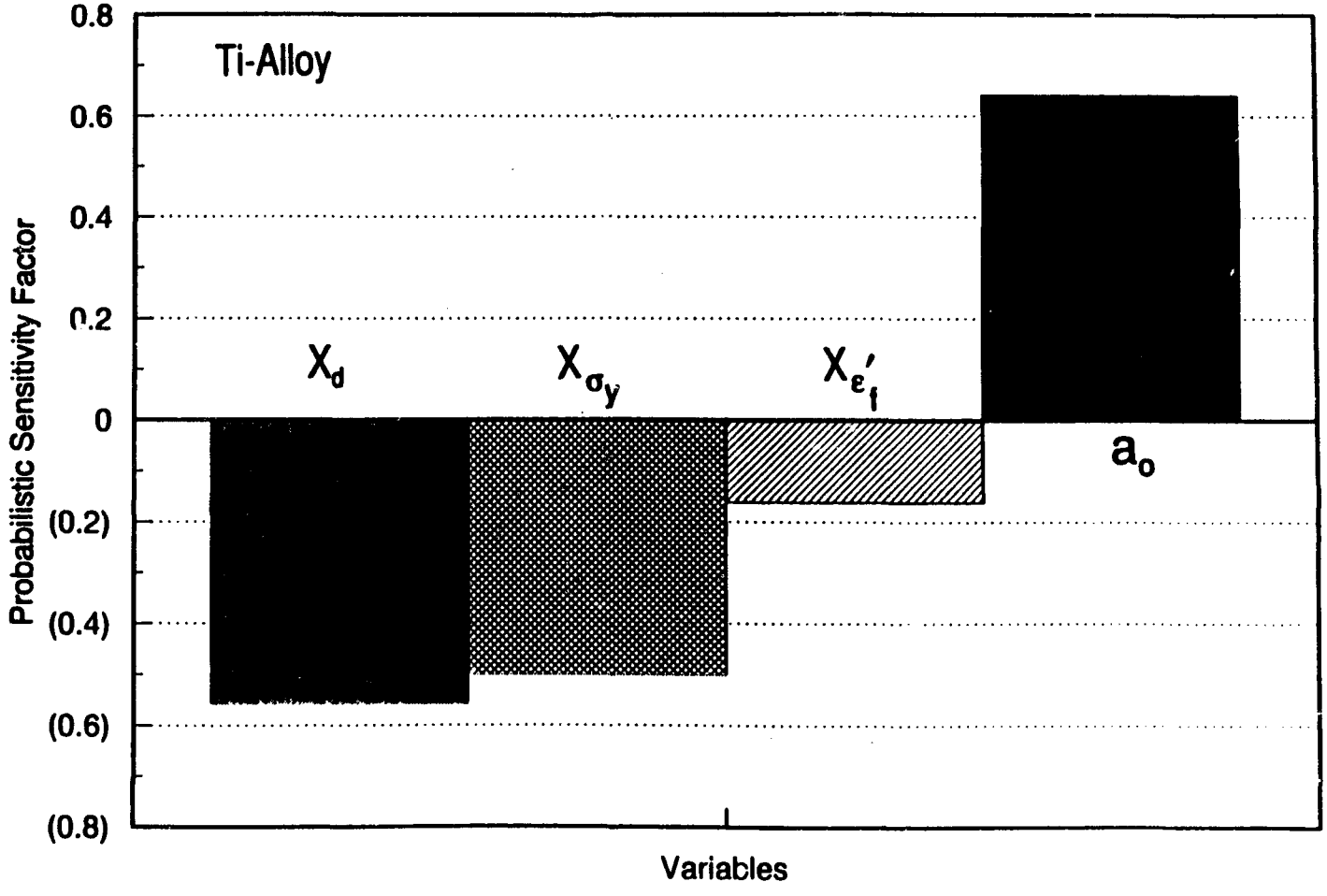

Figure 11. Calculated values of the probability sensitivity factor for the yield stress, fatigue ductility coefficient, dislocation barrier spacing, and initial crack size random variables for the CDF calculation for a Ti-alloy.

APPENDIX F

"Probabilistic Fatigue Life Prediction Methods for Small and Large Fatigue Cracks"

T. Y. Torng and R. C. McClung

[An earlier version of this manuscript was presented and published as paper AIAA-94-1509, AIAA/ASME/ASCE/AHS/ASC 35th Structures, Structural Dynamics, and Materials Conference, April 1994, pp. 1514-1524.]

[Selected portions of this revised manuscript and Appendix D have been combined to develop a manuscript entitled, "Analysis of Small Fatigue Cracks in HSLA-80 Steel," by R. C. McClung and T. Y. Torng, to be submitted for publication]

PROBABILISTIC FATIGUE LIFE PREDICTION METHODS FOR SMALL AND LARGE FATIGUE CRACKS

T. Y. Torng and R. C. McClung
Southwest Research Institute

INTRODUCTION

Fatigue crack growth (FCG) is fundamentally a random phenomenon because of the macroscopic variation (from specimen to specimen) as well as the microscopic variation (along the crack path in a single specimen). This randomness may be most apparent and most significant for small cracks, when crack-microstructure interactions are also most significant. Small crack growth rate data are often characterized by great variability, especially in comparison to growth rate data for large cracks outside of the near-threshold region. Because of this large variability, simple deterministic schemes to compute small crack-dominated life may not be satisfactory. Algorithms based on best estimates such as mean values cannot account for the significant possibility of non-conservatively faster growth. Attempts to "envelope" the data with upper bound crack growth curves may be excessively conservative, leading to unnecessary rejection of safe hardware.

Therefore, small crack growth is a particularly good candidate for probabilistic life prediction methodologies. Unfortunately, small crack growth also presents special obstacles to developing probabilistic models. In particular, it is often difficult to collect raw FCG data of sufficient quality and quantity to compute necessary probabilistic parameters. Crack length measurement is expensive and often cumbersome for small cracks. Small crack initiation and growth is especially unpredictable, and so it is nearly impossible to obtain data at fixed crack lengths or fixed growth intervals. Smooth specimens are characterized by multiple microcrack initiation and growth, so it is not easy to identify *a priori* a single dominant crack, and different microcracks may interact or link up later in life. These difficulties are not insurmountable, but they do influence the path to a solution.

One of the goals of the subject research program is to develop probabilistic fatigue life prediction methods based on the growth of both small and large cracks. This particular goal is guided by two central criteria. The first criterion is that these methods will reflect some genuine understanding of the physical sources of uncertainty in small crack and large crack growth, and that the mathematical methodologies will, in some way, reflect this understanding. This criterion excludes some existing probabilistic FCG methodologies which cannot be linked to the physical process of small crack growth. The second criterion is that these methods will retain sufficient mathematical simplicity to permit their practical use in engineering contexts. This criterion excludes other methodologies which may be theoretically attractive but are scientifically or mathematically complex.

In this report, various potential sources of uncertainty in FCG are discussed, with special attention to small crack behavior and microstructural influences. Next, the two steps necessary to the development of probabilistic fatigue life methods are addressed: (a) the derivation of an appropriate stochastic FCG model, and (b) the selection of a robust, efficient, and accurate probabilistic method. Several simple example problems are posed and solved to illustrate various physical and mathematical issues.

SOURCES OF SCATTER IN FCG DATA

Before attempting to develop engineering life models based on probabilistic treatments of the data, it is important to understand different potential sources of the FCG rate variability. These understandings should provide additional insight into the observed increase in scatter for small cracks.

Actual fatigue crack growth data for both large cracks and small cracks are shown in Figure 1 for the HSLA-80 steel. Small crack data were obtained from both rotating, fully-reversed bending tests (Specimens 353 and 354) and three-point bend tests (Specimen 347), while large crack tests were conducted on compact tension specimens. Here the correlating parameter ΔK is defined as $\Delta K = K_{max} - K_{min}$ when $R \geq 0$, and $\Delta K = K_{max}$ when $R < 0$. As noted previously (see Appendix D), the correlation of these particular large crack and small crack data based on this definition of ΔK gives similar results to a correlation based on ΔK_{eff}.

Note that small cracks and large cracks grow at similar rates in the traditional large-crack power-law regime. However, the small cracks can grow at applied stress intensity factors which are smaller than the traditional long crack threshold value (in this case, the large crack ΔK_{th} is about 7.5 MPa•m$^{1/2}$). While both large cracks and small cracks exhibit some growth rate variability, the scatter in small crack growth rates in the low ΔK regime is generally much greater.

In the following paragraphs, some different sources of uncertainty are identified and briefly discussed, with a special emphasis on small crack behavior and microstructural issues.

Crack growth increment rate

In general, the FCG testing procedure measures the crack size at pre-selected increments of cycles in order to determine the crack growth rate. The crack growth increment rate is defined as the crack growth rate between any two adjacent time intervals. This growth rate can be viewed as the microscopic variation along the crack path of a single specimen. With enough specimen growth data, a distribution function can be constructed for each crack growth increment. The "scatter" of the FCG increment rate is described by the coefficient of variation (COV), which is simply the standard deviation divided by the mean value.

At least two physical arguments support the potential decrease of the FCG increment rate COV as the crack grows. First of all, when the small crack is small relative to characteristic microstructural dimensions, such as the grain size, and when the driving force is on the same order as the threshold resistance to crack growth (the condition for nonpropagating cracks), a large variability in growth rate (including crack arrest) is to be expected. When the crack becomes large relative to the microstructure, and the driving force easily overcomes local microstructural barriers to crack advance, the variability should decrease.

The second physical argument is mathematically based. Even if the variability (the standard deviation) in the crack growth increment rate remains unchanged with further crack growth, the significance of this variability decreases as the FCG increment rate increases (i.e., the COV decreases as the mean value increases). Put another way, as the crack length grows and the average FCG rate increases, minor variations in crack growth during a given increment become less and less significant. When the total crack length is small, these minor variations in crack growth have a large impact on calculated growth rate scatter (the COV is larger).

Measurement (estimation) error

Errors in the measurement of crack length can have a large impact on FCG rates for small cracks, when the crack length a and crack growth increment Δa are small compared to the measurement resolution. However, the same estimation error can typically be ignored in the large crack regime, because both a and Δa are large compared to estimation error. This estimation error can sometimes be reduced using improved experimental procedures or instrumentation.

Crack superposition effect during crack growth

Crack growth usually starts from a small initial crack and then gradually increases increment-by-increment. The final crack size, a_F, is equal to the sum of the initial crack size, a_I, and crack growth increments, δa_i:

$$a_F = a_I + \sum_{i=1}^{n} \delta a_i \tag{1}$$

The true distributions for both a_I and δa_i are very difficult to determine. However, it can be easily proved that both a_I and δa_i are dependent non-negative random properties. As discussed in the "crack growth increment rate" section, the mean value and COV of the crack growth increment rate will respectively increase and decrease with time. Therefore, these δa_i distributions may be correlated. With the assumption of independence, the final crack size, a_F, becomes a random property and its mean, standard deviation, and COV become approximately

$$\mu_{a_F} = \mu_{a_I} + \sum_{i=1}^{n} \mu_{\delta a_i} \tag{2}$$

$$\sigma_{a_F} = \sqrt{\sigma_{a_I}^2 + \sum_{i=1}^{n} \sigma_{\delta a_i}^2} \tag{3}$$

and

$$COV_{a_F} = \frac{\sigma_{a_F}}{\mu_{a_F}} \tag{4}$$

respectively. Because both a_I and δa_i have non-negative mean values, the coefficient of variation (σ_{a_F}/μ_{a_F}) of the final crack size will continuously be reduced as more increments are included. Compared with the initial crack size and each individual crack growth increment, the resulting final crack coefficient of variation is significantly smaller. The mean or standard deviation of each crack growth increment rate may be affected by other factors, of course, but the trend of reducing the COV should remain the same.

This mathematical phenomenon can be interpreted physically as an averaging effect. As cracks increase in length and grow faster, the change in crack length during fixed measurement intervals also gradually increases. This larger crack growth increment permits more averaging of local perturbations in growth rate along the crack path, so that the average growth rate per increment $\Delta a/\Delta N$ is closer to the true mean.

A similar behavior can also be observed in large crack test data (e.g., Virkler *et al.* [1]) even when the initial crack size is relatively large. In the Ortiz [2] analysis of the Virkler data, a larger variability was observed for shorter crack lengths, even though these crack lengths were considerably larger than the traditional "small crack" regime. In other words, the first few increments have larger variability. These test data converged faster (smaller variability) than typical small crack data because they started at larger initial crack sizes.

Example 1

In order to illustrate some of these issues, a simple example problem was formulated and solved. An initial crack size (10^{-6} meter) and the initial crack growth increment rate (10^{-6} meter/2000 cycles) were assumed to be independent normally distributed functions with mean and standard deviation equal to 10 and 5, respectively. For the second and the following increments, the mean value was assumed to increase at a rate of 1% of the crack size; the standard deviation was assumed to decrease at a rate of 0.5% of the crack size (but with a lower bound limit = 2). In other words, for a crack of length $100(10^{-6})$ meter, the mean value and standard deviation of the next increment rate become 11 and 4.5 (10^{-6} meter/2000 cycles), respectively. An estimation error at each measurement was also assumed to be a normally distributed random variable with mean = 0 and standard deviation = 10^{-6} meter.

Based on these assumptions, a Monte Carlo method was used to simulate the crack growth process. The results for a total of eight simulations are shown in Figure 2. The results are qualitatively similar to the actual experimental data in Figure 1: large variability in the small crack regime, and relatively smaller variability in the large crack regime.

This simple model permits the evaluation of different sources of scatter in the small crack regime. For example, Figure 3(a) shows the results of simulations in which the increment rate standard deviation was not decreased with crack growth. Figure 3(b) gives the results for a set of simulations in which estimation error was assumed equal to zero. Figure 3(c) illustrates the effect of larger initial crack sizes. Note that in all three cases, the scatter in growth rates still reduces appreciably as the cracks reach a certain length.

Example 1A

Of course, the specific results in these simulations are dependent on the specific numerical assumptions made about various sources of scatter. In order to generate simulations which were more realistic, a set of the HSLA-80 small crack data (specimens 353/354) was analyzed to estimate the distributions of the initial crack size, measurement error, and crack growth increment rate. Because the available data sets were relatively small, several assumptions were required.

Observations of crack nucleation conducted previously (see Appendix A) found that small cracks initiated at inclusions in the as-received material. Therefore, the initial crack size distribution was set equal to the inclusion size distribution. Statistical analysis of inclusion size measurements from the as-received HSLA 80 steel found that inclusion size had a Weibull distribution with parameters $\alpha = 1.59$ and $\beta = 4.27 \cdot 10^{-6}$ meter.

In this particular example, the estimation, or measurement, error was relatively small. Acetate replicas were taken of the specimen surface, and the actual crack length measurement was based on inspection of the replica in the scanning electron microscope. This measurement technique has extremely high resolution, on the order of $0.1 \cdot 10^{-6}$ meter. Based on this observation, the estimation error was assumed to be normally distributed with mean equal to zero and standard deviation equal to $0.1 \cdot 10^{-6}$ meter.

The crack growth increment rate, as suggested, was modeled as a random variable. However, the mean and standard deviation of this random variable was assumed to be a cycle- or time-dependent function, $d(N)$, where N represents the cycle number. To validate this assumption and obtain the mean and standard deviation of this crack growth rate distribution, the following analysis procedure was used:

1. For each set of crack growth data (a vs. N) corresponding to a single crack, a second-order polynomial function was constructed from a linear regression of $\log_{10}(a)$ vs. $\log_{10}(N)$.
2. The overall cycle range of interest, [N_F(final cycle) - N_I (initial cycle)] was identified, and then partitioned into J intervals of equal width ΔN.
3. For each cycle increment, the crack growth increment was calculated from each second-order function developed in step 1. The mean and standard deviation of the crack growth increment rate were then calculated, respectively, as follows,

$$\mu_{(da/dN)_j} = \frac{1}{k}\sum_{i=1}^{k}\left(\frac{\Delta a}{\Delta N}\right)_i \tag{5}$$

$$\sigma_{(da/dN)_j} = \sqrt{\frac{\sum_{i=1}^{k}\left(\left(\frac{\Delta a}{\Delta N}\right)_i - \mu_{(da/dN)_j}\right)^2}{k-1}} \tag{6}$$

where k represents the total number of data sets and j represents the jth crack growth increment (total = J).

4. Based on all these computed values of $\mu_{(da/dN)_j}$ and $\sigma_{(da/dN)_j}$, the time-dependent functions for the mean value of the crack growth increment rate, $d_{\mu_{(da/dN)_j}}(N)$, and the coefficient of variation (= standard deviation divided by mean) of the crack growth increment rate, $d_{COV_{(da/dN)_j}}(N)$, were constructed.

Notice that the analysis procedure described in (1)-(4) is focused on crack-to-crack variability, rather than point-to-point variability as an individual crack grows. This approach was chosen for several reasons. First of all, point-to-point data will also include the effects of measurement error as well as averaging phenomena. In this analysis, however, the intended focus was a characterization of the crack growth increment rate, independent of measurement and averaging effects. The regression procedure used to characterize each individual crack serves to minimize these other effects, leaving only the true variation from crack-to-crack. Second, since each crack is growing through an independent sample of the microstructure, this procedure should be more successful in isolating genuine microstructurally-induced variations, which is the intended goal of this particular analysis. This information should then be equally transferable to describe microstructurally-induced scatter from point-to-point for a single crack. Third, this regression procedure also insures that the

data from each crack will be weighted equally. If point-to-point data from different cracks were pooled, cracks with more data points (typically, from cracks which were growing slower) could bias the analysis. Fourth, a rigorous treatment of point-to-point scatter requires considerably more crack growth data (and of a higher quality) than is practical to generate for small cracks. And fifth, since the ultimate stochastic life issue involves variability from crack-to-crack (how long until the fastest crack grows to failure?), this is an appropriate focus earlier in the analysis.

This procedure enables $d_{\mu_{(da/dN)_j}}(N)$ and $d_{COV_{(da/dN)_j}}(N)$ to be estimated. However, it should be noted that the limited available data do not make it possible to rigorously assess the distribution type and the quality of these statistical assumptions. Nevertheless, to demonstrate the concept, it has been assumed that the crack growth increment rate is a lognormally distributed function with mean $\mu_{(da/dN)_j}$ and standard deviation $\sigma_{(da/dN)_j}$ at each crack growth increment.

In this particular example, an polynomial expression for the mean value of the crack growth increment rate, $d_{log10\left(\mu_{(da/dN)_j}\right)}(N)$, was developed from a linear regression of the $\log_{10}(da/dN)$ vs. $\log_{10}(N)$ data. A similar linear regression for the standard deviation, $d_{log10\left(COV_{(da/dN)_j}\right)}(N)$, was judged to be an unsatisfactory description of the data at larger values of N. Instead, a simple empirical relationship was devised and judged to be of satisfactory quality for demonstration purposes. The mean and standard deviation of crack growth increment rate at the jth interval ($j \cdot \Delta N$) was then calculated as

$$\mu_{(da/dN)_j} = 10^{\left[d_{log10\left(\mu_{(da/dN)_j}\right)}(j \cdot \Delta N)\right]} \tag{7}$$

$$\sigma_{(da/dN)_j} = 10^{\left[d_{log10\left(\mu_{(da/dN)_j}\right)}(j \cdot \Delta N) + d_{log10\left(COV_{(da/dN)_j}\right)}(j \cdot \Delta N)\right]} \tag{8}$$

With all the distributions defined, a simulation program was created to simulate the crack growth. The simulated results are shown in Figure 4, which are superimposed with the original experimental data. The trends of the simulated data match reasonably well with the original experimental data. The slight disagreement in slope at larger crack sizes arises because insufficient experimental data was available to properly calculate the crack growth increment rate distributions in this regime.

These examples demonstrate that good analysis strategy can be used to understand different sources of uncertainty more clearly. In principle, this capability should also facilitate more accurate interpretation of the sources of scatter for different applications, and ultimately some predictive capability for small crack growth rate variability. These fundamental understandings of FCG rate scatter may also have direct implications for life prediction. For example, apparent scatter which is largely a mathematical artifact of the analysis process should have a different impact on life prediction than real scatter which is driven by microstructure-crack interactions at low ΔK.

Further study is required to select appropriate, physically-meaningful values for the various distributions. In different applications, one or more sources of scatter may be dominant. For example, the estimation error was relatively insignificant in these simulations, because the measurement process being modeled has extremely high resolution. In some other applications,

measurement error can be a dominant source of scatter in small crack growth rates [3]. Nevertheless, a simple conceptual model of this sort provides a basis for comparing these different sources more rigorously and thereby gaining fundamental insights into the behavior of small cracks.

Fundamental microstructural effects

At the most fundamental level, the growth rate of a fatigue crack is controlled by the inherent resistance of the material microstructure to deformation and damage near the tip of the growing crack. Chan [4] has developed a set of micromechanical scaling laws which describe the effects of critical microstructural parameters on FCG rates. The scaling laws assume that FCG occurs as the result of low-cycle fatigue failure of a crack-tip element whose width and height correspond to the dislocation cell size and barrier spacing, respectively. These laws suggest that the effects of microstructure on FCG can be described in terms of a dimensionless microstructural parameter ξ, which is defined in terms of yield stress σ_Y, fatigue ductility ε_f', dislocation cell size (striation spacing) s, and dislocation barrier spacing d. The resulting FCG equation in the intermittent growth regime is

$$\frac{da}{dN} = \xi^{1/b}(2s)^{1-1/b}\left[\frac{\Delta K}{E}\right]^{2/b} X(t) \tag{9}$$

where

$$\xi = \frac{Es}{4\sigma_Y \varepsilon_f' d} \tag{10}$$

Here E is Young's modulus and b is the fatigue ductility exponent. Both σ_Y and ε_f' are also functions of the dislocation barrier spacing, d.

Variations in material microstructure (e.g., variations in the dislocation barrier spacing) from location to location within a given component (local variations) or from heat to heat of material (global variation) should therefore lead to variations in FCG rate. A probabilistic treatment of the Chan micromechanical model is discussed in Appendix E.

LIFE PREDICTION MODELS WHICH TREAT SCATTER

Uncertainty modeling

Before introducing the life prediction models, it is useful to introduce statistical strategies which will be used to quantify the random properties, including the crack initiation size and the critical crack size. The uncertainties identified must be carefully modeled so that the calculated fatigue life is unbiased and accurate. In general, there exist various types of uncertainties which can be broadly classified as being either reducible or irreducible [5]. Irreducible uncertainties are intrinsic to nature and beyond our ability to control, e.g., material properties. Reducible uncertainties are attributed to estimation error, modeling error, and human error, and cannot be completely avoided. The effects of reducible uncertainties, however, can be attenuated by additional testing, more accurate modeling, and better quality control measures.

Given enough test data, the irreducible uncertainties can be modeled as random variables with selected distribution types, means, and standard deviations by using proper statistic tools. The same analysis strategy may be applied to the reducible uncertainties, but the resulting means or standard deviations may not be the true means or standard deviations because of either estimation or human error. Thus, for the reducible uncertainties, an additional random variable may be used to account for the modeling errors and random means or standard deviations may be used to account for those estimation error or human error.

The effects of irreducible types of uncertainty are reflected in the calculated reliability, whereas the effects of reducible types of uncertainties are reflected in a confidence bound on the calculated reliability result [5]. In other words, with the existence of reducible type of uncertainty such as uncertain mean and standard deviation, the reliability itself becomes a random variable.

Critical crack size distribution. Some distribution for the critical crack size is required to complete the mathematical formulation. In practice, the final crack size often has a relatively weak effect on the total FCG life, so accurate determination of this distribution may be of less importance.

Stochastic fatigue crack growth models

An appropriate stochastic fatigue crack growth (SFCG) model should be as simple as possible while maintaining a reasonable accuracy for the prediction of the FCG damage accumulation. The SFCG must be able to address the small crack regime (large variability) as well as the large crack regime (small variability). Thus, the selected SFCG must be able to predict the fatigue life reasonably without underestimating the life in the small crack regime or overestimating the life in the large crack regime.

The model of Ortiz [2] is an intriguing SFCG option, because it attempts to address the influence of microstructure on rate variation along the crack path. This proposed model uses a random FCG model to deal with the macroscopic variation, and an additional random noise model to deal with the microscopic variation. As a result, this model needs the probability distribution functions of the coefficients of random FCG, the probability distribution function of the variance of random noise, and the correlation length of the autocorrelation function of random noise.

Unfortunately, the Ortiz model requires a large number of replicate test data to construct accurately the random parameters such as the joint distribution of the coefficients of random FCG and the variance of random noise. The quantity and quality of available small crack data is typically not good enough to construct all these parameters. In addition to the data limitation, the Ortiz model also requires the crack growth measurements, a vs N, at constant growth increments, Δa, so that the correlation length can be determined more exactly. This requirement stands in contrast to the usual experimental procedure, which generates FCG data at constant ΔN increments. Several other stochastic FCG growth models also share the same fundamental limitation, including the Markov chain and semi-Markovian models [7, 8]. Construction of an accurate Markov transition matrix usually requires a large data base.

When only limited data are available, a lognormal random variable model proposed by Yang et al. [9, 10, 11] is useful. This model uses the simplest mathematical model for which the analytical solution may be derivable, and it can easily be understood by engineers. Because this model does not consider the crack correlation length, crack growth parameters and the model statistics can be estimated from a limited quantity of baseline test results, which is all that is available in many practical applications.

To account for microstructural effects, a non-infinite correlation time (or correlation distance in the Ortiz model) has been proposed [9, 11]. The resulting stochastic model, called a lognormal random process model, is composed of a random FCG law and a stochastic process, i.e.,

$$\frac{da}{dN} = f(\xi, \Delta K, a, R) X_{\xi}(t) \tag{11}$$

where da/dN is the crack growth rate and $f(\xi, \Delta K, a, R)$ is a user-defined function (FCG model) of microstructural features (ξ), stress intensity factor range (ΔK), crack size (a), stress ratio (R). When microstructural features are addressed explicitly, scaling laws such as those proposed by Chan [4] can be employed as the function f. $X_{\xi}(t)$ represents a non-negative stationary lognormal random process which will be used to account for the combined effect of unknown contributions toward changing the crack growth rate with time, t (expressed in terms of the number of cycles, N). $X_{\xi}(t)$ is also considered to be a function of microstructural features.

In general, the lognormal random process model or Ortiz model can be used to solve the problems described in Refs [2, 9, 10] because small crack data are not available or considered. Small crack data, however, exhibit much greater growth rate variability (cf. Figure 1) for reasons discussed earlier. In principle, an ideal model can be created based on both initial crack size and increment crack size distributions, and the life can then be predicted accurately using these distributions. To obtain all of the necessary distributions, however, an enormous number of tests is required. In most fatigue tests, especially for small cracks, data are difficult to acquire and limited in quantity and/or quality.

Thus, an enhanced model is proposed to deal with the nonlinear variability phenomenon while maintaining a computationally simple model for the probabilistic analysis. This enhanced model first uses the same analysis strategy proposed for the lognormal random variable model to obtain the basic trends of mean value crack growth. Some additional enhancements are then added to account for the nonlinear variability exhibited by the actual FCG data. Before formally introducing this enhanced model, some background issues related to the construction of a regular lognormal random variable model are discussed first.

A lognormal random variable model

To construct this lognormal random variable model successfully, the following key factors, which can influence the accuracy of the prediction, must be addressed.

An appropriate fatigue crack growth model. The choice of the crack growth law has a significant impact on crack growth predictions. A poor fit may introduce a low frequency signal into the residuals, which increases the variance and adds to the correlation of the residuals. The well-known Paris law may be adequate for the power-law FCG regime and, as indicated by Figure 1, this power-law relationship may be extrapolated downward as an engineering estimate of small crack growth rates. For some materials, as discussed in Ref. [4], the power-law regime may be further subdivided into intermittent and continuous growth regimes. In this case a simple Paris law is inadequate and a bilinear model may be the best choice. In general, the lognormal random variable model is obtained from Eq. (11) as

$$\log\left(\frac{da}{dN}\right) = \log(f(\xi, \Delta K, a, R)) + \log(X_\xi(t))$$

$$= \log(f(\xi, \Delta K, a, R)) + Z_\xi(t) \qquad (12)$$

Equal number of data points for each test specimen. In the small crack data sets generated in this study, each crack growth specimen (and often each crack) has an unequal number of data points. In particular, more crack size measurements were taken for slow growth specimens/cracks than for fast ones. This may introduce some bias to the crack growth rate calculated. As such, it clearly violates the statistical premise that each specimen is of equal weight. Consequently, the resulting statistical FCG predictions are biased toward the nonconservative side: the stochastic model tends to predict a longer propagation life or smaller crack size. To circumvent such an error due to an unequal number of measurements for each specimen, additional data points for the primary data (a versus N or $\log(da/dN)$ vs $\text{Log}(\Delta K)$) may be added artificially to the fast crack growth specimens. In this work, each available data set was fitted using least squares regression with the selected fatigue model to get the parameters of the model. Additional data points were then generated over a global range of ΔK. These artificial points were used only to assist in the evaluation of crack-to-crack scatter, not point-to-point scatter within a single data set.

Data processing procedure. According to the small crack data generated in this study, each crack growth data set contains very large statistical dispersion, especially in the low ΔK regime. As discussed earlier, these statistical dispersions may be caused by crack measurement error (or human error), crack superposition effects, microstructural effects, etc. Among the available data processing methods, the secant method retains the original statistical dispersion of the crack growth rate data more accurately than any of the incremental polynomial methods which reduce the undesirable statistical variability by smoothing out the original crack growth rate. As discussed by Ortiz, these 5-, 7-, or 9-point incremental polynomial methods may distort the original behavior of the data. For the simple lognormal random variable model, which incorporates all the uncertainties into a single lognormal random variable, the mean behavior is more important. In this case, the polynomial methods may be more acceptable.

Goodness-of-fit test. To validate the accuracy of the model, Kolmogorov-Smirnov (K-S) tests for goodness-of-fit should be used to determine the observed K-S statistics of $Z_M(t)$ (a normally distributed variable). These statistics will then be used to determine if the normal distribution is acceptable or not, at a certain significance level, given the available data sets. For problems with either few data sets or bad quality data, the use of this lognormal random variable model must be carefully examined.

Example 2: Lognormal random variable model

One example of the SFCG model in application to a particular HSLA-80 data set is shown in Figure 5. Here the lines describing the 10%, 50% (mean value), and 90% probability of exceedence in growth rate as computed from the SFCG model are superimposed on the raw crack growth data from [6], with a simple Paris Law as the user-selected FCG model. Final results are listed in Table 1. The model generally accounts for the uncertainties. However, in the higher ΔK region (longer cracks), the estimates may be overconservative.

Table 1. Summary of results from Example 2

Data Set	Paris Coef. C	Paris Expo. m	Std. Dev. σ_Z
353/354	1.004E-12	2.8662	0.187

An enhanced lognormal random variable model

This enhanced lognormal random variable model is based on the same philosophy and mathematics as the lognormal random variable model, with additional consideration given to the different variabilities exhibited in the small crack and large crack regimes. In the following paragraphs, only the enhanced features of the model will be discussed further.

As shown in Figure 5, in the small crack regime many data points fall outside of the 90 percent and 10 percent bounds, while in the larger crack regime the bounds seem overly conservative. In order to improve the lognormal random variable model while maintaining its computational simplicity, the stochastic random variable, $Z(t)$ was modified. Originally, $Z(t)$ had a mean value equal to zero and a fixed standard deviation value, σ_Z. To accommodate the increased scatter in the small crack regime, the standard deviation σ_Z was modeled as a time-dependent function so that σ_Z became larger in the small crack regime and smaller in the large crack regime.

To acquire this time dependent function for $Z(t)$, an analysis procedure was proposed as follows:

1. For each set of crack growth rate data (da/dN vs. ΔK) corresponding to a single crack, a linear approximation function was constructed from a linear regression of $\log_{10}(da/dN)$ vs. $\log_{10}(\Delta K)$.
2. The overall ΔK range of interest, [ΔK_F (final ΔK) - ΔK_I (initial ΔK)], was identified, and then partitioned into J intervals of equal width, $\delta\Delta K$.
3. For each increment of ΔK, the crack growth rate was calculated from each function developed in step 1. The mean and standard deviation of the crack growth rate were then calculated as

$$\mu_{log10(da/dN)_j} = \frac{1}{k}\sum_{i=1}^{k} log10\left(\frac{da}{dN}\right)_i \tag{13}$$

$$\sigma_{log10(da/dN)_j} = \sqrt{\frac{\sum_{i=1}^{k}\left(log10\left(\frac{da}{dN}\right)_i - \mu_{log10(da/dN)_j}\right)^2}{k-1}} \tag{14}$$

where k represents the total number of data sets, and j represents the jth ΔK increment (total = J). It is reasonable to select a best-fitted distribution to represent these data. In addition, the confidence level for these data can also be constructed for probability assessment.

4. Given enough data, a normal distribution is assumed. In other words, the mean ($\mu_{log10(da/dN)_j}$) and standard deviation ($\sigma_{log10(da/dN)_j}$) calculated in Eqs. (13) and (14) can be used to determine the crack growth rate at any selected probability level. By collecting all crack growth rates at the same probability level (p%), a crack size dependent crack growth rate function, $C_{p\%}(\Delta K)$, can be constructed.

5. With $C_{p\%}(\Delta K)$, the crack growth rate at the $p\%$ level can be calculated as follows:

$$\frac{da}{dN_{p\%}}(\Delta K) = 10^{C_{p\%}(\Delta K)} \tag{15}$$

The final product of this proposed approach is a crack size dependent crack growth rate function, $C_{p\%}(\Delta K)$, which will be used to account for the time-dependent function, $Z(t)$.

Again, note that this particular analysis procedure focused on crack-to-crack scatter rather than point-to-point scatter for individual cracks. This approach was chosen for several of the same reasons cited earlier in the discussion of simulation models. An emphasis on genuine (microstructurally-induced?) scatter in the crack growth increment rate is appropriate because it is this scatter, not measurement error or averaging effects, which will have a genuine impact on total fatigue life.

Example 2A: Enhanced lognormal random variable model

To demonstrate the proposed approach, the same example solved in Example 2 using the lognormal random variable model is used. Because there are only six data sets (353/354), it is very difficult to justify a normal distribution for the crack growth rate at each ΔK level as suggested in the proposed procedure. However, for demonstration purpose, it is assumed that a normal distribution assumption can be used. Based on this assumption, three time-dependent crack growth rate functions, $da/dN_{5\%}(\Delta K)$, $da/dN_{50\%}(\Delta K)$, and $da/dN_{95\%}(\Delta K)$, are listed as follows:

$$\frac{da}{dN_{5\%}}(\Delta K) = 10^{C_{5\%}(\Delta K)} = 10^{-13+3.77*log10(\Delta K)-0.244*log10^2(\Delta K)} \tag{16}$$

$$\frac{da}{dN_{50\%}}(\Delta K) = 10^{C_{50\%}(\Delta K)} = 10^{-12+2.866*log10(\Delta K)} \tag{17}$$

$$\frac{da}{dN_{95\%}}(\Delta K) = 10^{C_{95\%}(\Delta K)} = 10^{-11+1.962*log10(\Delta K)+0.244*log10^2(\Delta K)} \tag{18}$$

In Figure 6, 95%, 50%, and 5% bounds of both lognormal random variable model and enhanced lognormal random variable model are superimposed with the original experimental data. As expected, enhanced model has a better fit with the original experimental data where great variability of the crack growth rate is observed in the small crack regime in comparison to the growth rate observed in the large crack outside of near-threshold region.

Example 3: Models for combined large and small crack data

An enhanced lognormal random variable model of this type can also be used to address small crack and large crack data together on a consistent basis. Example 3 demonstrates the different results obtained for a conventional lognormal rv model and an enhanced lognormal random variable model. The statistical results for the lognormal random variable model are given in Table 2. Details of the mathematical approach used to derive this particular enhanced lognormal random variable model are described in Ref. [12].

Figure 7 shows the Log(da/dN) vs Log(ΔK_{eff}) data from these two approaches. The enhanced lognormal rv model should lead to life predictions which are more accurate.

Table 2. Summary of results from Example 3

Data Set	Paris Coef. C	Paris Expo. m	Std. Dev. σ_Z
353/354/ 347/Large	4.58E-12	3.396	0.374

Both the simple and enhanced lognormal random variable models can be further increased in sophistication by considering more advanced forms of the user-defined FCG law, f. For example, the scaling laws proposed by Chan [4] can be employed. That selection is discussed in Appendix E.

Overview of probabilistic analysis methods

As noted earlier, complete solution of the probabilistic fatigue life problem requires two steps. Thus far, only one of these steps has been discussed, the development of an appropriate stochastic FCG model. The necessary second step is the development of a robust, efficient, and accurate probabilistic method to predict the fatigue life using the stochastic SFCG model.

In general, the probabilistic analysis method is developed to solve a limit-state function $g(\mathbf{X})$. Given the joint probability density function, $f_{\mathbf{X}}(\mathbf{x})$, the probability of failure can be formulated as

$$p_f = P(g \le 0)$$

$$= \int_{\Omega} \cdots \int f_{\mathbf{X}}(\mathbf{x}) d\mathbf{x} \tag{19}$$

where Ω is the failure region. This multiple integral is, in general, very difficult to evaluate. Alternatively, the Monte Carlo (MC) method provides a convenient, but usually time-consuming, solution.

The first step in the current probabilistic analysis method requires the transformation of a generally dependent, random vector $\mathbf{X}$ into an independent, standardized normal vector $\mathbf{u}$. The Rosenblatt transformation has been suggested when the joint distribution is available [5, 13]. If only the marginal distributions and the covariances are known, a transformation can be made to generate a joint normal distribution that satisfies the given correlation structure.

By transforming $g(\mathbf{X})$ to $g(\mathbf{u})$, the most probable point (MPP) in the u-space, $\mathbf{u}^*$, is located. The MPP $\mathbf{u}^*$ is the point that defines the minimum distance, β, from the origin ($\mathbf{u} = 0$ point) to the limit-state surface. This point is most probable because it has the maximum joint probability density on the limit-state surface. The MPP may be found by using optimization, advanced mean value (AMV), or other iteration schemes.

Next, the $g(\mathbf{u})$ or $g(\mathbf{X})$ function is approximated by a polynomial that approximates the true function in the vicinity of the MPP. Once the approximate function is obtained, the associated failure probability can be computed. If the $g(\mathbf{u})$ formulation is used, several analytical solutions are available for linear and quadratic functions [13, 14]. For example, the first-order reliability method (FORM) estimate is

$$P(g \le 0) \approx \Phi(-\beta), \tag{20}$$

and the asymptotic second-order reliability method (SORM) estimate, derived by Breitung [15], is

$$P(g \le 0) \approx \Phi(-\beta) \prod_{j=1}^{n-1} (1 + \beta\kappa_j)^{-1/2}, \quad \beta \to \infty \tag{21}$$

where $\Phi(\cdot)$ is the cdf of a standard normal distribution and κ_j, $j = 1, \ldots n-1$ are the main curvatures of the limit-state surface at $\mathbf{u}^*$.

However, for complex problems that require computation-intensive computer programs, it is very important to use an efficient method to calculate the cumulative distribution function of the response. The AMV and AMV+ methods were developed to search for the MPP with fewest extra g-function calculations by comparing with the conventional mean-based second-moment method (MVFOSM). AMV and AMV+ methodologies are discussed in greater detail in Ref. [16].

Fatigue life prediction using probabilistic methods

The choice of a specific probabilistic method depends on the complexity of the particular SFCG model under consideration. In the following, the probabilistic methods anticipated to be appropriate to different SFCG models are briefly discussed. Subsequent examples illustrate each of the three model types.

Lognormal random variable model. When a lognormal random variable model is used, an analytical function for the probability distribution for crack length at the given time or the probability distribution for time at the given crack length can be derived and used to predict the fatigue life. Because only one lognormal random variable is considered, this problem can be solved by most of the probabilistic approaches. Total required calculation effort is minimal. In addition, this model can easily be extended to include inspection and repair strategies.

Lognormal random variable model plus microstructural randomness. If the SFCG model also includes some detailed characterization of microstructural features, typically more random variables will be considered in the model. Therefore, more advanced probabilistic methods may be needed to solve the problem.

Enhanced lognormal random variable model. A different calculation strategy for this model is required by the time-dependent stochastic random variable, $Z(t)$(= Normal(μ_Z, $\sigma_Z \cdot C(\Delta K)$). Here the standard deviation of $Z(t)$ is controlled by a function of the stress intensity factor, $C(\Delta K)$. Because of $C(\Delta K)$, no explicit function for fatigue life can be derived directly, and a numerical integration may be required. To predict the fatigue life, an advanced mean value based method is proposed. This method requires the least number of life calculations to compute the probabilistic solution. Detailed discussion of this method is available in Ref. [16]. The other approach considered is Monte Carlo simulation. This method, however, requires many life calculations to obtain an accurate solution. Therefore, it may be unsuitable for this problem because the life integration may be time-consuming, especially for far-tail probability regions.

Example 4: Fatigue life prediction using lognormal and enhanced lognormal random variable models

The simple lognormal random variable model for small crack data introduced in Example 2 (cf. Figure 5) was used to perform life prediction. Here the analytical function was derived directly in closed form and then solved using a simple FORM method. The initial crack size and the crack initiation life selected for this data set were 9.43 μm and 10^4 cycles, respectively. The crack growth curves at 10%, 50% (mean value), and 90% can be easily calculated, as shown in Figure 8. As

predicted, the 90% and 10% curves have bounded the data well except in the small crack regime, where the lognormal random variable model failed to envelope the experimental *da/dN* data. The disagreement in this regime is also influenced by the specific selections of initial crack size and initiation life. Therefore, it is important that both values be selected carefully. Alternatively, a more complete formulation of the life prediction problem would also include some variability in initial crack size or initiation life.

Example 4A: Fatigue life prediction using an enhanced lognormal random variable model

In this example, the enhanced lognormal random variable model for small crack data introduced earlier and used in Example 2A was used to perform life prediction. Since the crack growth rate is a crack size dependent function, i.e., $C_{p\%}(\Delta K)$, no closed-form function could be derived to predict the fatigue life, and a numerical integration was required. The total life, N_T, which comprises the initiation life, N_I, plus the propagation life, N_P, was evaluated as

$$\begin{aligned} N_T &= N_I + N_P \\ &= N_I + \int_{a_0}^{a_C} \frac{1}{C_{p\%}(\Delta K)} da \\ &= N_I + \int_{a_0}^{a_C} \frac{1}{C_{p\%}(1.3\sigma_R\sqrt{a})} da \end{aligned} \tag{22}$$

where σ_R is the stress range (1080 MPa).

The same choices for initial crack size and crack initiation life were retained from Example 4. Therefore, in this example calculation the only random property is $C_{p\%}(\Delta K)$. To predict the total fatigue life at the 5%, 50%, and 95% level, equations (16), (17), and (18) were used. The fatigue crack growth rates predicted by this model are also shown in Figure 8. As expected, the enhanced lognormal random variable model predicts greater uncertainty in the small crack regime than the lognormal random variable model because it does account for larger variability. However, this model will gradually reduce the uncertainty to lower levels than the conventional lognormal random variable model as the crack grows into the large crack regime, because the crack growth rate of the enhanced model will converge faster than the lognormal model.

DISCUSSION

Progress has been achieved towards the stated goals of (1) better understanding the sources of scatter in large crack and small crack FCG data, and (2) developing simple probabilistic fatigue life prediction models which reflect these insights and which are suitable for engineering applications. Further work is required, however, to reach these goals.

Simple simulation models such as those exercised in Examples 1 and 1A should be improved through more careful study and analysis of available data. The incorporation of improved input distributions and more physically realistic crack growth relationships in these simulations should make it possible to mimic actual experimental data more closely. In principle, this capability should also facilitate more accurate interpretation of the sources of scatter for different applications, and

ultimately some predictive capability for small crack growth rate variability. These fundamental understandings of FCG rate scatter may also have direct implications for life prediction; e.g., perhaps apparent scatter which is largely a mathematical artifact of the analysis process would have a different impact on life prediction than real scatter which is driven by microstructure-crack interactions at low ΔK.

New probabilistic life models should also be linked more closely to these physical understandings. For example, it would be ideal if the formulation or calibration of the function $C(\Delta K)$ in the enhanced lognormal random variable model could be derived more directly from a physically meaningful description of the crack growth process. For example, it might be possible to calibrate $C(\Delta K)$ from a sophisticated simulation exercise, or to replace $C(\Delta K)$ with some direct function of crack size which reflects the mechanistic origins of scatter. Alternatively, expert rules might be developed to guide the construction of $C(\Delta K)$ when no experimental small crack data are available.

APPLICATIONS OF PROBABILISTIC MODELING

Development of the probabilistic models discussed above provides the opportunity and the technical foundation to solve additional aspects of the fatigue life problem.

Design strategy: probabilistic sensitivity factors. Probabilistic sensitivity factors are a significant by-product of the probabilistic analysis when advanced methods are employed. These factors provide guidance on the manner in which input uncertainties influence variability in the response function, identify those random variables which are most significant for this variability, and help to determine the optimum strategy for subsequent design analysis. They have the potential to play a stronger role in future efforts to design better critical experiments and, ultimately, to influence the direction of future engineering design strategies for naval and aerospace structures.

Life extension and management. Inspection and repair strategies are useful for extending the total fatigue life. However, calculation of the remaining life after an inspection and repair process introduces new challenges. To implement the analysis, the following quantities must be determined or developed: an initial quality of the damaged element before and after repair; a stochastic FCG model; a probability of detection curve, which is used to simulate a specific inspection technique; and advanced probabilistic methods for determining the probability of detection or remaining life. These expanded models can be used to determine both an inspection strategy (when to inspect) and a repair strategy (whether to replace or repair).

SUMMARY

The physical and mathematical sources of scatter in FCG rate data have been reviewed, giving special attention to variability in calculated growth rates for fatigue small cracks. An enhanced lognormal random variable model which can be extended to include microstructural effects has been developed to predict fatigue life for both small cracks and large cracks. This model reflects the general trend of increased scatter for small crack data, while retaining sufficient mathematical simplicity to be useful in engineering applications. Further work is required to better understand the relative quantitative importance of different sources of scatter for small cracks and large cracks,

including microstructural effects, and to more closely link the physical origins of this scatter with the engineering life prediction models. These probabilistic models could subsequently be extended to support life extension and life management, or to develop improved design strategies.

REFERENCES

1. D. A. Virkler, B. M. Hillberry, and P. K. Goel, "The Statistical Nature of Fatigue Crack Propagation," *ASME J. Engineering Materials and Technology*, Vol 101, 1979, pp. 148-153.

2. K. Ortiz and A. Kiremidjian, "Stochastic Modeling of Fatigue Crack Growth," *Engineering Fracture Mechanics*, Vol. 29, 1988, pp. 317-334.

3. J. M. Larsen, J. R. Jira, and K. S. Ravichandran, "Measurement of Small Cracks by Photomicroscopy: Experiments and Analysis," *Small-Crack Test Methods, ASTM STP 1149*, American Society for Testing and Materials, 1992, pp. 57-80.

4. K. C. Chan, "Scaling Laws For Fatigue Crack Growth Of Large Cracks In Steels," *Metallurgical Transactions A*, Vol 24A, November 1993, pp. 2473-2486 (see Appendix B).

5. A. H.-S. Ang, and W. H. Tang, *Probability Concept in Engineering Planning and Design, Volume II: Decision, Risk, and Reliability*, New York, John Wiley & Sons, Inc., 1984.

6. D. L. Davidson, K. C. Chan, and R. C. McClung, "Cu Bearing HSLA Steels: The Influence of Microstructure on Fatigue Crack Initiation and the Growth of Small Fatigue Cracks," to be submitted (see Appendix A).

7. F. Kozin and J. L. Bogdanoff, "A Critical Analysis of Some Probabilistic Models of Fatigue Crack Growth," *Engineering Fracture Mechanics*, Vol. 14, 1981, pp. 59-89.

8. F. H. Al-Sugair and A. S. Kiremidjian, "A Semi-Markovian Model For Low-Cycle Elastic-Plastic Fatigue Crack Growth," *Engineering Fracture Mechanics*, Vol. 34, 1989, pp. 1197-1207.

9. J. N. Yang, W. H. Hsi, and S. D. Manning, *Stochastic Crack Propagation With Applications To Durability and Damage Tolerance Analyses*, AFWAL-TR-85-3062, 1985.

10. G. C. Salivar, J. N. Yang, and B. J. Schwartz, "A Statistical Model For The Prediction of Fatigue Crack Growth Under A Block Type Spectrum Loading," *Engineering Fracture Mechanics*, Vol. 31, 1988, pp. 371-380.

11. Y. K. Lin and J. N. Yang, "A Stochastic Theory of Fatigue Crack Propagation," *AIAA Journal*, Vol. 23, 1985, pp. 117-124.

12. T. Y. Torng and R. C. McClung, "Probabilistic Fatigue Life Prediction Methods for Small and Large Fatigue Cracks," AIAA-94-1509, Proc. 35th Structures, Structural Dynamics, and Materials Conference, 1994, pp. 1514-1524.

13. H. O. Madsen, S. Krenk, S., and N. C. Lind, *Methods of Structural Safety*, Englewood Cliffs, New Jersey, Prentice Hall, Inc., 1986.

14. L. Tvedt, "Distribution of Quadratic Forms in Normal Space — Application to Structural Reliability," *Journal of Engineering Mechanics*, ASCE, Vol. 116, 1990, pp. 1183-1197.

15. K. Breitung, "Asymptotic Approximations for Probability Integrals," *Probabilistic Engineering Mechanics*, Vol. 4, No. 4, 1989, pp. 187-190.

16. Y.-T. Wu, O. H. Burnside, and T. A. Cruse, "Probabilistic Methods for Structural Response Analysis," *Computational Probabilistic Methods*, AMD-Vol. 93, ASME., 1988, pp. 1-14.

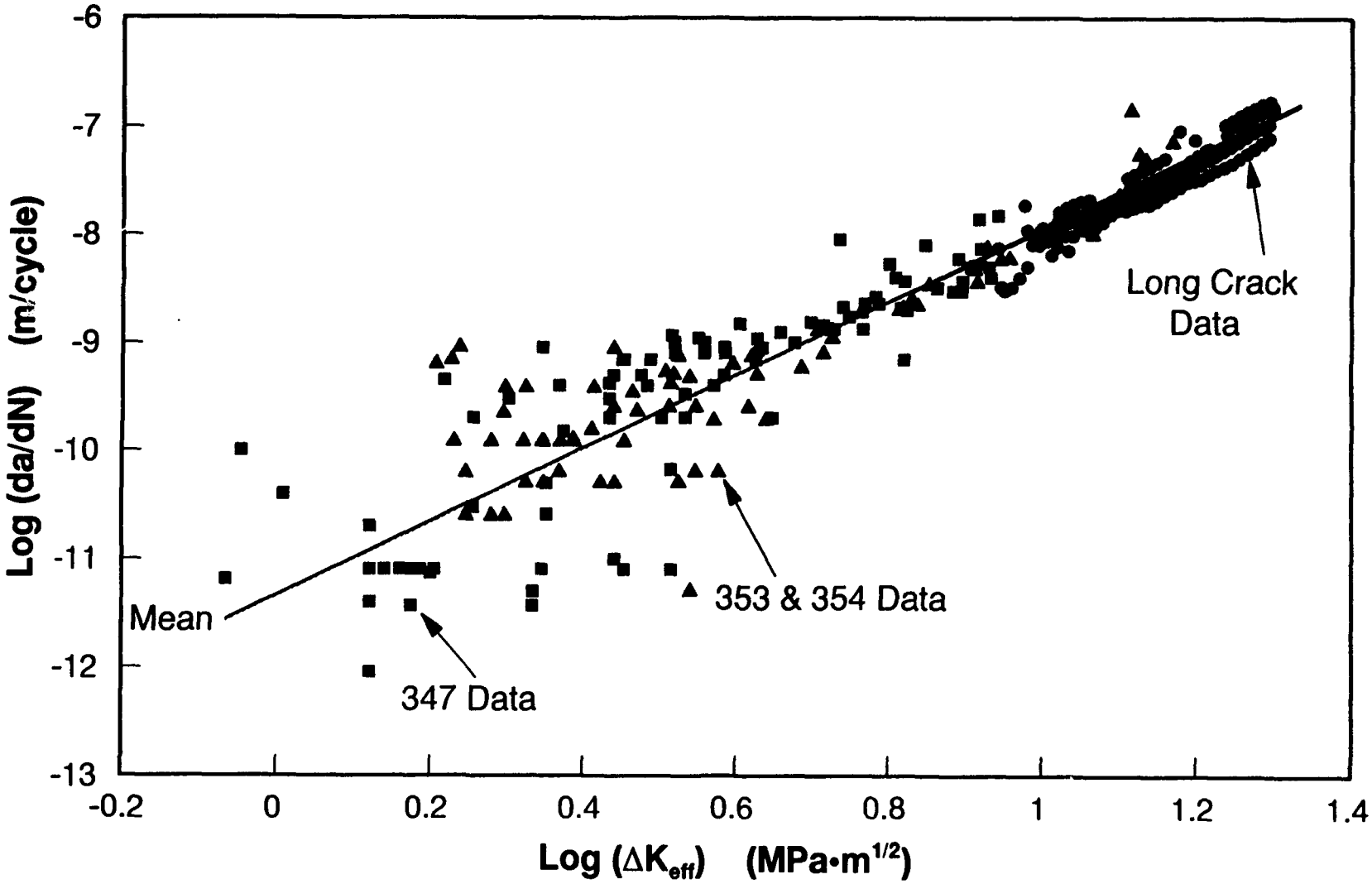

Figure 1. Growth rate data for small and large fatigue cracks in HSLA-80

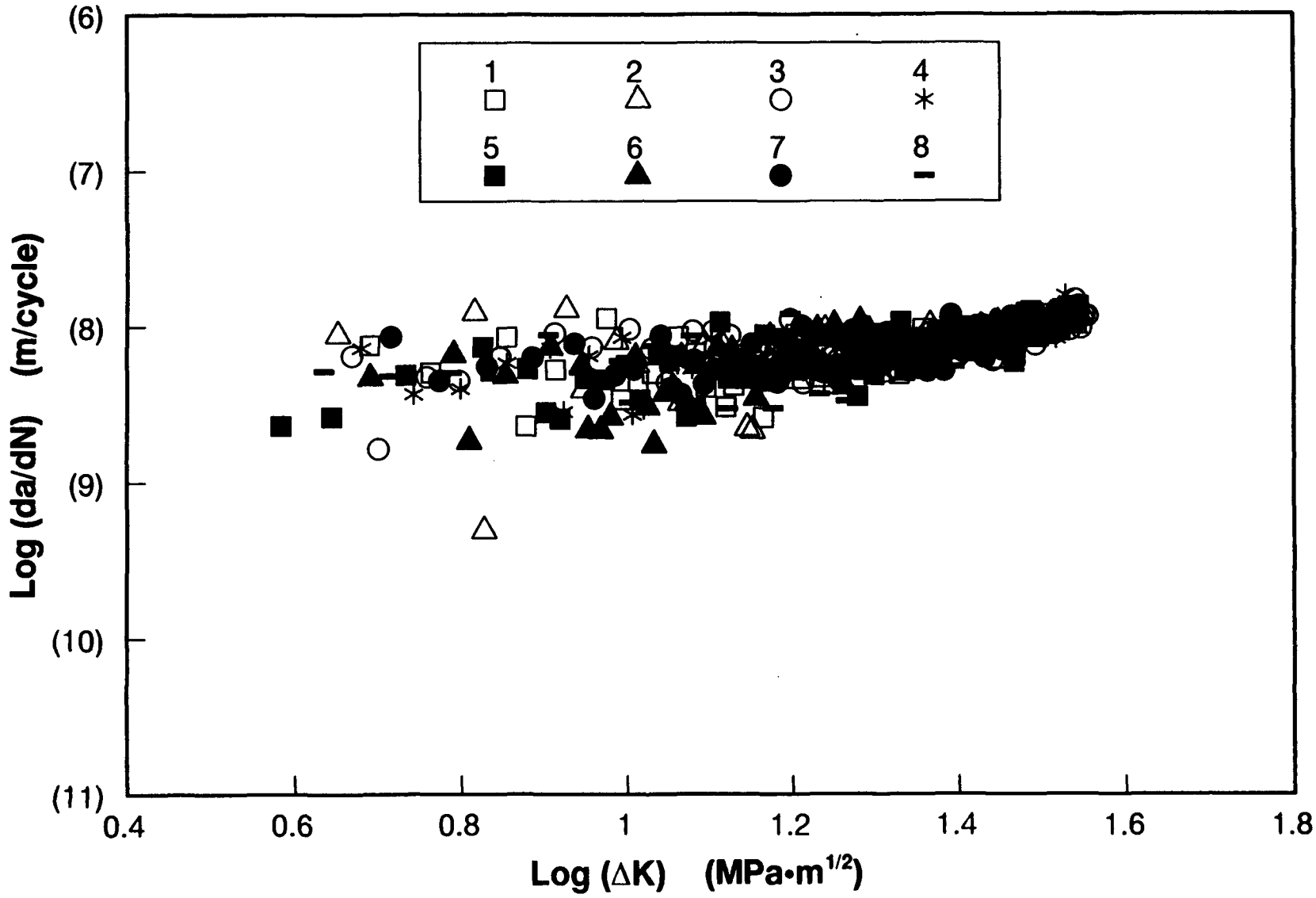

Figure 2. Simulated small crack growth rate data

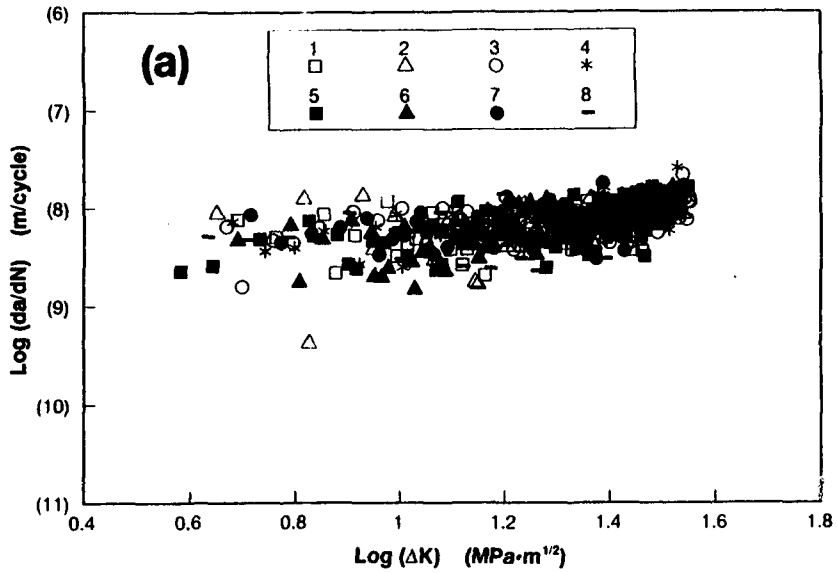

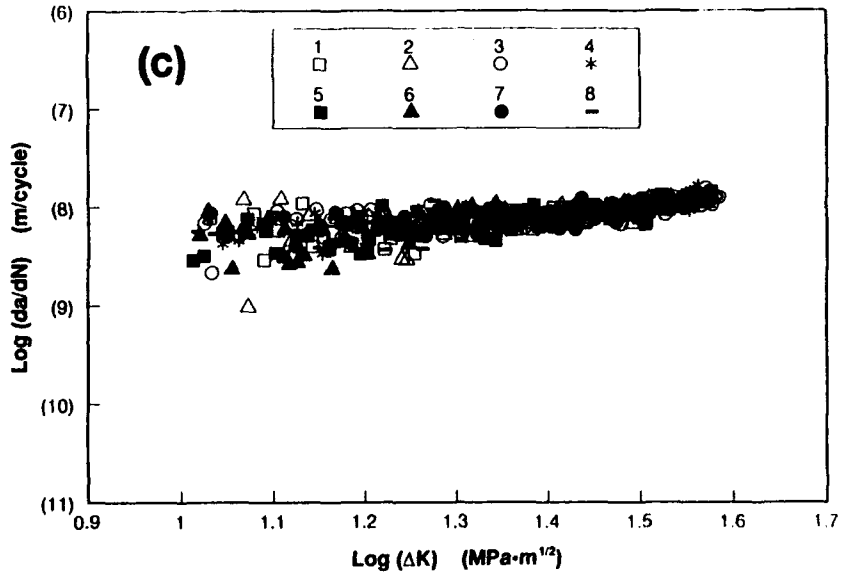

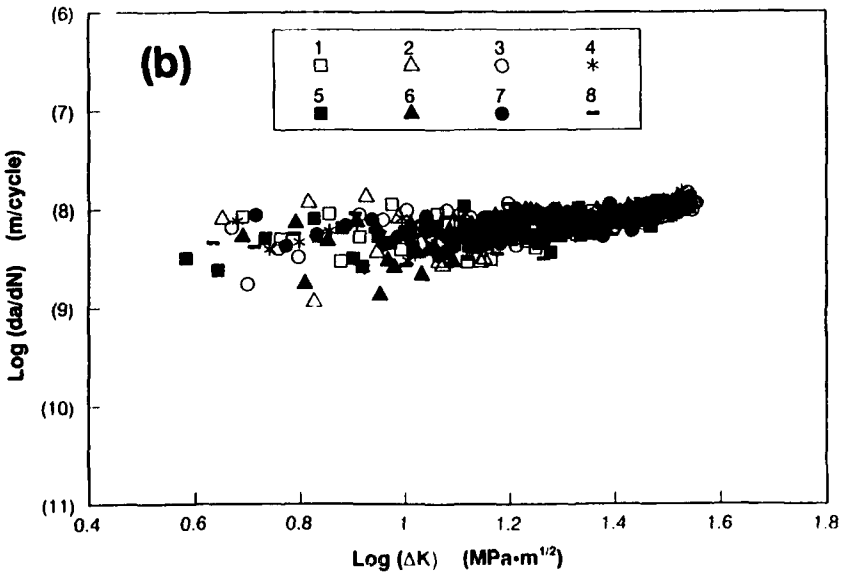

Figure 3. Simulated small crack growth rate data
(a) with constant increment standard deviation
(b) with estimation error set equal to zero
(c) with larger initial crack size

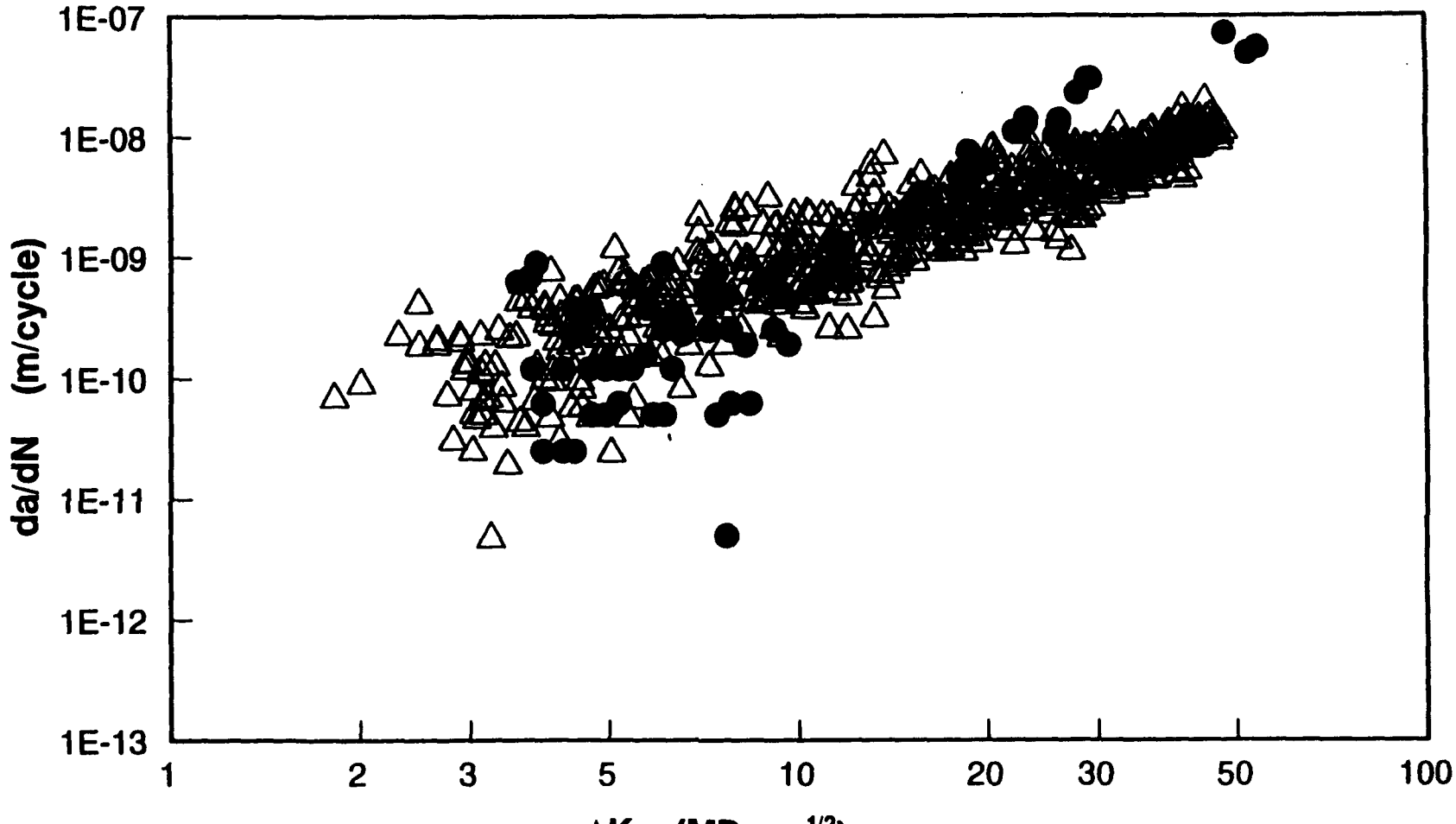

Figure 4. Simulated small crack growth rate data for HSLA-80

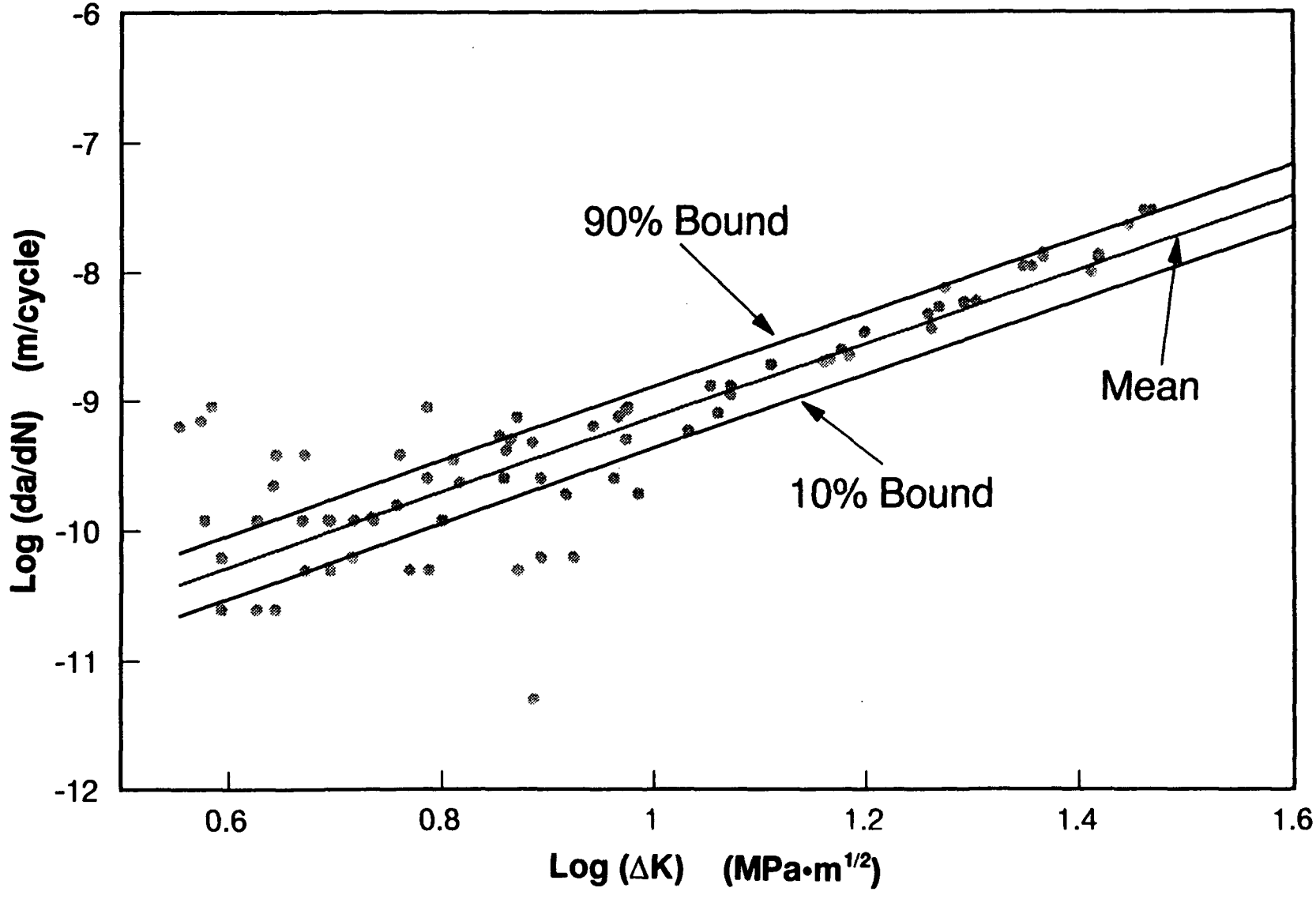

Figure 5. Illustration of the lognormal random variable FCG model

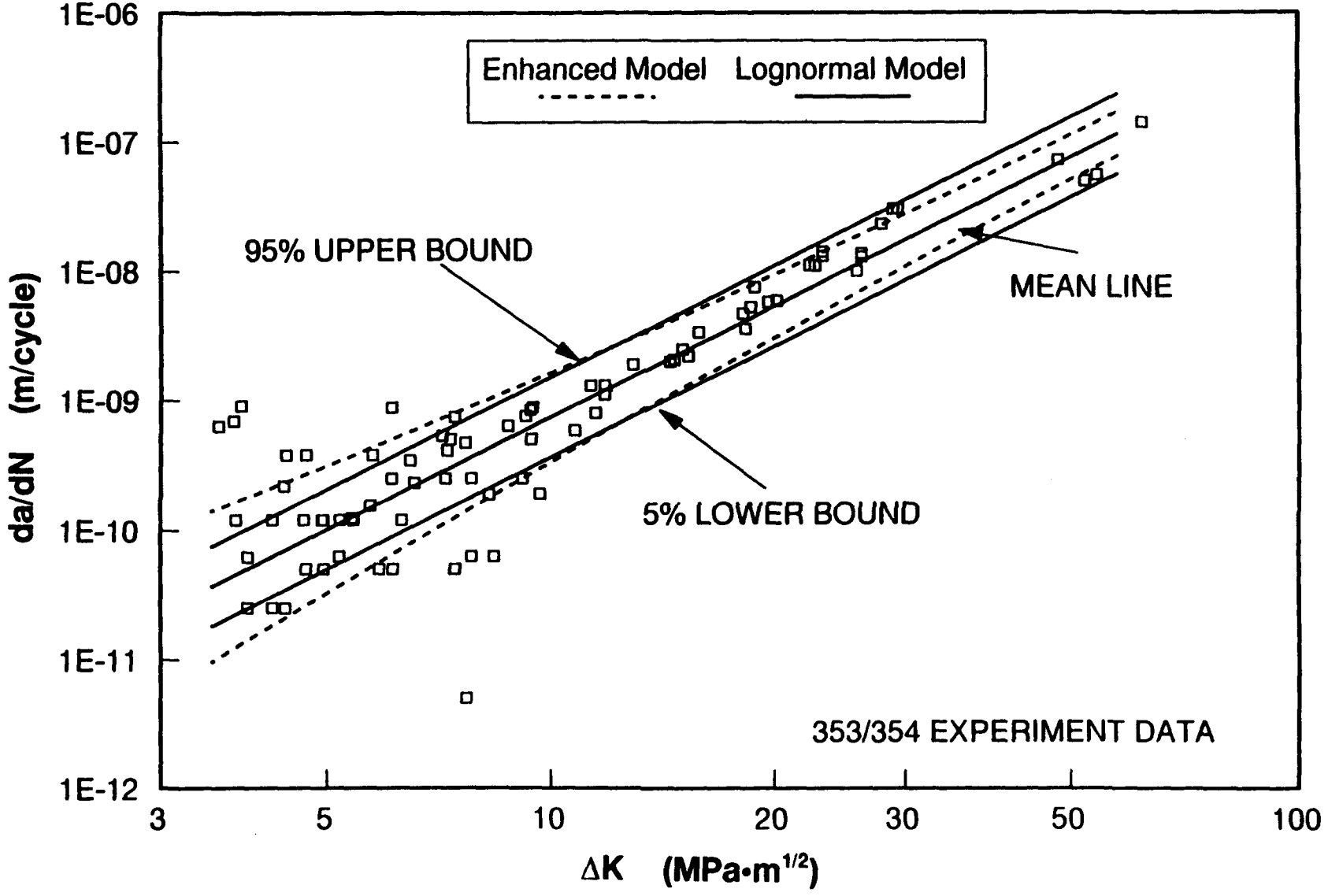

Figure 6. Illustration of the enhanced lognormal random variable FCG model

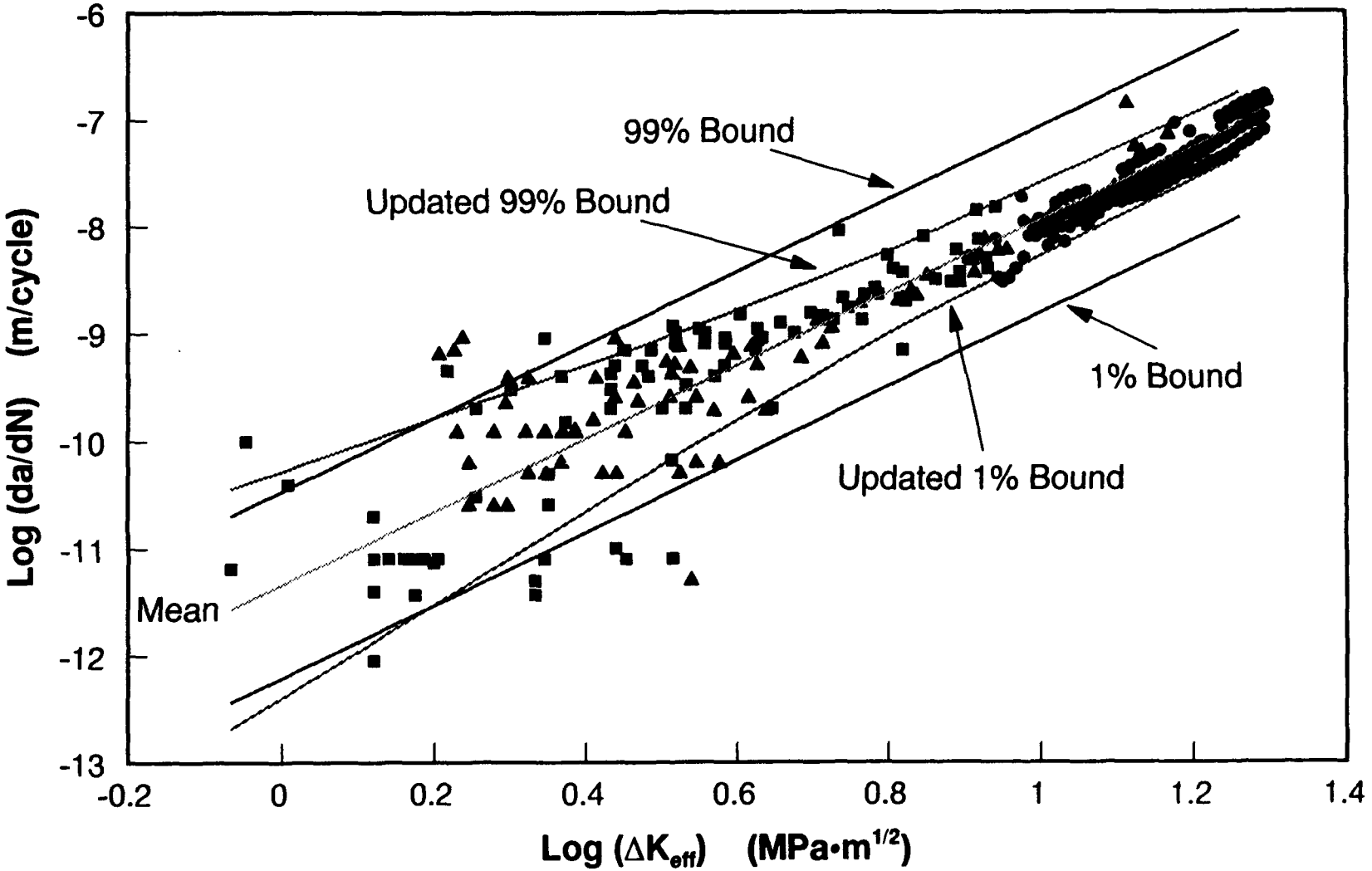

Figure 7. Illustration of the lognormal and enhanced lognormal random variable models for combined small and large crack data

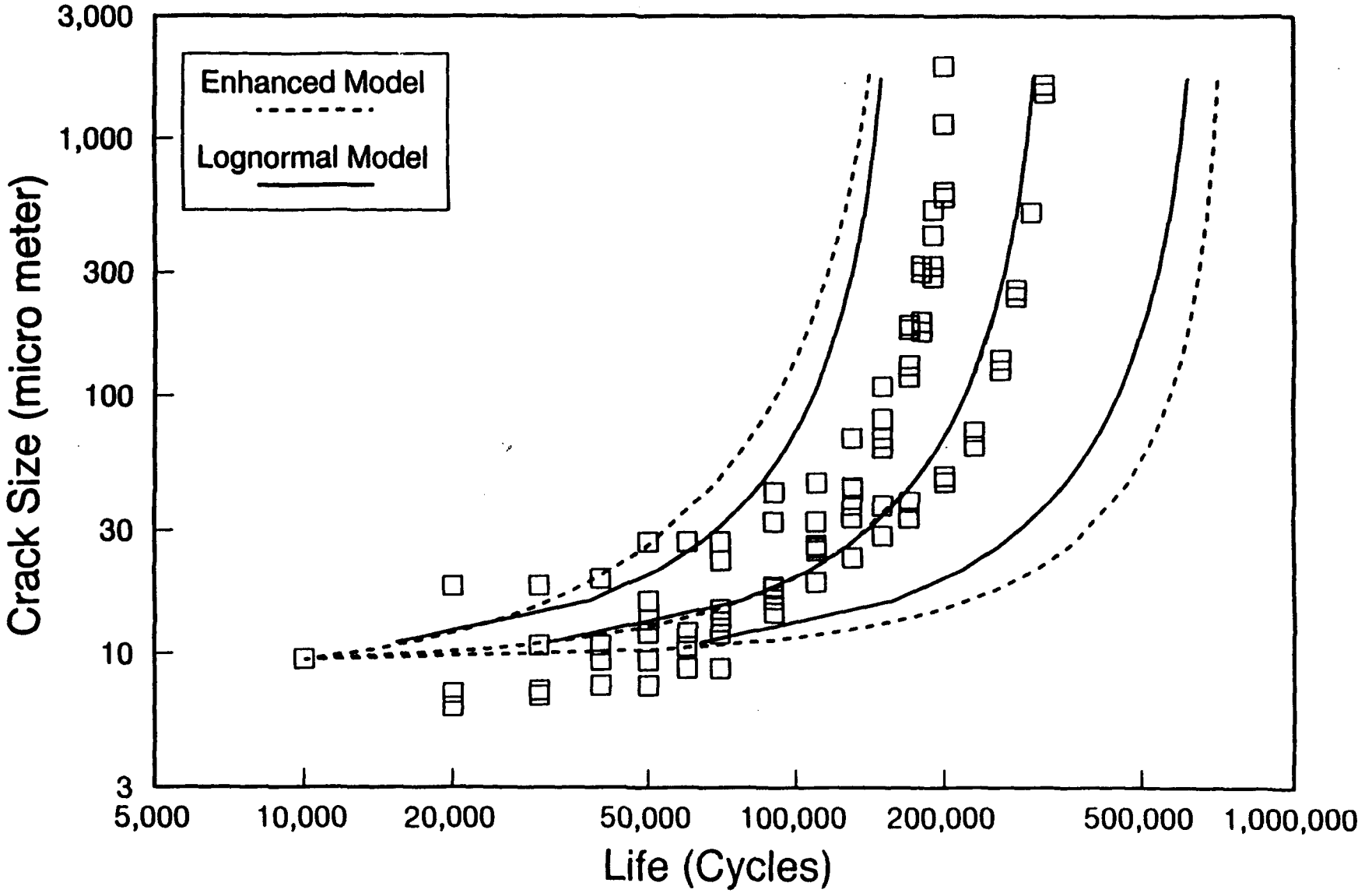

Figure 8. Sample life prediction results using lognormal and enhanced lognormal random variable models